Seismic Retrofit of Deficient Reinforced Concrete Shear Walls

Hamed Layssi

April, 2013

Department of Civil Engineering and Applied Mechanics

McGill University, Montreal

A thesis submitted to the Faculty of Graduate and Postdoctoral Studies

in partial fulfillment of the requirements of the degree of Doctor of Philosophy

Abstract

This research describes an experimental and analytical investigation to evaluate the seismic performance of poorly designed and detailed reinforced concrete (RC) flexural shear walls both in their as-built conditions and after being retrofitted. Older shear walls have several deficiencies which make them vulnerable in case of moderate to severe earthquakes. Full-scale shear wall specimens were constructed and tested under reversed cyclic loading.

Two different techniques were chosen to retrofit the deficient walls in order to improve the overall performance. A retrofit technique using Carbon Fibre Reinforced Polymer (CFRP), having minimum intervention, was studied to determine the seismic performance. A more labour-intensive repair technique, including the addition of a reinforced concrete jacket in the critical region (location of potential plastic hinging and lap splices of vertical bars) together with CFRP wrapping was also studied.

The responses obtained from experiments were used to develop behavioural models, capable of representing the global responses of the walls, as well as critical failure modes observed in the experiments. These models provide useful tools for predicting the complete reversed cyclic loading responses of shear walls.

The analytical models were used to predict the responses of a deficient prototype wall-frame structure in its original condition as well as after retrofit, subjected to different seismic hazard levels. This study enabled an evaluation of the performance of the prototype structure to determine the effectiveness of retrofit and repair measures.

Résumé

Cette recherche présente une étude expérimentale et analytique pour évaluer la performance sismique des murs des contreventements déficients avant et après réhabilitation sismique. Les murs représentent la construction typicalité des 1960's et ils sont plusieurs déficiences. Les murs à grande échelle ont été construits et soumises à des charges cycliques alternées.

Deux techniques différentes ont été choisies et examiné pour la réhabilitation sismique des murs déficients. Une méthode de dimensionnement de réhabilitation sismique, avec l'intervention minimale, utilisant de polymères renforcés de fibres de carbone (PRFC). La deuxième technique compris l'ajout d'une chemises en béton armé (renforcés de fibres d'acier et des armatures) dans la région critique (la région de rotule plastique potentielle et du chevauchement des armatures verticales), accompagnée PRFC pour l'amélioration résistance cisaillement de murs.

Les réponses obtenues à partir d'expériences fournissent des informations importantes sur les caractéristiques des murs des contreventements qui peuvent être utilisées pour développer modèles comportementaux et calibrer des techniques de prédictions numériques. Ces modèles sont capables de représenter les réponses globales des murs.

Les modèles numérique ont été utilisés pour prédire les réponses d'un vieux bâtiment (ossatures résistantes au moment munies de murs de contreventement) de cinq étages en béton armé dimensionne selon le code 1963 de l'ACI ((American Concrete Institute) et Code national du bâtiment 1965 du Canada (CNBC), et pourrait être vulnérables lors de séismes forts ou même modères. Le bâtiment est analyse (statique pushover et l'analyse dynamique de l'historique temporel) dans le régime non-linéaire avant et après réhabilitation séismique des murs.

“Sapere aude” ...

Acknowledgments

I would like to thank my supervisor, Professor Denis Mitchell, for his continuous support during the last five years at McGill. His wonderful and unique personality together with his great knowledge and experience were more than enough to enjoy every second of this long journey. With his bright and inspiring ideas and the freedom I was granted, I was able to discover more every single day. His great support and patience was crucial in dealing with the difficulties of being an international student.

I would also like to thank Dr. William Cook for his great support. The task of dealing with 6 tonne shear wall specimens could go nowhere unless I had his experience and expertise on my side. His contribution to the experimental phase of this study was vital.

The great support I received from technicians in the structural lab, Ron Sheppard, Marek Przykorski, John Bartczak is really appreciated.

I would like to thank Farshad Habibi for all the great moments we spent in the structural lab. He was a big help in all the ups and downs. The contribution of Payam Tehrani, Julie Reilly, Tristan Hogan, Hanif Shariff, Dana Saba, and Elena Chalmers in the different phases of this study is greatly appreciated.

The financial support from the Canadian Seismic Research Network (CSRN) funded by the Natural Sciences and Engineering Research Council of Canada (NSERC) is gratefully acknowledged.

My special thanks go to my lovely parents in Iran, for their generous and never ending supports during all years of my studies; with sacrifices they made, they paved the way for my academic life, in Iran and in Canada. Finally, I would like to thank my dearest wife, Azadeh Momeni, for her continuous supports and all the lovely moments she created. She has made my life an extraordinary journey. I feel guilty for missing her companionship so often during the course of this work.

To Azadeh jan;

for her great love, and all the amazing things she brought into my life;

&

To my beloved parents;

for their immense love and support.

Table of Contents

List of Figures

List of Tables

List of Symbols

A_b	Area of individual bar
A_{cv}	Area of the web of the walls, $0.8l_w b_w$
A_{ch}	cross-sectional area measured to the outside edges of transverse
A_g	Gross area of concrete section
A_s	area of longitudinal tension reinforcement
A_s	area of transverse reinforcement
A'_s	area of longitudinal compression reinforcement
$A_{s,bal}$	area of compression reinforcement
$A_{v,1}$	Area of transverse reinforcement in existing concrete
$A_{v,2}$	Area of transverse reinforcement in added FRSCC jacket
b_w	Web width
C_0	Modification factor to relate spectral displacement of an equivalent single-
C_1	Modification factor to relate expected
C_2	modification factor to represent the effect of pinching, as well as cyclic
C_m	Effective mass factor
c_b	Smallest cover or bar spacing
c_{vx}	Vertical distribution factor for pseudo-later forces (used in Static Pushover)
D	Guage length for average curvature determination
d	distance from extreme compression fiber to centroid of longitudinal tension
d_b	Nominal diameter of bar
d_{cs}	Smallest cover or bar spacing (CSA A23.2 notation)
E_c	Modulus of elasticity of concrete
E_s	Modulus of elasticity of steel reinforcement
E_f	Modulus of elasticity of CFRP material
F_a	The acceleration-based site coefficient
$F_{t,eff}$	Effective tensile strength of CFRP wrap
F_v	Velocity-based site coefficient
f'_c	Nominal compressive strength of concrete (lower-bound)

$f'_{c,e}$	Expected compressive strength of concrete
f_o	Axial stress in the wall element
f_r	Modulus of rupture
f_s	Stress in reinforcing steel bar (lap spliced bars)
f_{sp}	Tensile splitting strength of concrete
f_u	Ultimate strength of the reinforcing bars
f_y	Nominal yield stress of reinforcing materials (Lower bound)
$f_{y,e}$	Expected yield stress of reinforcing materials
$f_{y,h}$	Yield strength of the transverse reinforcement
G_c	Shear modulus
g	Gravity acceleration
h_c	centre-to-centre distance in the horizontal plane of the confining ties
h_w	Height of shear wall
I_g	Moment of inertia of gross concrete section
K_{lat}	Lateral stiffness of shear wall element (loading applied at the top)
k_{beam}	Rotational stiffness of beam-column element
k_e	Effective stiffness of the structure determined by idealization of pushover
k_{FRP}	Transverse reinforcement index
k_i	Initial stiffness of the structure obtained from mathematical model
k_s	Rotation stiffness of concentrated hinge at the ends of beam-column elements
k_{slip}	Rotational stiffness of elastic spring used for the effect of potential bar slip
$K_{rot,mem}$	Rotational stiffness of beam-column component (beam-column series with
k_{tr}	Transverse reinforcement index
L	Vertical distance of LVDT gauges
l_b	Provided lap splice length in existing member
l_d	development length of deformed bar in tension
l_h	unsupported length of hoops
l_w	Length of shear wall
$[M]$	Diagonal mass matrix
M_e	Expected moment capacity of beams and columns
M_f^+	Factored moment
M_n	Nominal moment resistance of section

M_r^+	Ultimate moment resistance of section
M_y	Yield moment of concrete section
m_i	Mass of storey i
N_u	Axial compression force on columns
n	Factor in Ibarra-Krawinkler Model used to avoid numerical problems
n_f	number of FRP layers
n_s	number of bars being spliced at a single failure plane
P_e	Design axial load
P_b	Axial load capacity at balanced condition
$Pinch_x$	Pinching factor for Hysteretic material
$Pinch_y$	Pinching factor for Hysteretic material
Q_D	Design action due to dead load
Q_L	Design action due to live load
Q_S	Design action due to snow load
Q_G	Design action due to gravity loads
R	Ratio of the elastic-strength demand to the yield-strength
r	Parameter that controls the nonlinear descending branch
r_{match}	ratio of the simulated response spectra over the period range of interest is
S_a	Spectral response acceleration
s	Vertical spacing of the ties
s_1	Spacing of transverse reinforcement in existing wall
s_2	Spacing of additional transverse reinforcement in the FRSCC jacket
s_h	Spacing of the hoops
T_i	Initial period of the structure
T_e	Effective period of the structure
t_f	thickness of the FRP layers
V_c	Shear resistance provided by concrete; & force correspond to shear cracking
V_{CFRP}	Shear resistance provided by CFRP wrap (or strips)
V_n	Nominal shear resistance of section
V_p	Column shear associated with plastic hinging of the beams
V_s	Shear resistance provided by steel
V_y	Lateral base shear corresponding to general yielding as determined by

W	Total weight of the building
W_x	Weight of storey x
x_p	strain at which the straight line descent begins in tension
x_n	strain at which the straight line descent begins in compression
α	Stiffness modification factors
α_c	coefficient defining the relative contribution of the concrete strength to the
α_m	Strain-hardening ratio for beam or column components
Δ_y	Yield displacement of wall
Δ_u	Ultimate displacement of wall
δ_t	Target displacement, ASCE-41
ε_c'	Strain corresponding to maximum compressive strength
ε_y	Yield strain of reinforcing steel
ε_u	strain corresponding with crushing of concrete
$\{\phi_1\}$	Mode shape vector
$\phi_{1,r}$	The ordinate of mode shape 1 at the roof
φ_y	Curvature corresponding to the yielding moment of section
Γ_1	First mode mass participation factor
γ_c	Shear strain corresponding to shear cracking
υ	Poisson's ratio for concrete
θ	Generalized deformation
θ_p	Plastic rotation capacity
ρ	Ratio of tension reinforcement
ρ'	Ratio of compression reinforcement
ρ_{bal}	Reinforcement ratio producing balanced strain conditions
ρ_t	Volumetric ratio of tie steel
υ_c	Stress corresponding to shear cracking
$\varepsilon_i^{\pm}, \sigma_i^{\pm}$	Strain-Stress points for Hysteretic Material calibration in OpenSees
$k_1; \psi_t; \alpha$	Bar location factor
$k_2; \psi_e; \beta$	Coating factor
$k_3; \lambda$	Concrete density factor
$k_4; \psi_s; \gamma$	Bar size factor

Chapter 1
Introduction

1.1. General

This thesis describes an experimental and analytical investigation to evaluate the seismic performance of poorly designed and detailed reinforced concrete (RC) flexural shear walls both in their as-built conditions and after being retrofitted. Older shear walls have several deficiencies which make them vulnerable in case of moderate to severe earthquakes. Full-scale shear wall specimens were constructed and tested under reversed cyclic loading (with load being applied near the tip of the walls).

Two different techniques were chosen to retrofit the deficient walls in order to improve the overall performance. A retrofit technique using Carbon Fibre Reinforced Polymer (CFRP), having minimum intervention, was studied to determine the seismic performance. A more labour-intensive repair technique, including the addition of a reinforced concrete jacket in the critical hinging region together with CFRP wrapping was studied.

The responses obtained from experiments were used to develop behavioural models, capable of representing the global responses of the walls, as well as critical failure modes observed in the experiments. These models provide useful tools for predicting the complete reversed cyclic loading responses of shear walls.

The analytical models were used to predict the responses of a deficient prototype wall-frame structure in its original condition as well as after retrofit. This study enabled an evaluation of the performance of the structure to determine the effectiveness of retrofit and repair measures.

1.2. The Need for this Research

Reinforced concrete (RC) shear walls have long been recognized as suitable structural systems, providing both lateral resistance and drift control in RC buildings. However older shear walls were typically designed mainly for combined actions of gravity loads and wind loading with no special seismic load consideration. Structures designed and built in the 1960's and 1970's, before modern seismic design and detailing requirements were developed, have a number of deficiencies.

Deficiencies in these older walls include: inadequate wall thickness with only one curtain of distributed horizontal and vertical reinforcement; inadequate lap splice lengths of the longitudinal reinforcement; lap splices located in regions of potential plastic hinging; inadequate confinement of the end regions of the walls; lack of control of the buckling of the flexural reinforcement; and insufficient amounts and poorly detailed transverse (shear) reinforcement. Experience from the 2010 Chile earthquake (Wallace, 2012; Saatcioglu, 2013) demonstrated that many thin shear walls were severely damaged.

While many experimental programs have been conducted on different aspects of modern shear walls, there is a lack of experimental results on the behaviour of thin shear walls with poor reinforcement details, corresponding to construction in the 1960's and 1970's. Furthermore, little research has been conducted on the retrofit of such deficient walls.

There is also a need to develop robust analytical tools for assessing the seismic performance of deficient shear walls. Experimental data from this research enabled the development of behavioural models, capable of capturing the global responses of the walls and potential failure modes.

1.3. Research Objectives

The main objectives of this study are to:

- Investigate the reversed cyclic loading behaviour of slender thin RC shear walls with deficiencies typical of the construction of the 1960's and 1970's.
- Investigate the effectiveness of different retrofit techniques in improving the reversed cyclic loading behaviour of deficient older shear walls.
- Develop behavioural models to predict the response of deficient and retrofitted shear walls.
- Perform nonlinear dynamic analyses of a prototype shear wall-frame structure before and after retrofit to assess the responses.
- Study the predicted responses of the wall-frame structures, before and after retrofit subjected to different levels of seismic hazard (i.e., Montreal and Vancouver)

1.4. Thesis Outline

A review of the literature including relevant experimental and analytical studies as well as the evolution of seismic design provisions since the early 1960's are summarized and presented in this chapter.

Chapter 2 describes the experimental research program and the testing method.

The results of the experimental program are summarized and discussed in Chapter 3. Comparative studies of the responses of the walls and the effectiveness of the retrofit and the repair techniques are assessed in this chapter.

Chapter 4 describes the development of behavioural models based on the experimental results.

Chapter 5 describes the prototype frame-wall structure, before and after retrofit as well as predicted responses using pushover analyses and non-linear time history analyses for two levels of seismic hazard (i.e., Montreal and Vancouver).

Chapter 6 provides conclusions from this experimental and analytical study and Chapter 7 highlights the original aspects of this research.

1.5. Literature Review

1.5.1. Development of Codes and Guidelines

1.5.1.1. ACI-318; 1963-2011

The design methodology in 1963 ACI code (ACI 318, 1963) is based on working stress design; however, an ultimate strength design approach was also introduced. Chapter 22 of this code required a minimum thickness of 6 in. (150 mm) for walls up to two storeys in height. This minimum thickness is increased by 1 in. (25 mm) for each 25 ft (7.6 m) below the top two storeys. This code requires an area of horizontal and vertical reinforcement not less than 0.0025 and 0.0015 times the area of the reinforced section of the wall, respectively. For walls more than 10 in. thick, there should be reinforcement for each direction placed in two layers parallel with the faces of the wall. The minimum bar size was limited to #3 (9.5 mm diameter) bars spaced not more than 18 in. (450 mm) on centres. Around openings and at wall boundaries, there shall be not less than two #5 bars (16 mm). The minimum lap splice length required for reinforcement of Grade 50 and 60 should not be less than 30 and 36 bar diameters, respectively.

The 1971 ACI Code (ACI 318, 1971) followed generally the same design and detailing requirements for reinforcement ratios and bar sizes as in the 1963 code, except that in Appendix A – “Special Seismic Provisions for Seismic Design”, the minimum areas of distributed horizontal and vertical reinforcement had to be at least 0.0025 times the area of the gross section of the wall. For shear walls with $P_e/P_b < 0.4$, (P_e, design axial load, and P_b, axial load capacity at balanced condition), additional vertical reinforcement was required near the boundary elements. The minimum amount of this concentrated reinforcement was $200\, b_w d/f_y$, where d is the distance between extreme compression fibre and the centre of concentrated reinforcement and b_w was the thickness of the wall. For walls with higher axial load levels, the amount of concentrated reinforcement had to be selected such that the wall could resist the combined actions of gravity and overturning moment.

The reinforcing steel in the boundary elements had to be confined with transverse reinforcement over their full height. The minimum amount of required transverse reinforcement in the boundary elements was $l_h \rho_s s_h / 2$, where $\rho_s = 0.45\left(\frac{A_g}{A_c} - 1\right)\frac{f'_c}{f_y}$, l_h was the unsupported length of hoops, and s_h was the spacing of the hoops. The minimum lap splice length of all vertical reinforcement was at least 30 bar diameters.

The 1977 ACI Code (ACI 318, 1977) had the same design and detailing requirements as the 1971 code, except that the 1977 code introduced minimum lap splice lengths which were modified for different Classes of splices.

The 1983 ACI Code (ACI 318, 1983) required a minimum area of 0.0025 times the gross section area for both longitudinal and transverse reinforcement. This reinforcement should not have spacing greater than 18 in. (450 mm). The portions of the shear walls, where the extreme fibre was subjected to stresses greater than $0.2f'_c$, should have boundary elements. The boundary elements had to be proportioned to carry all factored gravity loads on the wall, as well as the overturning moments resulting from earthquake loading.

The boundary elements had to be confined with transverse reinforcement spaced not more than the smaller of: one-quarter of the minimum member dimension and 4 in. (100 mm). The minimum amount of the transverse reinforcement was:

$$A_{sh} = min\begin{cases} 0.3\left(sh_c \frac{f'_c}{f_y}\right)\left(\frac{A_g}{A_{ch}} - 1\right) \\ 0.12sh_c \frac{f'_c}{f_y} \end{cases}$$

where h_c is the centre-to-centre distance in the horizontal plane of the confining ties, and s is the vertical spacing of the ties. The minimum development length for straight bars required by the 1983 Code was $2.5f_y d_b / 65\sqrt{f'_c}$ which had to be

modified in order to get the appropriate lap splice length, based on the Class of the lap splice.

The 1989 ACI code (ACI-318, 1989) requirements for the minimum development lengths and the lap splice lengths changed significantly, by modifying the required lengths for the effect of cover, bar spacing, bar diameter, and the presence of epoxy coating. The 1989 ACI Code prescribed two different Classes of lap splices: Class A, where only 50% or less of the reinforcement is spliced; and Class B where more than 50% of the reinforcement is lap spliced. For Class A splices the lap splice length is taken as the development length, and for Class B splices the lap splice length is taken as 1.3 times the development length. However, the seismic provisions remained identical to the previous version of the code.

The requirements for determining the minimum development length in the 1995 ACI Code (ACI-318, 1995) was:

$$l_d = \frac{3}{40}\frac{f_{y,e}}{\sqrt{f_c'}}\frac{\alpha\beta\gamma\lambda}{\frac{c_b + k_{tr}}{d_b}}d_b$$

Where, modification factors, α, β, γ, and λ account for the effect of bar location, bar coating, bar size, and the concrete density (λ taken greater than 1.0 for lightweight concrete), respectively. The factor, k_{tr}, is the effect of confinement and c_b is the maximum distance between bars. The seismic provisions for shear walls remained very similar to the previous version.

It should be noted that the 2008 and 2011 ACI Code (ACI-318, 2008, 2011) requires that development lengths of the longitudinal reinforcement be determined to develop 1.25 times the nominal yield stress. The 2011 ACI Code had basically the same expression for the minimum development length, but was reformatted as:

$$l_d = \frac{3}{40}\frac{f_y}{\lambda\sqrt{f_c'}}\frac{\psi_t\psi_e\psi_s}{\frac{c_b + k_{tr}}{d_b}}d_b$$

Where λ accounts for concrete density (λ is taken less than 1.0 for lightweight concrete).

1.5.1.2. CSA and NBCC; 1965-Present

The 1965 National Building Code of Canada (NBCC, 1965), subsection 4.5.8 requires a minimum thickness of 6 in. (150 mm) for walls. The required thickness was 8 in. (200 mm) for basement and foundation walls. The minimum ratios of horizontal and vertical reinforcement for the walls were 0.002 and 0.0012, respectively.

Special provisions for seismic design were introduced into Clause 19 of the 1973 CSA A23.3 Standard (CSA, 1973). The minimum ratios of horizontal and vertical reinforcement for ductile flexural walls were increased to 0.0025 and 0.0015, respectively. The maximum spacing of the steel was 18 in. (450 mm), but was reduced to 12 in. (300 mm) in the lower half of the structure.

CSA A23.3 required a minimum thickness of 6 in. (150 mm) for bearing walls. Walls more than 10 in. (250 mm) thick were required to have the uniformly distributed reinforcement in each direction, placed in two layers parallel with the face of the wall.

Ductile flexural walls required to have concentrated vertical reinforcement near each end of the wall designed for the combined actions of gravity load and overturning moment. In this calculation, the overturning moment should not be less than the cracking moment. In no case should the reinforcement be less than $0.002b_w d$ for intermediate or hard Grade steel or $0.0018b_w d$ for Grade 60 (414 MPa) steel. No more than 50% of the concentrated reinforcement was permitted to be spliced at the same location. Lap splice lengths were required to be 1.7 times the development length.

The CSA A23.3 (1977) was almost identical to the 1973 Code, except that metric units were used.

CSA A23.3 (CSA A 23.3, 1984) introduced capacity design in Clause 21-Special Provisions for Seismic Design. Brittle failure modes such as shear failure were avoided by designing the shear resistance of walls such that plastic hinging can be developed at the base of the wall. The length of the flexural compression zone in concrete walls without confinement reinforcement was limited to ensure ductile

response. The boundary elements of the walls were detailed to provide confinement and to prevent bar buckling by limiting the spacing of the closed hoops around the concentrated vertical reinforcing bars.

Using a performance-based approach, CSA A23.3 (CSA A23.3, 2004) requires an estimate of the wall global drift arising from the design earthquake forces and then ensuring that the compression zone length at the base of the wall does not exceed a limiting length (Adebar et al, 2005). These provisions also recommend the minimum reinforcement ratio of 0.0025 for both the longitudinal and transverse uniformly distributed reinforcement. The spacing of these bars is limited to 300 mm for the plastic hinging region and 450 mm for other regions. The Code requires that the transverse reinforcement be extended and anchored within a region of concentrated reinforcement to develop $1.25f_y$. Concentrated vertical reinforcement, consisting of at least four bars shall be placed in at least 2 layers at each end of the wall. The minimum concentrated reinforcement shall not be less than $0.0015b_w l_w$ for potential plastic hinge regions and $0.001b_w l_w$ for other regions. The concentrated vertical reinforcement shall be enclosed by ties having a diameter of at least 30% of that of the largest bar diameter and detailed as hoops and spacing shall not exceed the smallest of 6 longitudinal bar diameter, 24 tie diameters, one half of the least dimension of the member or the tie spacing required by special ductility demands. To ensure the ductility, the current code requires the inelastic rotational capacity of the wall in plastic hinging regions to be greater than the inelastic rotational demand.

1.5.1.3. Evaluation, Rehabilitation and Modeling Guidelines

Seismic evaluation and rehabilitation of existing structures have been of special interest during the last two decades. Several attempts have been made in order to introduce standard procedures for evaluation and rehabilitating substandard existing structures.

The ATC-40 (ATC, 1996) guidelines titled "*Seismic Evaluation and Retrofit of Concrete Buildings*" had a dual focus on technical issues (for engineers) and public policy (building owners, management, etc). ATC-40 presents a multiple objective

approach for seismic risk management. The analysis method proposed was a basic nonlinear static pushover analysis which was compared to a demand curve. Capacity Spectrum Method (CSM) was introduced, where both performance and demand curves were plotted in the spectral acceleration vs. spectral displacement domain in order to determine the expected performance.

FEMA 273 (FEMA, 1997), titled "*Guidelines for the* Seismic *Rehabilitation of Buildings"* intended to serve as a tool for design professionals. It was considered to work as a reference document and a nationally accepted guideline for seismic rehabilitation of buildings. It aimed to serve as a tool for engineers and at the same time, a reference document for building regulatory officials. FEMA 273 formed the foundation for future developments and implementation of building code provisions and standards for rehabilitation. This document was later updated forming FEMA 356 (FEMA, 2000) "*Pre Standard and Commentary for the Seismic Rehabilitation of Buildings"* and proposed as a pre standard document.

ASCE/SEI 41 (ASCE, 2006), titled *"Seismic Rehabilitation of Existing Buildings"* provides provisions and commentary that are based on FEMA 356. It presents different alternatives for evaluation, modeling and rehabilitation techniques. In the case of reinforced concrete structures, recommendations were made in order to update and revise the original version of the document (Elwood et al. 2007). These changes are presented in ASCE-41, supplement 1. These documents propose a standard approach for evaluating potential failure modes of structures. Based on available research and literature, different modeling parameters and analysis techniques are recommended.

Application of FEMA-695 (FEMA, 2010) has been put to test (NIST, 2010) for the purpose of quantification of building seismic performance factors in the case of existing structures. However, modeling techniques for deficient structures are still under development and require further research.

1.5.2. Previous Research

1.5.2.1. Squat Shear Walls

According to the current CSA Standard (2004), shear walls with shear span-to-depth ratio (h_w/l_w) equal to or less than 2.0 are classified as a squat shear walls. Squat shear walls are widely used as seismic force resistance systems in low-rise buildings. Many older unreinforced or lightly reinforced squat walls have poor details and exhibit poor behaviour with limited ductility.

Paulay et al. (1982) studied the ductility of earthquake resisting squat shear walls to investigate the possibility of achieving an acceptable level of energy dissipation by flexural yielding. Four shear walls with height to length ratio of 0.5 were constructed. Two of these units had 100 mm thick rectangular cross sections and two other walls included small flanges at both ends. The vertical reinforcement consisted of uniformly distributed bars in the web with additional bars at the wall's end or in the flanges. The vertical bars in the boundary zones were confined with 6 mm transverse hoops spaced at 50 mm centres to avoid premature buckling of the vertical reinforcement. Tests indicated the possibility of a predominantly flexural response involving considerable yielding of the flexural reinforcement. Sliding shear along the base is reported to be the main cause of loss of stiffness and strength as well as limited energy dissipation.

Taghdi et al (2000) carried out research on the seismic behaviour of partially reinforced masonry walls and reinforced concrete walls. The test program involved three pairs of unreinforced, partially reinforced and reinforced concrete blocks. The reinforced concrete walls had a height of 1800 mm and a length of 1800 mm and were reinforced using #3 bars at 800 mm spacing in the horizontal and vertical directions. Application of steel strips attached to the wall using through-thickness bolts was studied as a possible retrofit technique. Non retrofitted wall specimens showed no significant inelasticity with failure occurring by concrete crushing at the ends of the walls buckling of the vertical reinforcement. The failure of the retrofitted walls was due to sliding shear along the construction joint.

Kuang and Ho (2008) studied the performance of eight large-scale squat shear walls with height to length ratio of 1.0 and 1.5 under reversed cyclic loading. Two groups of walls were tested: walls with conventional reinforcement and walls with improved reinforcement detailing. The effects of aspect ratio, the amount of reinforcement and boundary region confinement were studied. Similar hysteretic behaviour was reported for both types of walls. Observations also showed that the inherent displacement ductility factor of 2.5 to 3 may generally be achieved for these walls without confinement of the boundary elements.

1.5.2.2. Slender Shear Walls

In contrast to squat walls, little experimental research is available on the performance of poorly designed and detailed slender shear walls. Most of the research in this area was carried out after the 1970's as seismic provisions were being introduced in standards and codes.

Cardenas and Magura (1973) studied the monotonic responses of six large rectangular cross section shear wall specimens of 21 ft height and 6 ft long. The walls were tested as a horizontal cantilever fixed at one end and subjected to loads at several locations over the wall height, representing wind or earthquake forces. Variables were the amount and distribution of vertical reinforcement and the effect of the moment to shear ratio. Results indicated that the strength of rectangular RC shear walls is generally governed by flexure rather than shear and that the amount and distribution of vertical reinforcement affects the ductility of walls.

Aktan and Bertero (1985) evaluated the seismic resistant provisions of the 1982 UBC code (ICBO, 1982), 1983 ACI Code (ACI-318, 1983) and ATC 3-06 (ATC, 1978) for the shear design of slender walls in mid-rise construction located in regions of high seismic risk. Both analytical and experimental studies were carried out on ten prototype frame-wall structures. The specimens had mainly barbell shape cross sections with spirally tied or square tied boundary elements. While all of the walls failed after flexural yielding of the reinforcement in the boundary elements, the amount of dissipated energy and final failure mechanism varied considerably. This study showed that the shear strength of walls determined in

accordance with the seismic design provisions of the 1980's may not be adequate as the shear demand is not based on actual axial-flexural capacity; and hence some premature shear failures may occur.

Wallace and Thomsen (1995) presented a displacement-based design procedure for two shear-wall buildings. The walls had rectangular, T-shaped, and channel-shaped cross sections, with aspect ratios (h_w/l_w) of 5 and 7.5. Experimental verification of the proposed displacement-based design approach was carried out in a separate research program (Thomsen and Wallace, 2004), where four one-quarter scale wall specimens were tested. Two rectangular cross sections and two T-shaped cross sections were chosen. The walls had a height of 3.66 m, a length of 1.22 m, and a thickness of 102 mm. The walls were well detailed for achieving ductility and energy dissipation. Under a constant axial load of approximately $0.1A_g f_c'$, cyclic lateral displacements were applied to the walls. It was reported that the large spacing of the hoops and crossties in the wall boundary elements led to the buckling of the longitudinal reinforcement at 2.5% drift. Experimental results of this study were later used to develop methods for the flexural modeling of the slender shear walls (Orakcal and Wallace, 2006).

1.5.2.3. Retrofit Techniques

The retrofit of existing shear walls and the repair of shear walls after a major seismic event have become topics of special interest among researchers and engineers over the past two decades (Kunnath et al. 1995; Seible et al. 1997; Mar et al. 2000; Julio et al. 2003; Thermou et al. 2007; Fardis, 2009). Several retrofit techniques have been developed and used in order to improve the seismic performance of RC buildings; however, little literature is available on the retrofit of slender shear walls.

Fiorato et al. (1983) studied the seismic behaviour of several earthquake resisting structural walls under incrementally increasing reversed cyclic loading (with and without axial load), before and after retrofit. Walls with barbell-shaped cross sections had a height of 4.6 m and a length of 1.90 m, with horizontal and vertical reinforcement ratios of 0.63 % and 0.29%. The damaged specimens from

the initial testing were retrofitted and subjected to reversed cyclic loading. The repair technique consisted of replacing the damaged webs of the original failed specimens, with or without increasing the web thickness and adding some diagonal reinforcement. The purpose of this research was to evaluate the damage that may occur in moderate or severe earthquakes. This research concluded that the replacement of the damaged concrete in the webs of structural walls is an easy and effective repair procedure. This sort of repair does not improve or modify the seismic performance of the specimens, but restored the strength and deformation capabilities.

Priestley and Seible (1995) investigated the application of composite fibre jackets bonded with a polymer matrix to the surface of structural elements of older masonry and concrete structures. These retrofit methods were aimed at improving several deficiencies: the low flexural strength of the plastic hinge zone; inadequate flexural ductility due to poorly detailed transverse reinforcement; and inadequate shear strength. This research demonstrated the effectiveness of composite material jackets and wall overlays as retrofit and repair solutions.

Paterson and Mitchell (2003) tested a series of four shear wall specimens under reversed cyclic loading in order to evaluate the effectiveness of two retrofit techniques for an existing structure in California. Walls in the as-built condition had non-ductile reinforcing details including lap splices in the longitudinal reinforcement in potential plastic hinging regions, inadequate confinement of the boundary regions, and inadequate anchorage of the transverse reinforcement. The wall specimens were 300 mm thick and 1200 long, with aspect ratio (h_w/l_w) of 2.7 and 3. One specimen had the vertical bars lap spliced at the base of the wall and the other had lap splicing 600 mm from the base of the wall. The concentrated reinforcement at each end of the wall consisted of two 25M bars, with 4 - 15M bars used as the vertical reinforcement. The horizontal steel consisted of 10M bars at 350 mm spacing, with these horizontal bars anchored at their ends by 90 degree hooks around the vertical bars. Seismic retrofit techniques involved the use of headed bars, carbon fibre wrap, and reinforced concrete collars at the base of the wall. The objective was to determine the effectiveness of the use of headed bars,

carbon fibre wraps, and RC collars on the retrofit of older walls. The reinforced concrete collar was effective in strengthening the lap splice region by avoiding the brittle behaviour of the lap splice soon after yielding of the main flexural reinforcement. This technique moved the plastic hinge to a location above the added concrete collar. The use of headed bars and CFRP wrap to confine the lap splices at a location above the wall base prevented bond failure under cyclic loading.

Antoniades et al. (2003) investigated different repair strategies such as replacing the damaged concrete by a high-strength mortar, lap-welding of fractured bars in the plastic hinge regions as well as strengthening using FRP wraps on low-slenderness reinforced concrete walls which were designed in accordance with modern code provisions. Walls were initially subjected to reversed cyclic loading to failure and later strengthened using fibre-reinforced polymer jackets. The anchorage of FRP strips by means of specially designed GFRP anchors, and the use of steel plates were also studied in this research. Properly anchored FRP strips resulted in strength increases of approximately 30% with respect to conventionally repaired walls; however the energy dissipation capacity of the original walls could not be restored.

1.5.2.4. Modeling and Analysis

Modeling and analyses have been progressively updated during the last two decades. Analyses techniques have moved from linear static to nonlinear dynamic, enabling more realistic modeling and simulations.

An appropriate technique for modeling shear wall components should be capable of predicting the inelastic responses of the walls by incorporating important materials characteristics and behavioural response features. Such a model should represent the migration of the neutral axis, tension stiffening, and the interaction of flexure-shear actions. Certain behavioural features such as the presence of lap spliced bars and the influence of bar slip should also be reflected in the models. Different modeling approaches for modeling shear walls include macro models

such as modified beam-column elements, to micro models such as finite element models and fibre elements.

Clough et al. (1965) proposed a macro-model using a two component element (an elasto-plastic beam + a linear elastic beam) combined in series to represent a vertical element (wall or column). This model, however, could not represent strength or stiffness degradation in cyclic loading. A one component macro model using a single element with lumped hinges at each end was proposed by Giberson (1967). It is assumed that the nonlinear deformations are lumped at the ends of elements and elements deform in double curvature. Different hysteretic rules were assigned to these one or two component elements to account for degradation in cyclic loading.

The Three Vertical Line Element Model (TVLM) proposed by Kabeyasawa et al. (1982) used two vertical springs to model the boundary elements, while a central multi-spring element is used to model rotational, shear and axial deformations of the wall. The TVLM was later extended by Vulcano (1988) to the Multiple Vertical Line Element Model (MVLM), where multiple vertical elements were used to represent different sections of the shear wall web. The model is reported to successfully represent important behavioural features of the shear walls. Orakcal et al. (2004; 2006) investigated the application of the MVLE model to model key response parameters associated with cyclic response of flexural walls.

Vecchio (1999) proposed a finite element algorithm in order to model RC components. This model uses a rectangular mesh, and incorporates the nonlinear material characteristics of the concrete and steel. The potential effect of slip (bar extension) at the base was not taken into account. The model provided good predictions of the responses of walls.

Belmouden and Lestuzzi (2007) studied the performance of RC walls using an inelastic multilayer flexibility-based finite element with multilayer interfaces (similar to fibres). The hysteretic behaviour of the walls including strength and stiffness degradation, pinching and potential effect of slip was modeled. Inelastic shear deformation mechanisms and confinement effects were also explicitly modelled. The models were in good agreement with experiments carried out on slender walls.

The application of fibre sections assigned to beam-column elements is becoming popular in modeling shear walls to predict the nonlinear response. NIST-GCR10-917-8 (2010) describes the application of this approach for modeling different shear walls (either flexural or shear dominated). These models are able to accurately capture global responses of the walls, and are easy to use for engineering purposes. These fibre elements have been recently implemented in commercial programs (SAP2000, 2011; Perform 3D, 2010).

Different behavioural features such as the effect of potential bar extension at the base of the walls and the presence of the lap spliced bars in different locations of the walls have been studied by researchers. Cho and Pincheira (2005) have studied the effect of lap splice length on the stress that could be developed in the lap spliced bars. The model is modified and implemented in the current edition of the ASCE/SEI 41 (2006) document. The potential impact of bar slip is also studied by many researchers (Belmouden and Lestuzzi, 2006; Massone et al., 2009). Zhao and Sritharan (2007) proposed a fibre-based nonlinear element in order to account for potential bar slip at the base of walls and columns.

Chapter 2
Experimental Programme

2.1. Introduction

The experimental programme was carried out in three stages:

- **Stage 1 -** Two pairs of identical, deficient shear walls were designed and constructed. The two pairs of walls differed only in the amount of concentrated flexural reinforcement at the ends of the walls. One wall from each pair was tested under reversed cyclic loading in their as-built condition (W1 and W2).
- **Stage 2 -** The second stage involved the development of an effective and economical retrofit technique to delay the failure modes observed in phase one, and to improve the reversed cyclic loading response of the deficient walls. The companions to W1 and W2, were retrofitted prior to testing and were subjected to reversed cyclic loading (WRT1 and WRT2).
- **Stage 3 -** In the last step, the effectiveness of a repair technique on the performance of previously tested and severely damaged walls was studied. After being tested to failure, the as-built wall specimens (W1 and W2) were repaired and were retested (WRP1 and WRP2).

All experiments were carried out in the Jamieson Structures Laboratory in the Department of Civil Engineering at McGill University.

2.2. Description of Test Specimens

The test specimens consisted of a foundation block, which was anchored to a strong floor and a shear wall that cantilevered out from the foundation block. The foundation block and the shear wall were cast monolithically. The walls were tested in a horizontal position, and the reversed cyclic loading was applied near the tip of each wall. The test specimen and the test setup are shown in Fig. 2-1.

The heavily reinforced foundation block was 2500 mm long, 1500 mm deep and 350 mm thick. This foundation block was designed and detailed to accommodate the probable moment resistance of the shear wall. The foundation block was reinforced with four 25M bars (500 mm^2 per bar) which were placed in two layers along the top and bottom that served as the main flexural reinforcement. A total of three 10M bars (100 mm^2 per bar) were placed along each side for crack control. The transverse reinforcement consisted of 10M closed stirrups at spacing of 100 mm near the wall – foundation block interface.

Starter bars (sticking out from the foundation block) lapped with the longitudinal bars of the wall at the base of the wall. The reinforcement details and cross section of the foundation block are shown in Fig. 2-2.

2.2.1. As-Built Walls W1 and W2

The design and detailing of the thin slender walls were chosen to simulate the critical potential plastic hinging region with poorly confined lap splices of the longitudinal reinforcement and single-leg, improperly anchored transverse reinforcement, which was typical in the construction of the 1960's.

Walls W1 and W2 were tested in their as-built condition. The two walls differ only in the amount of concentrated flexural reinforcement at the ends of the walls.

The cross section of walls W1 and W2 are shown in Fig. 2-3(a). The walls had cross-sectional dimensions of 150 mm by 1200 mm, and a total height of the 3400 mm from the base of the wall. The reversed cyclic loading was applied at a location 3.25 m from the base of the wall. The shear span-to-depth ratio in the direction of testing, h_w/l_w, was 2.7 and hence the walls can be classified as flexural shear walls ($h_w/l_w > 2.0$). It is noted that for walls with an aspect ratio equal to or less than 2.0, the CSA Standard (CSA, 2004) classifies the wall as a squat shear wall. The wall thickness of 150 mm satisfies the minimum thickness requirements of the 1963 ACI Code and NBCC 1965 for low-rise buildings.

The flexural reinforcement for W1 and W2 consists of 2-20M (300 mm^2 per bar) and 4-20M (placed in two layers), respectively. The reinforcement ratios of

concentrated reinforcement for walls W1 and W2 were 0.0033 and 0.0067, respectively.

Uniformly distributed longitudinal reinforcement consists of 3-10M (100 mm^2 per bar) with a uniform spacing of 277 mm for W1 and 260 mm for W2. The 1963 ACI Code required reinforcement ratios of 0.0015 in the longitudinal direction. The corresponding ratios for W1 and W2 were 0.0016.

For distributed transverse reinforcement, the reinforcement ratio required by the 1963 ACI was 0.0025. The transverse reinforcement consists of single leg 10M bars with a 90° hook having a $6d_b$ extension (≈ 60 mm) at each end. Fig. 2-3(b) illustrates the distribution of longitudinal and horizontal reinforcement.

The hook was oriented parallel to flexural reinforcement, and hence did not provide confinement of the lap splice or adequate anchorage of the transverse reinforcement (see Figs. 2-3(c) and 3-3(d)). The clear concrete cover, measured to the hook of the transverse reinforcement is 25 mm.

The lap splice lengths are about 30 times the bar diameter (600 mm for 20M bars and 350 mm for 10M bars). It is noted that the lap lengths are considerably shorter than that required by the current ACI Code (ACI Committee 318, 2011) and the lap splices are improperly located in a critical region of expected plastic hinging. These shorter lap splice lengths were chosen to conform to the 1963 ACI Code (ACI Committee 318, 1963) and the 1965 NBCC (NBCC, 1965) that required a tension lap splice length of 24 and 30 bar diameters for Grades 50 and 60 reinforcement, respectively. The lengths and positions of the lap splices are shown in Fig. 2-3(b).

The lap splices of both the 20M flexural reinforcement and 10M uniformly distributed vertical bars started at the base of the wall. The lap splice in the 20M bars ended 600 mm above the base of the wall while the lap splices in the 10M bars ended 350 mm above the base of the wall. The dowels extended 1000 mm inside the foundation block to provide sufficient development length.

For both W1 and W2, the spacing of the transverse reinforcement was 250 mm over most of the height of the walls. Additional transverse reinforcing bars were

provided at the location of the loading point near the tip of the wall. The first single leg transverse bar was located 125 mm from the base of the wall.

2.2.2. Retrofitted Walls WRT1 and WRT2

Walls WRT1 and WRT2 had the same structural details as their companion walls W1 and W2, with the concrete strengths being slightly higher for the retrofitted walls due to the increase in strength over time (see Table 2-1).

The objective of the retrofit measures was to improve the reversed cyclic loading performance with minimum intervention so that any brittle failure was delayed such that yielding of the concentrated reinforcement could occur. The goal of the retrofit was to achieve a displacement ductility of 2.0.

The minimum intervention retrofit technique involved only the use of carbon fibre wrap. A total length of 1800 mm ($1.5l_w = 1800\ mm$) from the base of the wall, involving the critical lap splice length and the potential plastic hinging region, was fully wrapped using a single layer of uni-directional CFRP. Above this region, the walls were strengthened in shear by applying uni-directional carbon fiber wrap strips of 100 mm width, with a uniform spacing of 250 mm, centre-to-centre. Details of the retrofit technique for walls WRT1 and WRT2 are illustrated in Fig. 2-4.

The preparation of the concrete surfaces and the application of the carbon fibre wrap were done in accordance with the requirements of ACI Committee 440 (2002). Prior to installation of the CFRP, the edges of the walls were ground down to a radius of 20 mm (see Fig. 2-5) so that the wrap would not be placed over any sharp corners. In addition, the concrete surfaces to be wrapped were roughened to improve the epoxy bonding of the CFRP wrap.

The Tyfo® SCH-41 carbon fibre wrap was applied by first rolling a mix of the Tyfo® S epoxy and Cab-O-Sil TS 720 silica fume onto the areas that were to be covered by the wrap. The strips of carbon fibre wrap were soaked in the epoxy for the purpose of fibre saturation and then placed on the wall (Fig. 2-6(a)).

The CFRP wrap was provided with an overlap length of 300 mm on one side of each wall. It is noted that a shorter lap would have been sufficient, however since

there was only one layer of carbon fibre, a conservatively longer lap length was provided. Fig. 2-6(b) shows wall WRT1 before testing.

2.2.3. Repaired Walls WRP1 and WRP2

The repair technique combined the use of steel fibre-reinforced self-consolidating concrete jacketing for improving the poor behaviour of the lap splice region that suffered bond failure in walls W1 and W2, and CFRP wrapping for improving the confinement and the shear strength of the rest of the walls. The minimum target displacement ductility was 2.0.

Walls W1 and W2 which had been tested to failure were repaired. It is noted that the walls were pushed back to their initial horizontal position at the end of original tests to avoid significant residual drifts or deformations. At the base, the damaged concrete was removed in the end regions of the walls over a length of 625 mm (600 mm lap length + 25 mm extra) and over a depth of 75 mm for W1 and 115 mm for W2 (see Figs. 2-7 and 2-8).

The new reinforced jacket added 100 mm to the thickness of the walls on each side, resulting in a total thickness of 350 mm in the lap splice region. The 1200 mm wall length was not increased to simulate the effects of the architectural constraints on an actual repair.

In order to increase both the flexural strength and stiffness of the lap splice region, supplementary headed bars, anchored properly into the foundation block, were added to the boundaries of this new section, prior to casting. The additional reinforcement required in the reinforced jacket was determined such that the factored resistance at the base of the wall was sufficient to develop the probable resistance at the end of the jacket assuming that the reinforcement at the end of the jacket developed a stress of $1.25f_y$. The added reinforcement consisted of 2-15M headed bars (200 mm^2 per bar) and 4-15M headed bars at each end of the walls WRP1 and WRP2, respectively. The bars were placed at the same level as the original 20M bars and were placed as close as possible to the sides of the original walls.

In addition, 6-10M headed bars, were added in the jacket in line with the original distributed reinforcement of W1 and W2 (see Fig. 2-7).

The added transverse reinforcement in the jacket consisted of 7 pairs of 10M U-shaped stirrups that overlapped in the central region of the wall. The details chosen enabled placement of the stirrups and the overlapping portions also had 180° hooks to improve their anchorage (see Fig. 2-7 and Figs. 2-8(a) and (b)). The added transverse reinforcement provided confinement to the lap splice region, additional shear capacity, and had a spacing of 5 times the 15M longitudinal bar diameter that delayed longitudinal bar buckling (ACI Committee 318, 2011).

The original wall surfaces were roughened and 16 mm diameter steel threaded rods were placed through the thickness of the wall that protruded into the jacket to provide the necessary shear transfer between the original concrete and the added jacket. The rods were designed such that the shear-friction resistance between the jacket concrete and the original concrete exceeded the force in the headed bars with a stress developed of $1.25f_y$. Steel washers, 36 mm in diameter, and nuts were used at each end of the threaded rods to provide anchorage.

2.3. Material properties

2.3.1. Concrete

The target strength of the concrete used in construction of the walls W1 and W2 was 30 MPa, a typical concrete strength for construction in the 1960's.

For each wall, the compressive strength (f_c'), the tensile splitting strength (f_{sp}) and the modulus of rupture (f_r), were determined at time the walls were being tested.

The cylinder specimens of 100 mm diameter and 200 mm height were tested for the compressive strength and the tensile splitting strength. In order to determine the strains, an extensometer was mounted on the cylinder specimens that were tested in compression. For the modulus of rupture, prisms of 100 mm × 100 mm × 400 mm were tested in a 4 point bending test setup.

The average concrete material properties for the walls are presented in Table 2-1. Figs. 2-9(a) and (b) illustrate the stress-strain relation for concrete in compression. It is noted that the average 28-day compressive strength of concrete was 27.0 MPa. Table 2-1 presents the material properties at the time of wall testing; there was a slight increase in the strengths of the concrete for the retrofitted walls that were tested at some time after walls W1 and W2.

Table- 2-1- Average concrete material properties

Wall	Concrete batch	Age	f_c'	ε_c'	f_r	f_{sp}	Slump	Air content
		Days	MPa	mm/mm	MPa	MPa	mm	%
W1	**#1**	122	31.2	0.0019	3.79	3.34	112	6.5
WRT1		278	32.4	0.0020	4.06	3.37		
W2	**#2**	198	30.4	0.0018	4.74	3.50	150	7.0
WRT2		303	32.8	0.0018	4.73	4.05		

2.3.2. Reinforcing Steel

The steel reinforcement consisted of Grade 400 (minimum specified yield strength of 400 MPa) deformed reinforcing bars, which is similar to the Grade 60 (414 MPa) steel commonly used in the 1960's.

For each bar size (10M, 15M, and 20M), three coupons were tested monotonically in tension up until their ultimate capacity. In order to measure the strain during the test, extensometers were attached to the bars. The averaged results of these tests are presented in Table 2.2. The average stress-strain relation for steel coupons are presented in Fig. 2-9(c).

Table- 2-2- Average reinforcing steel material properties

	Diameter	Area	f_y	ε_y	ε_{sh}	f_u
	mm	mm2	MPa	mm/mm	mm/mm	MPa
10M	11.3	100	478	0.0024	0.006	729
15M	16.0	200	426	0.0021	0.006	728
20M	19.5	300	460	0.0023	0.008	637

2.3.3. CFRP Material Properties

The composite laminate of carbon fibre and the epoxy has a design thickness of 1 mm and corresponding design strength of 834 MPa in the fibre direction with a breaking strain of 0.85% (see Table 2-3), according to the supplier's specifications (Fyfe, 2010). The carbon fibre wrap has negligible strength in the direction perpendicular to the main fibre direction.

Table- 2-3- Properties of CFRP (composite laminate and epoxy)

Composite laminate	**Design Value**
Ultimate Tensile Strength of the laminate in fibre direction	834 MPa
Elongation at Break	0.85 %
Tensile Modulus	82 GPa
Ultimate Tensile Strength 90 degrees to primary fibre	0 MPa
Nominal Laminate Thickness	1.0 mm
Properties of the Epoxy	**Typical Test Value**
Tensile Strength	72.4 MPa
Tensile Modulus	3.18 GPa
Elongation Percent	5.0 %
Flexural Strength	123.4 MPa
Flexural Modulus	3.12 GPa

2.3.4. Fibre Reinforced Concrete

The steel fibre-reinforced, self-consolidating concrete in the jacket of walls WRP1 and WRP2 consisted of a self-consolidating concrete, with a 28-day compressive strength of 40 MPa, with an addition of 0.5% by volume of 25 mm straight steel fibres. Fig. 2-9(d) shows the stress-strain relationship for this material. The steel fibres were used to improve the lap splices and the self-consolidating concrete was used to assist in the placement of the steel fibre-reinforced concrete in the congested jacket region. Fig. 2-8(c) shows the steel fibre used in the study. The flow test was carried out in order to determine the consistency and flowability of the steel fibre reinforced self-consolidating concrete (see Fig. 2-8(d)). The average

flow properties for WRP1 and WRP2 are presented in Table 3-4. The flowability of the fibre reinforced concrete resulted in sufficient workability for the retrofit and there were no problems with the consolidation of the concrete in the congested reinforced concrete sleeve region.

In the region outside of the jacket, CFRP wrap was used that was similar to the retrofit used for walls WRT1 and WRT2 (see details in Fig. 2-8).

Table- 2-4- Flow properties of fibre-reinforced self-consolidating concrete

Batch	Flow @ 4 sec.	Flow @ 30 sec. (stop)	Air content
	mm	mm	%
WRP1	580	600	13
WRP2	635	655	7

2.4. Behavioural Predictions

For each wall, the monotonic shear versus tip deflection response was predicted using RESPONSE 2000 (Bentz and Collins, 2000), which is a sectional analysis software for reinforced concrete and it is based on the modified compression field theory. The actual geometry of the wall specimens and the measured material properties for the steel and the concrete were used as the input parameters for the analysis.

The predicted flexural capacities for walls W1 and W2 were 386 kNm and 673 kNm, respectively. Assuming the shear span of 3250 mm, these values correspond to applied shear forces of 120.6 kN, and 207.8 kN. It is noted that these predictions assume that the longitudinal reinforcement is able to yield which was not the case due to the inadequate lap splicing of the reinforcement at the critical section in flexure.

In the case of the retrofitted walls, the effect of the CFRP wrap was to provide additional confinement to the critical lap splice region so that the flexural steel could yield. This aspect is discussed in Chapter 4. The effect of the CFRP on the

shear strength of the wall was estimated by treating the wrap as equivalent steel stirrups.

For the repaired walls, the critical section was shifted from the base of the wall to a region beyond the added jacket, and therefore, a higher flexural resistance was achieved due to the yielding of the longitudinal reinforcement. Due to the shorter lever arm from the applied load to the critical section in flexure, the predicted maximum shear load that can be endured will be 147.1 kN for WRP1 and 256.4 kN for WRP2.

2.5. Testing procedure

The shear walls were tested under reversed cyclic loading, with the loads applied near the tip of the walls. The shear walls of this study are representative of typical construction of the 1960's and early 1970's. The walls were used in relatively short buildings (5-6 storeys) and hence, the axial load imposed on the walls was small. Based on approximate tributary area to a shear wall, it is believed that applying the axial load on the wall does not affect the flexure dominant response of these walls, significantly. No axial load was applied in this experimental program.

2.5.1. Test Setup

The walls were tested in a horizontal position, cantilevered out from the reinforced foundation block that was anchored to the testing floor by post-tensioned high strength threaded rods. The foundation block was installed over 2 rigid steel supports and was aligned horizontally and vertically using capping compound. Four steel beams were installed on top of the foundation block, which were in turn post-tensioned to the strong floor using eight 38 mm diameter high-strength threaded rods. The threaded rods were pre-stressed to approximately 80% of their ultimate capacity.

Reversed cyclic loading was applied by hydraulic jacks at a distance of 3250 mm from the base of the wall (see Fig. 2-1(c)). Two pairs of hydraulic jacks were used for the purpose of positive and negative loading. The positive loading jacks were installed on the strong floor, over a rigid steel plate (50 mm thick) to push the tip of the shear wall in the upwards direction. For each wall, a steel plate (20 mm

thick, 100 mm width and 250 mm length) was welded to pre-installed steel plates cast into the wall at the location of applied loading. The load from the two jacks was transferred to the wall through a channel section and a roller.

The negative loading cycles were applied using two jacks which were installed under the strong floor. The negative loading was transferred to the channel section loading beam installed on top of the wall using two 32 mm diameter threaded rods. The loading beam was set into position using capping compound.

In order to avoid excessive lateral displacement of the wall, a bracing frame was placed 2200 mm from the base of the wall. The test setup and details are presented in Fig. 2-1.

2.5.2. Test Method

Each reversed cycle of loading consisted of positive (upwards loading near the tip of the wall) and negative loading (downwards loading near the tip of the wall). Fig. 2-10 illustrates the reversed cyclic loading histories of the four specimens tested. Three reversed cycles were carried at each load or deflection level. The walls were cycled to selected load levels up to general yielding. After general yielding the walls were cycled to multiples of the yield deflection ($1.5\Delta_y$, $2.0\Delta_y$, etc.).

The as-built walls W1 and W2 were tested entirely in load control until failure because flexural yielding did not occur. Retrofitted walls WRT1 and WRT2, and the repaired walls WRP1 and WRP2 which experienced flexural yielding, were tested in both load and deflection control. Testing was stopped at the positive and negative peaks of each cycle to take photographs and to determine crack widths and the cracking pattern.

2.5.3. Instrumentation

During loading, data was collected from the load cells, linear voltage differential transformers (LVDTs), and strain gauges on the reinforcing bars. A potentiometer was used to measure the tip deflection of the specimen at the loading point. In order to measure the displacements and deformation over the potential plastic hinge zone, combination of LVDTs were placed at the back of the walls, enabling the average curvature to be determined over this critical location (see Fig. 2-11(a).

Strain gauges were installed on the main flexural and transverse reinforcement of the walls and the dowel bar from the foundation block. The location of these strain gauges is shown in Fig. 2-11(b). The strains determined from the LVDTs were supplemented with strains obtained from the strain gauges.

A pair of LVDTs were installed at the back and the front of the foundation block, enabling the measurement of the rigid body rotation of the foundation block during the tests (see Fig. 2-11(c)).

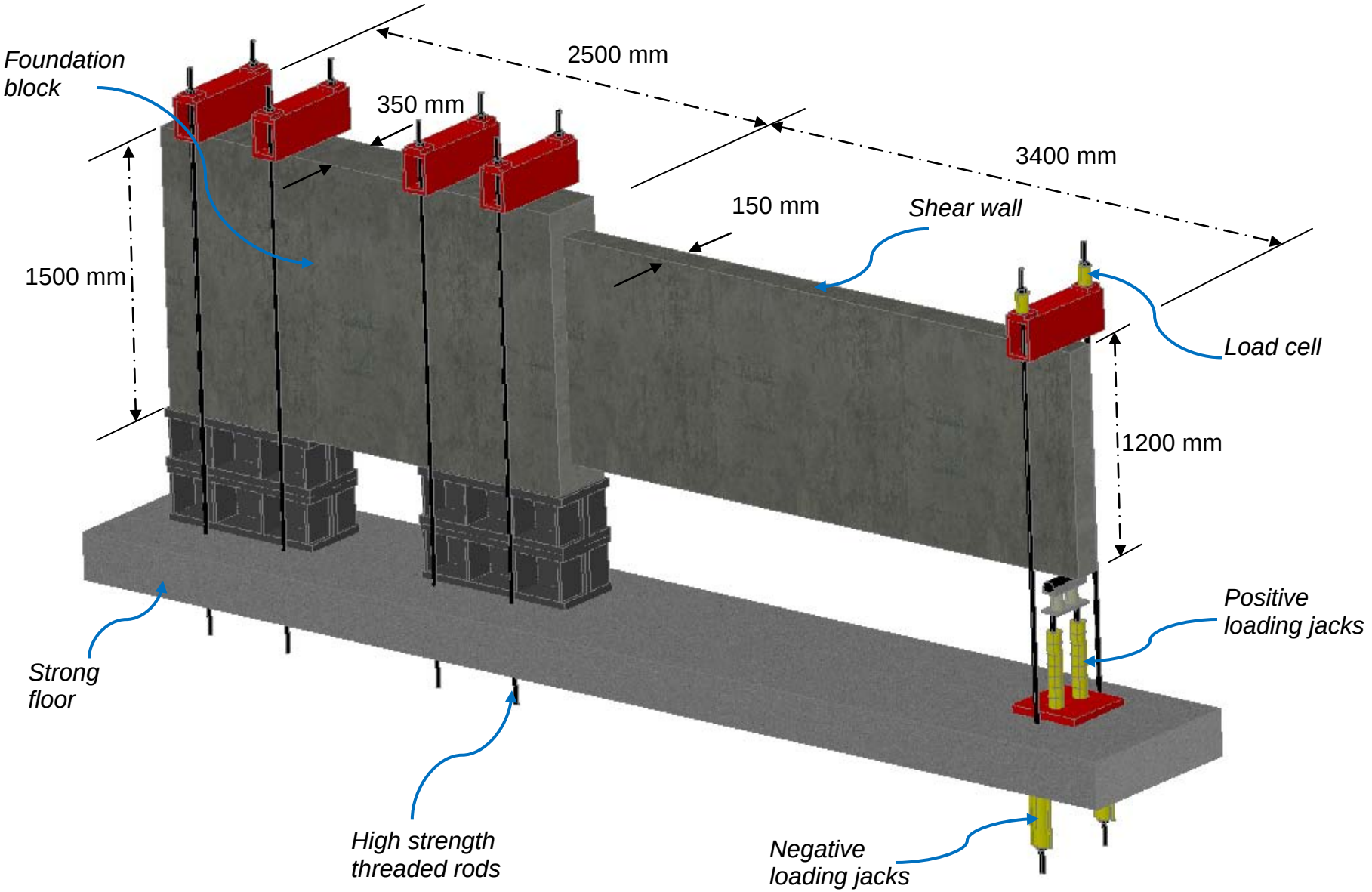

a) 3D Schematic view of the wall specimens and the test setup

(b) Wall W2 before test

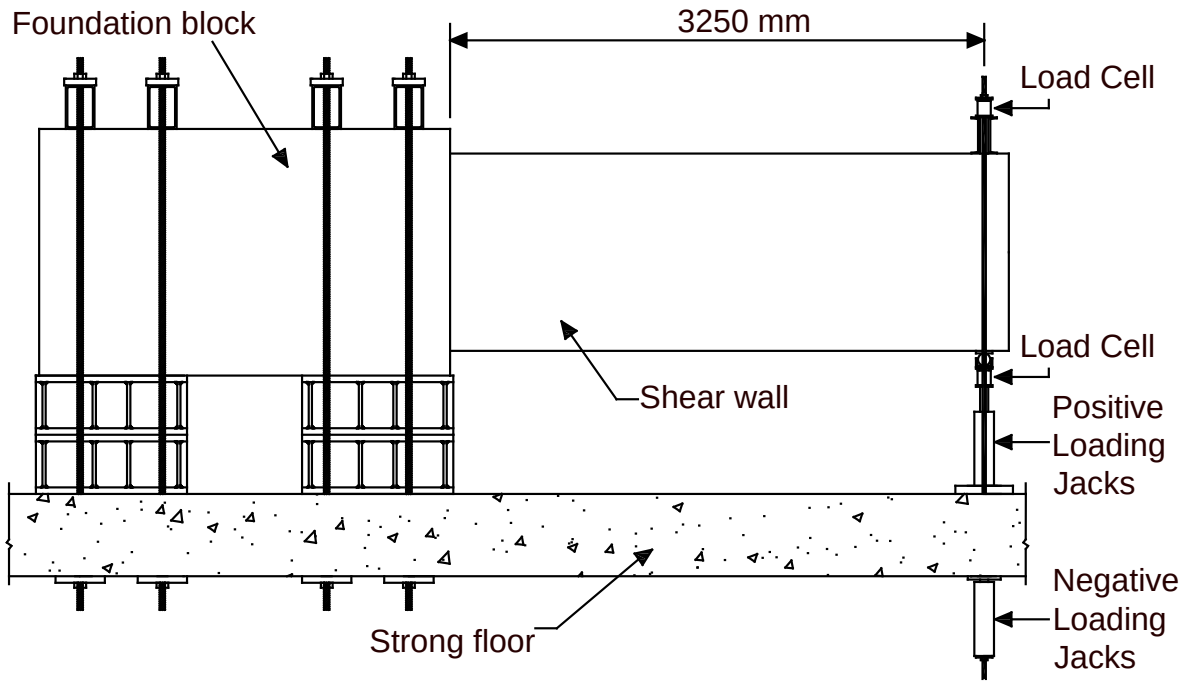

(c) Shear wall specimen

Fig. 2.1- Details of the test specimens

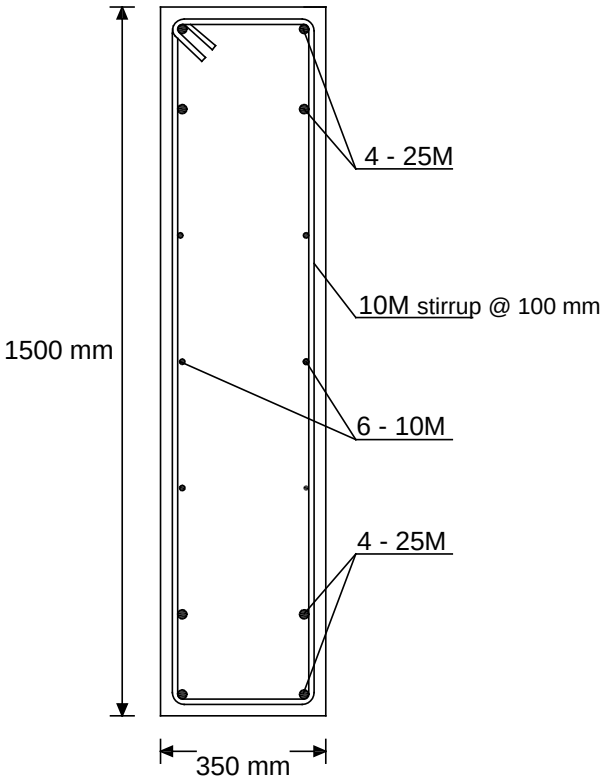

Fig. 2.2- Cross section of the foundation block

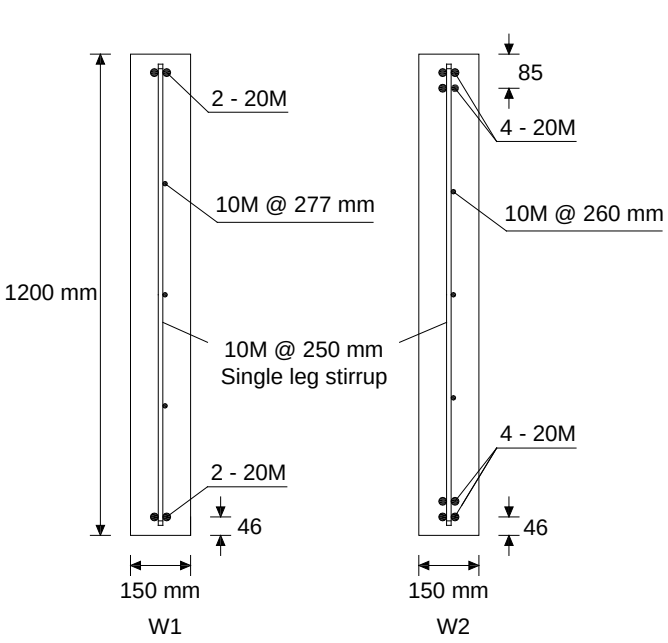

(a) Cross section of the as-built walls

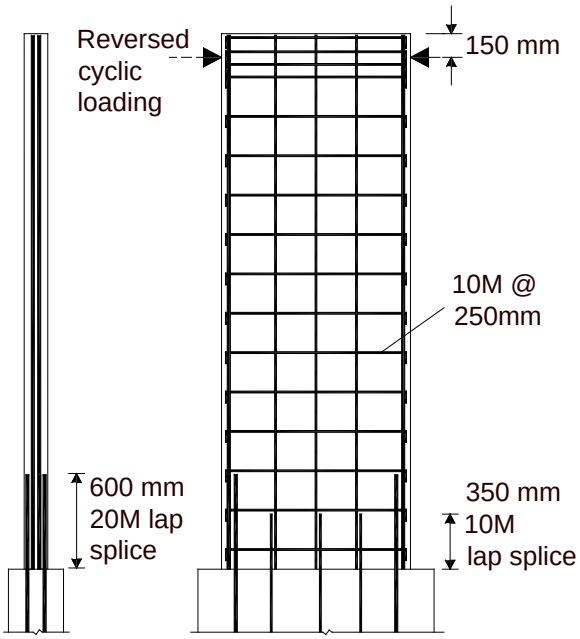

(b) detail of the single-leg transverse reinforcement

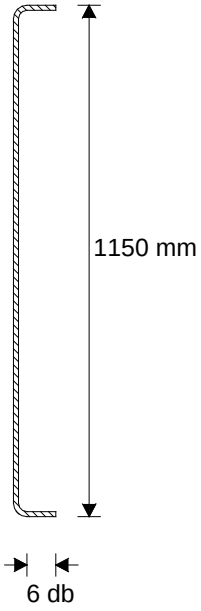

(c) Details of reinforcement and lap splices

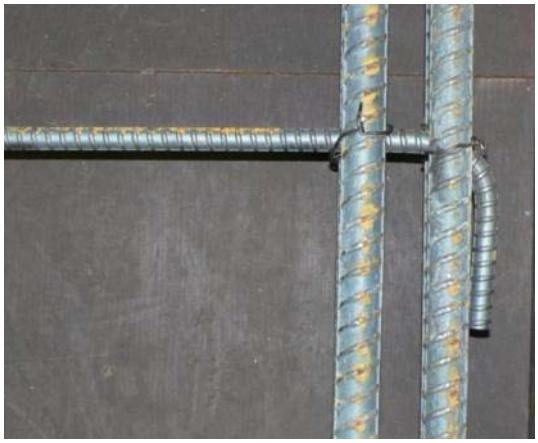

(d) anchorage of transverse reinforcement

Fig. 2.3- Details of walls W1 and W2

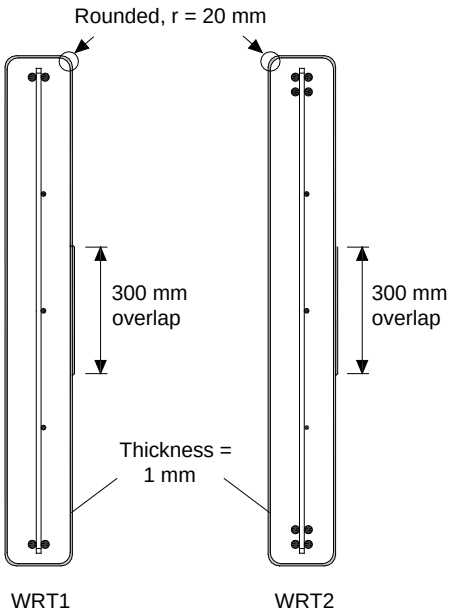

(a) Cross section of retrofitted walls

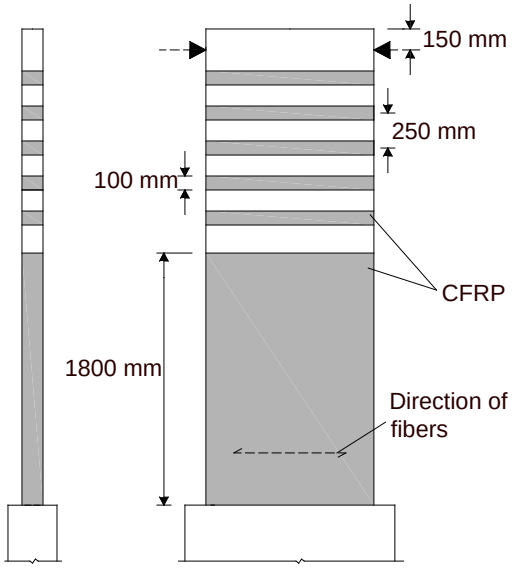

(b) Detail of retrofit technique

Fig. 2.4- Details of walls W1 and W2

(a) Full CFRP wrap zone

(b) CFRP strips zone

Fig. 2.5- Rounding the corners of the walls before installing the CFRP wrap

(a) Installing CFRP wrap

(b) Wall WRT1 before test

Fig. 2.6- CFRP wrap installation

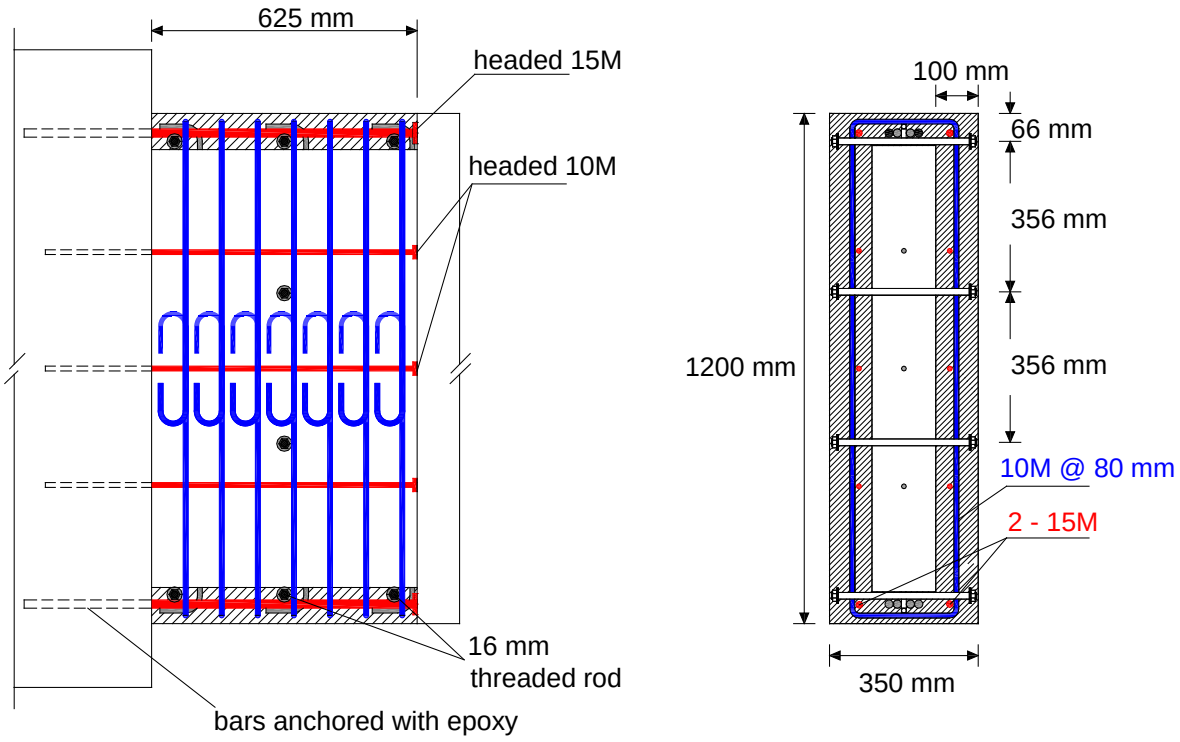

(a) WRP1

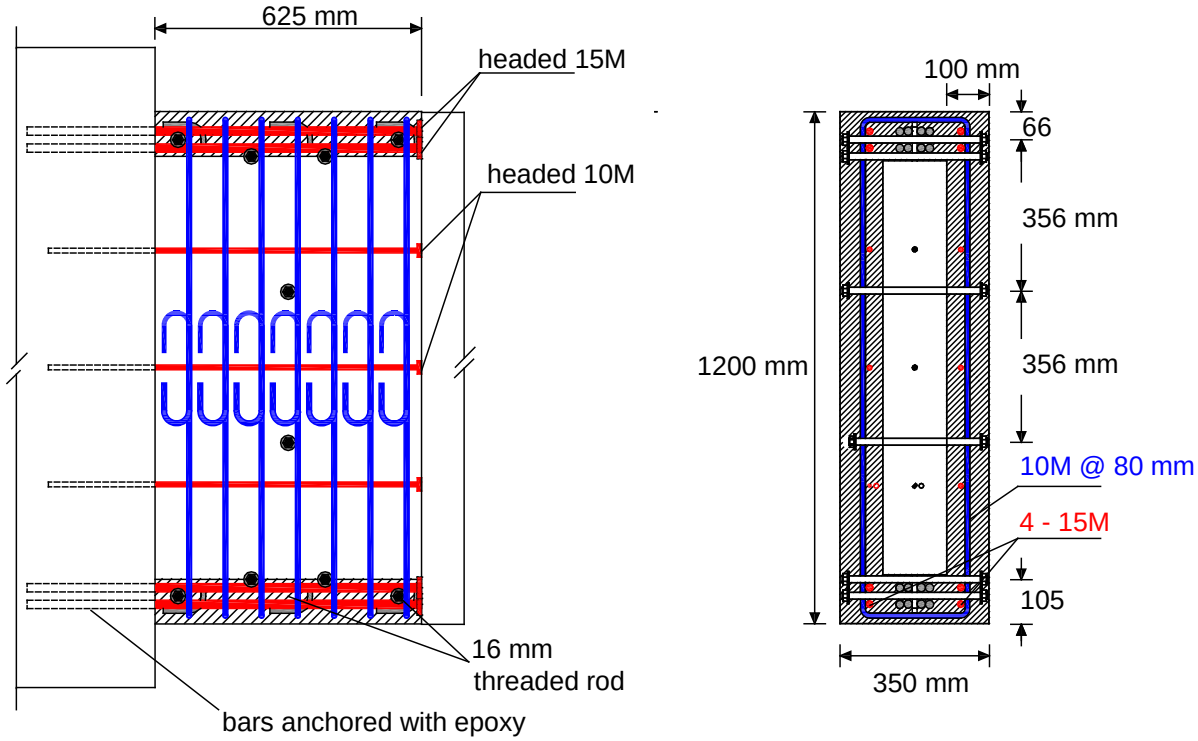

(b) WRP2

Fig. 2.7- Details of repaired walls WRP1 and WRP2: SCC with 0.5% steel fibres

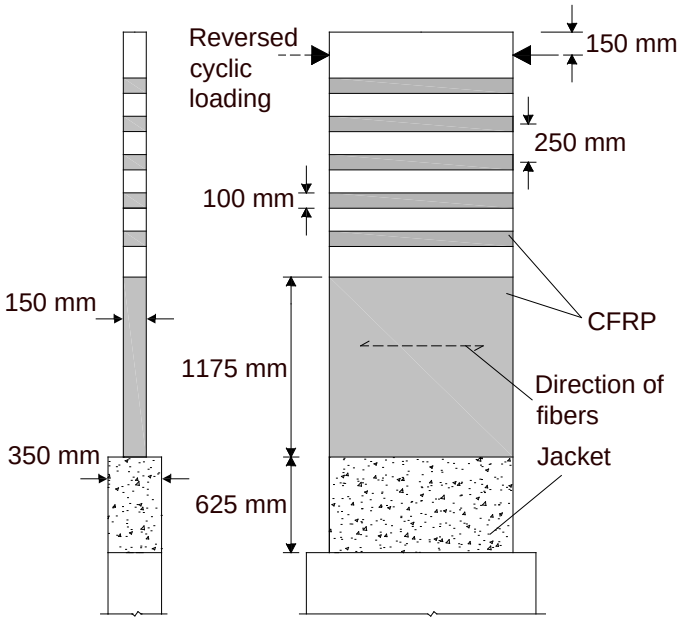

(a) Elevation view

(b) WRP1 jacket reinforcement

(c) Steel fibres

(d) SCC flow test

Fig. 2.8- Details of repaired walls WRP1 and WRP2

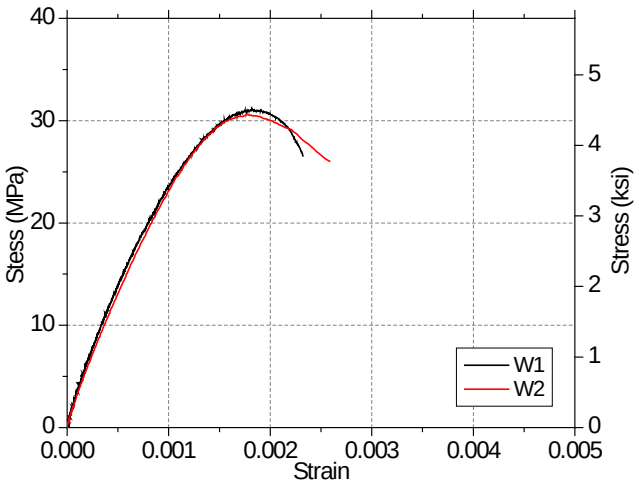

(a) W1 and W2

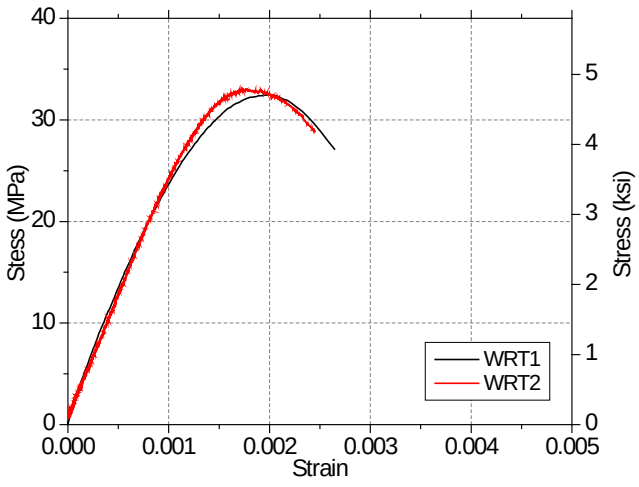

(b) WRT1 and WRT2

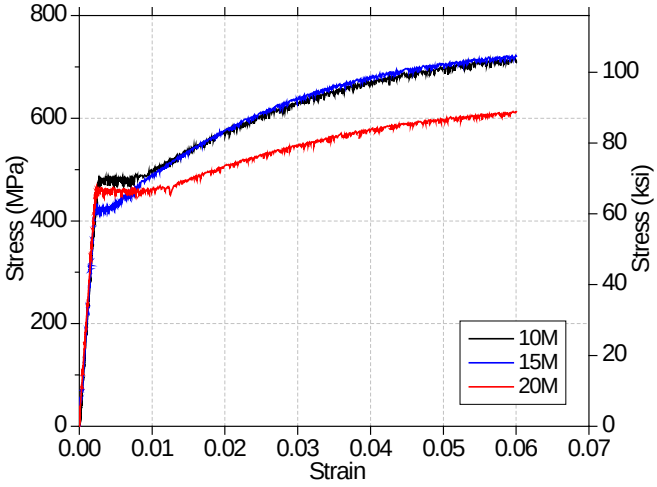

(c) W1 and W2

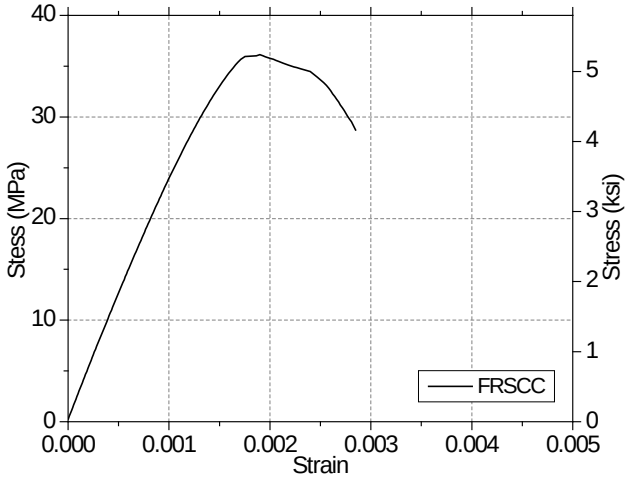

(d) FRSCC concrete used in Repair

Fig. 2.9- Fig. Average stress-strain relationships for concrete and steel material

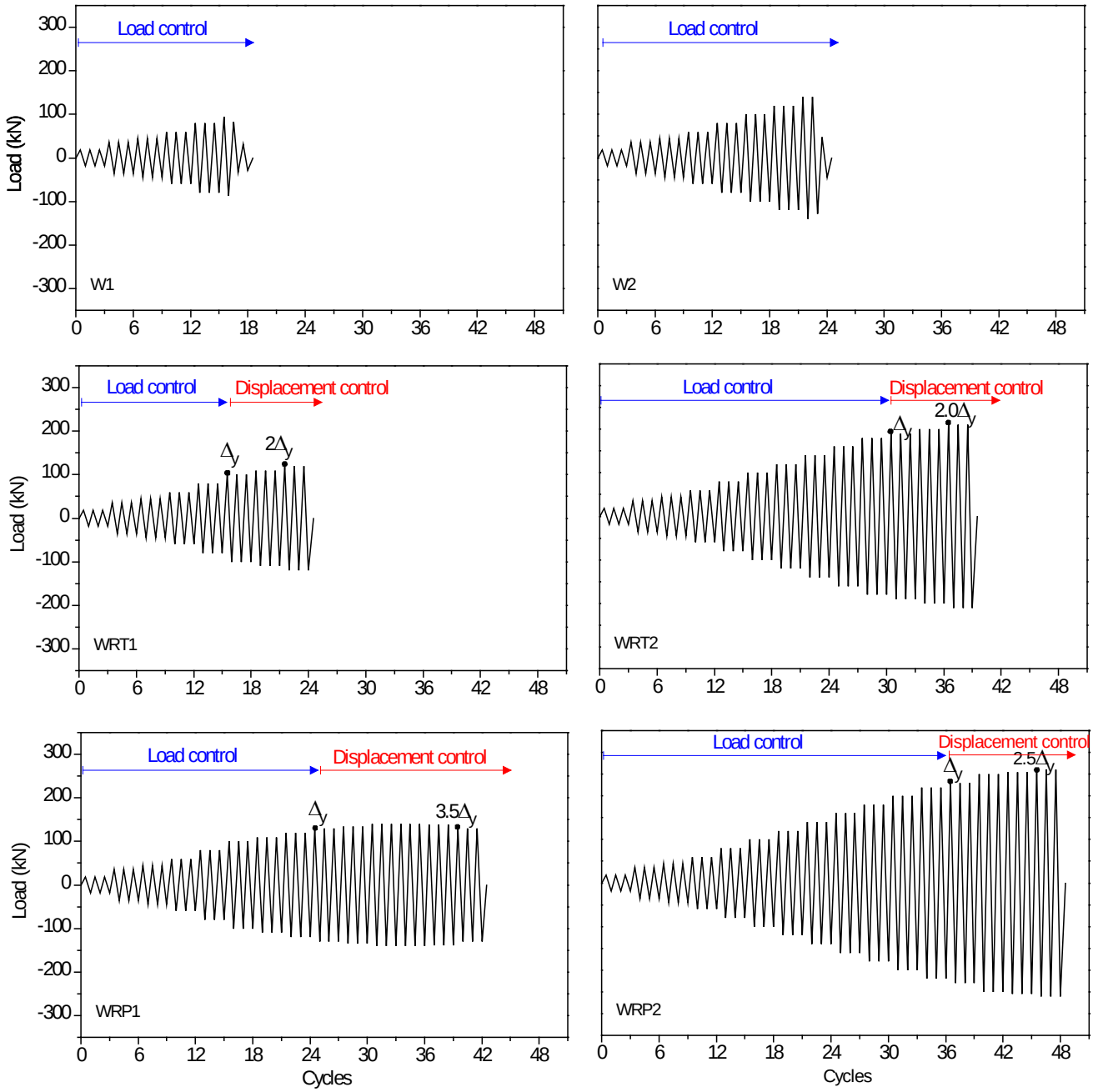

Fig. 2.10- Reversed cyclic loading histories

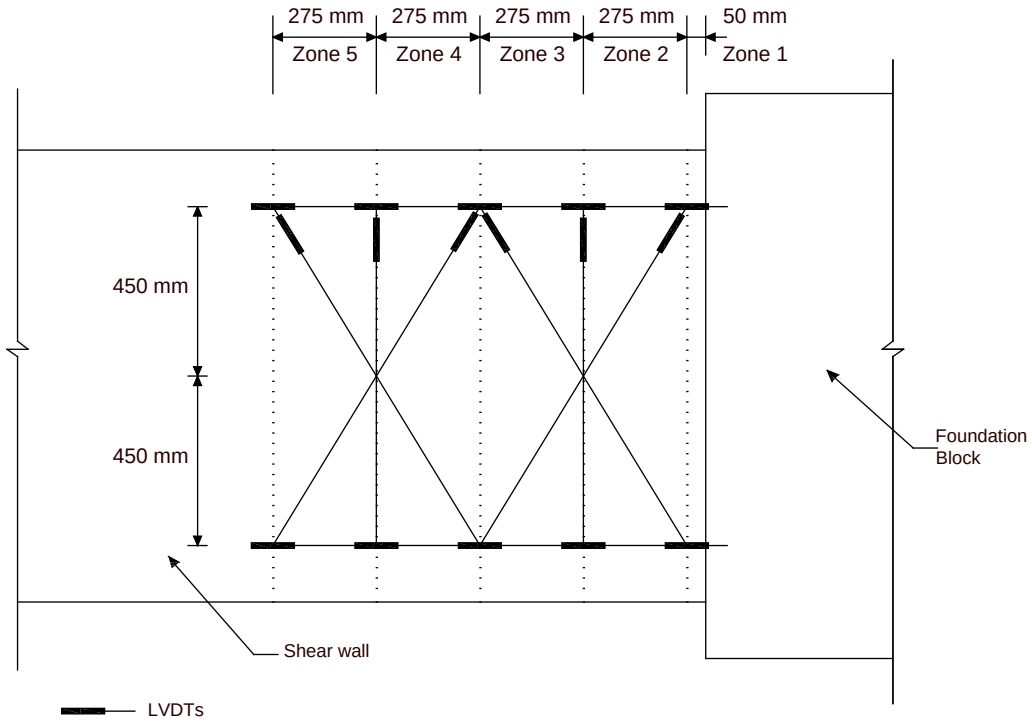

(a) LVDTs at the back of the walls

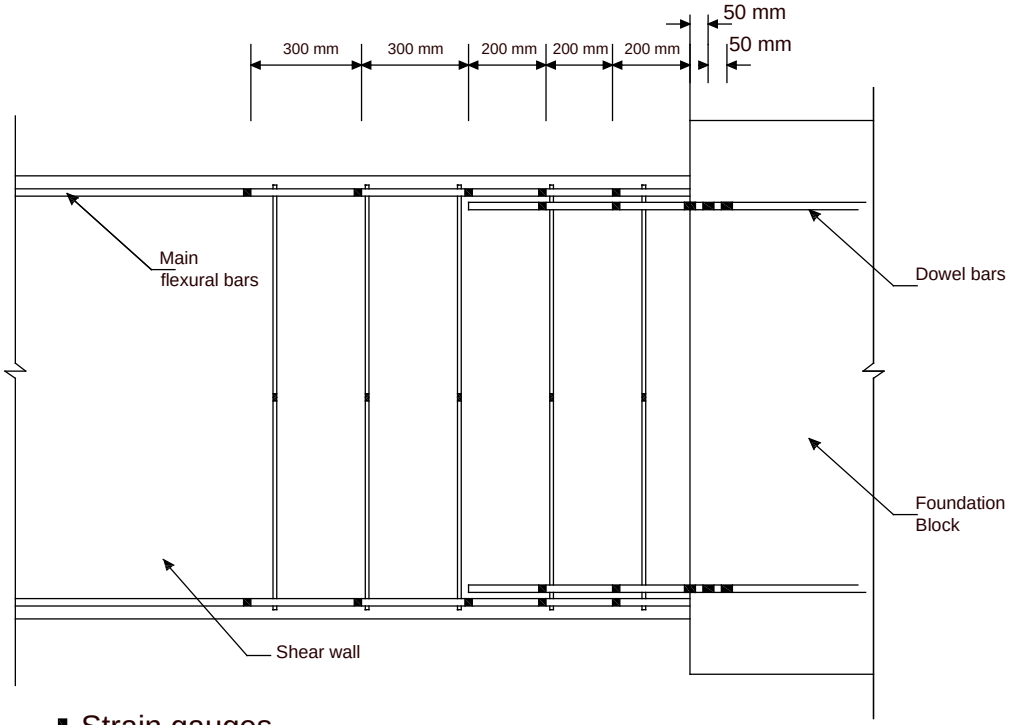

(b) Strain gauges over the main reinforcement and dowel bars

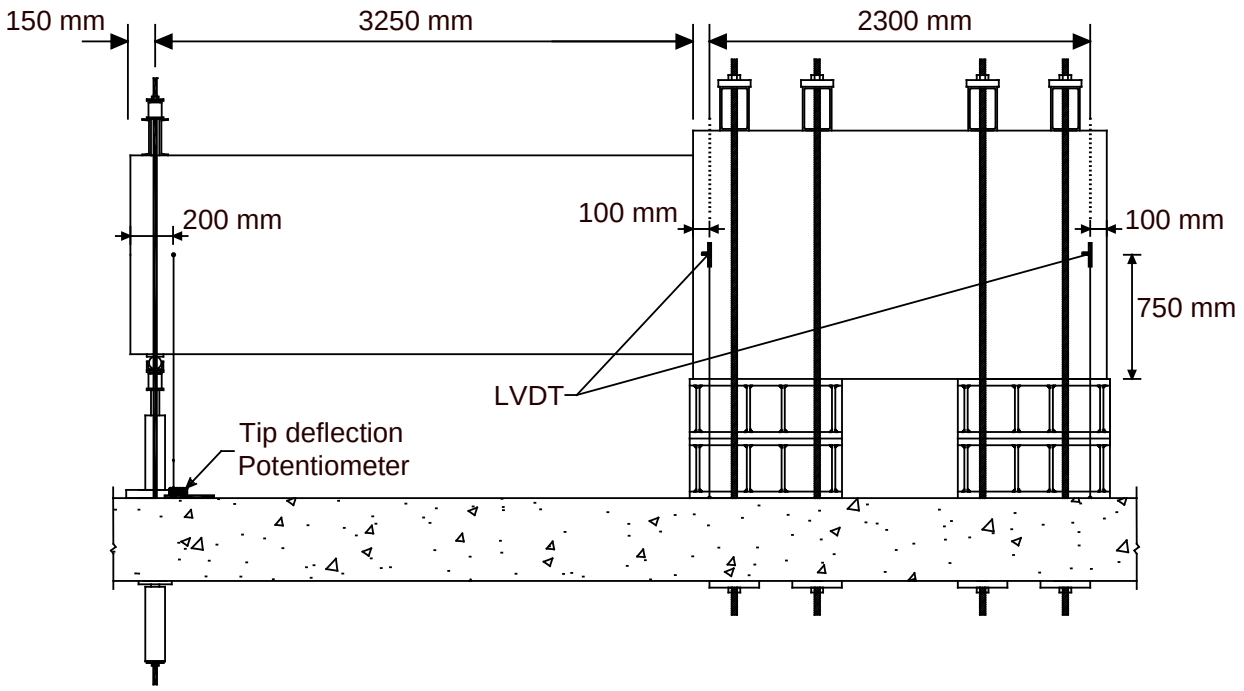

(c) Foundation block and tip deflection instrumentation

Fig. 2.11- The configuration of the LVDTs and strain gauges

Chapter 3
Experimental Results

3.1. Introduction

This chapter describes the results of the experimental investigation to evaluate the seismic behaviour of deficient shear walls under reversed cyclic loading. Walls W1 and W2 were tested under reversed cyclic loading in their as-built condition. A retrofit technique was chosen in order to achieve a performance objective, that is, to reach a displacement ductility of 2.0, with minimum intervention using CFRP wrap. Retrofitted walls WRT1 and WRT2 were tested in reversed cyclic loading to study the effectiveness of the retrofit technique.

After being tested to failure, walls W1 and W2 were repaired using reinforced concrete sleeving over the failed lap splice length and CFRP wrap. The repaired walls WRP1 and WRP2 were then tested under the reversed cyclic loading to investigate the effectiveness of the repair technique.

3.2. Behavioural Parameters

3.2.1. Applied Shear versus Tip Deflection

The applied shear versus tip deflection response was used to characterize the general behavioural aspects of each specimen. The tip deflection measurement from the potentiometer was adjusted for the rotation of the foundation block determined by the potentiometers located on the foundation block (see Fig. 2.12). The shear versus tip deflection responses were adjusted to include the effects of the self weight of the cantilevered wall as well as the loading devices.

The walls were cycled to selected load levels up to general yielding. After general yielding the walls were cycled to multiples of the yield deflection ($1.5\Delta_y$, $2.0\Delta_y$, etc.). The general yield deflection (Δ_y) was determined using the secant stiffness of the response as proposed by Park (1988). The maximum deflection at

which the wall could endure without the capacity dropping below 80% of the maximum load was considered as the ultimate deflection (Δ_u). The yield shear force was taken as the shear at the general yielding tip deflection, Δ_y. The displacement ductility was determined as the ratio Δ_u/Δ_y and was different in the positive and negative loading directions.

The maximum applied shear and the corresponding flexural moment induced at the critical section was determined for each wall. The critical section for walls W1, W2, WRT1 and WRT2 is located at the base of the walls, while for the repaired walls, WRP1 and WRP2 the critical section is shifted to the region beyond the added reinforced concrete jacket.

The flexural moment corresponding to the maximum applied shear for each wall was compared to the predicted flexural capacity, as given in Section 2.4.

3.2.2. Curvatures and Deformations

For each wall, the deformations were measured using a combination of LVDTs to form large rosettes with displacements measured on one face of each wall in the longitudinal, vertical and diagonal directions. The readings from these LVDTs enabled the calculation of the longitudinal strains, the transverse strains, the shear strains, and the principal strains.

The curvature was calculated as: $\varphi = (\delta_{top} - \delta_{bot})/DL$, where δ_{top} and δ_{bot} are the longitudinal deformations measure by LVDTs, L is the vertical distance between the top and the bottom LVDTs (900 mm) and D is the gauge length (50 mm for Zone 1 and 275 mm for Zone 4).

3.2.3. Strain Measurements

In order to study the strain histories of the main flexural reinforcement, dowel bars, and transverse reinforcement, the hysteretic shear versus strain responses were studied. These values enabled the determination of yielding of the reinforcement and the extent of yielding in different zones of the wall. Strain gauges on the dowel bars in the foundation block enabled the determination of the strain penetration in these bars. Strains for certain gauges that malfunctioned during testing were not

included in the plots. Strain measurements from the strain gauges were supplemented with average concrete strains obtained from the LVDTs.

3.2.4. Stiffness Degradation

The effective stiffness, k_{eff}, was calculated as the slope of the line connecting the positive and the negative peaks at each load/deflection stage (see Fig. 3-1). The ratio of the effective stiffness of each wall, k_{eff-u}, at the ultimate deflection to the effective stiffness at yield deflection, k_{eff-i}, was calculated in order to investigate the stiffness degradation.

3.2.5. Cumulative Dissipated Energy

The cumulative dissipated energy (CDE) is considered as the total area inside the hysteresis loops, calculated as:

$$CDE = \int_{loops} V.dy \approx \frac{1}{2}\sum_{i=1}^{n}(V_i + V_{i-1}).(y_i - y_{i-1})$$

, where V_i and y_i, are the applied shear and corresponding tip deflection, respectively. The numeric counter i covers the data set for the two variables (see Fig. 3-2).

3.3. Performance of Walls W1 and W2

Walls W1 and W2 were tested in their as-built condition. They are representative of very poorly detailed thin walls designed and constructed prior to the development of modern seismic design codes.

3.3.1. Shear versus Tip Deflection

The applied shear versus tip deflection responses of walls W1 and W2 are shown in Fig. 3-3. The key stages in the shear versus tip deflection responses for both walls are summarized in Tables 3-1, and 3-2.

The walls had a non-ductile response due to brittle splitting failures of the lap splices of the 20M bars, prior to the yielding of this main flexural reinforcement. These failures led to a significant drop in the shear. Fig. 3-4 shows the condition of

walls W1 and W2 at the end of the test. It can be seen that for both walls, the failure occurred along the entire length of the lap splices.

The predicted nominal flexural resistances of W1 and W2, assuming that the steel was capable of yielding), are 386 kNm and 673 kNm, respectively (see Section 3.4).

Wall W1 reached a maximum shear of 95.2 kN, corresponding to an applied moment of 309 kNm (80% of the predicted flexural capacity). The average deflection associated with the maximum shear was 11.12 mm (i.e., only 0.32 % lateral drift).

For wall W2, the maximum applied shear reached was 140.5 kN, corresponding to an applied moment of 455 kNm (68% of the predicted nominal flexural capacity). For W2, the maximum deflection corresponding to the maximum applied shear was 12.51 mm (0.38% lateral drift).

It is noted that these thin walls with extremely poor reinforcement details performed poorly, as expected, exhibiting a brittle failure mode and no ductility.

3.3.2. Moment – Curvature Responses

For walls W1 and W2, the experimental moment versus curvature responses are given in Fig. 3-5 for the critical section at the base of the wall. The curvatures corroborate the fact that yielding of the main flexural reinforcement did not occur. The curvature values in other zones are plotted in Fig. 3-6 and Fig. 3-7. It is noted that the values of curvature were very small for all regions.

3.3.3. Stiffness Degradation

The response of the walls did not indicate any significant yielding, and therefore, it was assumed that the walls responded in an elastic manner. Consequently, no stiffness degradation parameter was calculated for walls W1 and W2.

3.3.4. Cumulative Dissipated Energy

Walls W1 and W2 did not experience any yielding since the lap splices failed in a brittle manner. The walls responded mainly in the elastic range and the areas

inside the hysteretic loops were small, and therefore, the cumulative dissipated energy was very low for both walls (i.e., 1.4 kNm for W1 and 2.5 kNm for W2).

3.3.5. Strains

Figs. 3-8 and 3-9 show the distribution of the strains in the flexural reinforcement (longitudinal bars) at the peak of each load/deflection level. The strain gauges at the base of the wall on the dowel reinforcement are at the critical section and therefore, experiences the maximum strains.

For wall W1, the maximum measured strain at the base of the wall was 2369 microstrain at the peak cycle of 17a (positive loading) and 2000 microstrain at the peak cycle of 16b (negative loading), when the lap splice bond failed in a brittle manner at these load levels and the wall was not able to endure further loading. The hysteretic applied shear versus local strain response of W1 is plotted for this critical section (see Fig. 3-10(a)). It is noted that the maximum measured strain in one bar only just reached the yield strain for this reinforcement having strain of 2300 microstrain. Due to the brittle failure mode and low measured strains it was judged that general yielding did not occur.

The maximum measured strain at the critical section for wall W2 was 1557 microstrain at the peak cycle of 23a (positive loading) and 1854 microstrain at the peak cycle of 23b (negative loading). It should be noted that the strain values are far below yielding. The maximum strains are lower compared to wall W1 due to the larger amount of flexural reinforcing steel. Fig. 3-10(b) shows the shear versus strain response for this critical section.

The longitudinal reinforcement remained elastic except for localised yielding of one dowel bar at the base of wall W1. The yield at this point did not spread into the foundation, nor to other regions of the wall.

For both walls, the strains were measured on the transverse (shear) reinforcement, and were plotted against the distance from the base of the walls. Generally, the strain measurements did not indicate any yielding except for the transverse bar located at 1125 mm from the base of wall W2 where the strain just reached the yield strain (Fig. 3-11). These values were supplemented with the

average strains measured by the vertical LVDTs located at the distances of 325 mm and 875 mm from the base of the walls. The shear vs. average vertical strains for W1 and W2 are shown in Fig. 3-12.

3.4. Performance of Walls WRT1 and WRT2

The objective of the retrofit was to improve the overall response of the shear wall such that displacement ductility of 2.0 could be achieved. The retrofit technique was chosen to improve the confinement of the boundary regions over the critical potential plastic hinging zone, and to improve the shear capacity of the walls with minimum intervention.

3.4.1. Shear versus Tip Deflection

Fig. 3-13 shows the shear versus tip deflection responses of walls WRT1 and WRT2. The responses of the walls indicate that the premature brittle failures of the lap splices were delayed and the walls exhibited a more ductile response. The target load/tip deflection levels for both walls are summarized in Tables 3-3, and 3-4.

The average yield deflection for wall WRT1 was 11.95 mm, and the ultimate yield deflection was 23.6 mm (displacement ductility of 2.0 and lateral drift of 0.73%). WRT1 experienced a maximum shear of 115 kN, corresponding to an applied moment of 373.8 kNm (21% increase in the flexural resistance compared to un-retrofitted wall W1). The wall retrofit enabled the wall to achieve to 97% of the predicted flexural capacity of W1.

For WRT2, the average yield deflection was 17.0 mm and the ultimate deflection was judged to be 34.8 mm (1.1% lateral drift), resulting in a displacement ductility of 2.0. Wall W2 was able to endure a maximum shear force of 216 kNm (applied moment of 702 kNm) which is a 54% increase in the flexural resistance compared to the un-retrofitted wall W2. WRT2 was able to get to 104% of the predicted flexural capacity.

The retrofit technique was effective in improving the reversed cyclic loading performance of the walls WRT1 and WRT2. The retrofit technique delayed the

brittle failure of the lap splices, and resulted in the yielding of the concentrated flexural reinforcement.

3.4.2. Moment – Curvature Responses

The average moment versus curvature responses of the walls WRT1 and WRT2 at the critical section of maximum flexural moment are plotted in Fig. 3-14. The responses show yielding has occurred at the base of the wall and the curvature values are higher compared to the non-retrofitted companions. The average moment vs. curvature for other regions of the retrofitted walls are illustrated in Figs. 3-15 and 3-16. The values of curvature at these regions are very low.

3.4.3. Stiffness Degradation

The average stiffness of the walls WRT1 and WRT2 at the yield deflection were 8.6 kN/mm and 10.8 kN/mm, respectively. The stiffness of walls WRT1 and WRT2 at displacement ductility of 2.0 were 4.1kN/mm and 5.7kN/mm, respectively. The stiffness degradation ratio for WRT1 is therefore 0.48 for wall WRT1 and 0.52 for wall WRT2.

3.4.4. Cumulative Dissipated Energy

The cumulative dissipated energy for WRT1 and WRT2 are 9.5 kNm and 40.9 kNm, respectively. The retrofitted walls dissipated considerably larger amounts of energy compared to their non-retrofitted companions.

3.4.5. Strains

Strains measured on the main longitudinal bars and the dowel bars indicate that yielding occurred at the critical section as well as spreading of yield along the bars and yield penetration into the foundation. The carbon fibre strips were effective in controlling diagonal shear cracking, above the base.

Wall WRT1 experienced a maximum strain of 2400 microstrain at the base of the wall. The strain values at the same location in WRT2 reached 2800 microstrain (see Fig. 3-17, 3-18, and 3-19).

For WRT1, the measured strain values over the lap region indicated that some of the bars yielded. For WRT2, the strains in the lap splice region exceeded the

yield strain in all of the concentrated reinforcement. WRT2 performed somewhat better than WRT1 because the improved application of the CFRP wrap. There were some problems in applying the CFRP wrap for WRT1, with this being the first wall that was retrofitted with the CFRP wrap.

The strains on the transverse reinforcement did not reach the yield strain. These measurements were supplemented with the average strain determined from the LVDTs at 2 locations (see Figs. 3-20 and 3-21).

3.5. Performance of Walls WRP1 and WRP2

The performance objectives in the design of the repaired walls were to improve the overall response of previously damaged shear walls in terms of stiffness, flexural resistance, shear resistance and confinement of the lap splice region, such that the repaired walls could achieve a minimum displacement ductility greater than 2.0.

3.6. Shear versus tip deflection

The shear versus tip deflection responses of WRP1 and WRP2 are presented in Fig. 3-22. Wall WRP1 experienced a maximum shear load of 157 kN (32% increase in the flexural capacity compared to W1). The average yield deflection was 14.46 mm, and the ultimate deflection the wall achieved was 47.97 mm (a lateral drift of 1.48 %), resulting in displacement ductility of 3.3. The target load and tip deflection levels for both walls are summarized in Tables 3-5, and 3-6.

The maximum applied shear for wall WRP2 was 270 kNm (32% increase in the flexural capacity compared to W1). The average yield deflection was 23.60 mm, and the ultimate deflection the wall achieved was 56.60 mm (a lateral drift of 1.74 %), resulting in displacement ductility of 2.4.

The monotonic predicted flexural capacity for WRP1 and WRP2 are 147.2 kN and 256.7 kN, respectively. The test values for the flexural capacities are 7% and 5% higher than the predicted values, for WRP1 and WRP2.

The resistance of the walls gradually degraded due to crushing of the concrete just outside of the reinforced jacket. This was associated with debonding of the

CFRP wrap at this region which was followed by rupture of the CFRP (see Fig. 3-23).

It is noted that for walls WRP1 and WRP2, the critical section (lap splices in the maximum moment location) was shifted from the base of the wall to a location at the end of the SFRSCC jacket (625 mm from the base of the wall). The repair prevented the failure of the lap splices, and both specimens had a large reserve of strength after general yielding.

3.6.1. Moment – Curvature Responses

Fig. 3-24 shows the average moment versus average curvature for the new critical section (beyond the jacket: zone 4). It should be noted that the curvature plot for the new plastic hinge region shows bigger hysteresis loops as a result of larger deformations.

The average moment versus curvature for other regions (zone 1, zone 2, zone 3, and zone 5) are plotted in Figs. 3-25 and 4-26. For both WRP1 and WRP2, the shear vs. curvature in zone 5 indicates that the yielding has spread to a distance of at least 275 mm beyond the jacket, forming a plastic hinge.

The curvature values at the base of the wall were very small, indicating no significant inelastic deformations at this location.

3.6.2. Stiffness degradation

The stiffness degradation ratio for WRP1 and WRP2 is calculated in a similar approach to the retrofitted walls. The stiffness degradation ratios for WRP1 and WRP2 are 0.31 and 0.45, respectively.

It should be noted that the smaller values indicate that more stiffness degradation in both walls since they were previously tested. On the other hand, these walls exhibited a more ductile response compared to the retrofitted walls, and therefore, more load/deflection cycles led to significant loss of stiffness at the end of testing.

3.6.3. Cumulative Dissipated Energy

The hysteresis loops indicate that a significant amount of energy was dissipated through the formation of plastic hinging in walls WRP1 and WRP2. The cumulative dissipated energy for walls WRP1 and WRP2 were 95kNm and 104 kNm, respectively. Fig. 3-27 compares the amount of cumulative dissipated energy for the walls compared to their retrofitted and non-retrofitted (as-built) companions.

3.6.4. Strains

Some of the strain gauges were broken since the walls were previously tested in the as-built condition. However, some new strain gauges were provided for the existing steel and the new headed bars during the repair phase.

The strains were measured for the additional 15M headed bars at the base of the walls. It is noted that the reinforced concrete sleeve was designed to be capacity-protected. The strain values measured at this location were 0.0021 for WRP1 and 0.002 for WRP2 (which indicates no significant yielding has occurred at the base of the walls).

The strain value at the critical location beyond the added jacket (625 mm from the base) reached the yield strain of 0.0023 (see Fig. 3-28). For both WRP1 and WRP2, strain measurements indicate the spreading of yielding over a region of at least 275mm beyond jacket.

Table 3-1- Key stages in the response of wall W1

Cycle	General Description	Applied shear (kN)	Tip deflection (mm)
1A	$0.48M_{cr}$	18	0
1B		-18	-0.3
4A	$0.97M_{cr}$	36	-0.62
4B		-36	-1.78
7A	$0.43V_{y,*}$	45	2.79
7B		-45	-3.82
10A	$0.57V_{y,*}$	60	4.72
10B		-60	-6.23
13A	$0.76V_{y,*}$	80	7.51
13B		-80	-9.85
16A	$0.90V_{y,*}$	95	10.5
16B		-85	-11.53

$V_{y,}^{*}$: is the estimated yield shear for W1

Table 3-2- Key stages in the response of wall W2

Cycle	General Description	Applied shear kN	Tip deflection mm
1A	$0.48M_{cr}$	17.8	0.59
1B		-20.2	-0.3
4A	$0.98M_{cr}$	36	1.38
4B		-36	-0.86
7A	$0.24V_{y,*}$	45	2.27
7B		-45	-1.8
10A	$0.32V_{y,*}$	-60	-2.88
10B		60	3.86
13A	$0.43V_{y,*}$	80	5.54
13B		-80	-4.75
16A	$0.54V_{y,*}$	100	7.95
16B		-100	-6.76
19A	$0.65V_{y,*}$	120	10.15
19B		-120	-9.29
22A	$0.76V_{y,*}$	140	12.68
22B		-140	-12.3

$V_{y,}^{*}$: is the estimated yield shear for W2

Table 3-3- Key stages in the response of wall WRT1

Cycle	General Description	Applied shear (kN)	Tip deflection (mm)
1A	$0.48M_{cr}$	18	0.1
1B		-18	-0.35
4A	$0.95M_{cr}$	36	0.6
4B		-36	-0.8
7A	$0.43V_y$	45	3.9
7B		-45	-3.19
10A	$0.57V_y$	60	5.2
10B		-60	-4.8
13A	$0.76V_y$	80	7.9
13B		-80	-7.6
16A	$0.95V_y$	100	11.18
16B		-100	-10.56
19A	$1.5\Delta_y$	108	16.6
19B		-114	-15.9
22A	$2.0\Delta_y$	90	23.9
22B		-97	-23.1

Table 3-4- Key stages in the response of wall WRT2

Cycle	General Description	Applied shear (kN)	Tip deflection (mm)
1A	$0.48M_{cr}$	18	0.47
1B		-18	-0.1
4A	$0.95M_{cr}$	36	1.3
4B		-36	-0.65
7A	$0.24V_y$	45	1.9
7B		-45	-1.1
10A	$0.32V_y$	60	3.3
10B		-60	-2.4
13A	$0.43V_y$	80	5.3
13B		-80	-3.9
16A	$0.54V_y$	100	7.25
16B		-100	-5.7
19A	$0.65V_y$	120	9.23
19B		-120	-7.6
22A	$0.76V_y$	140	11.4
22B		-140	-9.7
25A	$0.86V_y$	160	14.1
25B		-160	-11.8
28A	$0.97V_y$	180	17.3
28B		-180	-14.2
31A	$1.03V_y$	191	21.17
31B		-190	-15.68
34B	$1.5\Delta_y$	202	27.6
34B		-207	-24.4
37A	$2.0\Delta_y$	175	36
37B		-215	-33

Table 3-5- Key stages in the response of wall WRP1

Cycle	General Description	Applied shear (kN)	Tip deflection (mm)
1A	$0.47M_{cr}$	18	0
1B		-18.59	-0.71
4A	$0.94M_{cr}$	36	1.03
4B		-36	-1.87
7A	$0.34V_y$	45	1.71
7B		-45	-2.73
10A	$0.45V_y$	60	3.04
10B		-60	-4.35
13A	$0.6V_y$	-80	-8.46
13B		100	7.12
16A	$0.75V_y$	-100	-10.52
16B		120	9.76
19A	$0.90V_y$	-120	-13.3
19B		132	12.46
22A	V_y, $1.0\Delta_y$	-132	-15.3
22B		138	18.7
25A	$1.5\Delta_y$	-147	-22.1
25B		143	25.5
28A	$2.0\Delta_y$	-154	-28.8
28B		140	32.3
31A	$2.5\Delta_y$	-153	-35.7
31B		136	39.1
34A	$3.0\Delta_y$	-153	-42.5
34B		136	45.9
37A	$3.5\Delta_y$	-152	-49.3
37B		111	52.7
40A	$4.0\Delta_y$	-125	-56.1
40B		60	3.04

Table 3-6- Key stages in the response of wall WRP2

Cycle	General Description	Applied shear (kN)	Tip deflection (mm)
1A	$0.48M_{cr}$	18.2	0.97
1B		-18.8	-0.53
4A	$0.94M_{cr}$	36	2.18
4B		-36	-1.45
7A	$0.19V_y$	45	2.94
7B		-45.1	-2
10A	$0.26V_y$	60.5	4.11
10B		-60.5	-3.03
13A	$0.34V_y$	80.4	5.83
13B		-80.7	-4.54
16A	$0.43V_y$	100	7.44
16B		-100	-5.94
19A	$0.51V_y$	120	9.19
19B		-120	-7.51
22A	$0.6V_y$	140.2	11.3
22B		-140	-9
25A	$0.68V_y$	160	13.6
25B		-160	-10.5
28A	$0.77V_y$	180	16.4
28B		-180	-12.4
31A	$0.85V_y$	200	19.41
31B		-200	-14.54
34A	$0.94V_y$	220	23.4
34B		-220	-17.13
37A	V_y, D_y	227	27.6
37B		-232	-18.4
40A	$1.5\Delta_y$	255	37.7
40B		-253	-29.6
43A	$2.0\Delta_y$	260	48.9
43B		-262	-40.8
46A	$2.5\Delta_y$	264	60.2
46B		-270	-51.2
49A	$3.0\Delta_y$	231	71.4
49B		-206	-63.3

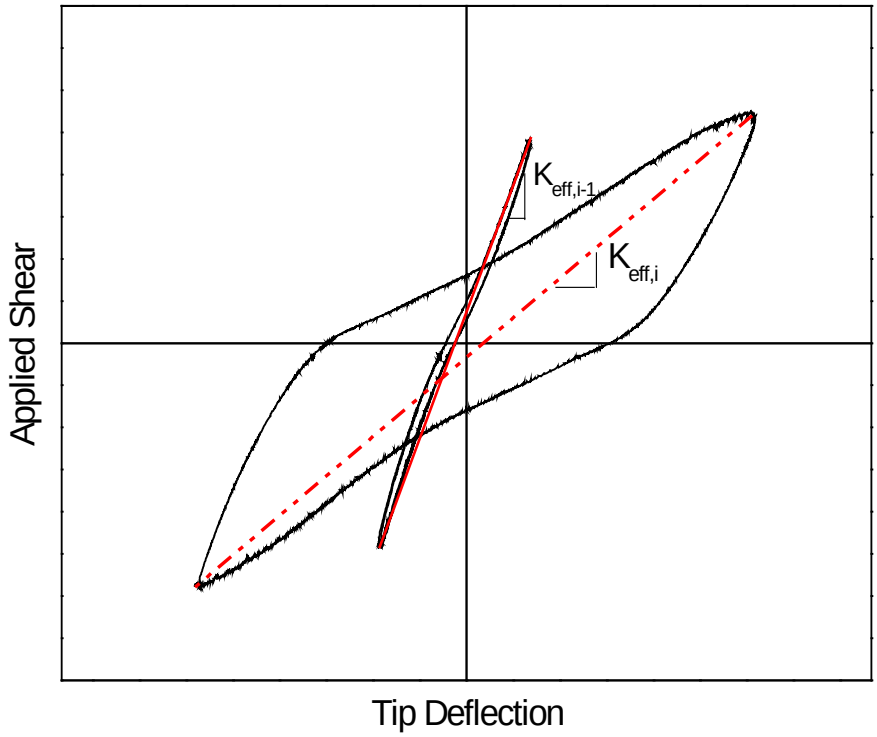

Fig. 3-1- Determining stiffness degradation

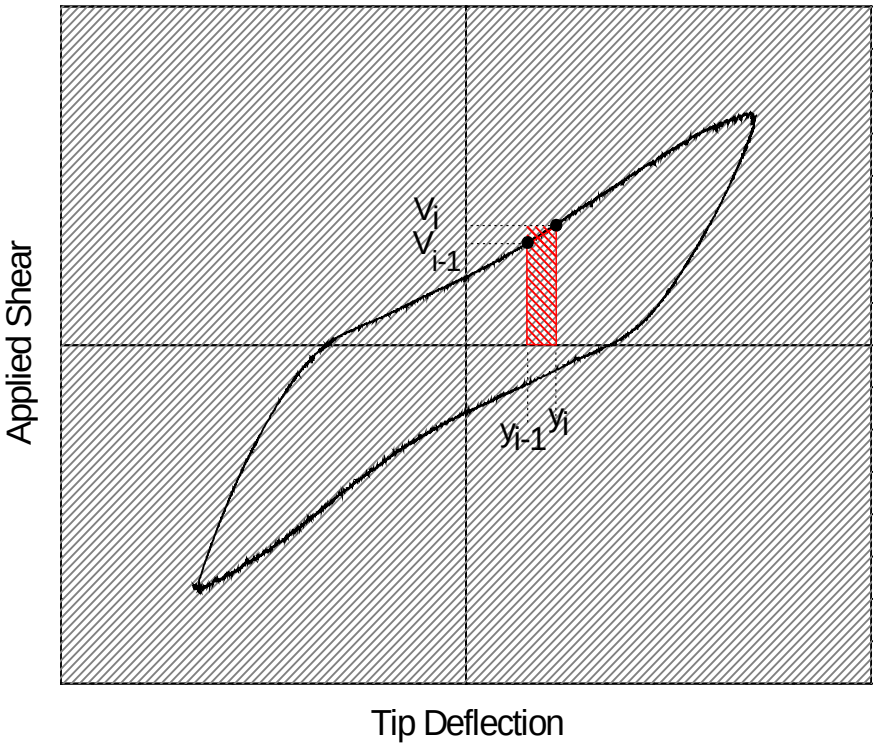

Fig. 3-2- Cumulative dissipated energy (area under the hysteretic loops)

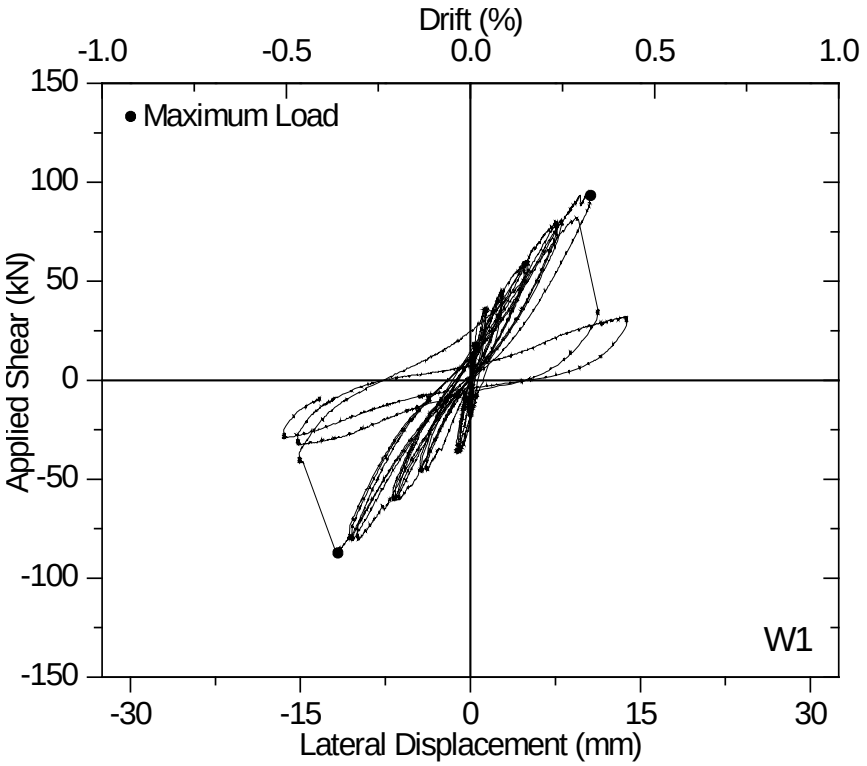

(a) W1

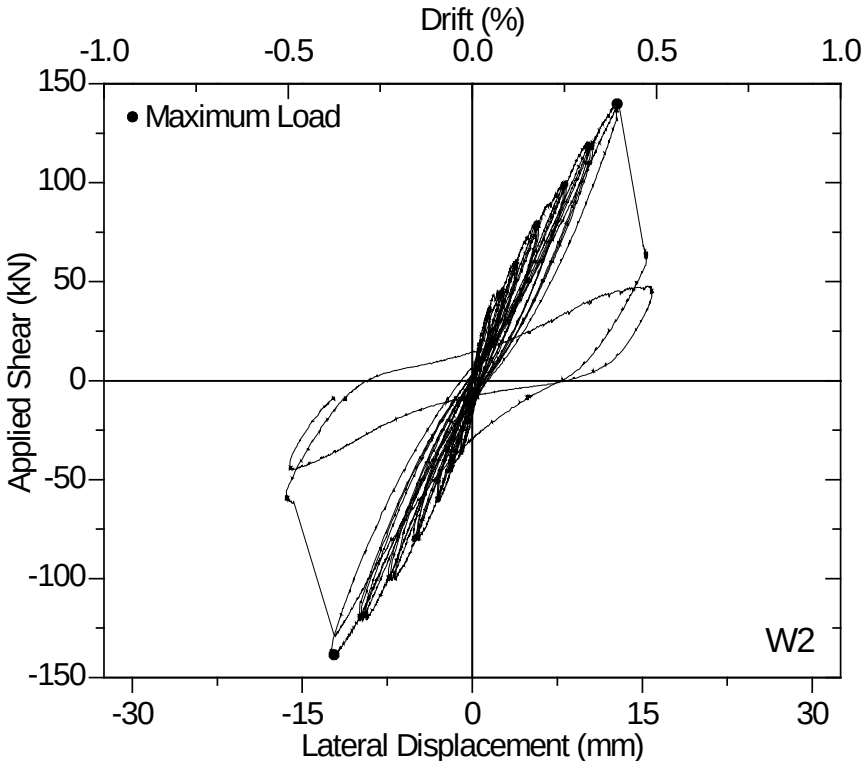

(b) W2

Fig. 3-3- Applied shear versus tip deflection responses

(a) W1

(b) W2

Fig. 3-4- Condition of the original walls at the end of testing

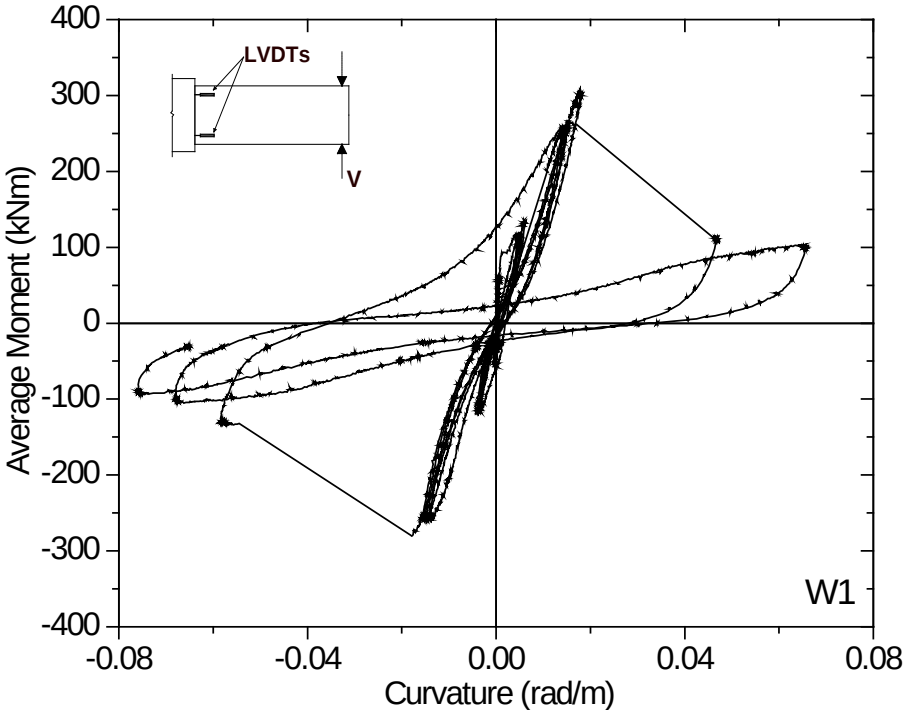

(a) W1

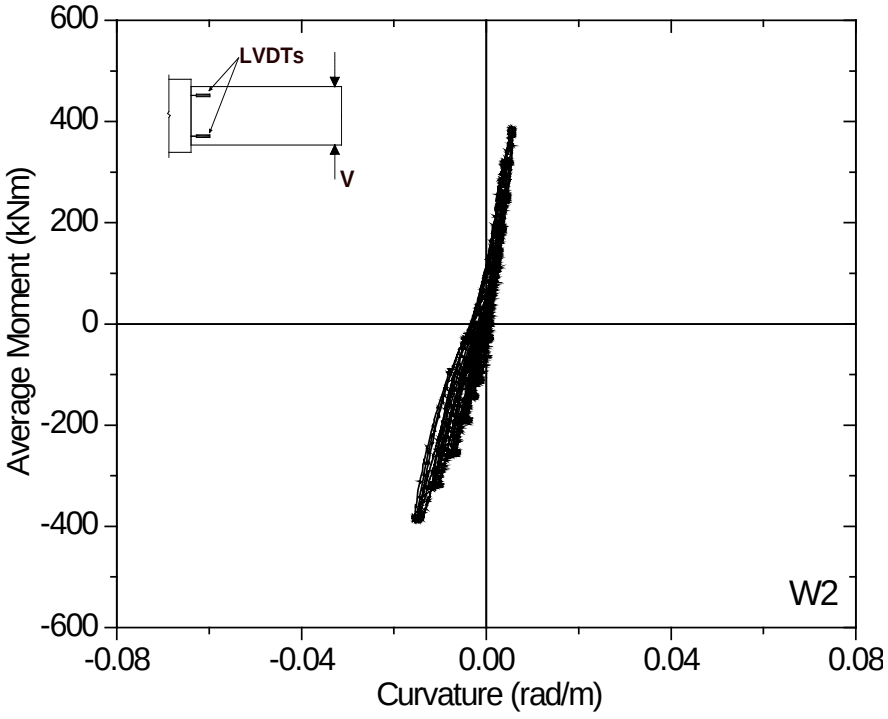

(b) W2

Fig. 3-5- Average moment versus curvature at the base of the walls

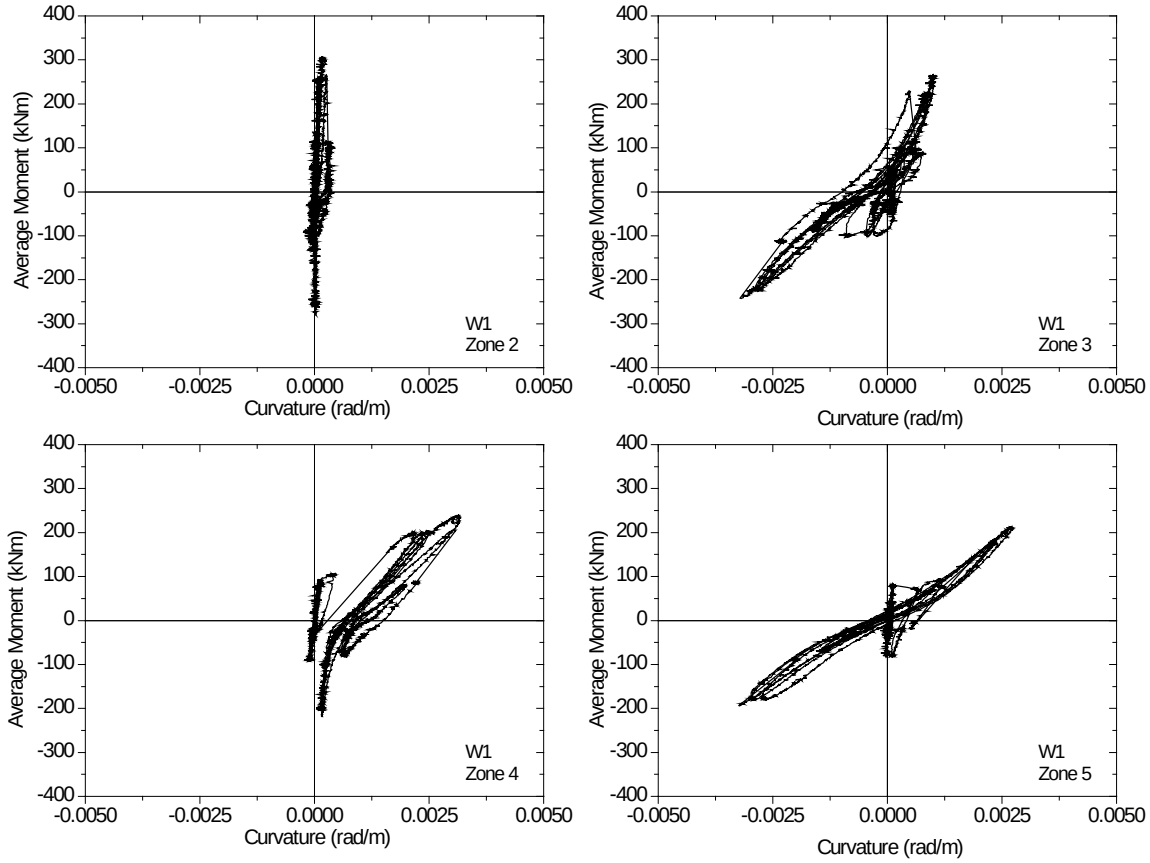

Fig. 3-6- Average moment versus curvature at zones 2, 3, 4, and 5 for wall W1

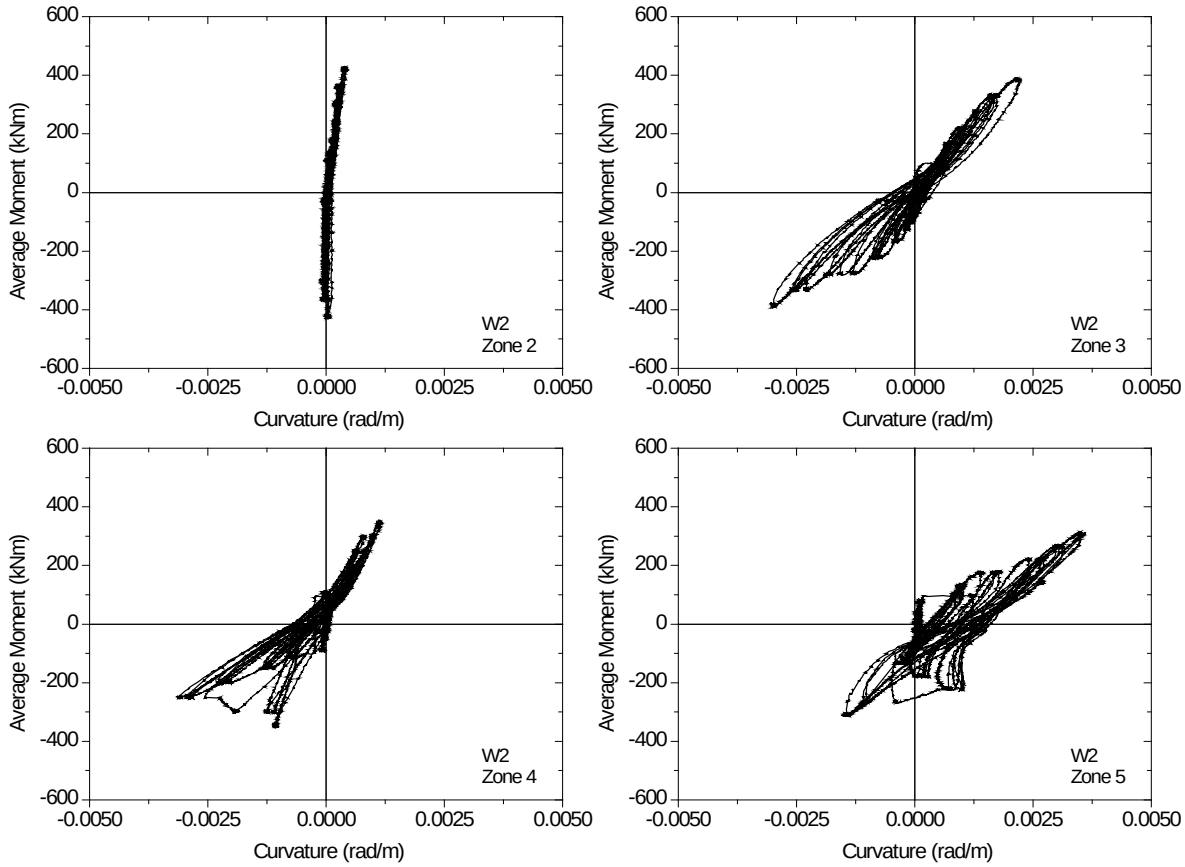

Fig. 3-7- Average moment versus curvature at zones 2, 3, 4, and 5 for wall W2

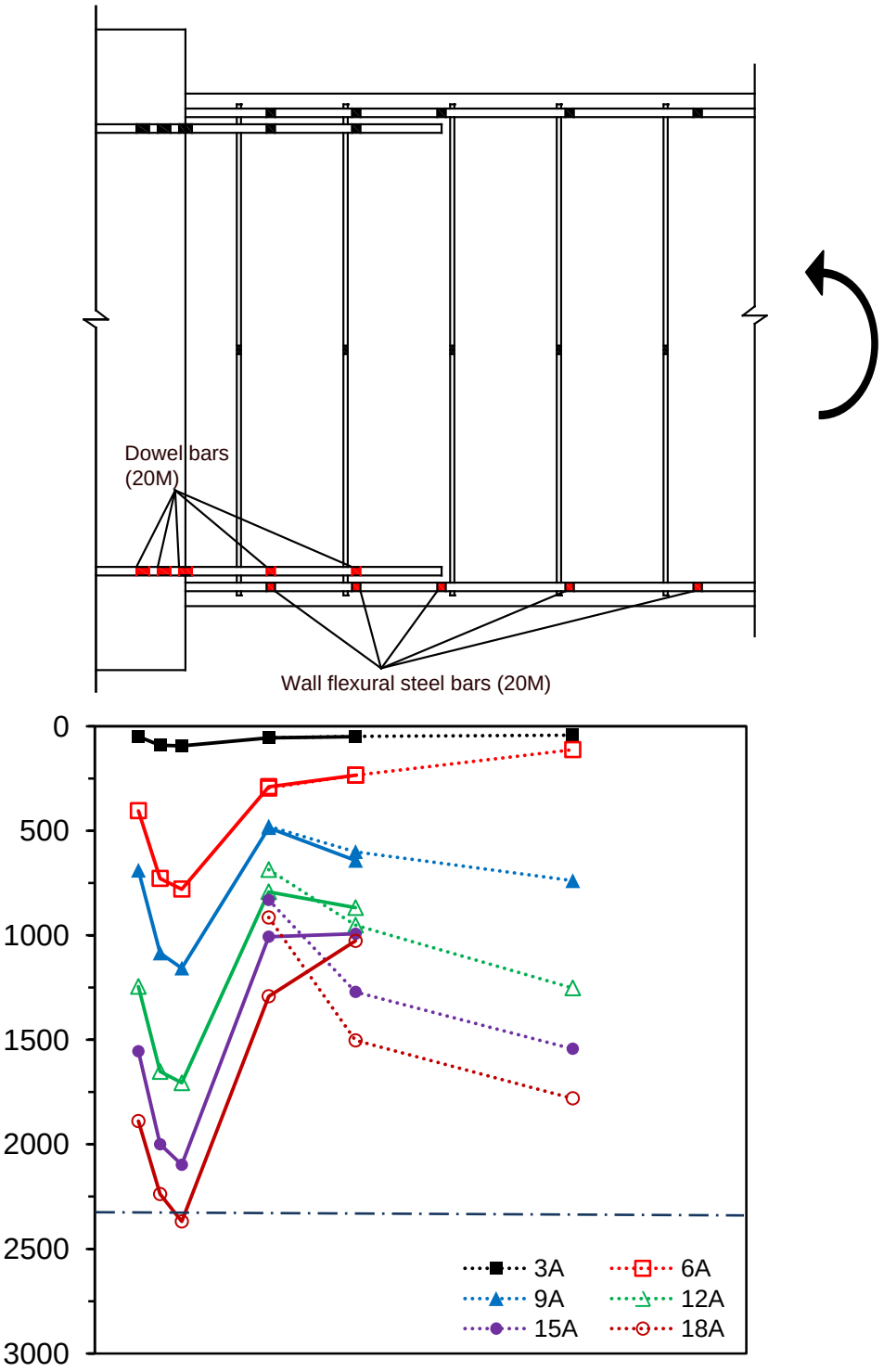

Fig. 3-8- Strains in the dowel bars and the main flexural bars-W1

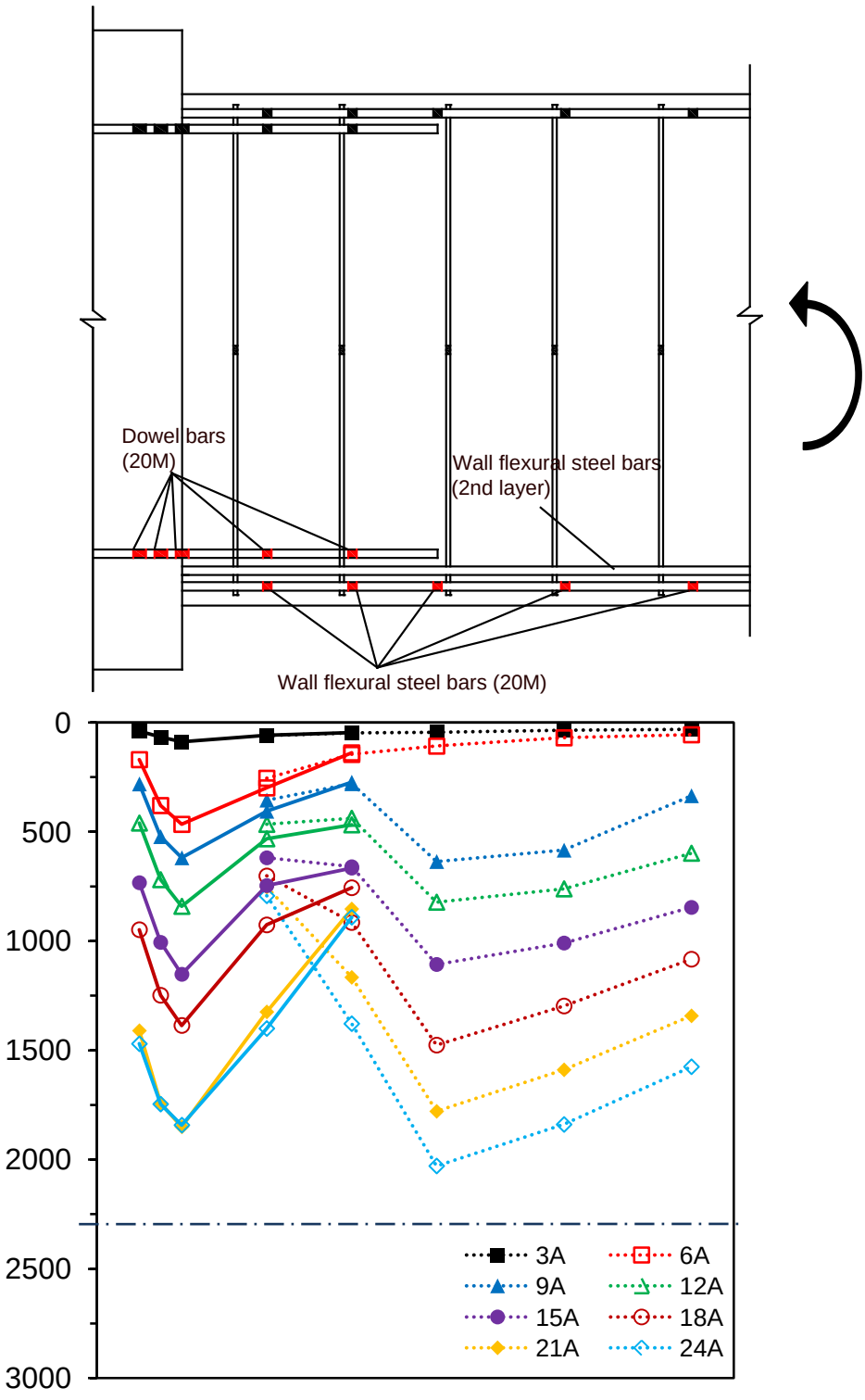

Fig. 3-9- Strain in the dowel bars and the main flexural bars-W2

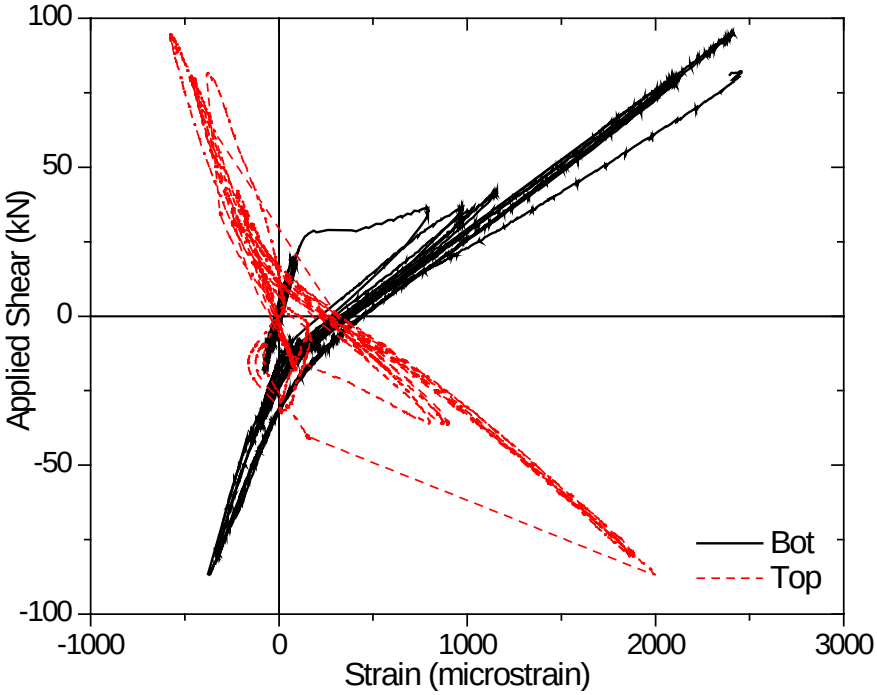

(a) W1

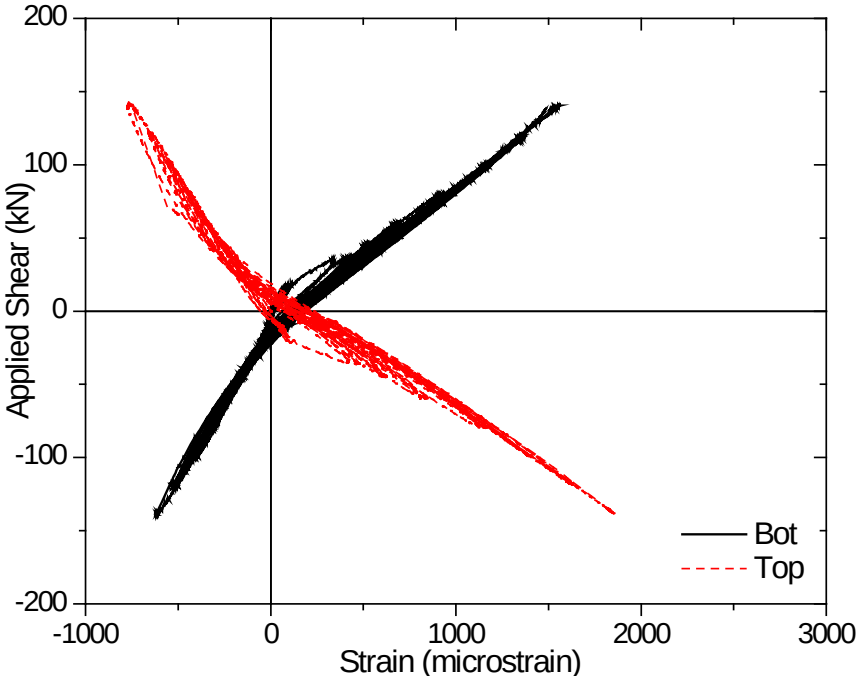

(b) W2

Fig. 3-10- Applied shear vs. strain on the top and bottom dowel bars the base of the walls

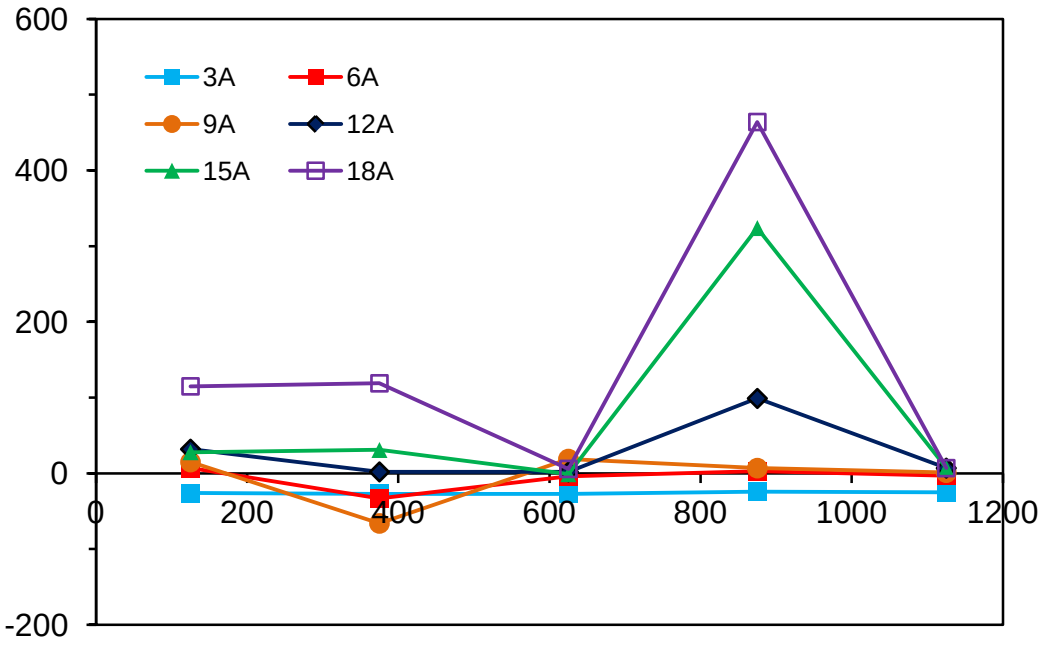

(a) W1

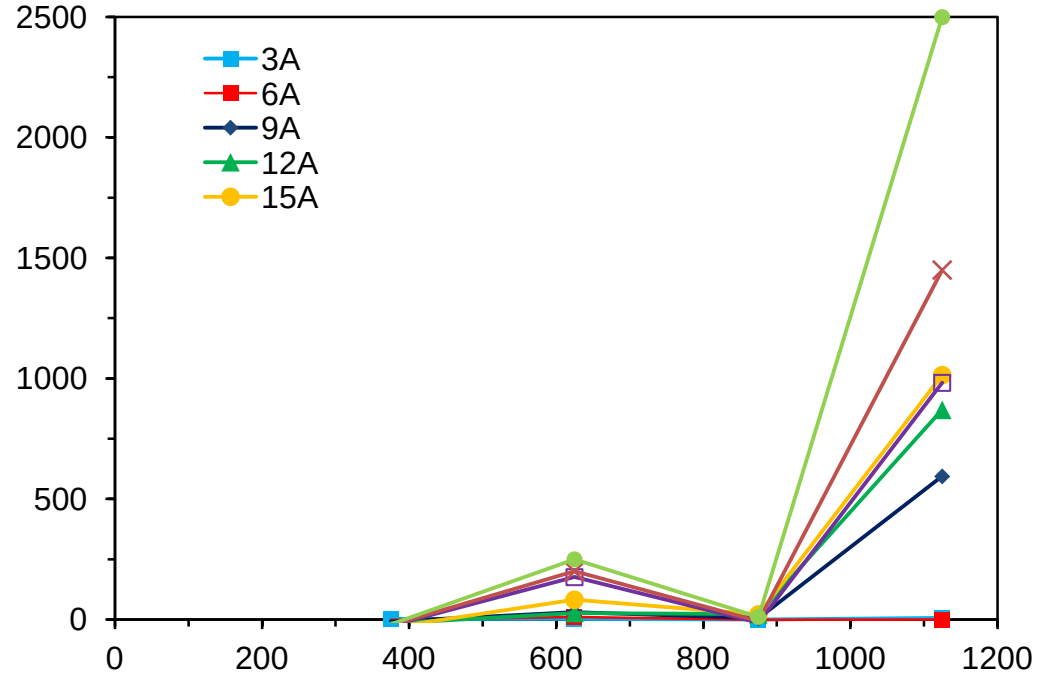

(b) W2

Fig. 3-11- Strain on the transverse reinforcement vs. distance from the base of the walls

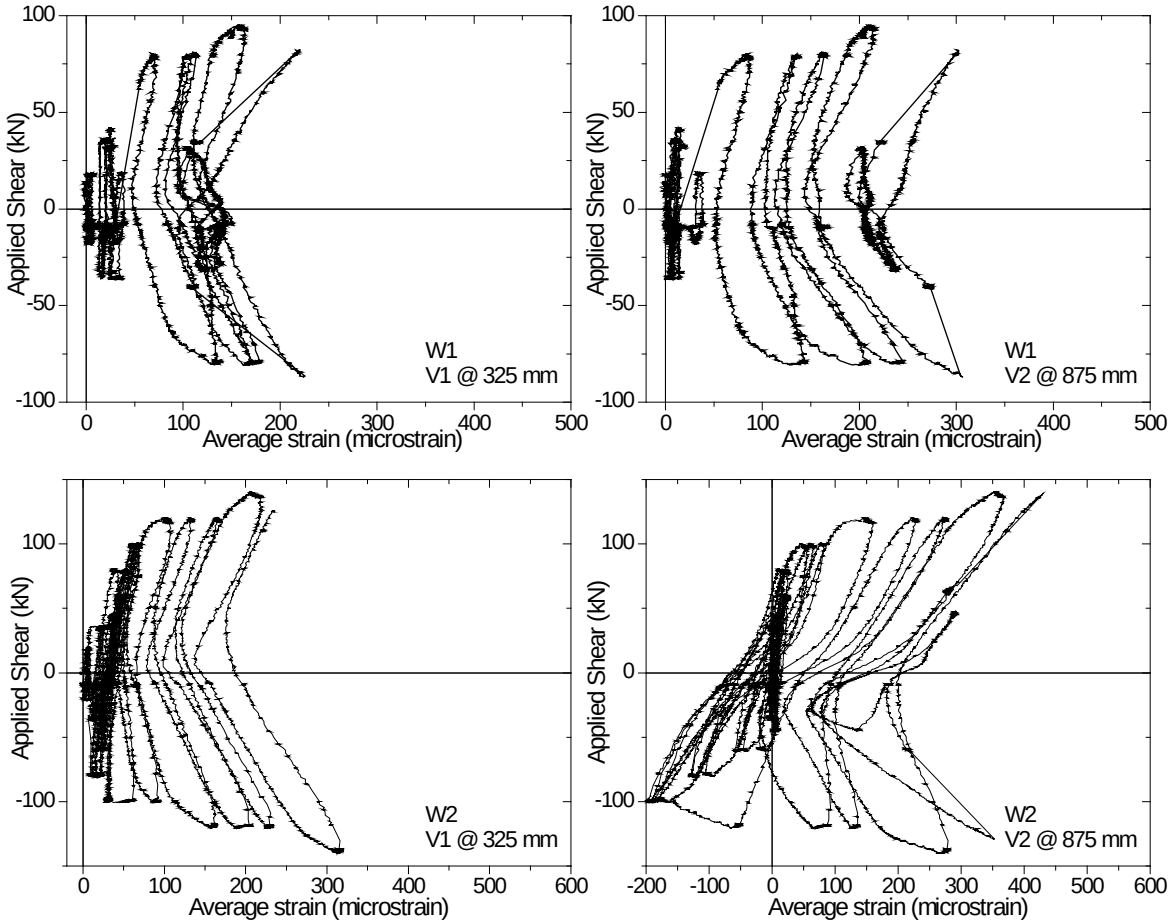

Fig. 3-12- Applied shear vs. average strains from the vertical LVDTs

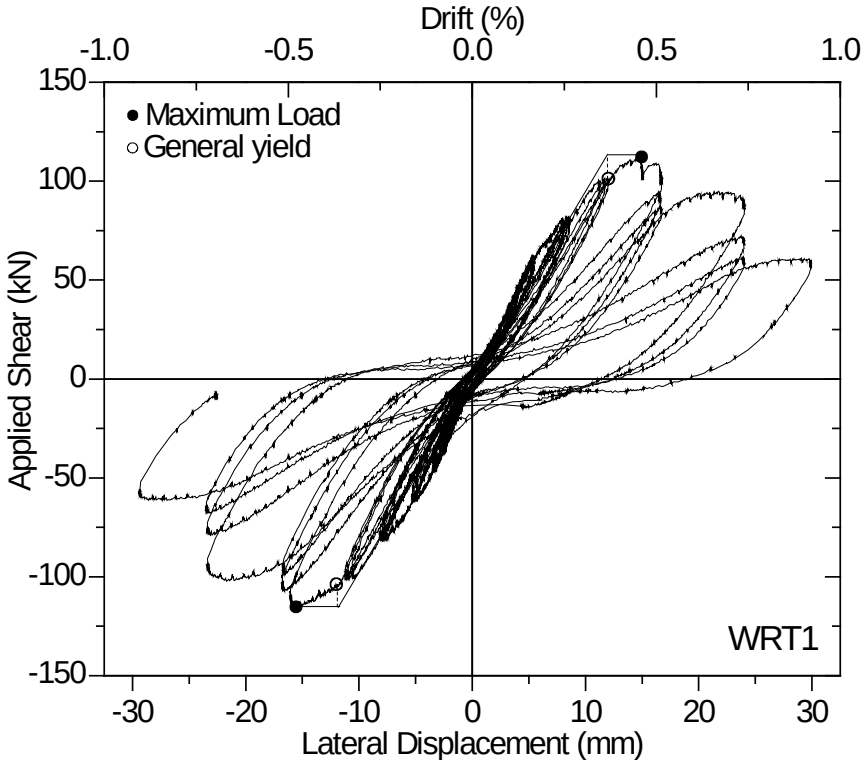

(a) WRT1

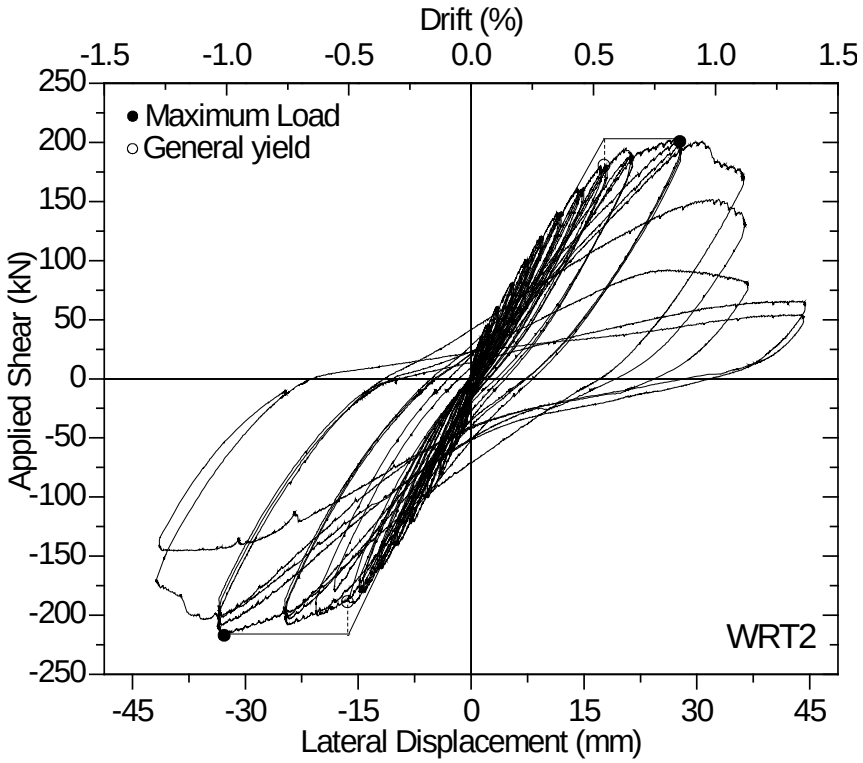

(b) WRT2

Fig. 3-13- Applied shear versus tip deflection responses

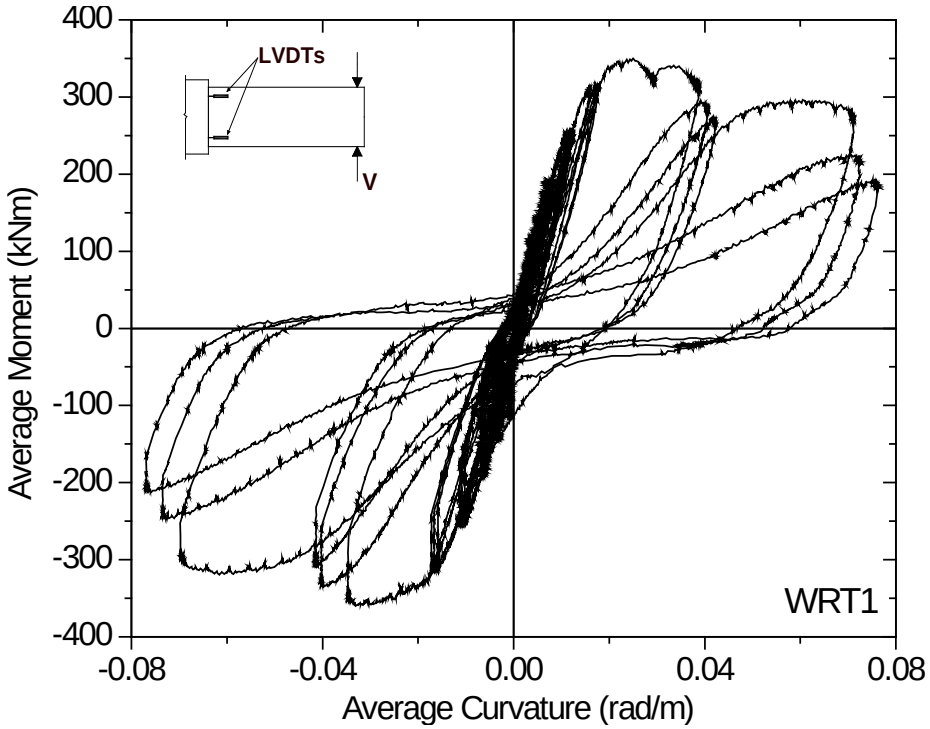

(a) WRT1

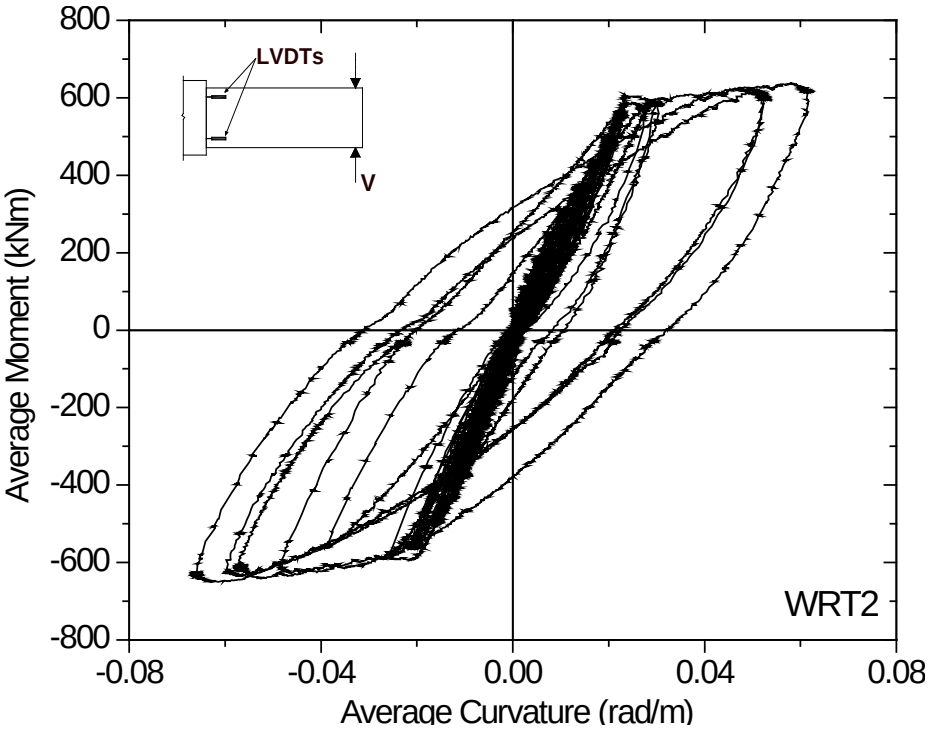

(b) WRT2

Fig. 3-14- Average moment versus curvature

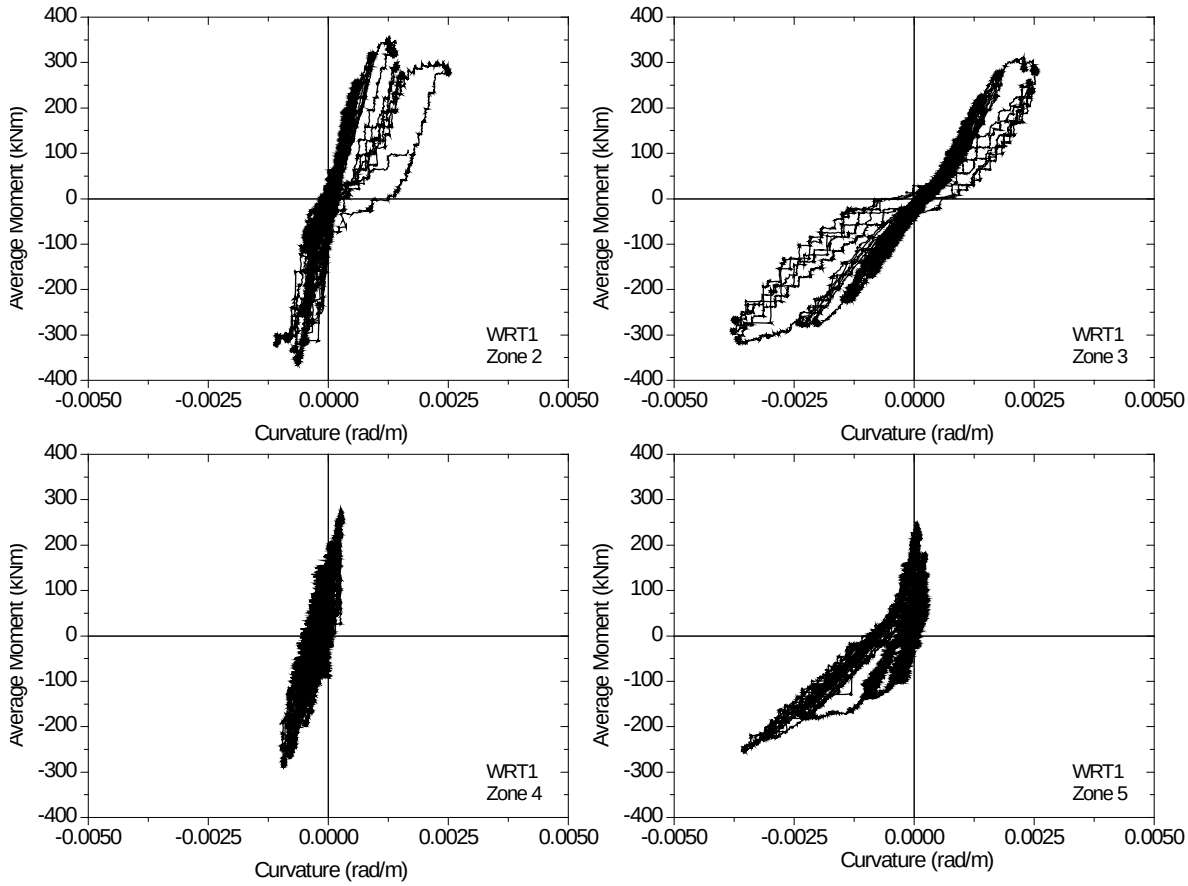

Fig. 3-15- Average moment versus curvature at zones 2, 3, 4, and 5 for wall WRT1

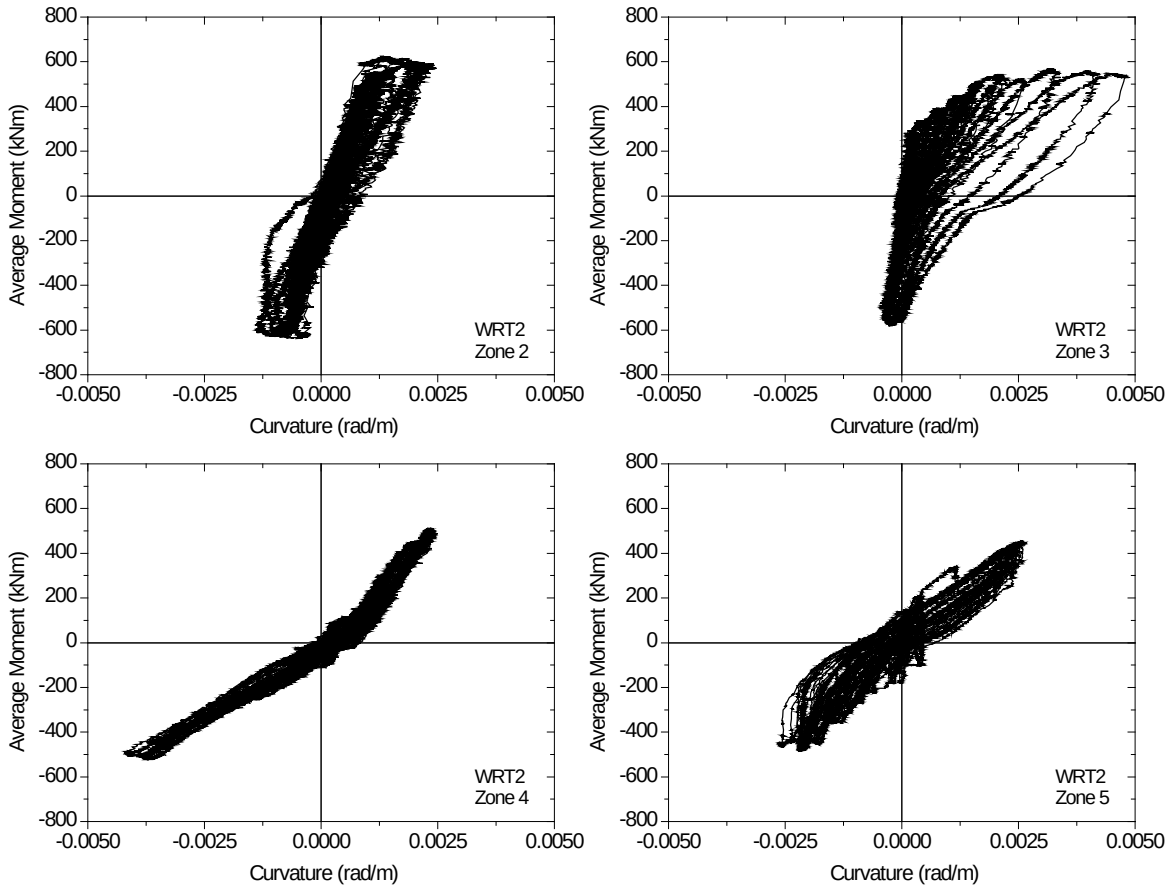

Fig. 3-16- Average moment versus curvature at zones 2, 3, 4, and 5 for wall WRT2

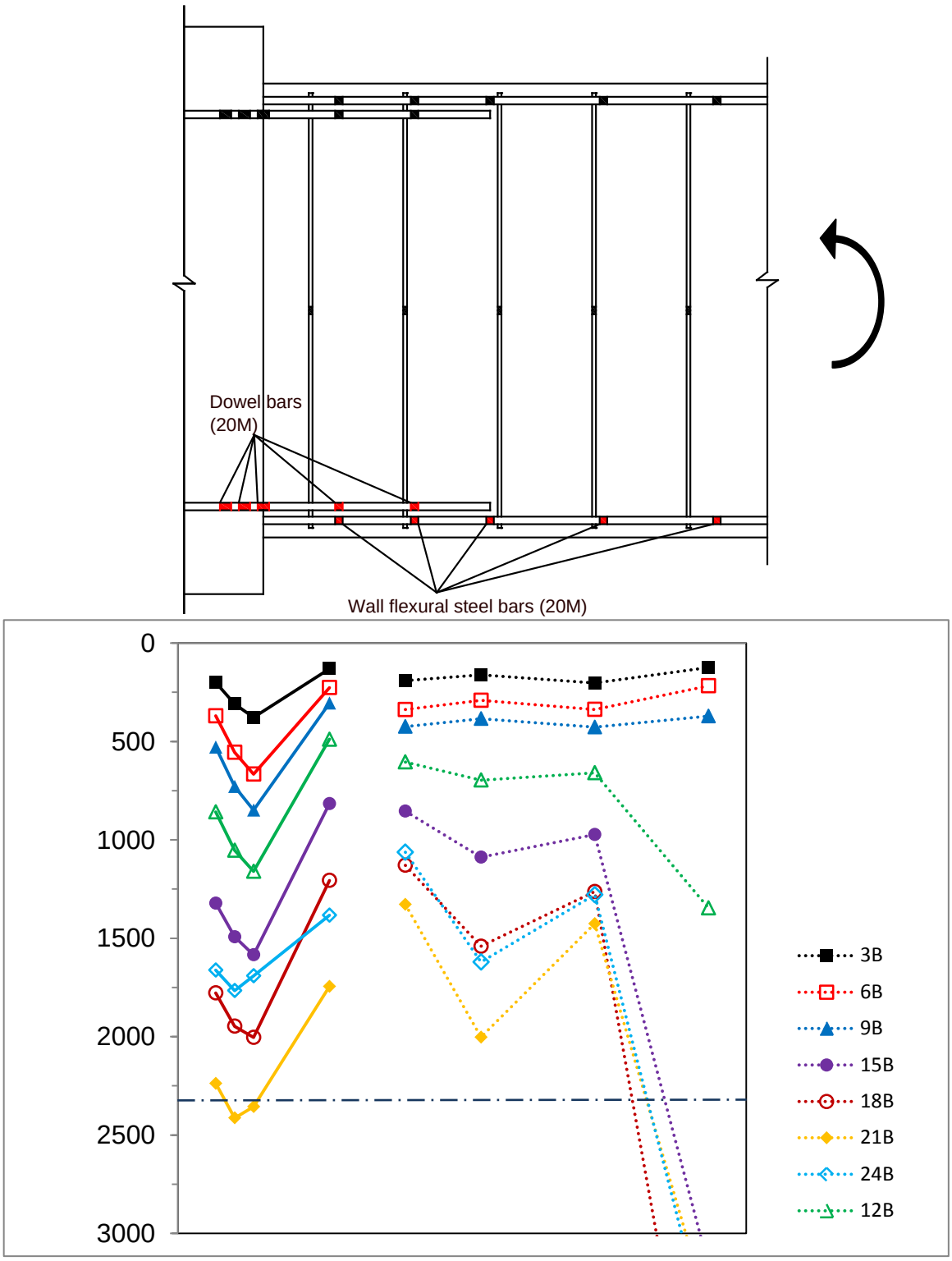

Fig. 3-17- Strains in the dowel bars and the main flexural bars-WRT1

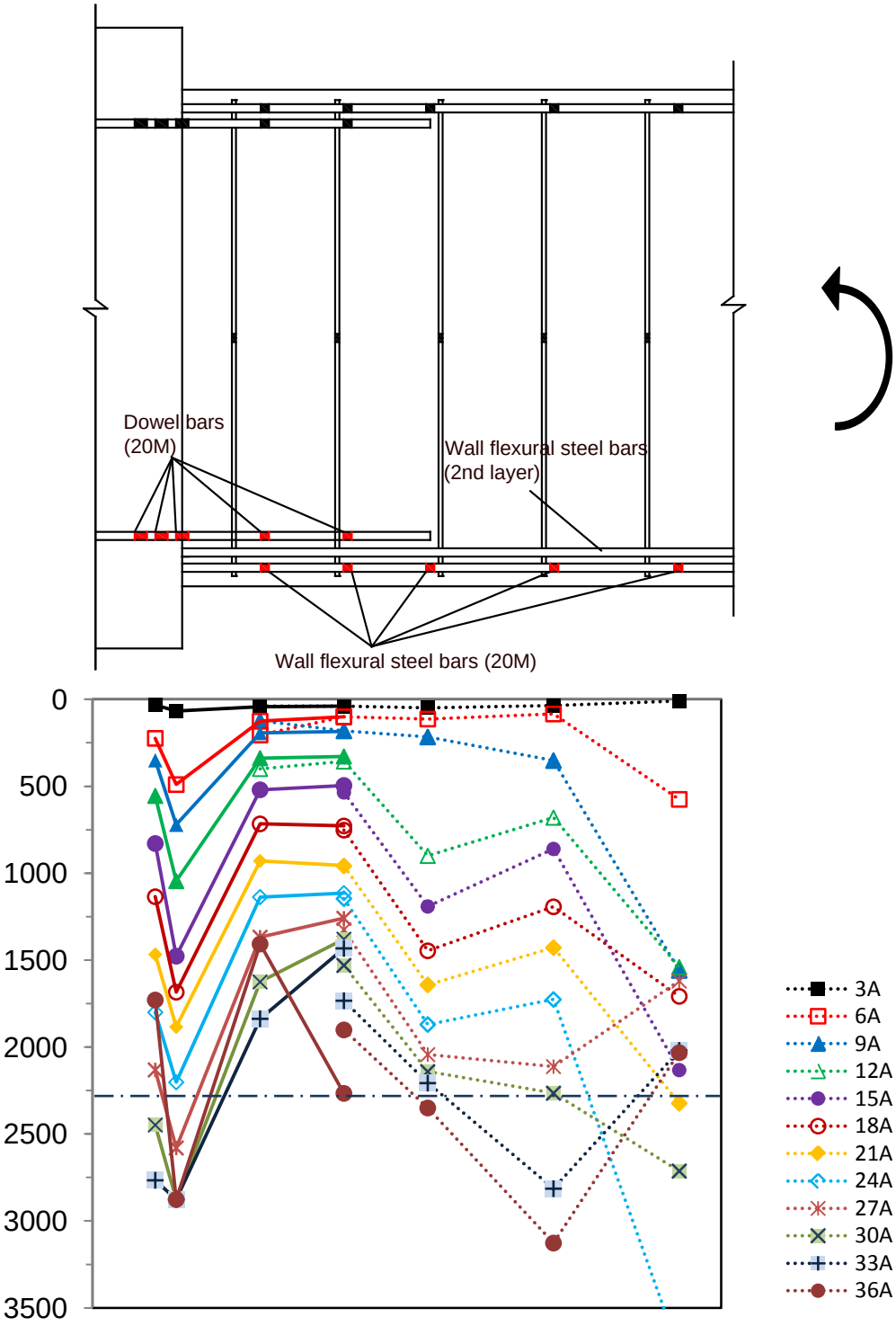

Fig. 3-18- Strains in the dowel bars and the main flexural bars-WRT2

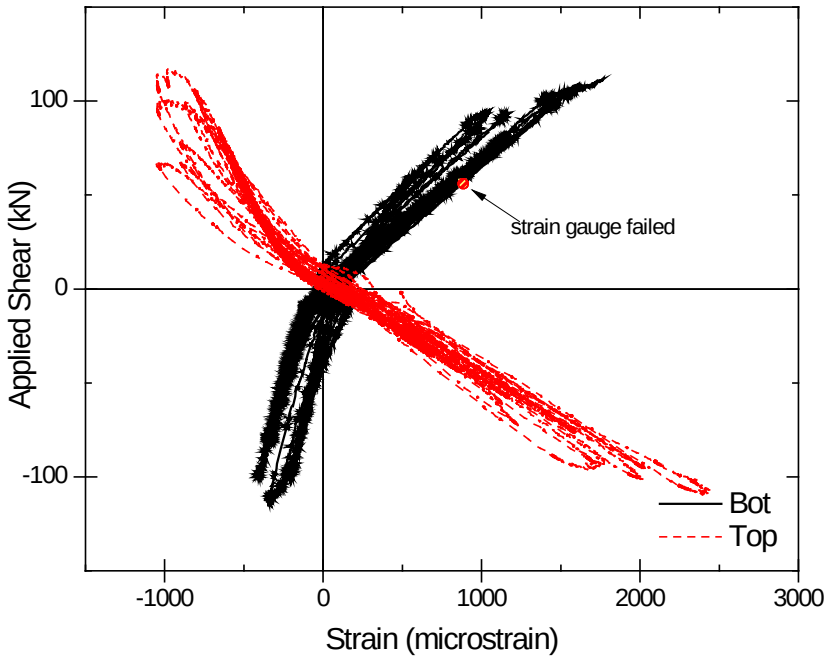

(a) WRT1

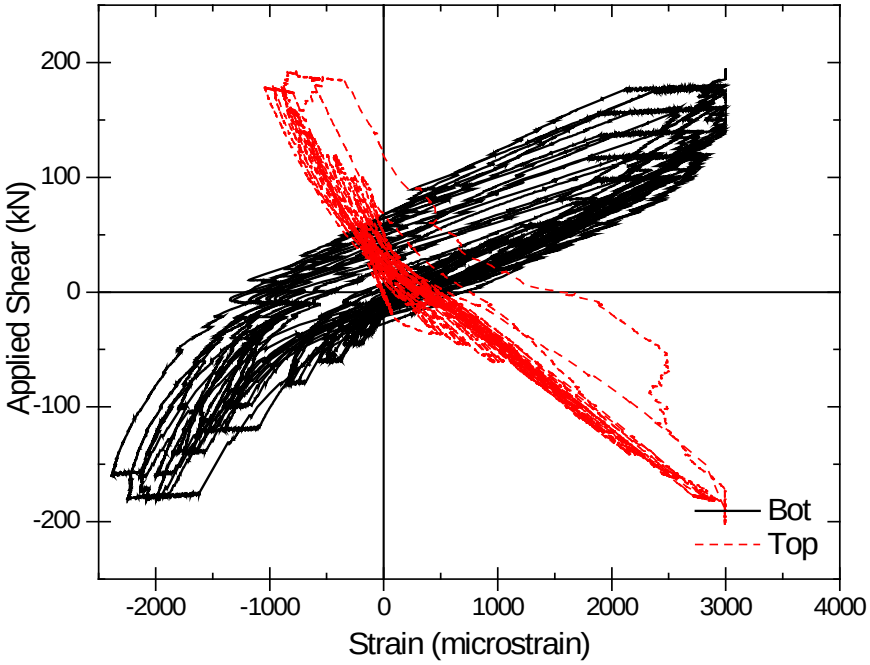

(b) WRT2

Fig. 3-19- Applied shear vs. strains in the top and bottom dowel bars the base of the walls

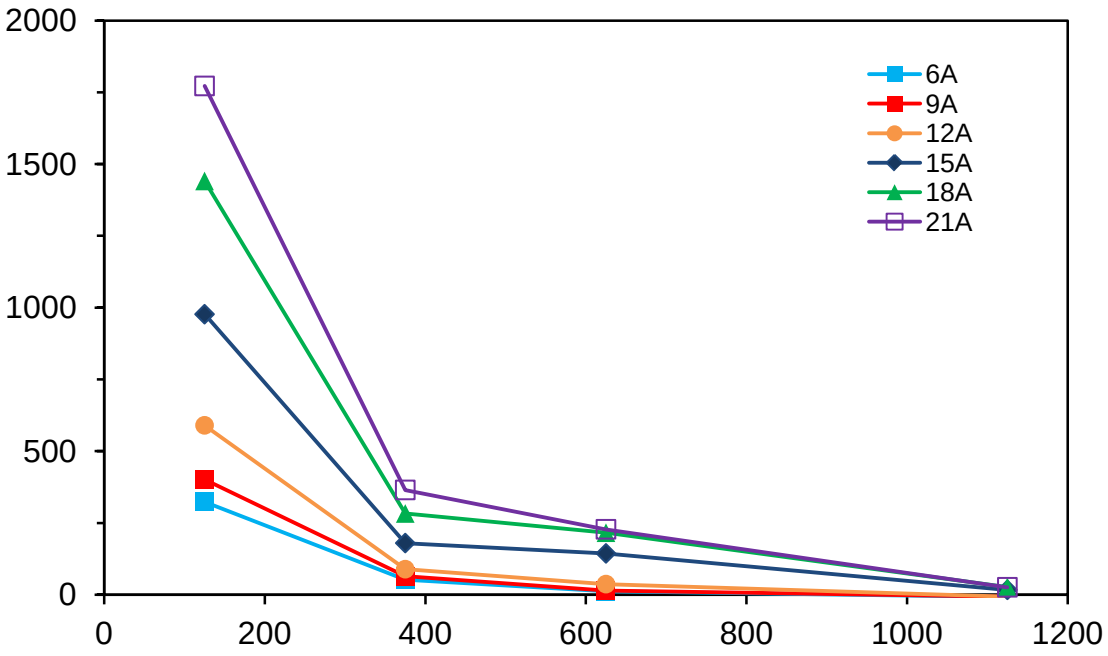

(a) WRT1

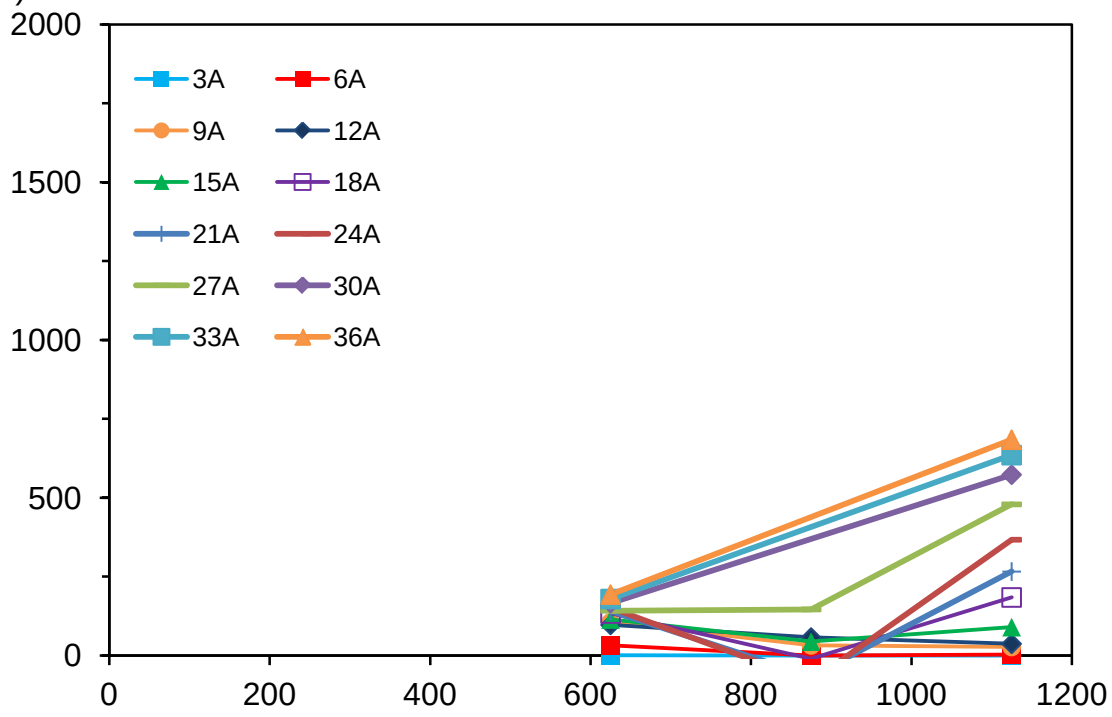

(b) WRT2

Fig. 3-20- Strains in the transverse reinforcement vs. distance from the base of the wall

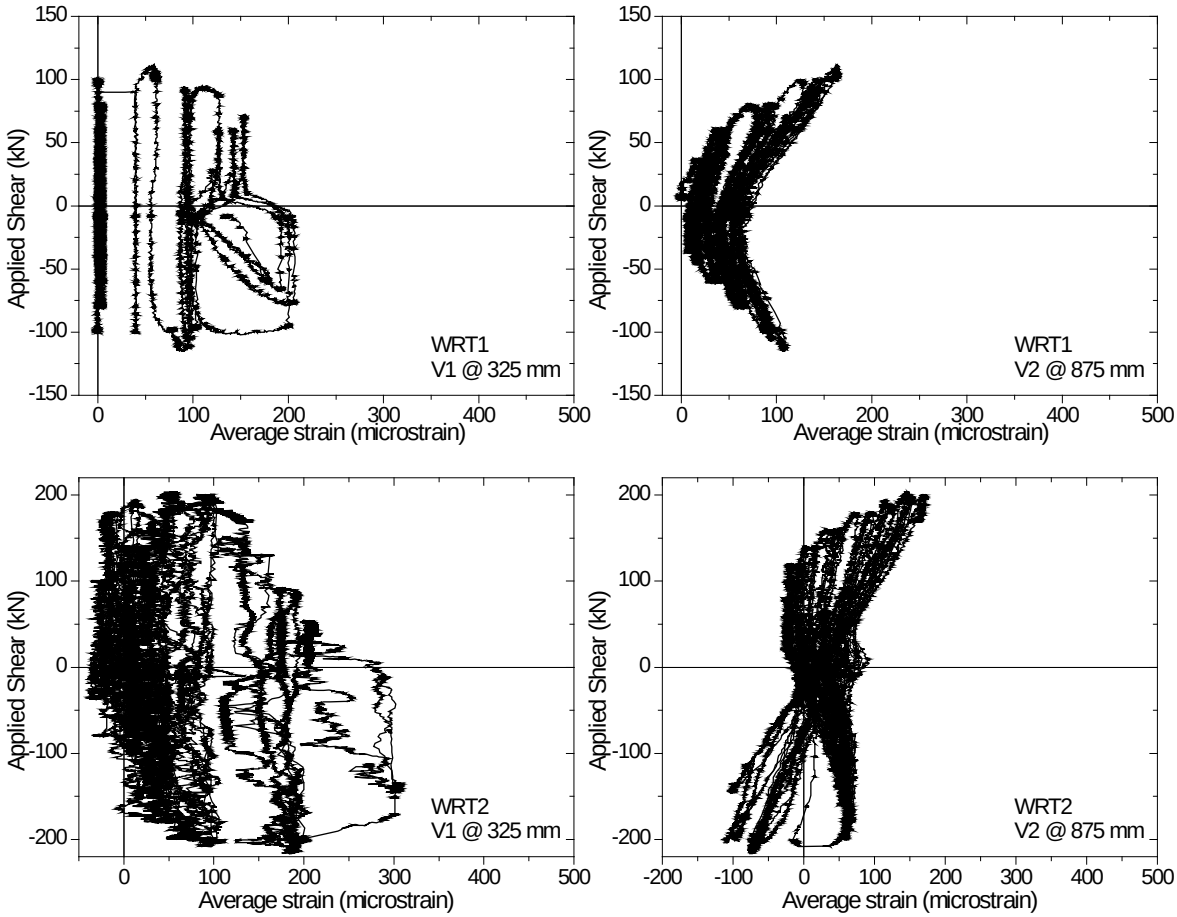

Fig. 3-21- Applied shear vs. average strains from the vertical LVDTs

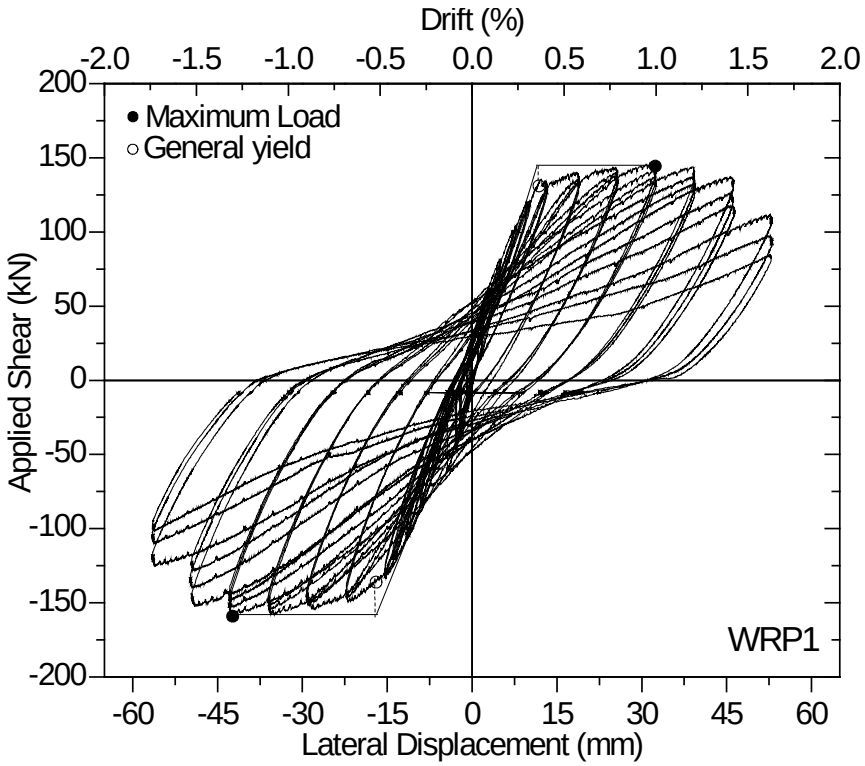

(a) WRP1

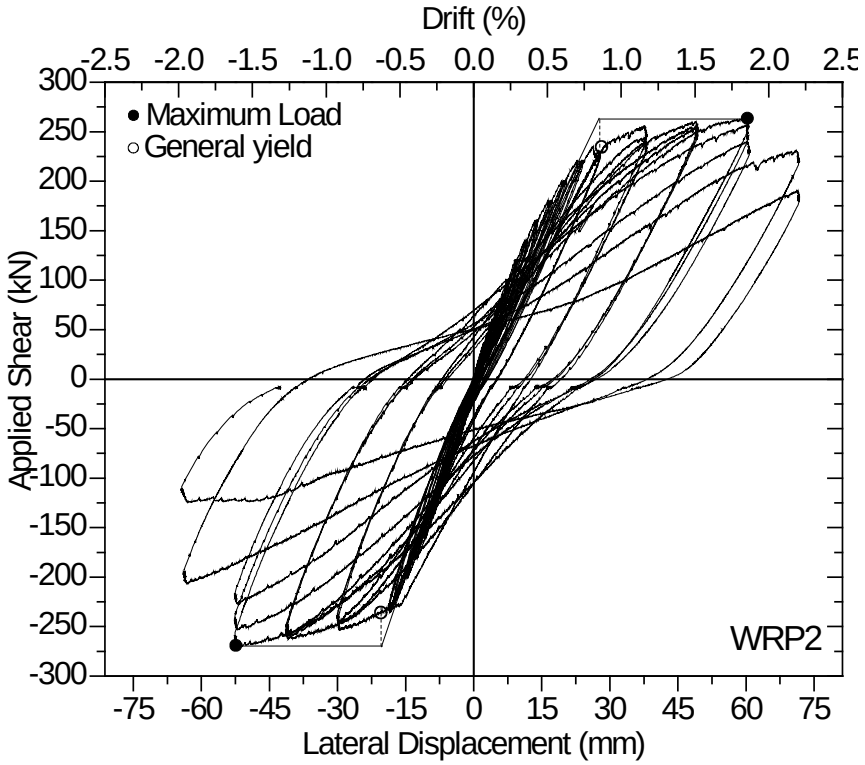

(b) WRP2

Fig. 3-22- Applied shear versus tip deflection responses

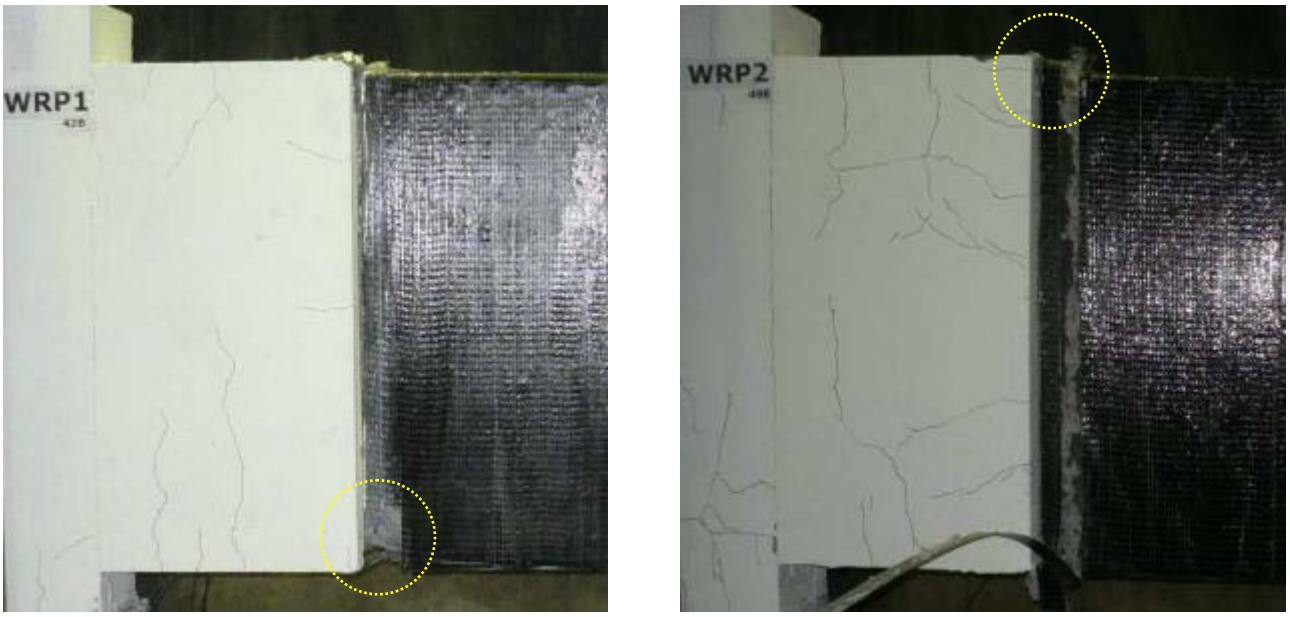

(a) Concrete crushing beyond jacket

(b) Close-up view of concrete crushing and fiber rupture
Fig. 3-23- Repaired walls at the end of testing

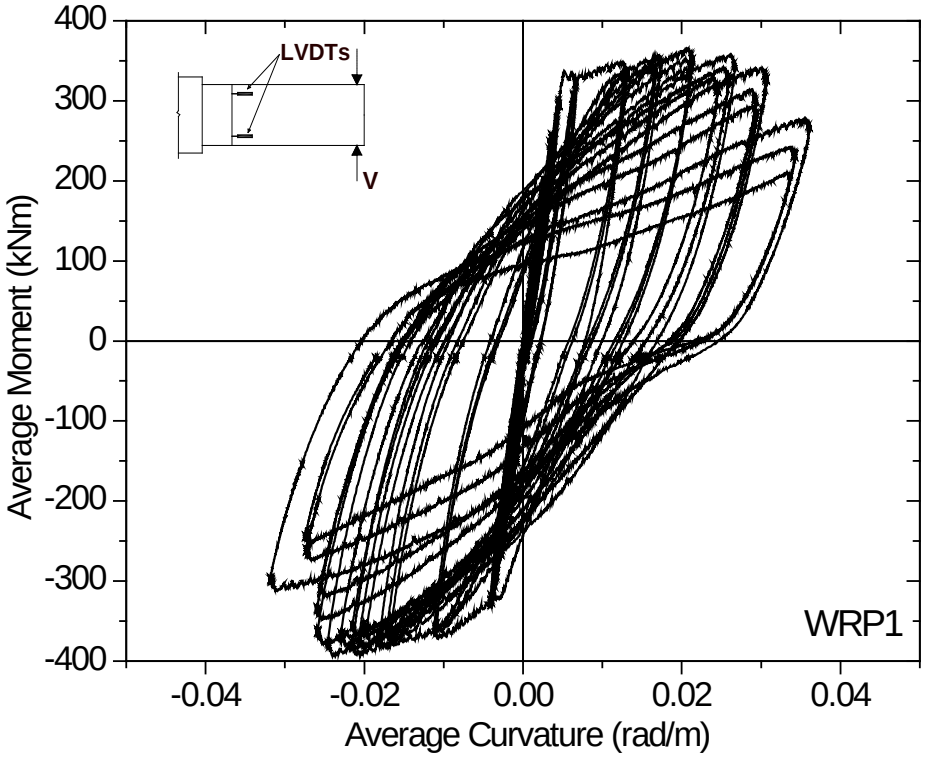

(a) WRP1

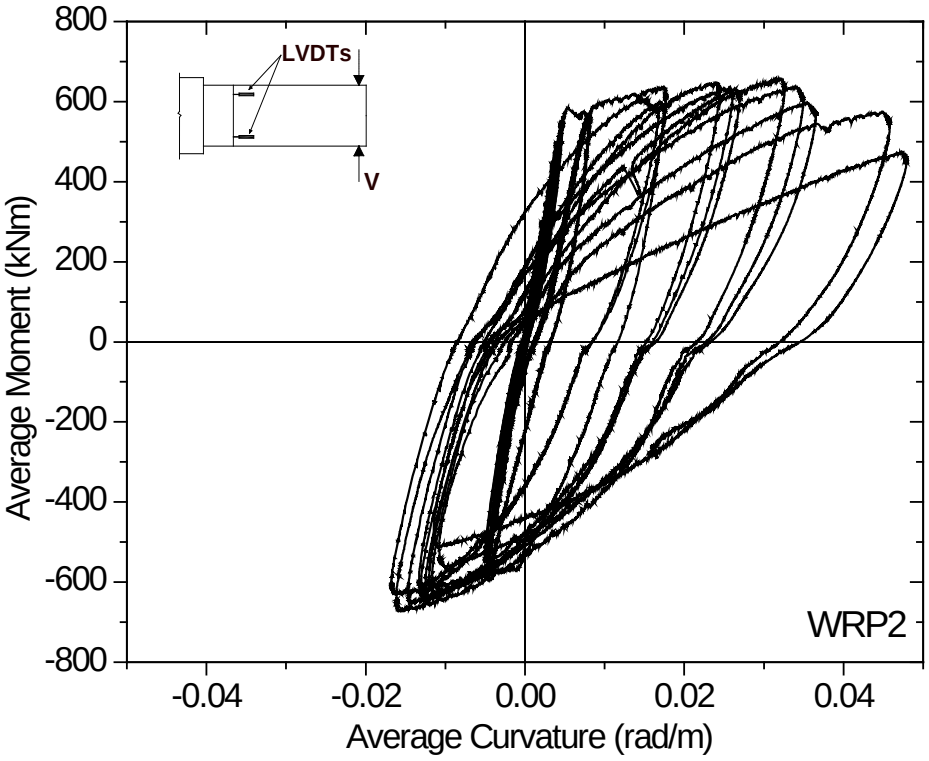

(b) WRP2

Fig. 3-24- Average moment vs. curvature at the new critical section (Zone 4)

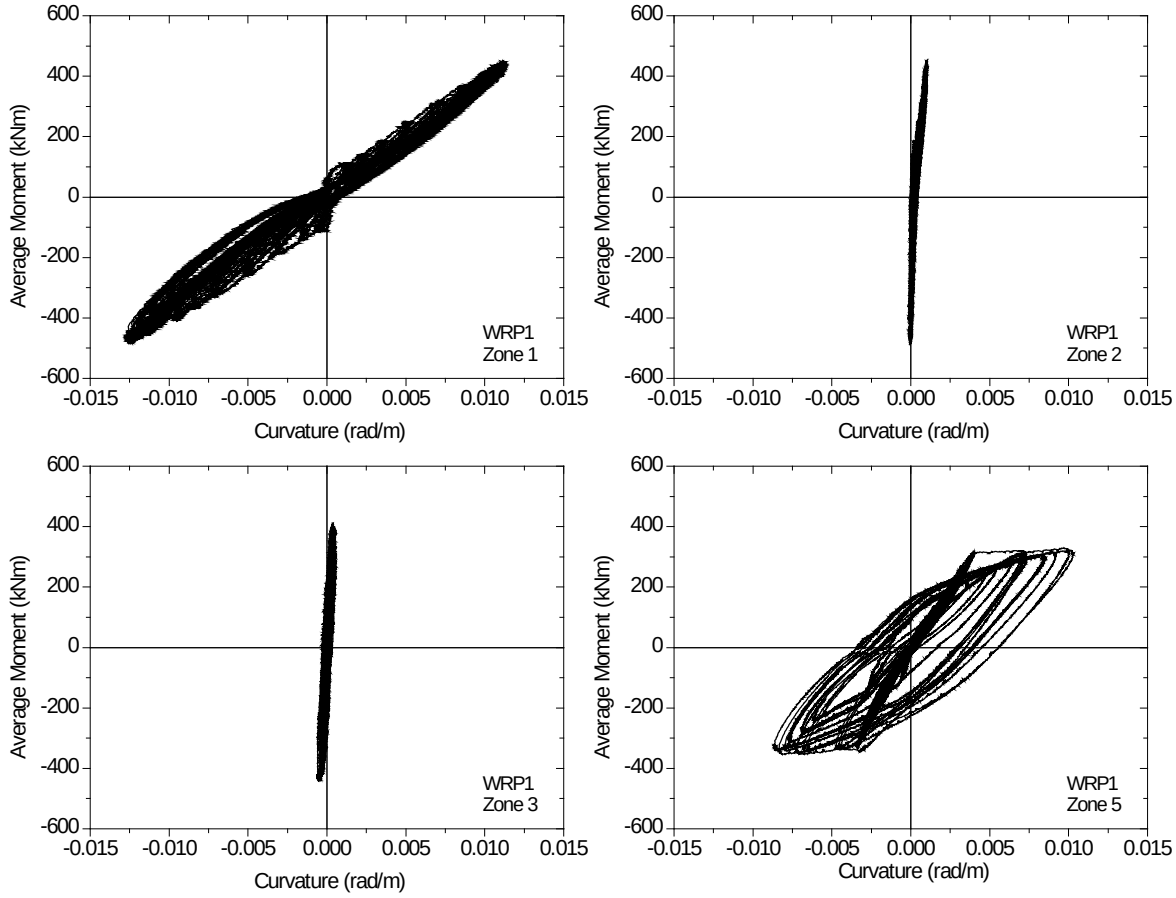

Fig. 3-25- Average moment versus curvature at zones 2, 3, 4, and 5 for wall WRP1

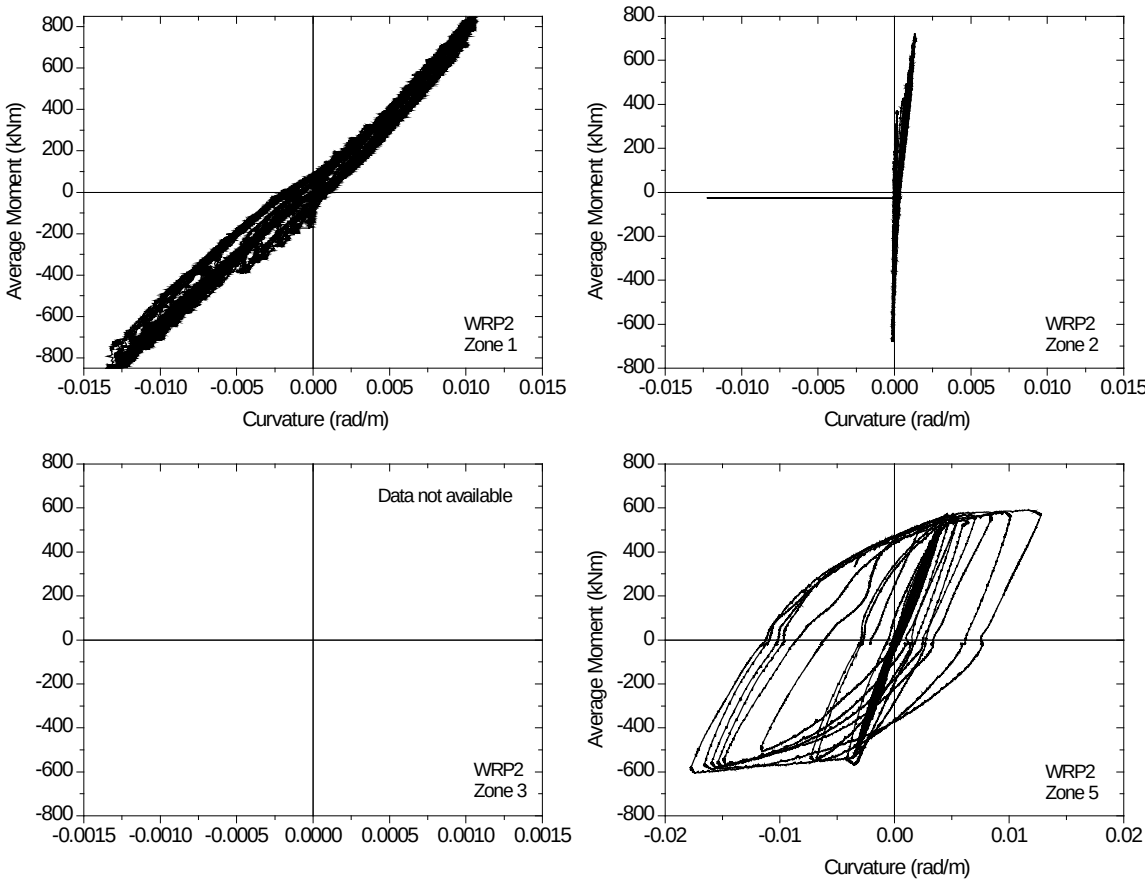

Fig. 3-26- Average moment versus curvature at zones 2, 3, 4, and 5 for wall WRT2

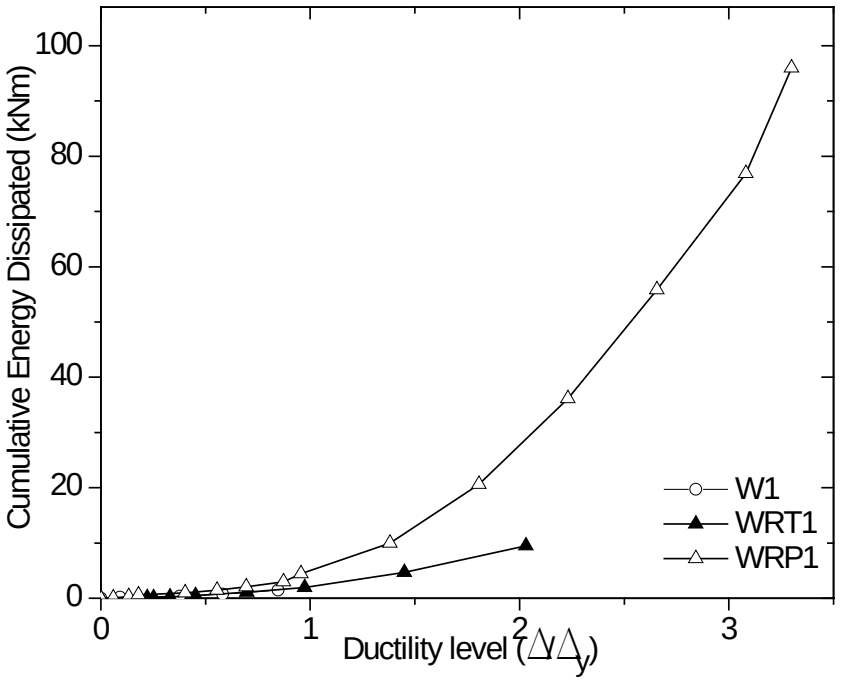

(a) W1, WRT1, and WRP1

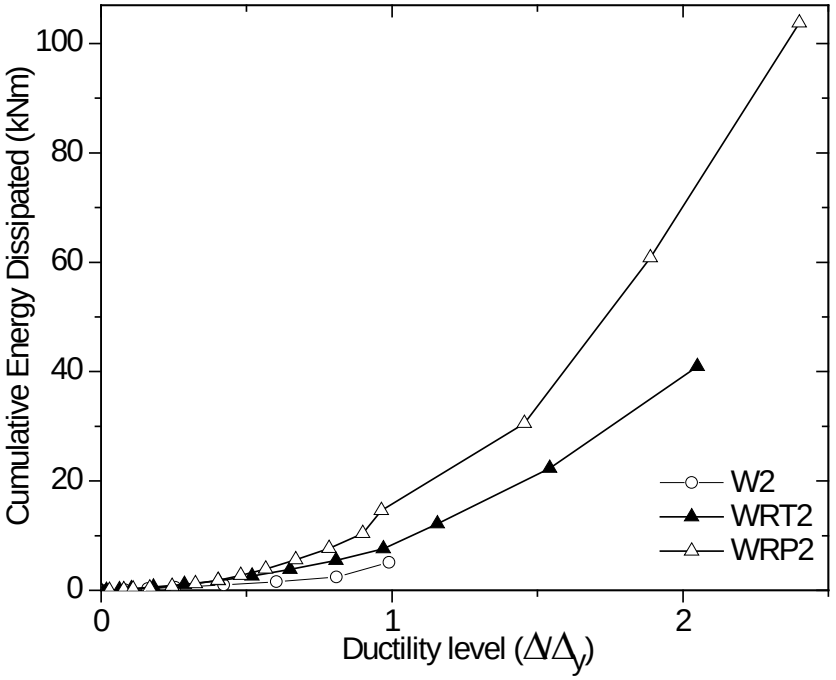

(b) W2, WRT2, and WRP2

Fig. 3-27- Cumulative dissipated energy versus ductility

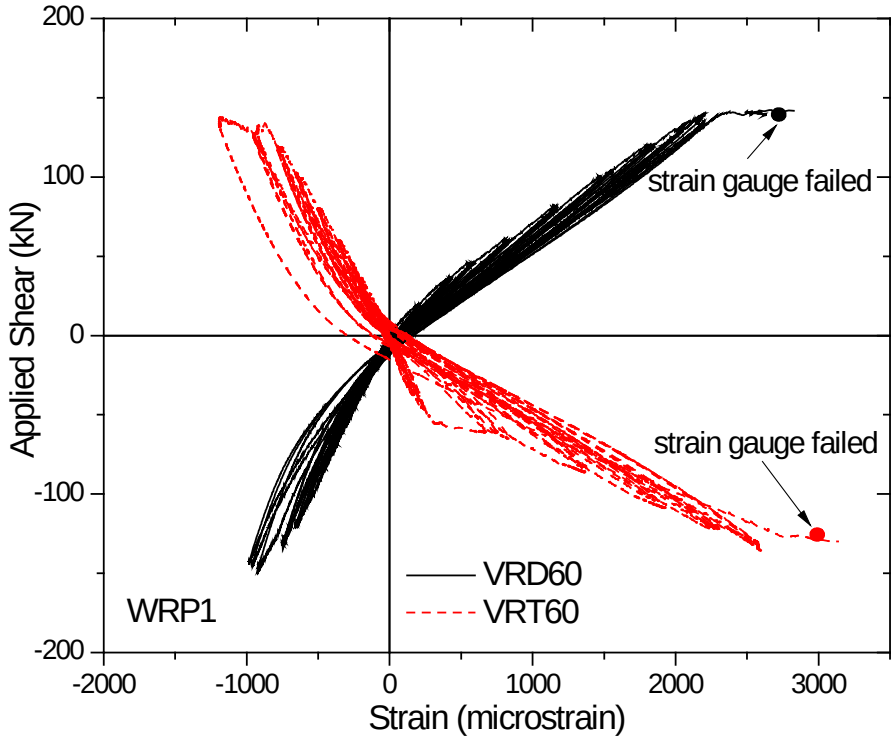

(a) WRP1

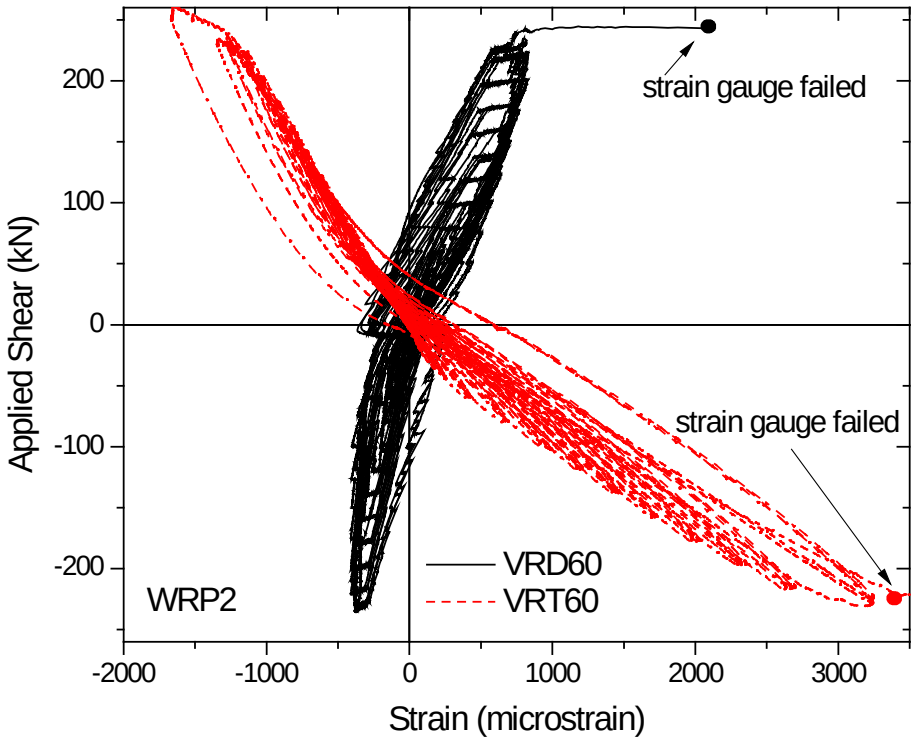

(b) WRP2

Fig. 3-28- Strain on wall flexural steel at the critical section (600 mm from the base)

Chapter 4
Behavioural Models

4.1. Introduction

The behavioural modeling techniques are described in this chapter. ASCE/SEI 41 (2006) proposes simplified approaches for modeling shear walls. Acceptance criteria are based on different performance levels for the wall components. These recommendations are compared with the experimental results.

The behavioural model should represent important material characteristics (steel and concrete) as well as important behavioural features. These features include shear and flexural deformations, bar buckling, bar slippage, and influence of lap splices.

Phenomenological models are widely used for engineering and research purposes. These models were preferred to more sophisticated finite element methods because of their simplicity.

This chapter will describe the techniques used for modeling the reversed cyclic loading behaviour of the poorly detailed walls. The inelastic flexural response of the shear walls were modeled using fiber elements. The shear deformations were modeled using a zero-length translational shear spring (un-coupled) and the potential impact of reinforcement slip on the response of the wall is modeled using a zero-length rotational spring.

The validity of the proposed models was verified with the experimental results from this study and the shear walls tested by Paterson and Mitchell (2003).

The fibre element has been recently implemented in commercial software's (i. e., Perform3D, SAP2000). The software "Open System for Earthquake Engineering Simulation-OpenSees" (McKenna, 1997) was used for modeling and analysis.

4.2. Material Models and Calibration

4.2.1. Concrete

Average compressive stress vs. strain relationships are shown for the concrete materials for the four wall specimens tested in this study (see Fig. 4-1). The important characteristics for concrete, such as: unconfined compressive strength ($f_c^{'}$), concrete peak strain ($\varepsilon_c^{'}$), and modulus of elasticity (E_c), and splitting tensile strength (f_{sp}) were determined by testing 100 mm diameter by 200 mm long cylinders (see section 2.3.1).

An appropriate model for concrete material should represent different concrete properties in compression and tension both for monotonic and cyclic loading and unloading. Several hysteretic constitutive models have been developed for accurate modeling of unconfined and confined concrete materials (i.e., Kent and Park, 1971; Saatcioglu and Razvi, 1992; Chang and Mander, 1994).

The original Kent and Park (1971) model for concrete was modified by Park et al. (1982). In the original model, the ascending part of the stress strain curve of concrete was considered to be unaffected by the confining effect of the transverse reinforcement. The slope of the descending part was a function of the amount of transverse reinforcement and the ratio between the core dimensions and the tie spacing.

Scott et al. (1982) and Park et al. (1982) proposed modifications to the original model by making an allowance for the enhancement in the concrete strength and the peak strain due to confinement. The increase in the confined concrete strength is a function of $\rho_t f_{yh}$, where ρ_t is the volumetric ratio of tie steel; *and* f_{yh} is the yield strength of the transverse reinforcement. The slope of the descending part of the curve remained the same as in the original model up to a stress of 20% of the maximum, beyond which a constant concrete stress is assumed.

Chang and Mander (1994) developed a generalized model which is capable of simulating the hysteretic behavior of confined and unconfined concrete in cyclic compression and tension. The envelope for the cyclic stress-strain behavior is derived from the monotonic curve. These envelopes provide a very good prediction

of the shape of both the pre-peak and post-peak branches of the stress-strain relationship.

Modified versions of the Kent and Park model and the Chang and Mander model are implemented in the OpenSees platform (*Concrete07: Chang and Mander*, and *Concrete02: Kent and Park*). It has been reported (NIST, 2010) that models using the *Concrete07* material model are generally matching better with experimental data than Concrete02, but some convergence problems have been reported.

Fig. 4-2 illustrates the simplified Chang and Mander model implemented in the OpenSees platform. The following parameters are used to calibrate these models:

- concrete compressive strength, $f_c^{'}$
- concrete strain at maximum compressive strength, $\varepsilon_c^{'}$
- Initial Elastic modulus of the concrete, E_c
- tensile strength of concrete, f_t
- tensile strain at max tensile strength of concrete, ε_t
- x_p , defines the strain at which the straight line descent begins in tension
- x_n, defines the strain at which the straight line descent begins in compression
- r , parameter that controls the nonlinear shape of descending branch

For each wall specimen, the Concrete07 material was calibrated with the available test data. Non-tested parameters were calculated and calibrated based on available data in the literature. For the repaired specimens, WRP1 and WRP2, it was assumed that concrete material properties did not change significantly, compared to the as-built specimens, W1 and W2. The tested properties of fibre-reinforced self-consolidating concrete, were used for calibrating the material model.

The tensile strength for cyclic modeling is expected to be well below the values obtained from monotonic tests. However, neglecting the contribution of concrete in tension results in a lower prediction of the wall lateral stiffness and a slightly lower prediction of the wall lateral strength compared with results that include the contribution of concrete in tension (Orakcal et al 2004). Therefore, the value of

tensile strength of concrete in modeling is limited to $f_t = 0.4\sqrt{f_c'}$ (MPa). Table 4-1 summarizes the Concrete07 parameters which were used for analysis.

Equations 4-1 to 4-4 (Chang and Mander, 1994) could be used as alternatives where experimental data is not available. In this study, the modulus of elasticity for concrete was chosen as the initial slop of the stress-strain plot (E_c = 27,100 MPa).

$$E_c = 8{,}200\left(f_c'\right)^{3/8} \quad \text{Eq. 4-1}$$

$$f_t = 0.40\sqrt{f_c'} \quad \text{Eq. 4-2}$$

$$\varepsilon_t = \frac{2f_t}{E_c} \quad \text{Eq. 4-3}$$

$$r = \frac{f_c'}{5.2} - 1.9 \quad \text{Eq. 4-4}$$

Table 4-1- Cocnrete07 calibrated parameters

Wall	f_c'	ε_c'	E_c	f_{sp}	$0.40\sqrt{f_c'}$	ε_t	x_p	x_n	r
	MPa	≈	MPa	MPa	MPa	≈			
W1, WRP1	31	0.002	27100	3.3	2.2	0.0003	2	2.3	4.1
WRT1	32	0.002	27100	3.4	2.3	0.0003	2	2.3	4.3
W2, WRP2	30	0.002	27100	3.5	2.2	0.0004	2	2.3	3.9
WRT2	33	0.002	27100	4.1	2.3	0.0004	2	2.3	4.4

4.2.2. Reinforcing Steel

The average stress vs. strain relationships for the reinforcing bars used in this study are shown in Fig. 4-3.

The most important characteristics for the steel are: yield strength (f_y), Modulus of elasticity, (E_s), ultimate strength (f_u), ultimate strain (ε_u), which are derived from the monotonic tensile testing of the reinforcing bars.

A bilinear model for the steel is the simplest model, however, such a model does not account for the Bauschinger effect.

The Giuffré-Menegotto-Pinto (1970, 1973) model which was modified by Filippou, Popov, and Bertero (1983) is a numerically efficient model which is capable of capturing the nonlinear hysteretic response of reinforcing bars, including isotropic strain hardening, and is in good agreement with experimental results (Orakcal et al. 2004; Elnashai and Izzuddin, 1993). These models are incorporated in the OpenSees Steel02 model. The OpenSees *ReinforcingSteel* material model is based on the Chang and Mander (1994) uni-axial steel model and is capable of capturing the isotropic hardening. The material is intended to work as uni-axial fibres; however, there are convergence difficulties when subject to cyclic loading.

A simple uni-axial bilinear hysteretic material (designated as *Hysteretic Material*) capable of representing force and deformation pinching is also available. The material is used for its simplicity and is utilized in the NIST (2010) model. The *Hysteretic* material was used for modeling purposes.

Fig. 4-4 shows the defining envelope for rebar modeling. In this model, the yield plateau region is not considered, and it is assumed that the hardening branch is linear. The following parameters are used to define the *Hysteretic* material:

- 1st, 2nd and 3rd points in positive loading: $\varepsilon_1^+, \sigma_1^+,\ \varepsilon_2^+, \sigma_2^+,\ \varepsilon_3^+, \sigma_3^+$
- 1st, 2nd and 3rd points in negative loading: $\varepsilon_1^-, \sigma_1^-,\ \varepsilon_2^-, \sigma_2^-,\ \varepsilon_3^-, \sigma_3^-$
- $Pinch_x$, and $Pinch_y$: pinching parameters for strain, and stress, respectively. The values are selected based on the hysteretic responses obtained from experiments
- d_1, and d_2: Damage parameters due to ductility, and energy, respectively

The calibrated parameters for the steel material are summarized in Table 4-2.

Table 4-2- Hysteretic material calibrated parameters

	10M		15M		20M	
$\varepsilon_1^+, \sigma_1^+$ *	0.0022	65	0.0022	65	0.0022	65
$\varepsilon_2^+, \sigma_2^+$	0.05	105	0.05	105	0.05	105
$\varepsilon_3^+, \sigma_3^+$	0.06	10	0.06	10	0.06	10
$\varepsilon_1^-, \sigma_1^-$	-0.0022	-65	-0.0022	-65	-0.0022	-65
$\varepsilon_2^-, \sigma_2^-$	-0.05	-105	-0.05	-105	-0.05	-105
$\varepsilon_3^-, \sigma_3^-$	-0.06	-10	-0.06	-10	-0.06	-10
$Pinch_x$ **	0.6		0.6		0.6	
$Pinch_y$	0.4		0.4		0.4	
d_1	0		0		0	
d_2	0		0		0	

* σ is in ksi units

** chosen to match experimental data of this study

4.3. Mathematical Model

The mathematical model should accurately represent global and local response features.

The inelastic behaviour of the walls was modeled using displacement-based beam-column elements. The ASCE/SEI 41 (2006) allows for the use of an equivalent beam-column element in modeling shear walls. Since the aspect ratio of the walls is $h_w/l_w = 2.7$, flexural deformations are expected to be dominant in the global response of the walls, however, the effect of shear deformations was taken into account using a zero-length translational shear spring. Shear deformations and flexural deformations are uncoupled.

The wall is divided into sub-elements in order to accurately model the response of the walls. It is reported (NIST, 2010) that an element size close to the expected plastic hinge length will improve the accuracy of the analytical model.

It is assumed that the foundation block acts a fully fixed support. The effect of the relative rotation of the foundation (as a rigid body) was measured and the tip deflection of the wall was corrected for this rotation.

4.3.1. Fibre Displacement-based Beam-Column Element

A displacement-based beam-column element with a fibre cross section was used in order to model the shear wall components. The fibre displacement-based beam-column element was proposed by Taucer et al. (1991) and was based on a displacement formulation that allows for distributed plasticity modeling which would allow yielding to occur at any location along the element. The nonlinear response of the element is therefore derived from the nonlinear stress-strain relationships for each individual fibre.

For the displacement-based approach, the deformations are interpolated from an approximate displacement field. The principle of virtual displacements (PVD) is used to form the element equilibrium relationship (OpenSees, 2011). Constant axial strain and linear curvature distribution are enforced along the element length in order to approximate the nonlinear response of the element.

The section force-deformation relation is determined by integration of the stress-strain relationship in each fibre. The displacement-based element is sensitive to the number of elements used to model the wall, and to the length of an element at the location of potential plastic hinging. Best results are reported for element sizes close to the plastic hinge length (Wallace et al, 2004). Different number of element sizes was studied in order to optimize the results.

In order to represent higher order distributions of deformations, application of a finer mesh is encouraged. The cross section of the shear wall is divided into concrete and steel fibres and the global force-deformation response of the section is derived by integration of the stresses in the fibres over the cross section (Taucer et al, 1991). Fibre elements enable accurate estimation of local response parameters such as sectional curvature and material strain values (NIST, 2010).

Fig. 4-5 shows a schematic view of discretizing the cross section into concrete and steel fibres. A refined mesh would result in better estimates of deformations

along the element; however, it would be computationally more time consuming. A concrete mesh size of 150 mm by 150 mm was reported to be accurate enough (NIST, 2010). In this study a finer mesh size of 75 mm by 75 mm was used to model the concrete. Each steel reinforcing bar was modeled as a single fibre.

It should be noted that since the formulation of the fibre displacement-based beam-column element is based on sectional analysis, it does not model bond slip effects and neglects the effect of shear deformations. Therefore, additional behavioural features should be included in the model to appropriately model these phenomena.

4.3.2. Shear Deformation

Modeling the interaction of nonlinear flexural and shear actions is complicated. The nonlinear shear deformations are reported to be the result of coupling between axial-bending and shear behaviour.

Elwood et al. (2007) proposed a generalized multi-linear shear model for modeling nonlinear shear deformations in wall components (see Fig. 4-6). Several key features such as cracking, yielding in shear, and degradation of strength, as well as the residual strength are reflected in this backbone model. This model was a modified version of an older model presented in FEMA 356 (2006), which was later adapted by ASCE/SEI 41 (2006).

These models have been adopted in the NIST model (2010); however, different behavioural models were used for the shear spring for shear-critical and flexure-critical wall components, since it is expected that yielding in flexure limits the shear demand in the wall.

The OpenSees platform does not provide a reliable element for appropriate modeling of the interaction of shear deformations and flexure deformations. The flexure-shear interaction displacement-based beam-column element, which is available at this time (January 2013), only works for monotonic loading, despite using cyclic material properties as input parameters.

Consequently, a combination of displacement-based beam-column element and a translational shear spring to account for shear deformations (in global response)

has become a common practice among researchers and engineers (NISTGCR10-917-8, 2010). However, the deformations remain uncoupled.

In this study, shear deformations were considered in the model, using an uncoupled translational shear spring. The characteristics of this spring are described in Fig. 4-7.

4.3.3. Bar Slip

Bar extension as a result of strain penetration into the foundation affects the response of the structural components. Bar slip contributes to softening of the response of the elements. (Cho and Pincheira, 2006; Zhao and Sritharan, 2007; Massone et al. 2009). Therefore, models should consider the effect of strain penetration. Sectional analysis does not account for bond slip.

ASCE-41 and FEMA 356 take into account the softening effect of the bar slip by modifying the effective stiffness of structural components. These modification factors account for cracked section properties, but in the update to the ASCE/SEI 41 concrete provisions (Elwood et al. 2007), the potential impact of bar slip is also included.

The effect of strain penetration was included in the models by adding rotational springs at the base of the walls to account for softening of the load-versus-deformation response. Simplified models use linear elastic rotational springs to account for softening effects due to bar slip. These models assume that a crack forms along the entire length of the base of the wall and reduces the flexural rigidity of the wall, leading to a softer moment-rotation response.

Zhao and Sritharan (2007) proposed a new material model (implemented into OpenSees as Bond-SP01) assigned to the reinforcing bars in a zero-length section to account for the effect of strain penetration in fully anchored reinforcing bars. The nodes for the zero length section elements should be constrained in the shear direction (for transferring shear actions). Fig. 4-8 describes the properties of the model.

4.3.4. Lap splices

Failure of lap splices is a common deficiency in structural components of existing structures. The potential impact of lap splice failure should be reflected in the mathematical models. FEMA 356 (2000) as well as the ASCE/SEI 41 (2006) followed the same procedure for the capacity of lap spliced reinforcement. Both models modify and reduce the stress that could be developed in lap spliced bars based on the ratio of the available lap splice length, l_b, to the required lap splice length, l_d.

$$f_s = \left(\frac{l_b}{l_d}\right) f_y \qquad \text{Eq. 4-5}$$

The required lap splice length should be determined according to ACI-318, Clause 12 (Eq. 4-6). CSA A23.3 (2004) proposes a similar equation for the development length of straight bars (Eq. 4-7). The CSA provisions are based on the ACI provisions. However, one difference between the two equations comes from how they take into account the spacing of lap spliced bars, with CSA being less conservative.

$$l_d = \begin{cases} \dfrac{f_y}{1.1\lambda\sqrt{f_c'}} \dfrac{\psi_t \psi_e \psi_s}{\dfrac{c_b + k_{tr}}{d_b}} d_b & \text{ACI-318 (2011)} \quad \text{Eq. 4-6} \\ 1.15 \dfrac{k_1 k_2 k_3 k_4}{d_{cs} + k_{tr}} \dfrac{f_y}{\sqrt{f_c'}} A_b & \text{CSA A23.3 (2004)} \quad \text{Eq. 4-7} \end{cases}$$

It should be noted that the value of $(c_b + k_{tr})/d_b$ should be limited to 2.5 to prevent pullout failure. Table 4.3 describes the parameters and corresponding values used in Eq.4-6 and Eq. 4-7.

Table 4-3- Description of parameters for calculating development length

	Description	Units	Approximate value
f_y	Average yield stress of steel	N/mm^2	460[1]
$f_c^{'}$	Average compressive strength of concrete	N/mm^2	31
$k_1;\psi_t$	Bar location factor	-	1.0
$k_2;\psi_e$	Coating factor	-	1.0
$k_3;\lambda$	Concrete density factor	Normal	1.0
$k_4;\psi_s$	Bar size factor	-	0.8
$d_{cs};c_b$	Smallest cover or bar spacing*	mm	40[2]
k_{tr}	Effect of transverse reinforcement	mm	
d_b	Nominal diameter of bar	mm	20
A_b	Area of individual bar	mm^2	300

[1] Test value used as a lower bound value in calculations

[2] $d_{cs};c_b$ is determined as the minimum of c_{b1}, c_{b2}, c_{b3}: see Fig. 4-9

It should be noted that in ASCE/SEI 41, l_d is taken as the tension development length and not the lap spliced length as defined in the ACI code and CSA standard. On the other hand, the seismic provisions of Chapter 21 of ACI-318 (2011) requires that the minimum lap splice length at the location of yielding be at least 1.25 times the value calculated for f_y in tension (Clause 21.9.2.3). In other words, the minimum lap splice length required for new construction should be modified by 1.3 for Class B lap splices, and by 1.25 for the expected yield stress in the bars in plastic hinge regions. Thus, the minimum lap splice length for design is 1.6 (1.25×1.3) times the development length l_d or the splice length.

The Canadian Guidelines for Seismic Evaluation and Retrofit (2013) specify that the expected yield strength of the steel is taken as 1.15 times the lower bound yield stress. This differs from ASCE-41 and for the Grade 400 steel used in this study, the expected yield is $1.15 \times 400 = 460\ MPa$. This yield stress of 460 MPa corresponds to the average yield stress determined from tests.

The update to ASCE-41 (Elwood et al. 2007; ASCE/SEI 41, Supplement 1, 2007) substitutes Eq. 4-5 with a nonlinear formula (Eq. 4-8), which also accounts for the expected increase in the yield stress of the reinforcement:

$$f_s = 1.25 \left(\frac{l_b}{l_d} \right)^{2/3} f_y \qquad \text{Eq. 4-8}$$

The modification factor of 1.25 in Eq. 4-8 was introduced (Elwood et al., 2007) to account for the expected over-strength in the reinforcement. This equation is a modified version of a model proposed by Cho and Pincheira (2006):

$$f_s = \left(\frac{l_b}{0.8 l_d} \right)^{2/3} f_y \qquad \text{Eq. 4-9}$$

The multiplier 0.8 accounts for the conservatism of the development length equation of ACI 318 (Eq. 4-6).

4.4. Experimental Results vs. ASCE-41

The responses of the shear walls obtained from this research have been compared with the modeling recommendations of ASCE-41, section 6-7. For each set of experiments, backbone curves are developed and compared with the experimental results.

4.4.1. Walls W1 and W2

For walls W1 and W2, the lap spliced bars failed well below the predicted general yielding of the walls. It was found that the lap splices in both walls failed in a side splitting mode. As a result of the brittle lap splice failure, it is assumed that a force control approach would be appropriate to describe the responses of these walls.

The potential impact of the presence of the lap splice is taken into account by determining the maximum stress that could be developed in the lap spliced bars according to ASCE/SEI 41 and ASCE/SEI 41, Supplement 1.

The shear capacity of the walls, WRT1 and WRT2 can be determined as proposed by ACI-318 (Eq. 4-10):

$$V_n = A_{cv}(\alpha_c \sqrt{f_c'} + \rho_t f_y) = (0.8 \times 1200 \times 150) \times (0.17\sqrt{30} + 0) = 170\ kN \quad \text{Eq. 4-10}$$

where A_{cv} is the area of the web of the walls ($0.8 l_w \times b_w$), α_c is the coefficient defining the relative contribution of the concrete strength to the nominal wall shear strength, and ρ_t is the percentage of transverse reinforcement to gross area of the wall section. For $h_w / l_w \geq 2$, the value of α_c is 0.17 according to ACI recommendations. Neglecting the effect of the poorly detailed transverse reinforcement, the predicted nominal shear capacity of the walls is $V_n = 170\ kN$ and hence, the walls are predicted to be controlled by flexure.

4.4.1.1. ASCE-41 and FEMA 356

The lap splice length for the 20M bars in walls W1 and W2 was 600 mm. In these approaches, the minimum required lap splice length is taken equal to the ACI development length in accordance with Eq. 4-6. For determining the required length, the material properties determined from testing are used as the expected material properties. Hence, the required lap splice length is:

$$l_d = \frac{f_{y,e}}{1.1\lambda\sqrt{f_{c,e}'}} \frac{\psi_t \psi_e \psi_s}{\frac{c_b + k_{tr}}{d_b}} d_b = \frac{(460)}{1.1 \times 1 \times \sqrt{31}} \frac{1 \times 1 \times 0.8}{\frac{40}{20}} \times 20 \approx 600\ mm$$

In calculating the required lap splice length for the 20M bars, the details of the transverse reinforcement are such that k_{tr} can be taken as zero. By using ASCE-41 equation, the maximum stress that could be developed in the lap spliced bars is:

$$f_s = \frac{l_b}{l_d} f_y = \frac{600}{600} \times 460 = 460\ MPa$$

The update to ASCE-41 for calculating the capacity of lap spliced bars yields higher capacities compared to the original version; however, this value is limited to the upper-bound value of the yield stress of the reinforcement for force-controlled actions (as it is the case for W1 and W2):

$$f_s = 1.25\left(\frac{l_b}{l_d}\right)^{2/3} f_y \le f_y \rightarrow f_s = 460\ MPa$$

For the case of walls W1 and W2, it can be seen that both ASCE-41 and the updated version (Supplement 1) will lead to the same backbone curves.

The yield stresses in the above equations were taken as the average yield stress obtained from material testing (lower bound value). The stiffness of the walls is estimated using the modification factors of ASCE-41 and FEMA 356. The walls are assumed as cantilevers with loads being applied at the tip of the walls; therefore, the lateral stiffness can be calculated as:

$$K_{lat} = \alpha \frac{3E_c I_g}{h^3} \qquad \text{Eq. 4-11}$$

where E_c is the concrete modulus of elasticity, I_g is the gross section moment of inertia, and h is the height of the walls measured to the loading point (i.e., 3250 mm). Using the recommendations of ASCE/DEI 41 (2006) and FEMA 356 (2000), the stiffness should be reduced to 50% ($\alpha = 0.5$) to account for cracked section properties.

The calculated parameters for the backbone curves for walls W1 and W2 are summarized and presented in Table 4-4. Fig. 4-10 shows the load versus displacement test results (W1 and W2) versus the backbone curves developed according to ASCE/SEI 41 and FEMA 356.

The ASCE-41 predictions over-estimate both the stiffness and strength for these poorly detailed thin walls.

Table 4-4- Backbone parameters versus test results

	ASCE-41 and FEMA 356				*Experiments*			
	l_b/l_d	f_s	$V_{lat\ @Mn}$*	K_{eff}	$\varepsilon_{s,avg}$**	f_s	V_{lat}	K_{eff}
		MPa	kNm	kN/mm	-	MPa	kN	kN/mm
W1	1	460	119	24.7	0.0021	437	309	8.5
W2	1	460	207	24.7	0.0017	341.2	455	11.2

* Assuming a yield strain of $\varepsilon_y = 0.0023$

** Average of maximum steel strains at the ends of the walls

.

4.4.1.2. Proposed Model

This section describes a model that is proposed for poorly detailed thin walls with lap splices at the critical section.

The softer response could be a result of bar slip and the resulting crack at the wall-foundation interface. The stiffness of the walls is in better agreement with $\alpha = 0.3$. The reduced capacity of walls W1 and W2 is due to premature failure of the lap splices in tension.

In determining the maximum stress that can be developed in the lap spliced bars, it was concluded that the required lap splice length should take account of the effect of the modification factor corresponding to the Class of the splice as well as taking account of the expected yield stress in a plastic hinge region. The ASCE-41 approach is mainly based on experimental data from column tests (Lynn, 2001; Melek and Wallace, 2004; Cho and Pincheira, 2006) rather than shear wall tests. In addition, the ACI seismic design provisions require lap lengths increased by a factor of 1.25.

It is proposed that the ACI -318 (2011) method for calculating the required lap splice length be used. Therefore, the required lap splice length for walls W1 and W2 are:

Required development length of straight bars in tension, $l_d = 600\ mm$;

Required lap splice length (Class B splice), $1.3l_d = 780\ mm$;

Therefore, the maximum stress that can be developed is determined as follows:

$$f_s = \frac{l_b}{l_d}.f_{y,e} = \frac{600}{780} \times 460 = 354\ MPa$$

The lateral forces associated with the flexural resistance of the walls when a tensile stress of 354 MPa is reached in the reinforcement are 92 kN and 164 kN, for walls W1 and W2, respectively. This proposed approach seems is in better agreement with the experimental results as shown in Fig. 4-10.

4.4.2. Walls WRT1 and WRT2

The CFRP retrofitted walls, WRT1 and WRT2, experienced delayed and gradual failure of bond along the lap spliced bars. Their responses displayed some ductility, reaching a displacement ductility of about 2.0; however, the responses of these walls were affected by degradation of bond along the lap spliced bars, which in turn led to a reduction of load carrying capacity (but not less than 80% of maximum load before reaching a displacement ductility of 2.0); therefore the behaviour of the retrofitted walls was modeled as deformation-controlled actions.

Several researchers have studied the effect of FRP on the bond strength of tension lap splices in columns (Priestley et al. 1996; Seible et al. 1997; Hamad et al. 2004; Harries et al. 2006; Harajli and Khalil, 2008; Thai and Pimanmas, 2009). Paterson and Mitchell (2001) tested shear walls with deficiencies in the lap splice region. It was reported that the CFRP retrofit and headed bars can be an effective approach in improving the reversed cyclic loading performance of shear walls. The experimental results of this study, on the other hand, show the positive effect of CFRP on the performance of bond and the lap splices.

Harajli (2008) studied the bond strength of lap spliced bars confined by FRP and determined an equivalent confinement factor, k_{FRP}, to be added to the confining effect of transverse reinforcement, k_{tr}, in Eq. 4-6. This confinement factor is given as:

$$K_{FRP} = \frac{E_f n_f t_f}{1000 n_s} \qquad \text{Eq. 4-12}$$

where E_f is the modulus of elasticity of the FRP, n_f is the number of FRP layers, t_f is the thickness of the FRP layers, and n_s is the number of bars being spliced at a single failure plane. Hence for specimens WRT1 and WRT2 the equivalent confinement factor is:

$$K_{FRP} = \frac{E_f n_f t_f}{1000 n_s} = \frac{82000 \times 1 \times 1}{1000 \times 2} = 41$$

In order to account for the beneficial effects of concrete cover and the confinement provided by the FRP it is necessary to adjust the ACI Code expression for tension development length to include the term K_{FRP}:

$$\frac{c_b + K_{FRP}}{d_b} = \frac{40 + 41}{20} = 4.05 \leq 2.5$$

Using the development length expression from the ACI Code, the steel stress, f_s, that can be developed, including the effects of FRP confinement can be calculated as:

$$f_s = \frac{1.1\sqrt{f_c'}\left(\frac{c_b + K_{tr}}{d_b}\right)\lambda l_d}{\psi_t \psi_e \psi_s d_b} = \frac{1.1\sqrt{30}(2.5) \times 1 \times 600}{1 \times 1 \times 0.8 \times 20} = 565\ MPa$$

It is noted that with the CFRP wrap, yielding is predicted to occur.

4.4.2.1. ASCE-41 and ASCE-41, Supplement 1

For a ductile response, ASCE-41 and the updated version, provide modeling parameters which are based on the available literature. The parameters take into account the ductility of the walls, which in turn is a function of confinement of the boundary element at the location of plastic hinging, the axial load level, and the shear capacity of the wall which depends on the amount of the transverse reinforcement and other available confinement.

The contribution of CFRP wrap and strips to the shear capacity of the walls can be approximated as:

$$V_{CFRP} = \frac{(2\, t_f w_f l_w) \times F_{t,eff}}{s_f} \qquad \text{Eq. 4-13}$$

, where t_f is the thickness of the CFRP composite layer, w_f is the equivalent width of the CFRP strips, $F_{t,eff}$ is the effective tensile strength of CFRP composite, and s_f is the spacing of CFRP strips. The multiplier, 2, is to account for CFRP layers on both sides of the walls. The effective tensile strength of the FRP is taken as 30% of the specified nominal ultimate strength (Balaguru et al. 2009).

Assuming a perfect bond between the concrete and the CFRP composite layers, the shear strength provided by CFRP is determined as:

$$V_{CFRP} = \frac{(2 \times 1.0 \times 100 \times 1200) \times (0.3 \times 834)}{250} \approx 240\ kN$$

Hence, the shear capacity of the walls is:

$$V_u = V_c + V_{CFRP} = 170 + 240 = 410\ kN$$

The global responses of the walls were dominated by flexure, and the design shear associated with nominal moment capacity of walls W1 and W2 are 118 kN and 208 kN, respectively. The required shear in both cases is considerably below the shear capacity of the walls (410 kN) and therefore, the value of $\frac{V}{t_w l_w \sqrt{f_c'}}$ (used in ASCE-41 to categorize the walls) is considered to be less than 4.0. On the other hand, the axial load is assumed to be negligible for these tests.

The modeling parameters (see Fig. 4-11) according to ASCE/SEI 41 and ASCE-41, supplement 1 are summarized in Table 4-5.

Table 4-5- ASCE-41 Nonlinear modeling parameters for flexural walls (adopted from ASCE-41, supplement 1)

	Plastic hinge rotation θ *(Rad)*		Residual Strength
Condition	**a**	**b**	**c**
Confined Boundary	0.015	0.020	0.75
Unconfined Boundary	0.008	0.015	0.60

ASCE-41(2006) recommends that when the spacing of the transverse bars does not exceed 1/3 of the effective depth of the section, the lap splice is able to sustain this stress to high ductility demand. For larger spacings, the stress that could be developed in the lap spliced bars, f_s, at a ductility of 1.0 should be reduced linearly to $0.2\,f_s$ at a ductility of 2.0.

While the CFRP retrofit has improved the performance of the bond strength along the lap splice, and has prevented the premature and brittle failure of the lap splices, the confining effect on the boundary elements is somewhat limited, resulting in a maximum displacement ductility of about 2.0.

4.4.2.2. Proposed Model

The proposed model for thin walls with short lap splices retrofitted with CFRP results in general yielding and a maximum ductility of 2.0. It is assumed that the CFRP retrofit does not affect the flexural stiffness of the walls significantly; therefore, the stiffness of WRT1 and WRT2 remain the same as the stiffnesses for W1 and W2.

According to ASCE-41, the plastic hinge length can be estimated as $0.5\,l_w$, that is, $0.5 \times 1200 = 600\ mm$. Hence the tip deflection due to hinging can be determined from the rotation, θ, of the plastic hinge as:

$$\Delta = \theta \times \left(3250 - \frac{60}{2} \right)$$

The resulting backbone relationships for WRT1 and WRT2 are shown in Fig. 4-12. It is noted that the stiffness and resistance proposed by ASCE-41 are over-estimated. The proposed model incorporates degradation of the lap splice and can reasonably describe the response of these CFRP retrofitted walls.

The plastic hinge length could significantly affect the global response of the walls. It should be noted that in the presence of insufficient lap splice bars at the location of plastic hinging, the potential hinging length is over-estimated in $0.5\,l_w$. More experimental results are needed for more accurate predictions.

4.4.3. Walls WRP1 and WRP2

WRP1 and WRP2 were assumed to have a properly confined lap splice region with the help of additional transverse reinforcement and fibre-reinforced concrete jacketing, which successfully shifted the potential plastic hinging to beyond the jacket. For these walls, no lap splice failure was observed in the experiments, and therefore, no lap splice model was considered due to the excellent confinement provided.

However, the flexural yielding of the bars beyond the Self-Consolidating Concrete (SCC) jacket, as well as potential bar pull-out at the interface of wall and the foundation is an important behavioural feature. The responses of repaired walls were dominated by flexural yielding followed by crushing of the concrete beneath the CFRP. The CFRP experienced rupturing at higher ductility levels.

Assuming a perfect shear connection between the existing web of the walls and the added concrete jacket, the nominal moment capacity of the jacketed region for WRP1 and WRP2 is 750 kNm and 1290 kNm, respectively. The flexural capacity of the SCC jacket retrofitted section is significantly more than the shear associated with plastic hinging of the critical section beyond the jacket (471 kNm for WRP1 and 838 kNm for WRP2).

The strains measured along the lap spliced bars in the confined section indicate that no significant yielding occurred in this region, and therefore, it was concluded that the deformations of the new jacket remained essentially elastic. Hence, elastic deformations of this portion are included in the prediction of the tip displacement. Hence, the new retrofitted section will increase the stiffness of the wall.

Fig. 4-13 shows the response of the walls retrofitted with SCC jacketing, as well as the predictions using the ASCE/SEI 41 (2006) recommendations for WRP1 and WRP2. A better fit for the initial loading stiffness was achieved when the stiffness was reduced to 30% of the gross stiffness. The modeling parameters are in good agreement with experimental results.

4.5. Predicted Responses of Wall Specimens

Fibre element models were developed using the material models described in section 4-2. For the predictions, the analytical model was subjected to the same deformation history as the experiments.

In the experiments, the loading was applied in two stages: the pre-yielding stage which was load-controlled, and the post-yielding stage, which was displacement controlled. For analysis purposes, however, the displacement control integrator was used, with corresponding displacements. Fig. 4-14 describes the displacement protocols that were used for analysis.

The Analytical model for the walls is shown schematically in Fig. 4-15. The flexural responses of the walls were modeled using displacement beam-column elements in OpenSees. The translational shear spring takes into account shear deformations, and the rotational spring accounts for bond slip at the base of the walls.

4.5.1. Displacement-Based Beam-Column Element

The flexural response of the walls was modeled with a displacement-based beam-column element. The height of the wall is divided into six beam-column elements to accurately model the flexural response of the walls. The displacement based beam-column element is sensitive to the number of sub elements, and using a “finer mesh” is necessary for accurate predictions of the internal forces and reactions. The size of the sub elements is kept constant (500 mm long) except for the element near the loading point where a longer element was used (725 mm). The nonlinear deformations in this region are limited and they do not affect the global response significantly.

4.5.2. Translational shear spring

The translational shear spring is calibrated to predict the uncoupled shear deformations of a wall.

Sozen and Moehle (1993) have proposed the following equations for the shear spring:

$$\upsilon_c = 4\sqrt{f_c'}\sqrt{1+\frac{f_o}{4\sqrt{f_c'}}} \quad (psi)$$ Eq. 4-14

$$\gamma_c = k\frac{\upsilon_c}{G_c}$$ Eq. 4-15

where f_o is the axial stress, G_c is taken as $\frac{E_c}{2(1+\upsilon)} \approx 0.4E_c$ and k is the cross-sectional shape factor for shear (1.2 for a rectangular section). NIST (2010) limits the shear stress in the walls to 50% of nominal shear capacity determined according to ACI 2008, or $3\sqrt{f_c'}$ (psi), whichever is smaller.

The nominal shear capacity of the wall can be determined as:

$$V_c = A_{cv}(\alpha_c\sqrt{f_c'}) = (1200\times150)\times\left(0.17\sqrt{31}\right) = 170\ kN$$

According ti NIST (2010), $u_c = 1.38\ MPa$. Therefore, the shear strength corresponding to the shear cracking is determined as: $V_c = 207kN$ which is greater than 50% of the nominal shear strength (using ACI equation). As a result, the cracking shear strength is limited to $V_c = 85\ kN$. The corresponding shear strain is calculated as 0.00013. The initial slope will be 12410 MPa. The shear strength is capped to the nominal shear strength of the section (170 kN). Failure in shear is not modeled.

4.5.3. Bond-Slip Spring

An elastic rotational spring is assumed to adequately model the bond-slip response of the walls. Assuming a bond stress of $6\sqrt{f_c'}$ (psi unit), the rotational stiffness of the bond-slip spring can be determined based on the moment-curvature analysis of the wall section at its base:

$$k_{slip} = \frac{48\sqrt{f_c'}}{d_b f_s}\frac{M_y}{\Phi_y}$$ Eq. 4-16

For W1 and W2, the rotational stiffness of the slip spring is 363521kNm and 611703 kNm.

4.5.3.1. W1 and W2

For walls W1 and W2, it is assumed that the maximum stress that can be developed in the flexural reinforcing bars at the section with lap spliced bars is 285 MPa (see section 4.5.1-c). Fig. 4-16 shows the fibre-element model prediction against test results. It is assumed that the stress drops to a low value of 70 MPa after reaching it maximum capacity of 285 MPa to resemble the failure of the lap splice.

4.5.3.2. WRT1 and WRT2

For WRT1 and WRT2, it is assumed that the CFRP prevents the premature failure of the lap splices. However, degradation of bond is predicted between displacement ductilities of 1.0 and 2.0. The Hysteretic Material in OpenSees was calibrated to account for this degradation.

Fig. 4-17 shows the fibre-element model predictions versus the experimental results. The models are in good agreement with test results.

4.5.3.3. WRP1 and WRP2

The results of predictions using the fibre-element model are compared with the experimental results in Fig. 4-18. The reinforced concrete jacketing was designed such that flexural yielding would occur without failure of the lap splices and significant yielding occurred in the region just above the jacket. The predictions are in good agreement with the experimental results.

4.6. Fibre-Element Predictions of Walls Tested by Paterson and Mitchell (2003)

Two pair of slender shear walls were designed and tested by Paterson and Mitchell (2001, 2003) at McGill University. These walls were representative of a core wall of an existing structure in Berkeley, CA, built in the 1960's. The walls tested had a thickness of 300 mm, and a length of 1200 mm. The two sets of walls were similar except for their heights ($W1_{Pat}$: 3400 mm and $W2_{Pat}$: 3900 mm) and the location of lap splices. Fig. 4-19 shows detailing of the wall specimens. These walls were

tested before and after retrofit to study the reversed cyclic responses and the effectiveness of the retrofit.

4.6.1. As-Built Condition

Walls W1 and W2 were tested in their as-built condition. $W1_{Pat}$ had a total height of 3400 mm with lap splices (900 mm long for No. 25 flexural bars) at the potential plastic hinge region (at the base of the walls). W2 had a total height of 3900 mm with the lap splices starting 600 mm above the critical section at the base of the wall. This location of lap splice was chosen to simulate lap splices located in a region of high moment, but above the critical section, representing the lap splice at the first floor level. Both walls had identical cross sectional detailing as shown in Fig. 4-19(c).

In their as-built condition, these walls had better detailing than the walls tested in this study, with the thickness of the walls being 300 mm and the transverse reinforcement anchored with 90° bend hooks at the ends of the walls. The average compressive strength for $W1_{Pat}$ and $W2_{Pat}$ was 25.9 MPa and 33.4 MPa, respectively. The average yield stress for main flexural bars (No. 25) was 425 MPa.

The lap splice length for the No. 25 bars for both walls was 900 mm ($l_d \approx 36d_b$). The lap splice lengths in the original structure ($l_d \approx 24d_b$) were modified by the ratio of the yield stress of the steel reinforcement used in the experiments divided by the yield stress of the bars in the original structure.

The predicted nominal flexural resistance of $W1_{Pat}$ and $W2_{Pat}$, neglecting any strain hardening, is 644 kNm. Wall $W1_{Pat}$ was able to achieve yielding; however, its ductility was limited due to failure of the lap splices occurring at a ductility level of 1.5. The $36d_b$ lap splice length resulted in improved performance over the $30d_b$ lap splice length used in this experimental study. This longer lap splice length was able to develop yielding, but had limited ductility. The response of wall W2 was ductile and the wall could sustain its full capacity until a displacement ductility of

4.0 was achieved (when the load dropped to 80% of maximum load). The $36d_b$ lap splice length provided at a section above the base proved to be adequate to develop yielding and considerable ductility.

4.6.2. Retrofitted Walls

Two different retrofit techniques were used in order to improve the responses of the walls. The average compressive strengths of the concrete in W1 and W2 were 26.1 and 31.0 at the time of testing.

For W1R, the retrofit consisted of a combination of an added reinforced concrete collar at the location of the lap splices together with CFRP strengthening above the collar. The added reinforced concrete collar was attached to the original concrete using headed bars and additional pins were used at the ends of the wall to improve confinement (see Fig.4-20). This technique was successful in preventing the failure of the lap splices, and the wall could maintain its capacity up to a displacement ductility of 3.8. The retrofit of the lap splice region shifted the plastic hinge location to a location above the added concrete collar.

For W2R, a combination of headed bars and CFRP strips were used for the retrofit in order to improve the shear strength of the wall, as well as providing confinement over the lap splices. The CFRP wrap was epoxied to the concrete and additional anchorage was provided using headed bars. This wall was able to achieve a high displacement ductility level of 6.3, exhibiting considerable yielding at the base of the wall.

4.7. Predicted Responses of Walls tested by Paterson and Mitchell (2003)

The flexural responses of the walls were modeled using displacement beam-column elements in OpenSees. The translational shear spring takes into account shear deformations, and the rotational spring accounts for bond slip at the base of the walls. The concrete material parameters used in the fibre element model are given in Table 4-6. The reinforcing steel material properties are given in Table. 4-7.

Table 4-6- Concrete-07 calibrated parameters

Wall	f_c'	ε_c'	E_c	f_{sp}	$0.40\sqrt{f_c'}$	ε_t	x_p	χ_n	r
	MPa	≈	MPa	MPa	MPa	≈			
W1	25.9	0.002	27100	3.3	2.0	0.0003	2	2.3	3.1
W1R	26.1	0.002	27100	3.4	2.0	0.0003	2	2.3	3.1
W2	33.4	0.002	27100	3.5	2.3	0.0004	2	2.3	4.5
W2R	31	0.002	27100	4.1	2.2	0.0004	2	2.3	4.1

The predicted shear-displacement responses are compared with the experimental responses in Figs. 4-21 and 4-22. For all of the specimens, the steel was predicted to yield, including the as-built wall W1. The fibre element model is able to reasonably predict the reversed cyclic loading response of the walls tested by Paterson and Mitchell (2001).

Table 4-7- Hysteretic material calibrated parameters

	No. 25		**No. 15**		**No. 10**	
$\varepsilon_1^+, \sigma_1^+$ *	0.0022	61	0.0022	65	0.0022	46
$\varepsilon_2^+, \sigma_2^+$	0.05	95	0.05	100	0.05	65
$\varepsilon_3^+, \sigma_3^+$	0.06	10	0.06	10	0.06	10
$\varepsilon_1^-, \sigma_1^-$	-0.0022	-61	-0.0022	-65	-0.0022	-46
$\varepsilon_2^-, \sigma_2^-$	-0.05	-95	-0.05	-100	-0.05	-65
$\varepsilon_3^-, \sigma_3^-$	-0.06	-10	-0.06	-10	-0.06	-10
$Pinch_x$	0.6		0.6		0.6	
$Pinch_y$	0.4		0.4		0.4	
d_1	0		0		0	
d_2	0		0		0	

* σ is in ksi units

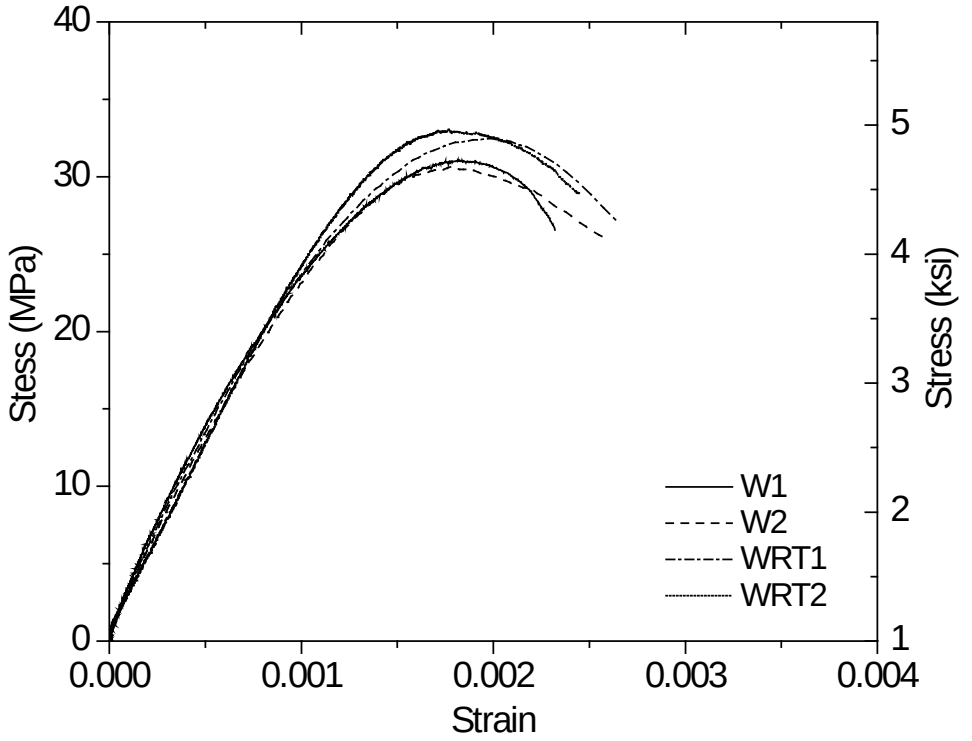

Fig. 4-1- Stress-strain response of concrete

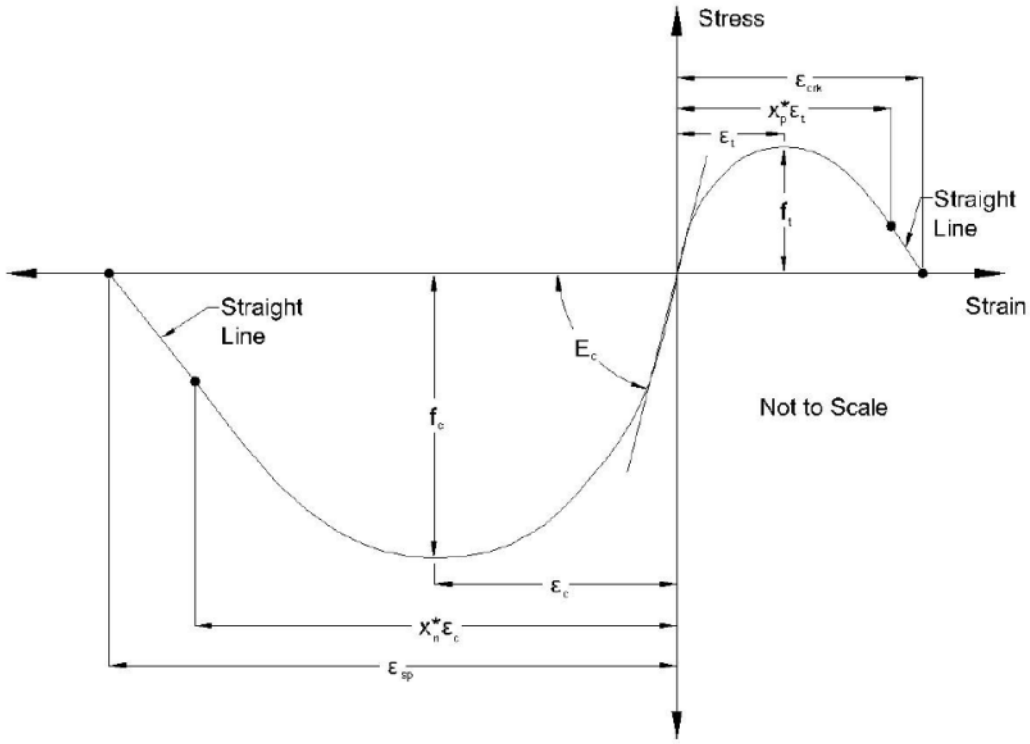

Fig. 4-2- Simplified Chang and Mander envelope for concrete (adapted from OpenSees manual, 2012)

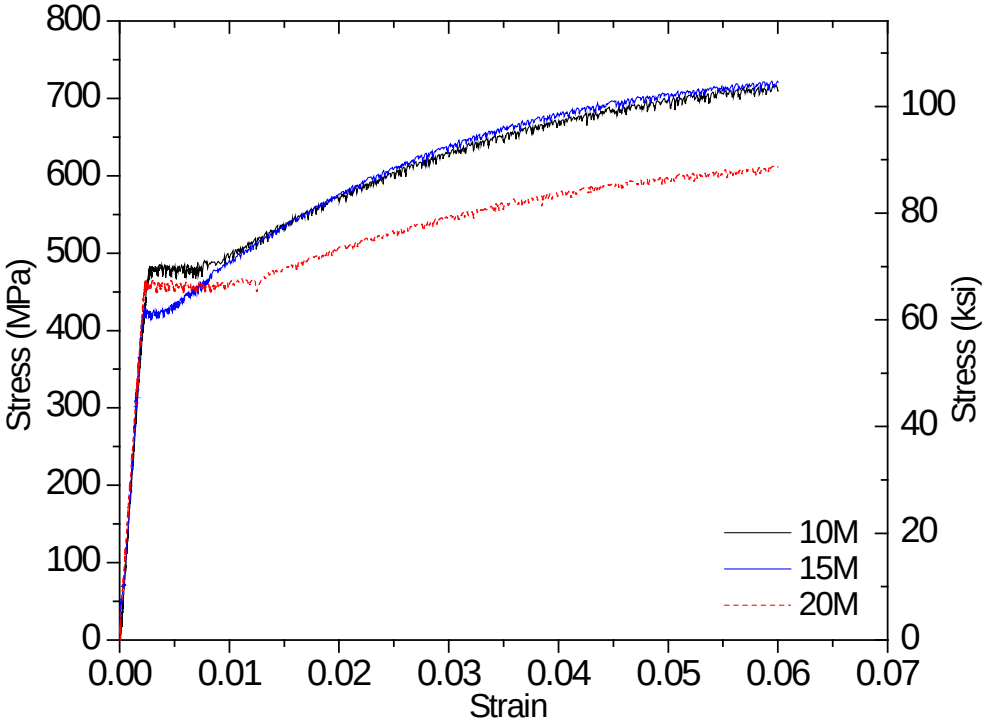

Fig. 4-3- Stress-strain relationship for reinforcing steel

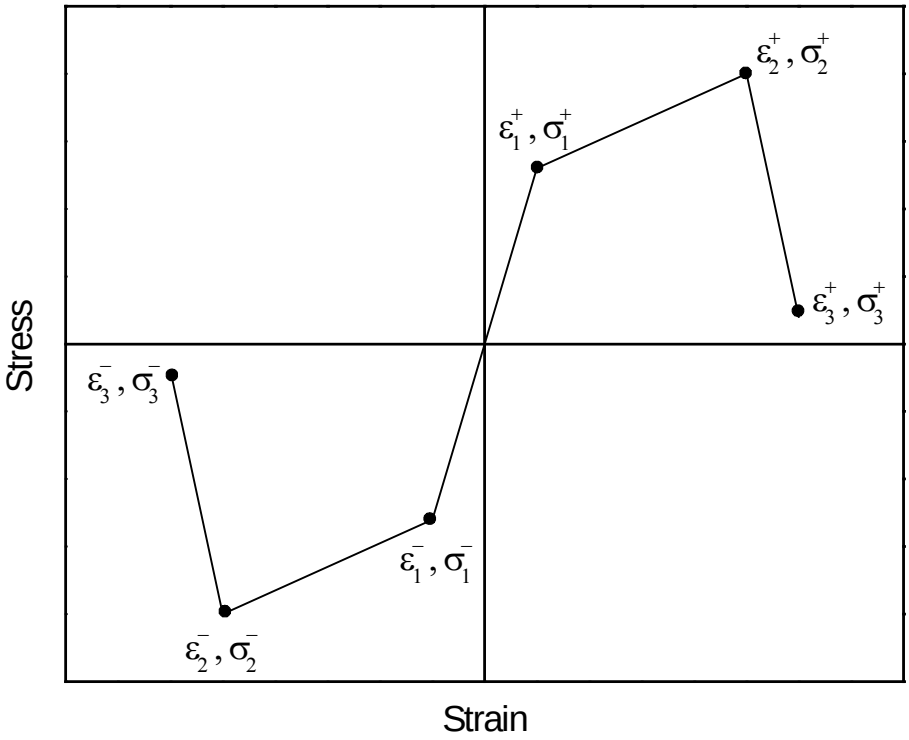

Fig. 4-4- Stress-strain relationship for steel (Hysteretic Material Model)

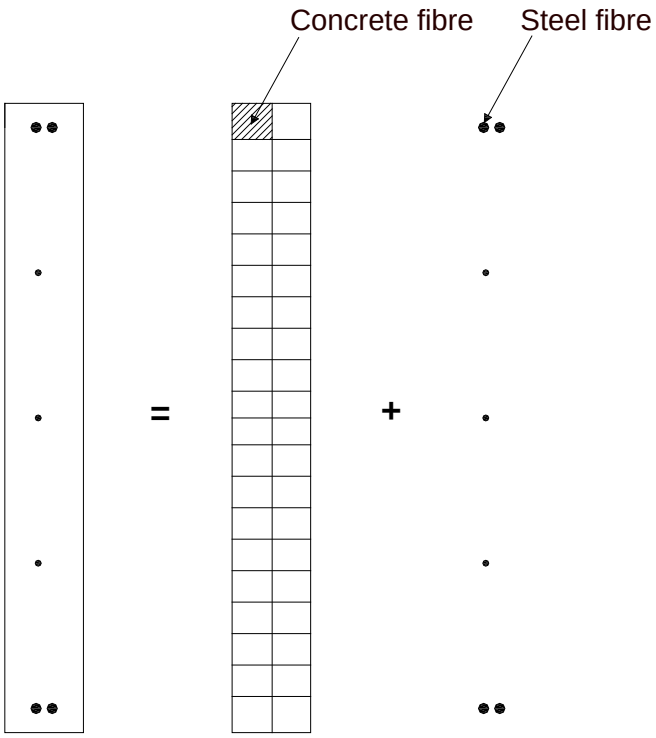

Fig. 4-5- Cross-sectional mesh(approximate 75 mm by 75 mm mesh arrangement)

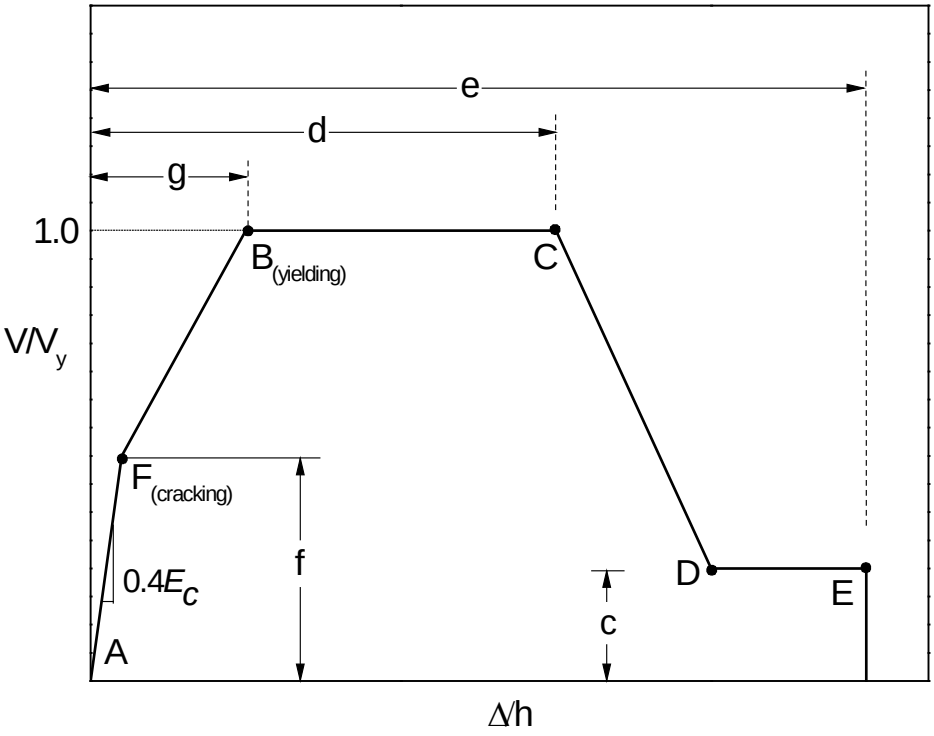

Fig. 4-6- Generalized Shear Model for shear walls (adapted from ASCE-41 supplement 1 and Elwood et al. 2007)

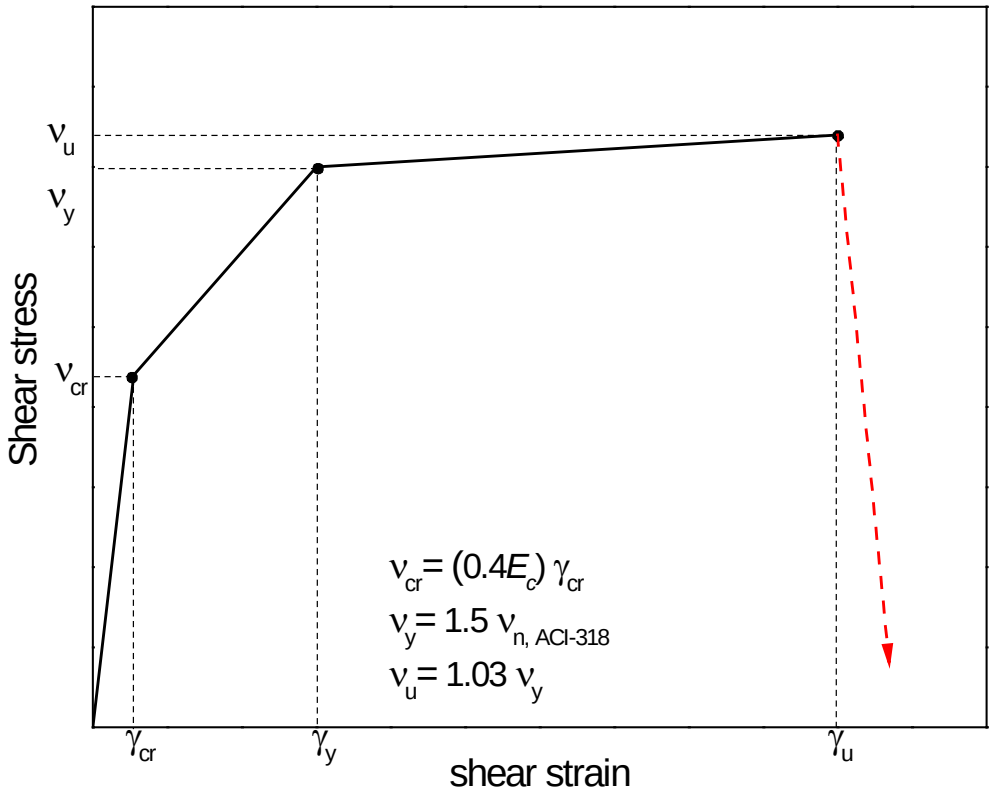

Fig. 4-7- Generalized Shear Model for shear walls (adapted from NISTGCR10-917-8, 2010)

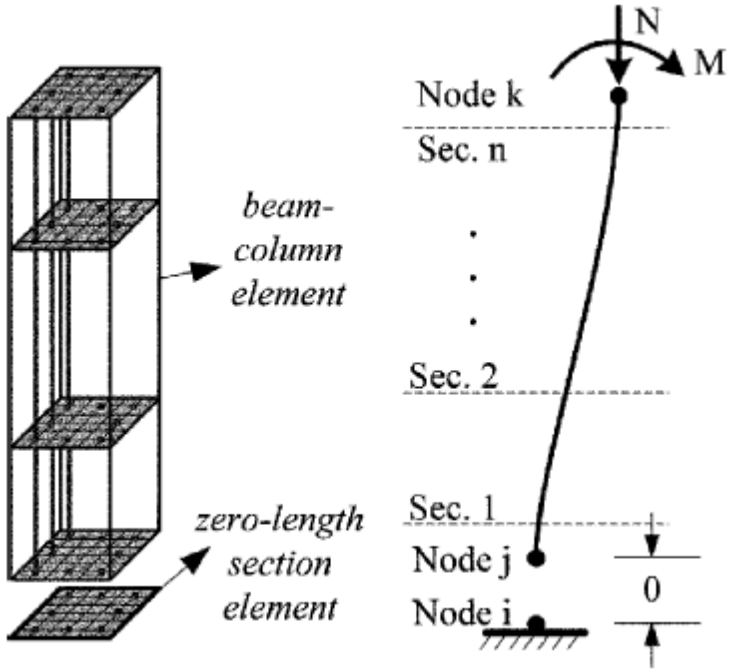

Fig. 4-8- Zero length section element used at the base for modelling the bar slip (adapted from Zhao and Siritharan, 2007)

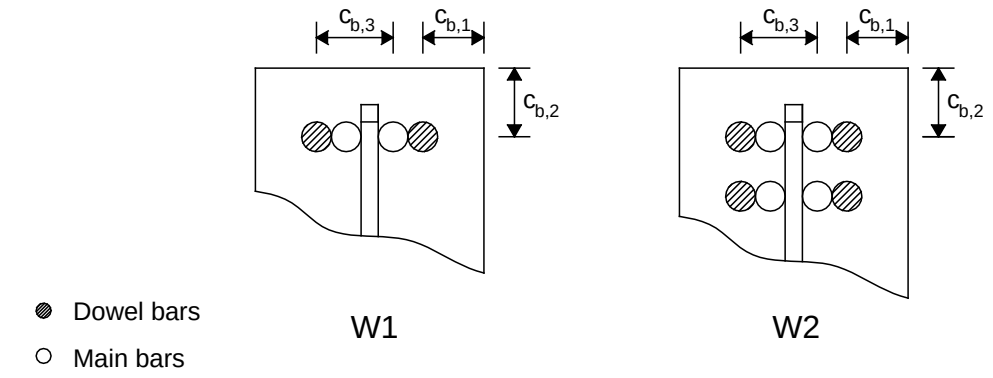

Fig. 4-9- Details of lap spliced bars

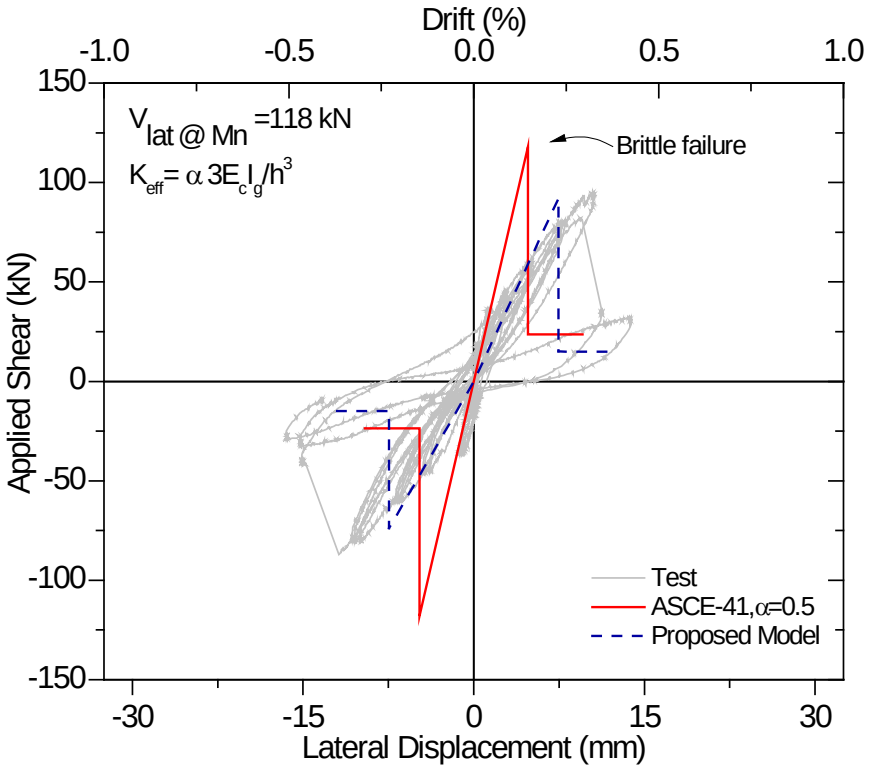

a) W1

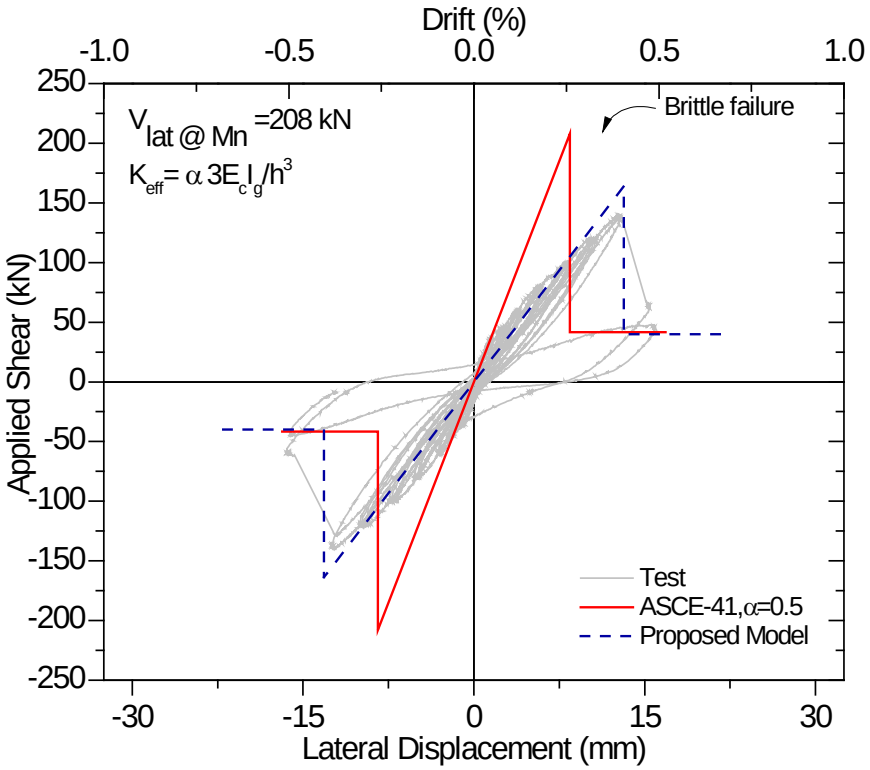

b) W2

Fig. 4-10- ASCE-41 backbone prediction, proposed backbone prediction and test results

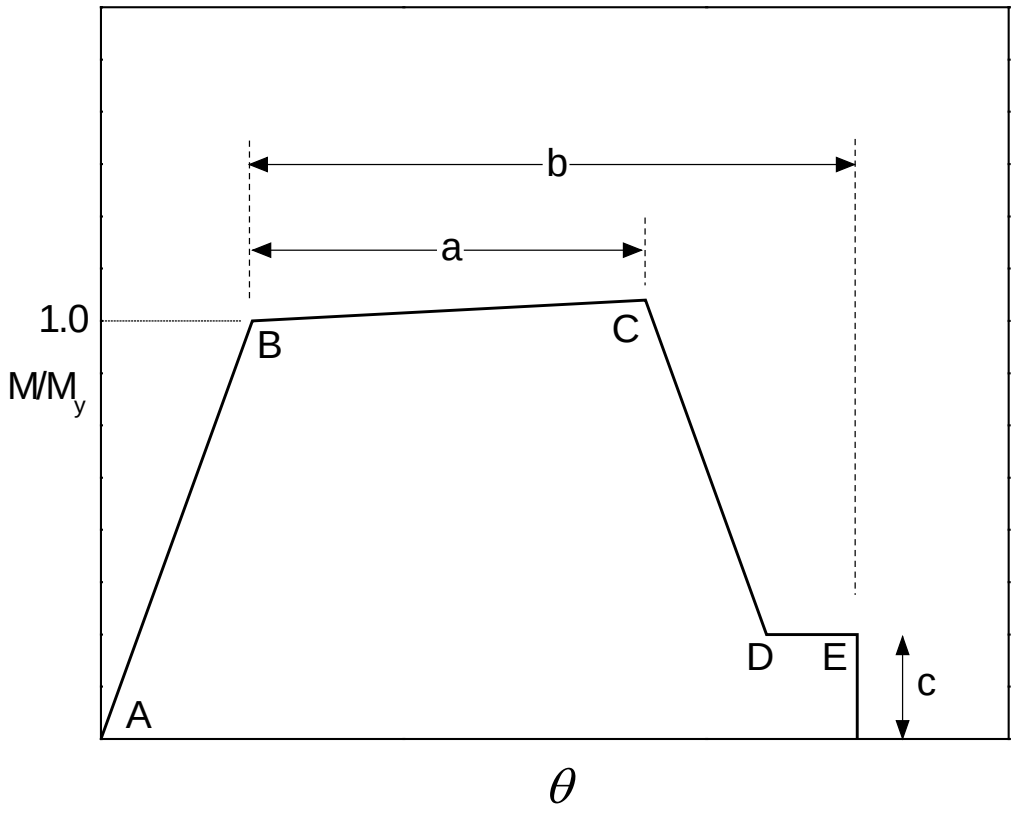

Fig. 4-11- Generalized Force-Deformation Relations (Adapted from ASCE-41)

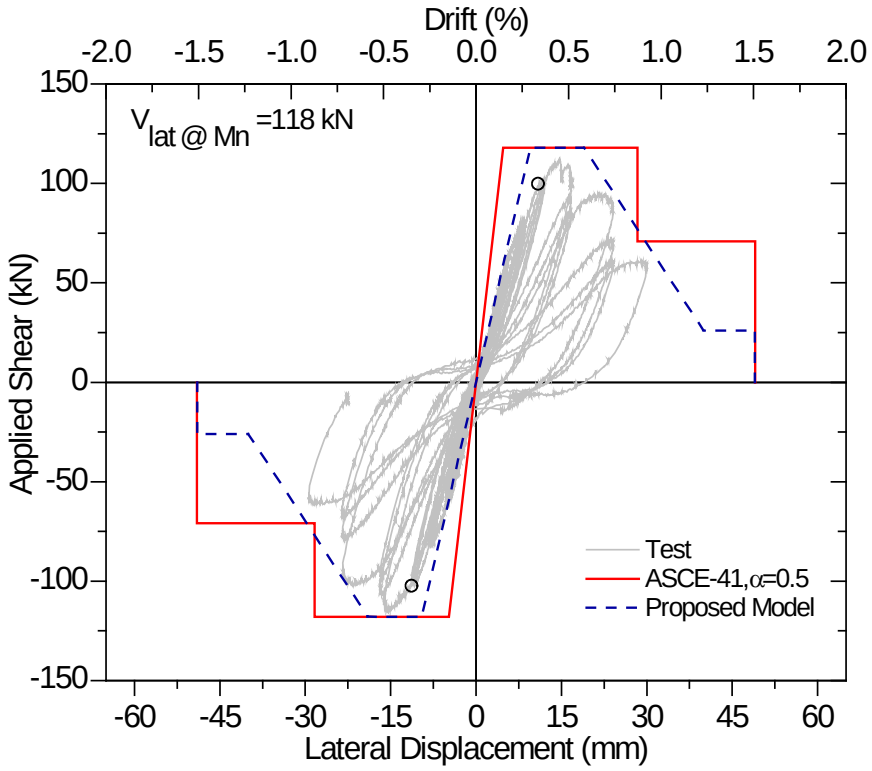

a) WRT1

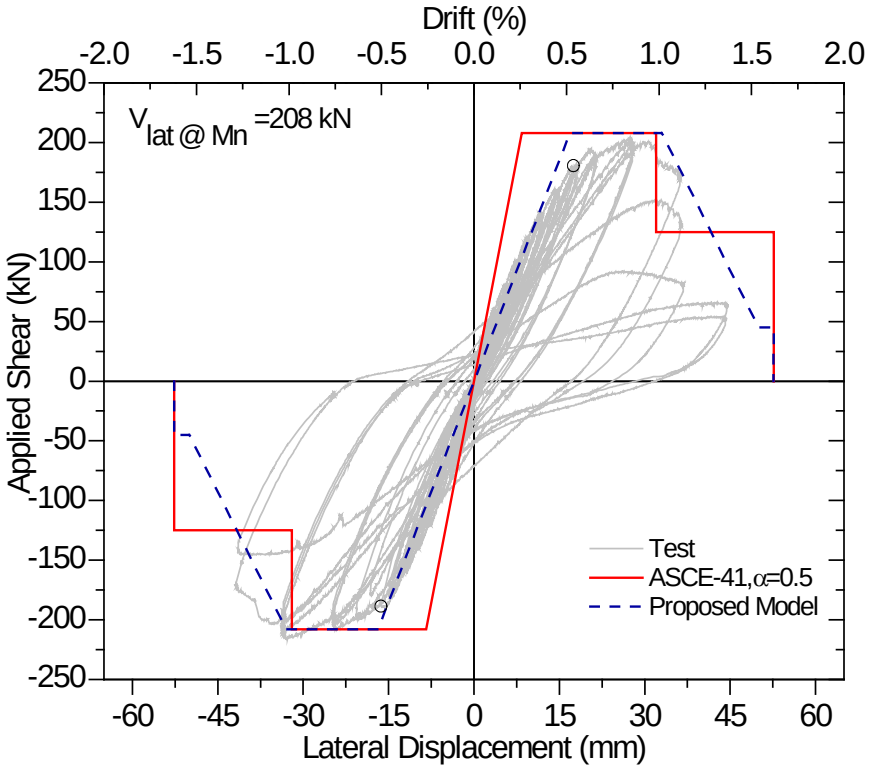

b) WRT2

Fig. 4-12- ASCE-41 backbone prediction, proposed backbone prediction & test results

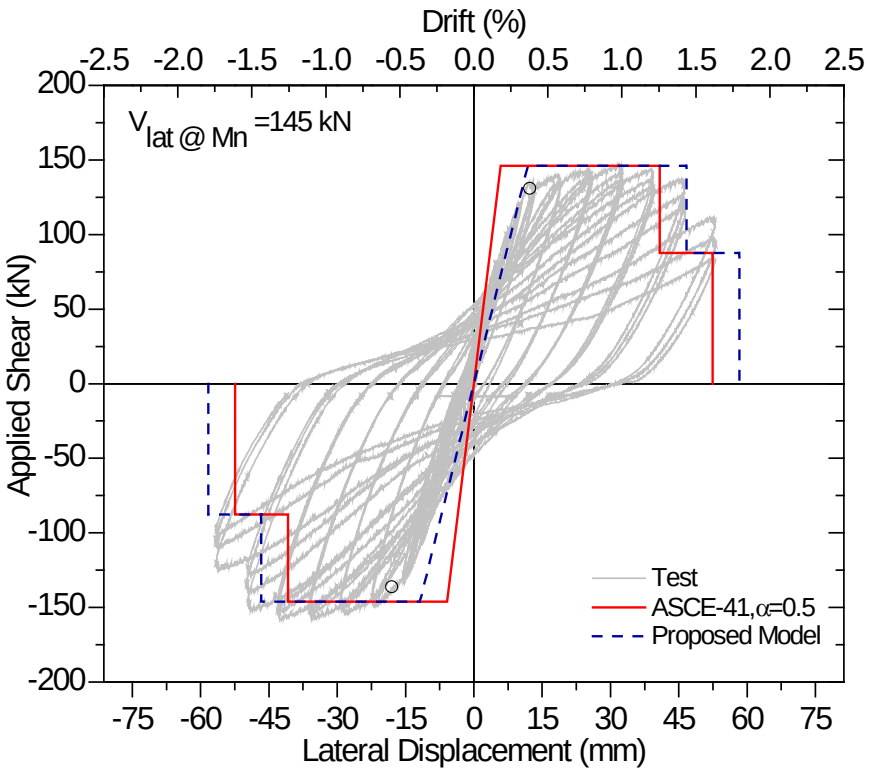

(a) WRP-1

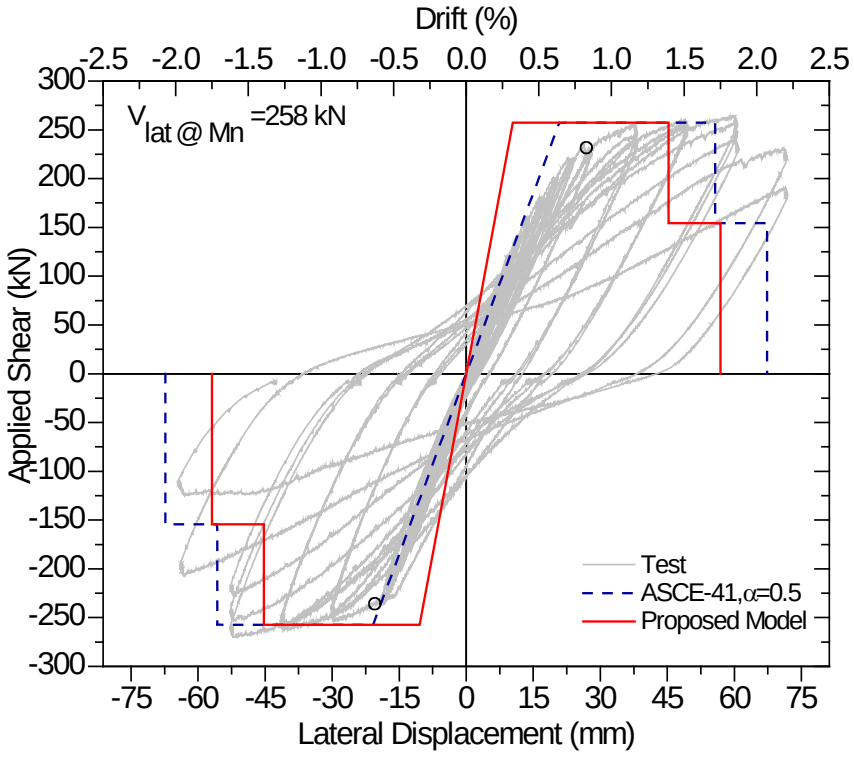

b) WRP2

Fig. 4-13- ASCE-41 backbone prediction, proposed backbone prediction and test results

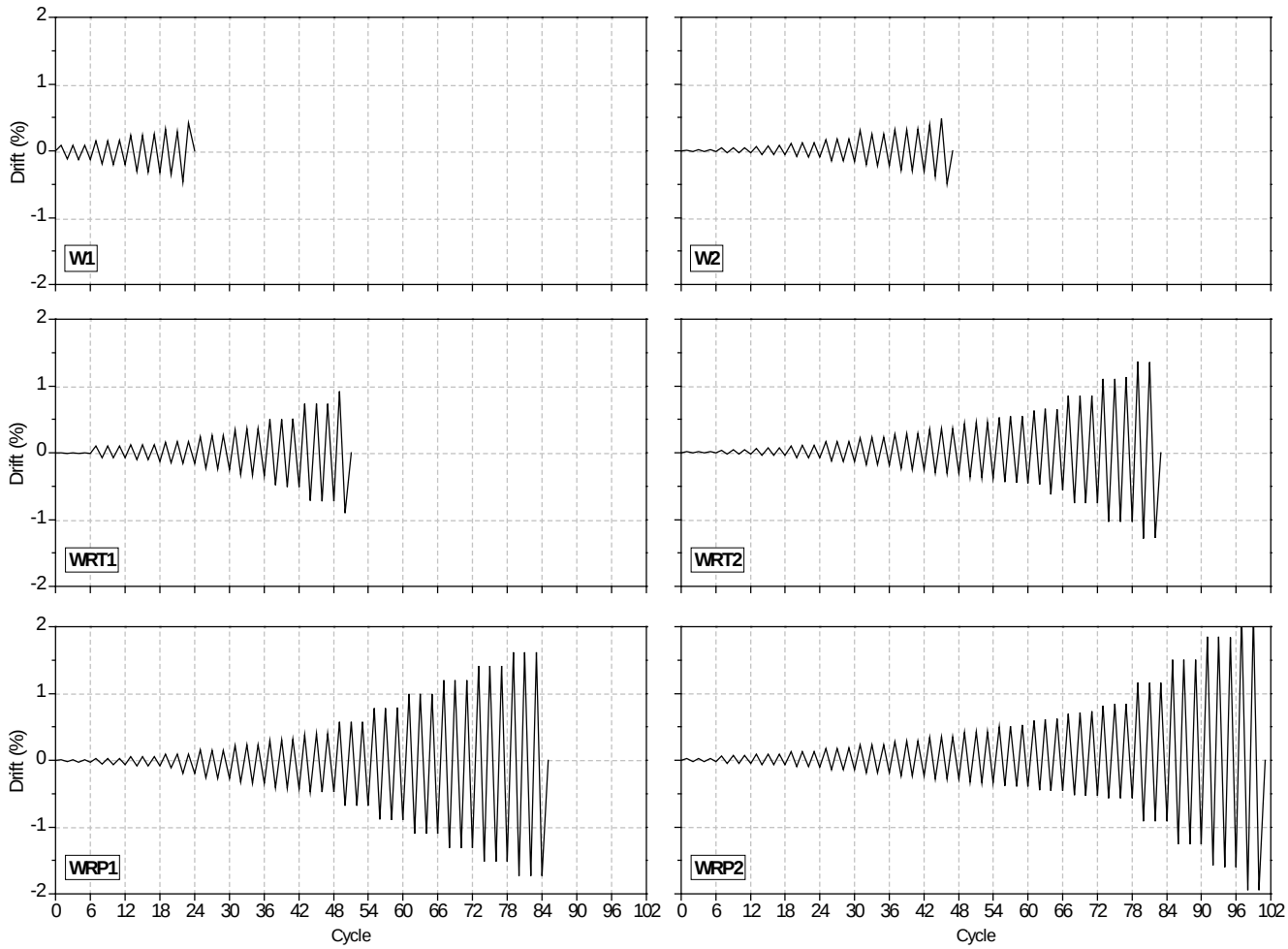

Fig. 4-14- Displacement histories for wall models

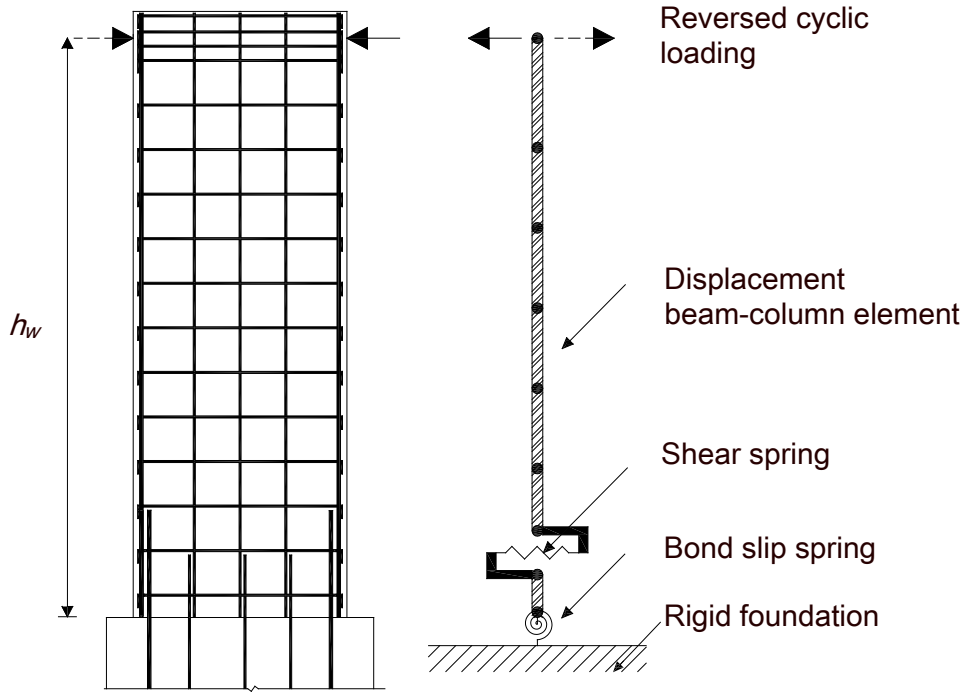

Fig. 4-15- Mathematical model for reversed-cyclic loading of walls

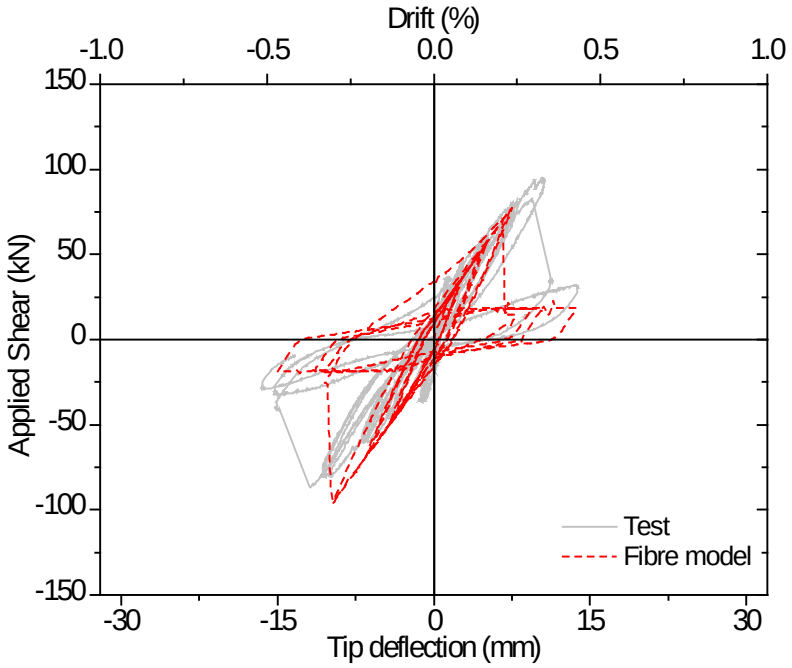

a) W1

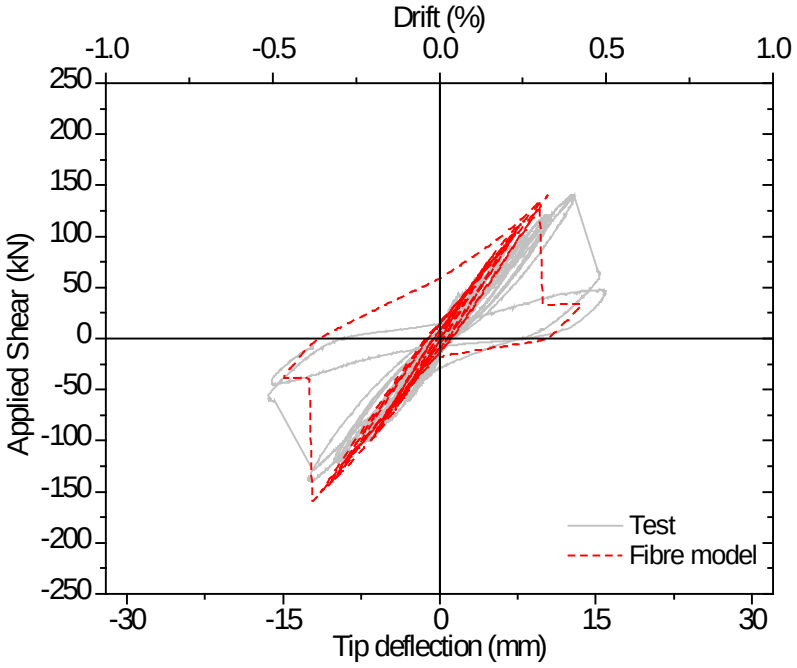

b) W2

Fig. 4-16- Fibre element analytical model versus Experimental results

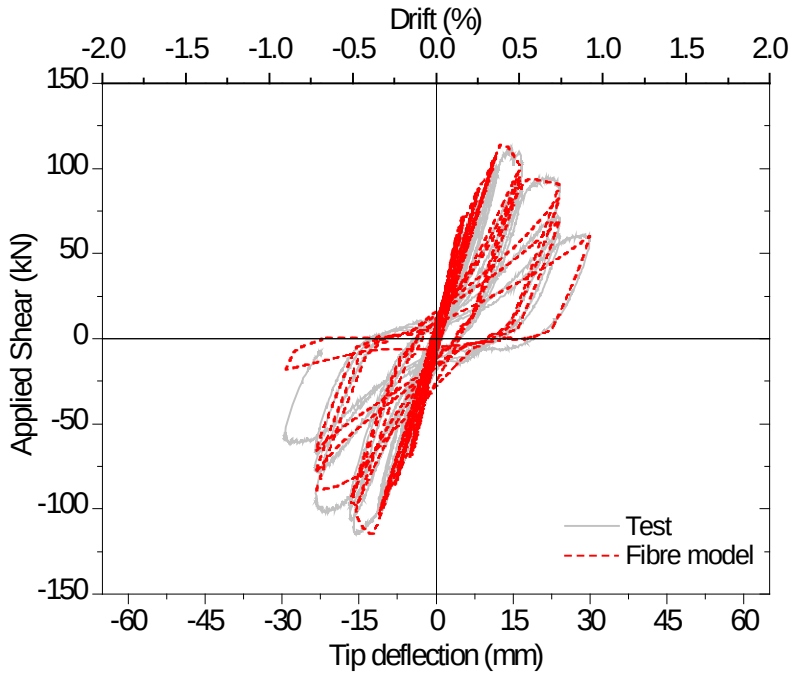

a) WRT1

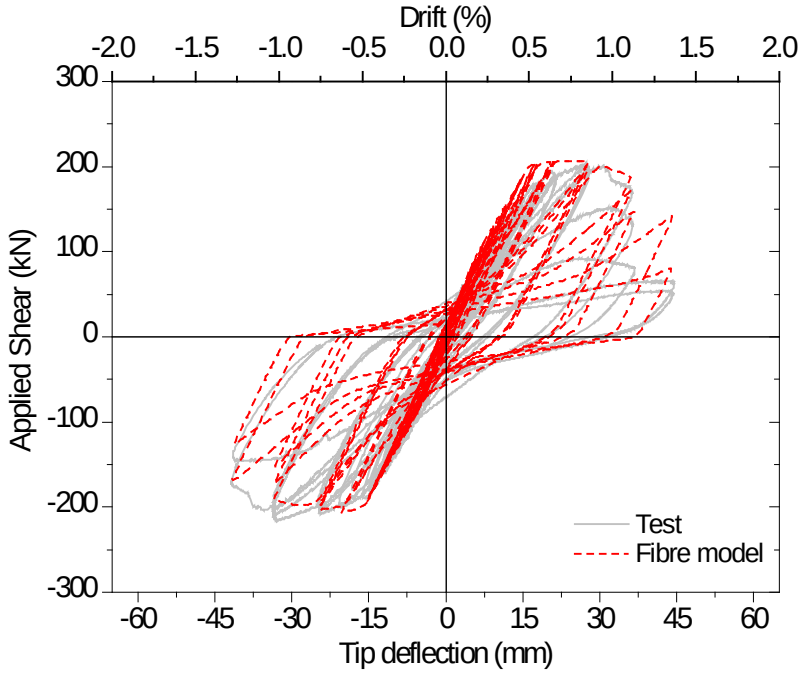

b) WRT2

Fig. 4-17- Fibre element analytical model versus Experimental results (CFRP Retrofitted)

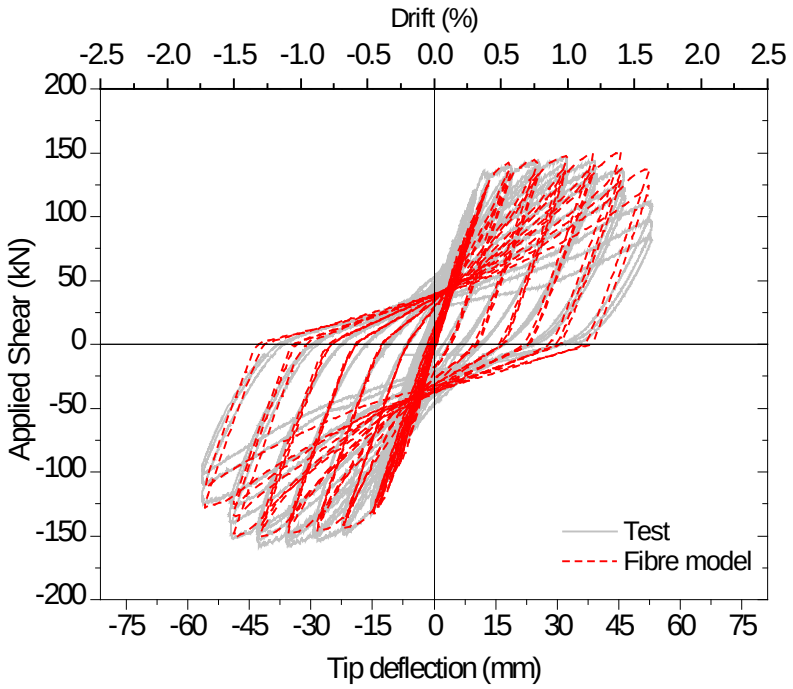

a) WRP1

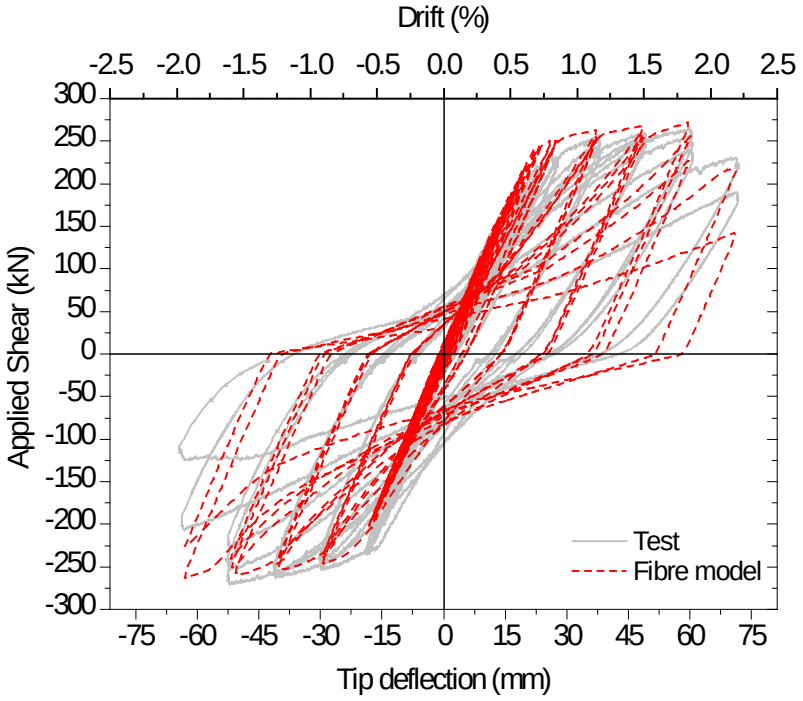

b) WRP2

Fig. 4-18- Fibre element analytical model versus Experimental results (SCC Jacket Retrofitted)

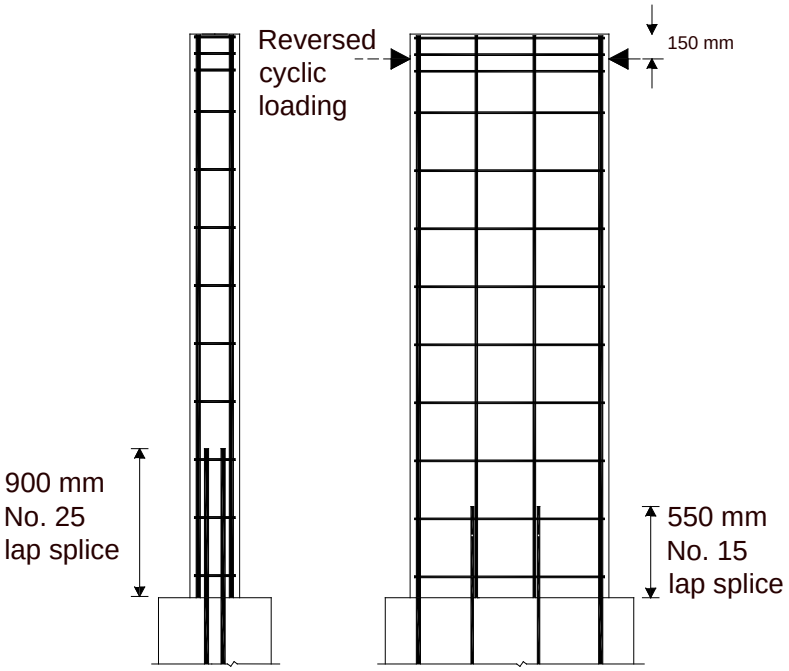

a) $W1_{Pat}$

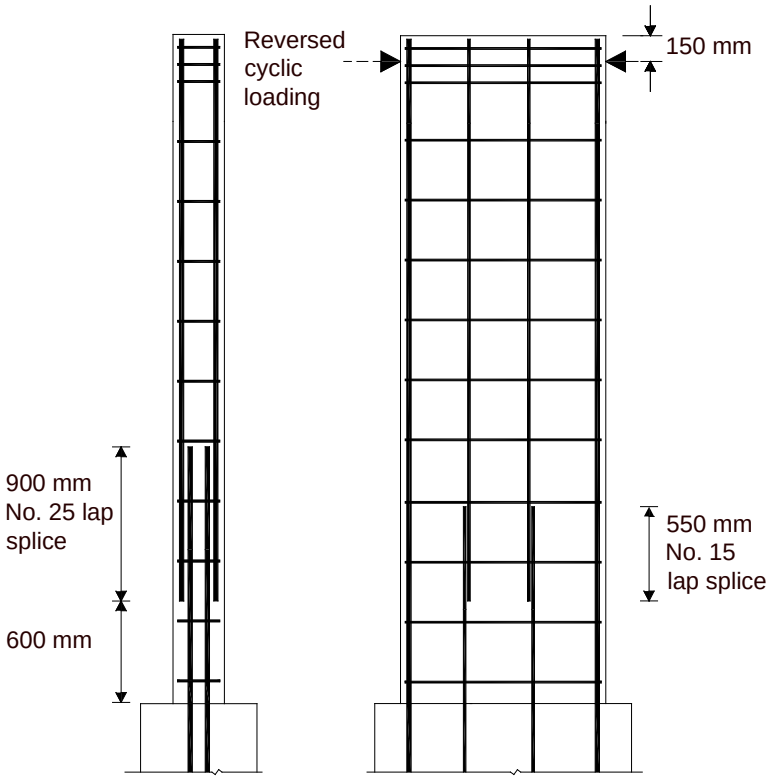

b) $W2_{Pat}$

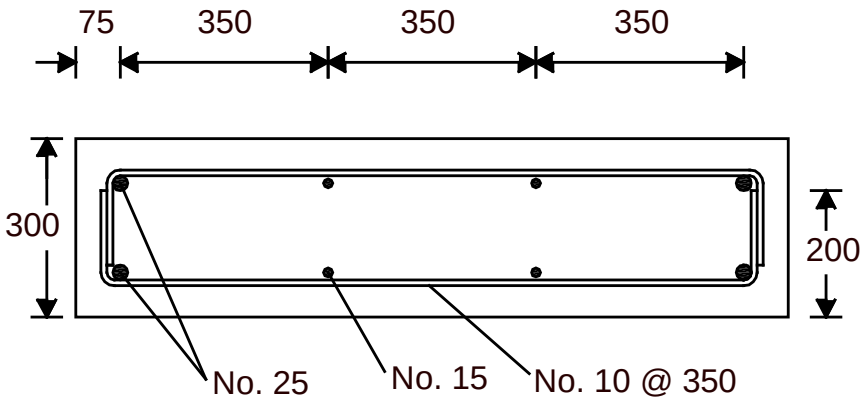

c) Cross-sectional details of the walls

Fig. 4-19- Details of walls $W1_{Pat}$ and $W2_{Pat}$ (adapted from Paterson and Mitchell, 2003)

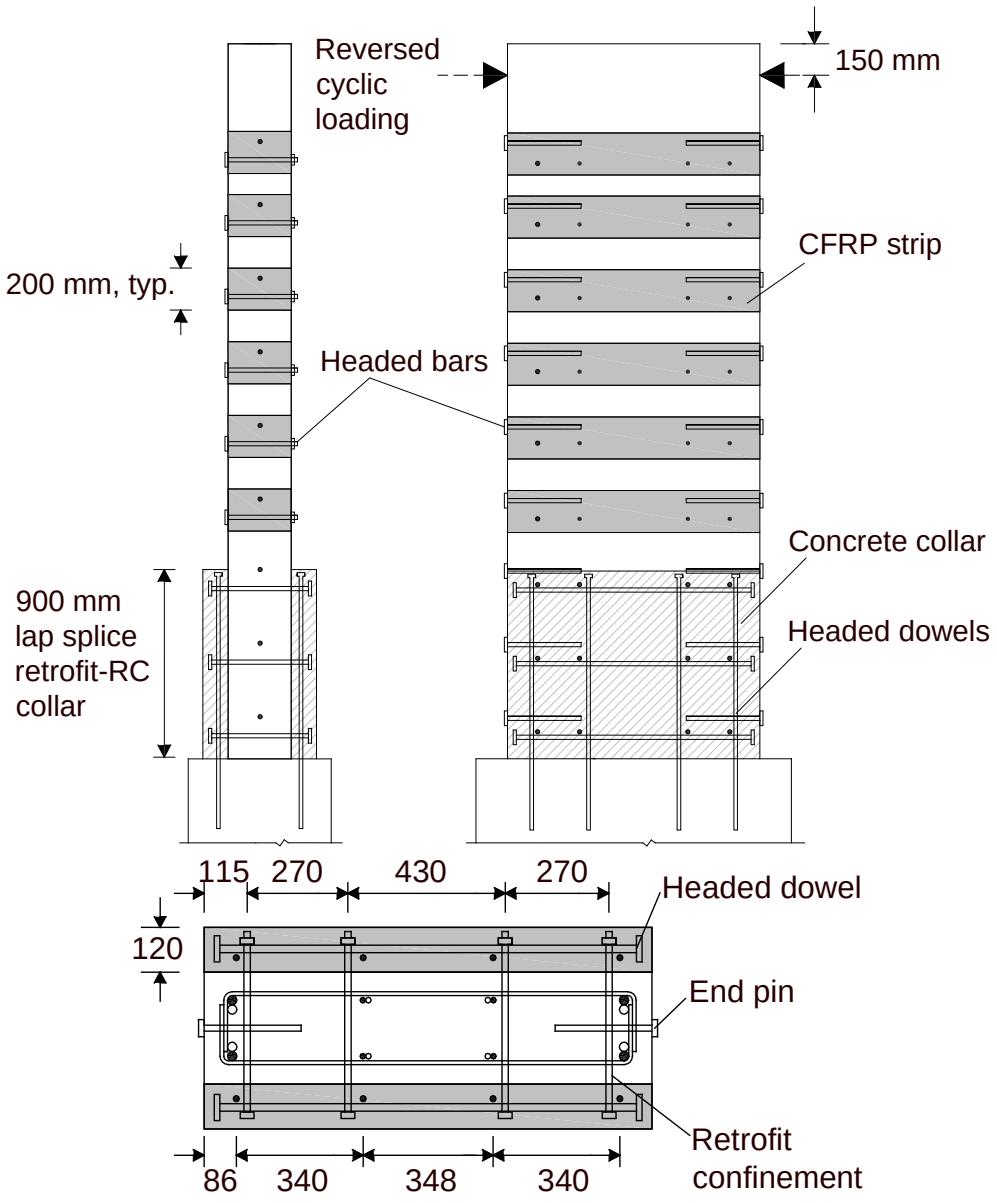
Reversed
cyclic
loading
150 mm
CFRP strip
200 mm, typ.
Headed bars
Concrete collar
Headed dowels
900 mm
lap splice
retrofit-RC
collar
115
270
430
270
Headed dowel
120
End pin
Retrofit
confinement
86
340
348
340

a) $W1R_{Pat}$

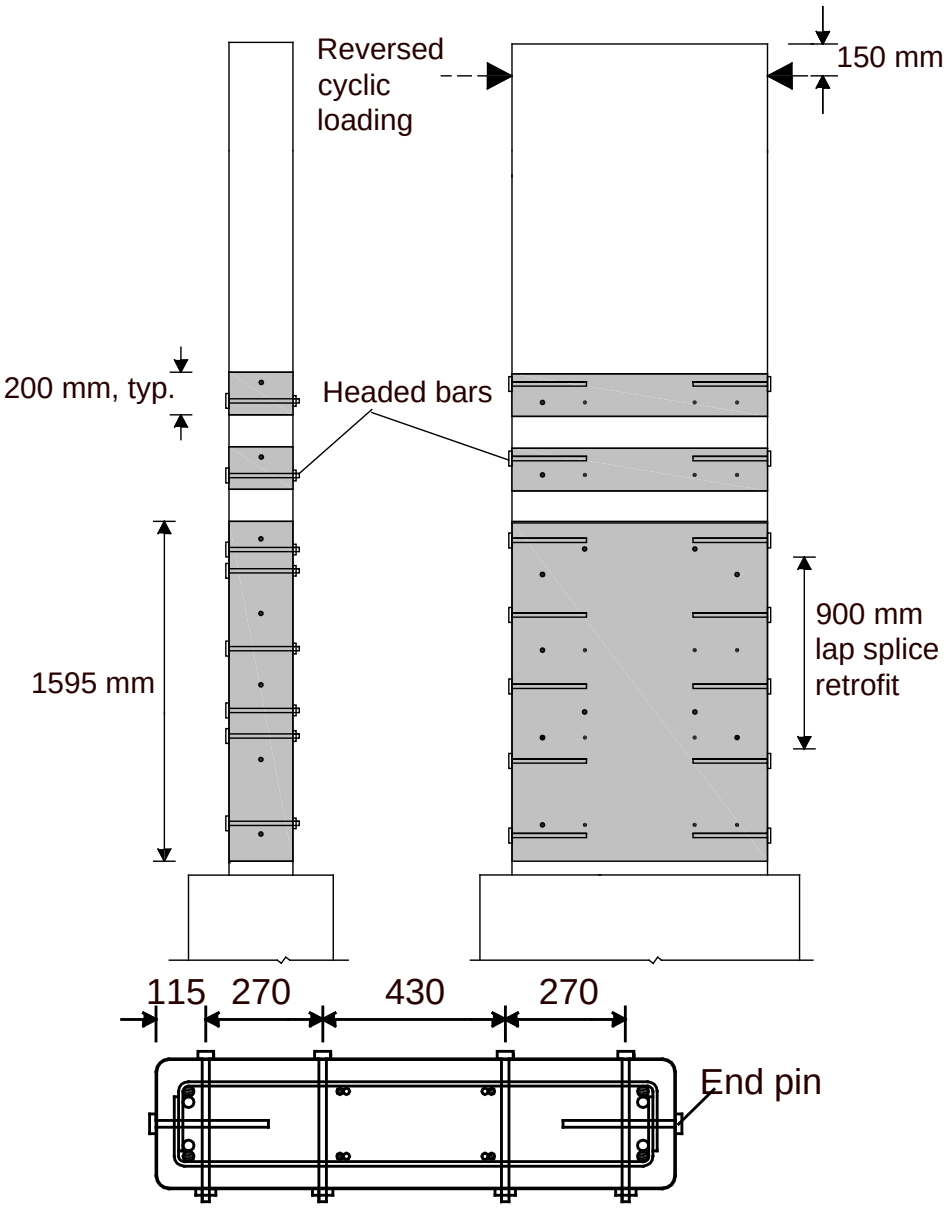

b) W2R

Fig. 4-20- Details of walls $W1R_{Pat}$ and $W2R_{Pat}$ (adapted from Paterson and Mitchell, 2003)

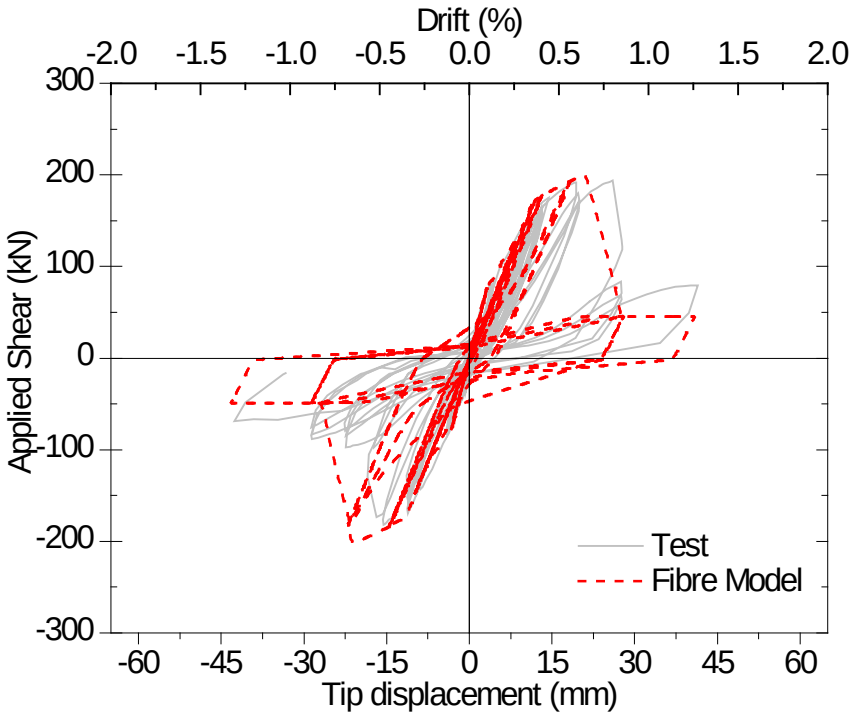

a) W1

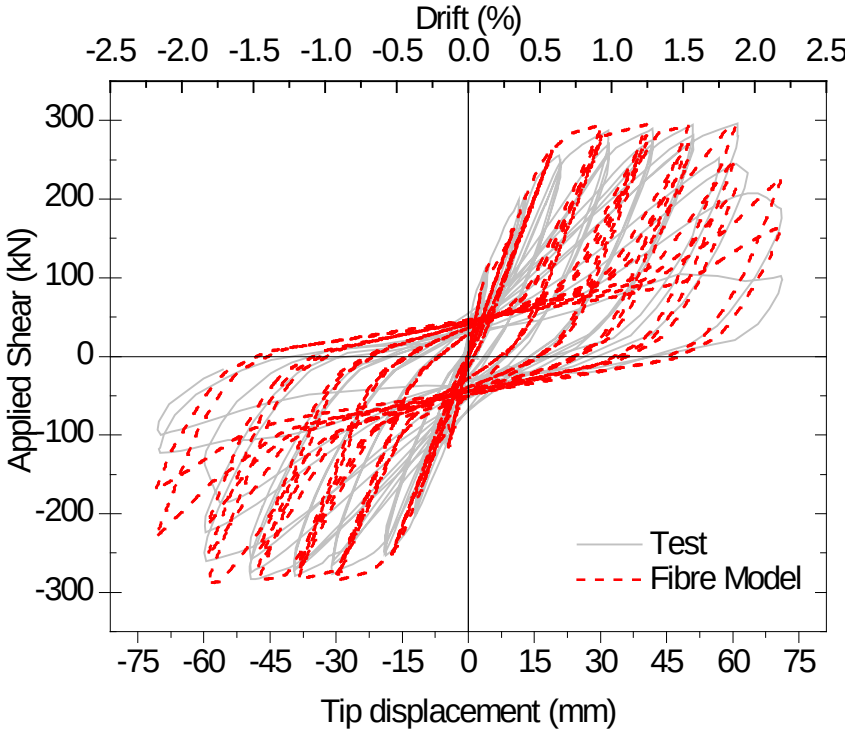

b) W1R

Fig. 4-21- Fibre element analytical model versus Experimental results ($W1_{Pat}$ and $W1R_{Pat}$)

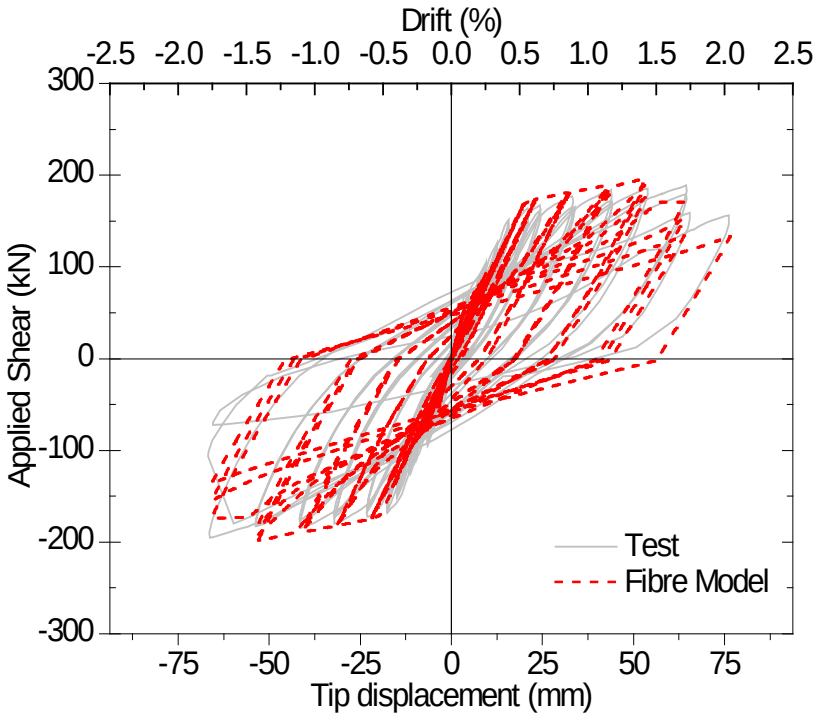

a) $W2_{Pat}$

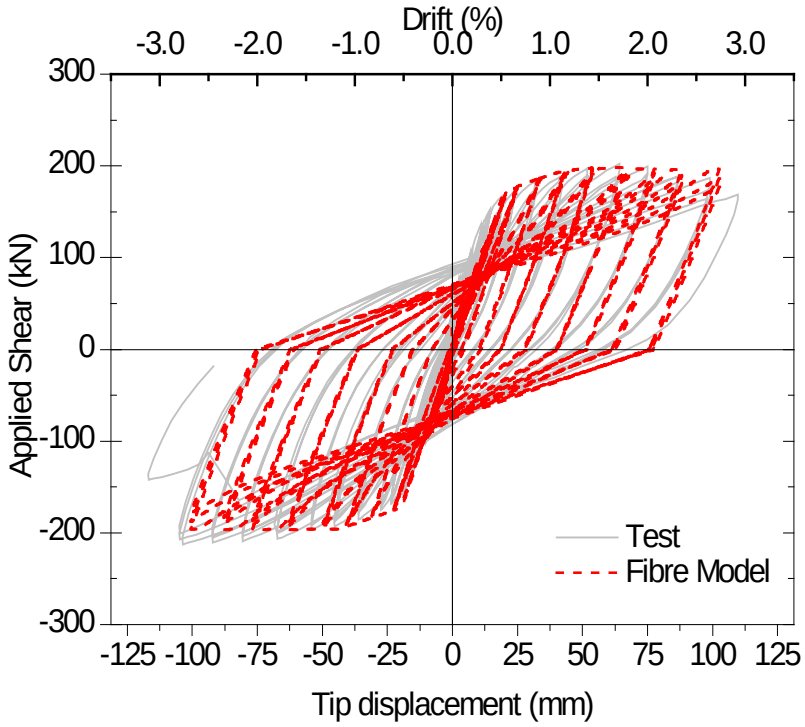

b) $W2R_{Pat}$

Fig. 4-22- Fibre element analytical model versus Experimental results (W2 and W2R)

Chapter 5
Predicting Seismic Response of Prototype RC Shear Wall Structures

5.1. Introduction

This chapter describes the modeling and analysis of a prototype RC frame-shear wall structure. The purpose is to investigate the effectiveness of the retrofit and the repair techniques proposed in this thesis in improving the global seismic performance of a prototype structure. The structural configuration and details of this prototype structure were chosen in order to represent the typical construction of the 1960's and early 1970's.

The detailed design information for this prototype structure is presented in this chapter. The prototype structure was designed and detailed to conform the 1963 ACI-318 Code (ACI, 1963) which was the basis for the concrete design provisions given in the 1965 National Building Code of Canada (NBCC, 1965). A linear static analysis was used in the design of the prototype structure.

The performance of the prototype structure was evaluated according to the recommendations of the ASCE-41 (2006) and ASCE-41, Supplement 1. OpenSees (v2.4.0, 2012) was used for the purpose of analyses. Response2000 (Bent and Collins, 2000) was used for sectional analysis.

The Imperial (U.S. customary) system of units is used in this chapter to match the units used in older construction and codes (both in Canada and the U.S.).

5.2. Description of the Prototype Structure

The selected prototype structure is a 5-storey reinforced concrete frame-shear wall structure. To represent different seismic hazard levels, Vancouver, British Columbia in the west, and Montreal, Quebec in the east were selected.

A rectangular, symmetrical frame configuration with two shear walls in each direction (see Fig. 5-1) was chosen as the prototype structure. The plan of the prototype structure is 78 ft in the X direction and 54 ft in the Y direction, measured centre-to-centre of the exterior columns.

The frame system consists of typical beams and columns with 5 bays in the X direction and 3 bays in the Y direction. The two shear walls in each direction of the building are located in the central bays of the exterior frames as illustrated in Fig. 5-1.

All the storey heights were 12 ft. The thickness of all of the shear walls is 8 in. (in accordance with the minimum thickness required by the 1963 ACI-318 Code (ACI, 1963) and the 1965 NBCC (NRC, 1965). The thickness is constant over the height of the building. The typical floor and the roof consisted of an 8 in. thick two-way slab supported by beams (see Fig. 5-1). Perspective views of the structural system are shown in Fig. 5-2.

5.2.1. Material Properties

The properties of the concrete and steel materials used to evaluate the prototype structure are given in Table 5-1. These properties were chosen to conform to the recommendations in ASCE-41, supplement 1 (ASCE, 2006). The lower bound values should be translated into expected values with ASCE-41 (ASCE, 2006) recommending factors of 1.5 for concrete and 1.25 for reinforcing steel, whereas the CSRN guidelines (CSRN, 2013) recommend factors of 1.3 and 1.15, respectively. Table 5.1 gives the lower-bound and expected material properties used for the original design and the seismic evaluation. The expected values conform to the recommended factors in the CSRN guidelines.

Table 5-1- Material properties

Material	Lower-Bound (ksi)	Expected Properties (ksi)
Unconfined concrete	$f_c^{'} = 3.5$	$f_{c,e}^{'} = 4.5$
Confined concrete (for FRSCC Retrofit)	-	$f_{c,e}^{'} = 5.0$
Steel reinforcement	$f_y = 50$	$f_{y,e} = 57.5$

5.2.2. Design of Original Building for Gravity and Wind Loading

The ultimate strength design method in accordance with practice in 1965 was used as the basis of design and detailing of the structural components in the prototype structure.

It is assumed that the prototype structure was designed to resist the actions due to gravity and wind loading. Since the prototype structure represents conventional construction of the 1960's, no seismic design was carried out.

The total dead load, including the self weight of the 8 in. thick slab, floor finishes, electrical and mechanical services, partitions and the roofing was assumed to be 150 psf. The live load was considered to be 50 psf for the floors and the roofs (snow load).

The wind load was assumed to be a uniform pressure of 40 psf. For each direction, the wind load was calculated based on the tributary area. The concentrated reinforcement at the ends of the shear walls were determined based on the factored wind loads. It was also assumed that the shear walls resisted 100% of this lateral load.

The calculation of the gravity loads and the wind load are presented in *Appendix B.*

The prototype structure was analyzed (linear static with no stiffness modification factors) in order to determine the gravity and the wind load actions in the beams, the columns, and the shear walls. For the design of the prototype structure the

lower-bound material properties given in Table 5-1 were used to represent values appropriate in the original design of the structure.

5.2.2.1. Beams

It was assumed that the gravity loads were uniformly distributed over the two-way slab. The tributary areas for determining the distribution of the slab loading to the perimeter beams is shown in Fig. 5-1. The interior beams in the Y direction are carrying more of the gravity load, while the exterior beams in the X direction are carrying lower gravity loads. Therefore, the interior beams in the Y direction were chosen for design. The same cross-sectional dimensions were chosen for all of the beams. The reinforcing details were assumed to be identical for both interior and exterior beams.

The maximum negative and positive moments were derived from the linear elastic analysis. The design moments of the exterior and interior beams at the critical sections are presented in Tables 5-2. The load factors and load combination of the 1963 ACI Code and the 1965 NBCC were used for design. The location for the critical moments is shown in Fig. 5-3.

Table 5-2- Factored bending moment (ft-kips): Y direction

Load Combination	Exterior frames			Interior Frames				
	AB	m_{AB}	BC	AB	m_{AB}	BA	BC	m_{BC}
1.5D+1.8L	-42.4	37.9	-73.5	-116.4	63.7	-108.8	-59.6	18.5
1.35 (D+L±W_Y)	-30.4	33.1	-63.7	-114.8	62.1	-83.4	-35.1	18.0
0.9D±1.35W_Y)	-46.5	19.4	-43.9	-66.5	32.9	-60.8	-40.7	10.4

The beams were designed for maximum positive and negative moments of 78.3 ft-kips and -127.8 ft-kips, respectively.

The cross section for the beams is shown in Fig. 5-4(a). The selected cross section provides factored positive and negative moment resistances of 75.5 ft-kips and 128.7 ft-kips, respectively. A safety factor of $\varphi = 0.9$ was used in flexural design of the beams.

The factored moment due to the gravity and the wind actions and the factored moment resistances of the designed beams are summarized in Table 5-3.

Table 5-3- Factored moment resistance vs. factored moment (Y direction)

Dimension (in)		M_n (ft-kips)		M_r (ft-kips)		M_f (ft-kips)	
b	*h*	M_n^+	M_n^-	M_r^+	M_r^-	M_f^+	M_f^-
14	18	83.9	-143	75.5	-128.7	78.3	-116.4

The maximum factored shear force in the beams is 34.4 kips. The concrete web could provide a maximum shear resistance of:

$$v_c = 2\ \varphi\sqrt{f_c'} = 2 \times 0.85 \times \sqrt{3500} = 100\ psi$$

Resulting in a concrete contribution of 21.8 kips and requiring a shear resistance from the transverse reinforcement of 12.6 kips. The maximum spacing of the transverse reinforcement was limited to $d/2 = 15.6 = 7.8\ in.$

The provision of #3 closed stirrups at a spacing of 7.5 in. satisfies the requirements for maximum spacing and the required shear resistance.

5.2.2.2. Columns

The cross-sectional dimensions of and reinforcement detailing was the same for all columns. The cross-sectional dimension of 18 in. by 18 in. (Gross area of 324 in^2) was chosen for the columns. Eight No. 7 bars, resulting in a reinforcement ratio of 1.48% (greater than minimum of 1.0%) were selected for these gravity-load columns. It is assumed that the transverse reinforcement consists of #4 ties, with 90° hooks at a spacing of 14 in. (chosen to satisfy spacing limit of $16d_b$). The resulting details are given in Fig. 5-4(b).

5.2.2.3. Shear Walls

It is assumed that the original shear walls were designed to resist 100% of the lateral wind loading. The minimum wall thickness of 8 in. for the shear walls was selected to satisfy the minimum thickness requirements of the 1963 ACI Code. The

thickness was kept constant through the entire height of the wall. The length of each wall is 14 ft.

The chosen details for the distributed horizontal reinforcement (transverse reinforcement) for these walls consisted of a single layer of #4 bars with a 10 in. spacing, giving a reinforcement ratio of 0.0025, which equals the required reinforcement ratio. The distributed vertical reinforcement consist of a single layer of #4 bars with a 15 in. spacing, resulting in a reinforcement ratio of 0.0017, which exceeds the required ratio of 0.0015.

The actions on the shear walls were determined from the linear static analyses and are summarized in Table 5-4. The amount of the concentrated reinforcement at the ends of the wall was chosen in order to provide the required factored moment resistance. The wall dimensions and details were chosen to be the same in the two directions (see Fig. 5-5(a)).

The walls have 4 #7 bars as the concentrated reinforcement at each end of the wall. The factored loads required by the 1965 NBCC for the different load cases are shown in Table 5-4. The controlling loading case for the design of the walls is 0.9D +1.35W. Table 5-5 gives the factored resistance for this loading case using the lower bound material properties used for the original design.

Table 5-4- Moment and Axial actions at the base of the walls

Load Combination	X direction		Y direction	
	P(kip)	M_f (ft-kip)	P(kip)	M_f (ft-kip)
1.35D+ 1.35 (L+W_x)	-486	2494	-	-
0.9D +1.35W_x	-270	2494	-	-
1.35D+ 1.35 (L+W_y)	-	-	-445	3602
0.9D +1.35W_y	-	-	-250	3602

Table 5-5- Factored bending moment capacity of the walls

	Axial load (kips)	M_f (ft-kips)	M_r (ft-kips)
X direction	-270	2494	3623
Y direction	-250	3602	3518

5.2.3. Design of Retrofit

The original walls were retrofitted using the methods previously described in Chapter 2.

5.2.3.1. CFRP Retrofit

The shear wall was fully wrapped with CFRP over the first two storeys, and was strengthened in shear using CFRP strips for the upper storeys. The cross sectional detail of the retrofit is shown in Fig. 5-5(b). The CFRP retrofit does not change geometry of the section. The CFRP retrofit will prevent premature failure of the lap splices such that the wall can display a limited ductility as determined by the experimental program. It was assumed that the CFRP retrofit does not change the stiffness of the wall.

5.2.3.2. FRSCC Retrofit

The FRSCC retrofit technique involved introduction of a FRSCC jacket over the first two storeys. The jacket increased the existing thickness of 8 in. (200 mm) to 14 in. (350 mm). The concrete over the lap splices of the concentrated reinforcement in the boundary elements was removed for depth equal to the concrete cover plus the bar diameter plus 1 in. (25 mm). The new FRSCC concrete was then added to increase the wall thickness. The new cross section keeps the existing wall length of 14 ft. Above the second storey the wall was entirely retrofitted using CFRP wraps to provide confinement for the lap splices in potential plastic hinge regions.

5.3. Seismic Modeling and Analyses

A two dimensional (2D) mathematical model, representing the exterior and interior bents (frames) in the Y direction, was developed and subjected to gravity and seismic loadings (see Fig. 5-6). Only one-half of the structure was modeled and the resulting lateral forces were multiplied by two to obtain the structure response. The wall was modeled using fibre elements at the centroid of the wall with rigid links from the centroid to the ends of the wall. The beams framing into the wall were fully

fixed to the wall. The interior frames were connected to the end frame using rigid truss links to represent a rigid diaphragm. Torsional effects were neglected in the analyses.

The purpose of the seismic analyses is to evaluate the original structure as well as the effectiveness of two different retrofit strategies (CFRP retrofit only and Fibre Reinforced SCC jacket) on the overall performance of the building. The analyses intend to show the significance of the retrofit techniques on seismic response of a prototype structure.

In the first model, the prototype structure is modeled in its original condition. This model is representative of poorly detailed existing wall-frame structures, with seismically deficient shear walls in both directions. The modelling technique is the same approach that was used to model the deficient shear walls in Chapter 4.

For the second model, CFRP wrapping is applied to the walls to improve the ductility of the shear walls. The CFRP retrofit does not increase the strength or the stiffness of the structure, but increases the ductility and energy absorption of the walls and hence the performance of the building.

For the third model, a SCC reinforced concrete jacket retrofit was applied over the first two storeys. This increases the stiffness and strength of the building.

The mathematical model consists of beams, columns, and shear walls. The contribution of the concrete slab to the strength and stiffness of this assembly was not taken into account. However, it was assumed that the 8 in. thick slab will provide a rigid diaphragm at all levels.

The nonlinear responses of the components were modeled using either the concentrated plasticity model (for the beams and columns) and distributed plasticity model (for the shear wall).

For the concentrated hinge model, the stiffness of the beams, and columns and the hinges at their ends were modified according to the recommendation of ASCE 41, supplement 1 (ASCE, 2006), Clause 6.3.1.2. The effective stiffnesses of beam and column elements for seismic analyses are based on the stiffness modification factors as given in Appendix C.

It should be noted that the stiffness and strength of columns depends on the axial load level. Therefore, these properties were modified for each column (see appendix C). The strength and stiffness of shear walls is directly derived from the material properties and cross-sectional details using the fibre element model.

The nonlinear response of the beams and columns were lumped at the ends using a zero-length rotational spring. The stiffness, strength, over-strength, and damping properties of these springs were modified according to Ibarra and Krawinkler (2005). It was assumed that the beams and columns will deflect in double curvature, and therefore, the rotational stiffness of the beams and columns can be approximated as:

$$K_{rot,mem} = \frac{6E_c I_{mem}}{l_{mem}}$$

The rotational springs at the ends of the beams and columns were chosen to have rotational stiffnesses of n (i.e., 10) times the rotational stiffness of the beams and column, to avoid unrealistic damping characteristics.

$$k_s = nk_{beam}$$

Assuming that the rotational springs are in series with the beam ends, the total stiffness of the beam-column element is derived as follows:

$$\frac{1}{K_{rot,mem}} = \frac{1}{K_s} + \frac{1}{K_{beam}} = \frac{n+1}{nK_{beam}}$$

Hence, the stiffness of the rotational spring and the elastic beam-column element can be modified as:

$K_s = (n+1)K_{mem}$, and $K_{beam} = \frac{n+1}{n}K_{mem}$

The over-strength factor for the plastic hinge can be modified as:

$$\alpha_s = \frac{(n+1)\alpha_{mem}}{n(1-\alpha_{mem})+1}$$

And α_m can be determined as:

$$\alpha_m = \frac{M_e - M_y}{\theta_p K_{mem}}$$

Where M_e and M_y are the expected capacity and yield moment, respectively, and θ_p is the pre-capping rotation capacity of the hinge.

Application of different hysteretic models was studied. For all hysteretic models, the ASCE/SEI backbone curve was used to define the monotonic responses. The hysteretic responses of the beam and column hinges were modeled using Modified Ibarra-Medina-Krawinkler (2005) deterioration model with Peak-Oriented model hysteretic response (Lignos and Krawinkler, 2012). The material is implemented in OpenSees platform (Lignos, 2012). It is noted that since no specific database on the responses of poorly detailed reinforced concrete beam and columns was available, no cyclic deterioration was assigned to the responses of the beams and columns ($\Lambda_s = \Lambda_c = \Lambda_a = \Lambda_k = 1000$). ATC 72-1 (PEER/ATC, 2010) modeling options 3 and 4 were employed for the beams and columns. In option 3, the shape of initial monotonic backbone from ASCE/SEI 41 was modified to represent deterioration. ATC 72-1 recommendations were used for modification. In the case of option 4, no credit was given to the negative post peak responses.

5.3.1. Beams

The beams were modeled as elastic beam-column elements. In the concentrated plasticity model, it is assumed that the nonlinear responses of the beams are restricted to their ends.

The spacing of the transverse reinforcement in the beams is 7.5 in. This spacing is larger than the $d/3 = 15.6/3 = 5.2$ *in.* and thus in accordance with the ASCE-41 requirements this transverse reinforcement is considered as non-conforming (NC).

In order to evaluate the significance of the level of shear in the beams, a pushover analysis was carried out in combination with dead load. This analysis resulted in a maximum shear force in the beams of 31 kips. Hence the non-dimensional shear stress level is:

$$\frac{V}{b_w d\sqrt{f'_c}} = \frac{31\times1000}{14\times15.6\times\sqrt{4500}} = 2.12 \le 3.0$$

This shear stress level is less than the value of 3 and the parameter accounting for the reinforcement ratios can be written as:

$$\frac{\rho-\rho'}{\rho_{bal}} = \frac{A_s - A'_s}{A_{s,bal}} = \frac{2.4-1.32}{6.26} = 0.17$$

The modeling parameters (see Fig. 5-7) were determined by interpolating the reinforcement ratio parameter between 0 and 0.5 resulting in values given in Table 5-7. Two cases are considered in Table 5-6, one with the original beam and the other with CFRP wrap around the web and bottom of the beam to increase confinement and shear resistance. With this CFRP wrap, the shear reinforcement is considered to be conforming, resulting in the values shown in Table 5-6. It is noted that the modeling parameters for the beam with the CFRP wrap are used only for the end of the beam framing into the wall, when these beams are retrofitted.

These parameters together with the numerical acceptance criteria of ASCE-41 were used to develop the concentrated plasticity models. The beams are “flexure controlled” and it is assumed that lap splice failure is avoided.

Table 5-6- Modeling parameters and acceptance criteria according to ASCE-41 (2006)

	Beams controlled by flexure			Plastic rotations (radians)		Residual strength ratio	Acceptance criteria for Plastic rotation*		
	$\frac{\rho-\rho'}{\rho_{bal}}$	Trans. Reinf.	$\frac{V}{b_w d\sqrt{f'_c}}$	*a*	*b*	*c*	IO	LS	CP
Original beam	0.17	NC	2.12	0.017	0.025	0.2	0.005	0.01	0.017
Beam with CFRP	0.17	C	2.12	0.023	0.043	0.2	0.008	0.017	0.023

* IO: Immediate occupancy, LS: Life safety, and CP: Collapse prevention

5.3.2. Columns

The nominal shear capacity, V_n, of the columns was calculated and compared with the shear corresponding to plastic hinging, V_p. Based on the ratio $V_p/(V_n/k)$, modeling parameters are determined. The factor, k, reflects the level of displacement ductility expected and was chosen to be 1.0 for a ductility level less than or equal to 2.0.

The nominal shear capacity of the columns is determined using the proposed equation in ASCE-41 (Eq. 5-1) and the term M/V will be taken as half the column height for these columns subjected to double curvature.

$$V_n = k\frac{A_v f_y d}{s} + \lambda k\left(\frac{6\sqrt{f_c'}}{M/Vd}.\sqrt{1+\frac{N_u}{6\sqrt{f_c'}A_g}}\right)0.8A_g \qquad \text{Eq. 5-1}$$

Table 5-7 gives the parameters used in calculating V_n:

Table 5-7- Parameters for calculating V_n

	Unit	Value	Description
b	*in.*	18	
h	*in.*	18	
A_g	in^2	324	
A_s	in^2	4.80	Longitudinal steel (8 #7)
A_v	in^2	0.40	Transverse steel (2 #4 legs)
d	*in.*	14.4	Taken as 0.8h
s	*in.*	14	Tie spacing
f_y	*psi*	57,500	
f_c'	*psi*	4,500	
k	-	1	
λ	-	1	Normal weight concrete
N_u	*lb*	300,000	
$M/(Vd)$		4.4*	$2.0 \le M/(Vd) \le 4.0$

* The value is limited to 4.0 in calculations

The nominal shear capacity of the columns can be determined as:

$$V_n = 1.0 \times \frac{2 \times 0.2 \times 57500 \times 0.8 \times 18}{14}$$
$$+ 1 \times 1 \times \left(\frac{6\sqrt{4500}}{4} \sqrt{1 + \frac{300000}{6\sqrt{4500} \times 18 \times 18}} \right) \times 0.8 \times 18 \times 18$$
$$= 23657 + 47381 = 71038 \text{ lb} = 71.0 \text{ kips}$$

The columns are stronger than the beams and hence the shear demand on the columns corresponds to plastic hinging in the beams. The sum of the positive and negative moments in the beams is 263.4 ft-kips, and hence the shear demand is:

$$V_p = \frac{M_b^+ + M_b^-}{h_u} = \frac{97.8 + 165.6}{(12 - 1.5)} = 25.1 \text{ kips}$$

Hence the ratio $V_p/(V_n/k) = 0.35$ and given the deficient detailing of the transverse reinforcement (large spacing, 90° hooks), the columns are classified in category ii of ASCE 41.

For determining the modeling parameters, the columns were categorized based on their axial load level. The exterior columns have $P/(A_g f_c')$ less than 0.1, while the interior columns have $P/(A_g f_c')$ of 0.2 at their bases. The modeling parameters given in Table 5-8 were determined by performing linear interpolations based on the axial load level, the transverse reinforcement ratio, and the normalized shear stress.

Table 5-8- Modeling parameters and acceptance criteria for exterior and interior columns, according to ASCE-41 for condition "ii"

			Plastic rotations (radians)		Residual strength ratio	Acceptance criteria*		
$\frac{P}{A_g f_c'}$	$\rho_v = \frac{A_v}{b_w s}$	$\frac{V}{b_w d\sqrt{f_c'}}$	a	b	c	IO	LS	CP
0.1	0.002	≤ 3	0.017	0.025	0.2	0.005	0.013	0.016
0.2	0.002	≤ 3	0.015	0.021	0.16	0.004	0.011	0.014

* IO: immediate occupancy, LS: life safety, and CP: collapse prevention

5.3.3. Shear Walls

The shear walls had a 14 ft (4.27 m) length and a 60 ft (18.29 m) height resulting in an aspect ratio of 4.3, and hence are classified as flexural walls (ASCE 41, 2006). The walls were modeled using fibre displacement-based beam-column elements which accounted for distributed plasticity over the height (see Chapter 4).

The cross section of the as-built wall was discretized into concrete and steel fibres. A rotational linear spring and a bi-linear translational shear spring were included to account for the effect of bar slip and shear deformations, respectively. Expected material properties were assumed for the concrete and the reinforcement.

5.3.3.1. Reinforcing Steel

The reinforcing steel was modeled as a bilinear *Hysteretic Material.* The expected properties of the steel were used and the pinching factors of Chapter 4 were used. The stress-strain relationship for the reinforcing steel is shown in Fig. 5-8(a).

It is assumed that the walls have a deficient lap splice at their base. The required development length (in tension) for straight bars is calculated according to ACI Code. A lap splice length of $30d_b$ was selected for #7 bars (81 mm diameter) in accordance with the 1963 ACI Code. This resulted in a lap splice length of 26 in.

The shear walls were modeled as equivalent displacement-based beam-column elements, with a fibre element section. The cross section of the walls (8 in. by 168 in.) was discretized into a rectangular mesh of 2 in. by 4 in. (50 by 100 mm). The steel reinforcement was modeled as individual fibres.

The 60 ft (18.29 m) high wall was divided into sub elements, with end nodes representing the 12 ft (3.66 m) height of each storey. In order to improve the accuracy of the internal forces, a finer mesh was used, dividing the height of each storey into 4 elements of equal length (see Fig. 5-9).

5.3.3.2. Concrete

The expected compressive strength of concrete was used as the basis of modeling. For monotonic analysis (i.e., Nonlinear Static Procedures), Concrete07

was calibrated and used in the models. However, for Nonlinear Dynamic Procedures, *Concrete02* was used as a result of better convergence. Table 5-9 summarized the calibrated parameters for both concrete materials. The monotonic envelopes (tension and compression) for Concrete02 and Concrete07 are shown in Figs. 5-8(b) and (c).

Table 5-9- Parameters for C02 and C07

Concrete 02	**Concrete 07**
$f_c' = 4500\ psi$	$f_c' = 4500\ psi$
$\varepsilon_{co} = 0.002$	$\varepsilon_{co} = \frac{(f_c')^{1/4}}{4000} = \frac{4500^{1/4}}{4000} = 0.002$
$E_c = \frac{2f_c'}{\varepsilon_{co}} = \frac{2 \times 4500}{0.002} = 4500\ ksi$	$E_c = 185{,}000 \sqrt[8]{f_{co}'^{\,3}}$ $= 185{,}000(4500)^{3/8} = 4336\ ksi$
$f_t \approx 0.3\ ksi$	$f_t \approx 4.5\sqrt{f_c'} = 0.3\ ksi$
$\lambda = 0.1$	$\varepsilon_t = \frac{2f_t}{E_c} = \frac{2 \times 0.3}{4336} \approx 0.00014$
$E_{ts} = \frac{f_t}{\varepsilon_t} = \frac{0.3}{0.0002} = 1500\ ksi$	$r = \frac{f_c'}{750} - 1.9 = \frac{4500}{750} - 1.9 = 4.1$

5.3.4. Gravity Loads

Table 5-10 shows the load actions that was combined with the actions due to seismic loads (ASCE 41, Clause 3.2.8, 2006).

Table 5-10- Load combinations to accompany actions due to seismic loading

$Q_G = 1.1(Q_D + Q^*_L + Q^*_S)$	Actions due to gravity and seismic are additive

* 25% of the unreduced design live load and 25% of snow load

Table 5-11 summarizes the gravity loads used for seismic analysis.

Table 5-11- Seismic weight and pseudo mass

Storey	D	L	$1.0D + 0.25L$	m_i	h_i	$w_i h_i$	$c_{vx} = \frac{(w_x h_x)}{\sum w_i h_i}$
	kips	kips	kips	$\frac{kip.s^2}{in.}$	in.	kip.in.	-
5	857.4	210.6	910.1	2.36	720	655236	0.32
4	923.4	210.6	976.1	2.53	576	562205	0.27
3	923.4	210.6	976.1	2.53	432	421654	0.20
2	923.4	210.6	976.1	2.53	288	281102	0.14
1	923.4	210.6	976.1	2.53	144	140551	0.07
			$\sum w_i = 4814.3$			2060748	

5.3.5. Seismic Effects

To represent two different levels of seismic hazard, Montreal and Vancouver were selected as the building sites (Eastern and Western Canada, respectively). For each location, acceleration response spectra for two different earthquake hazard levels corresponding to probabilities of exceedance of 2% in 50 years and 10% in 50 years (5% damped response spectrum) were used. Fig. 5-9 shows the design spectrum for Montreal and Vancouver.

A “Class C” soil is selected for the site conditions. The acceleration-based site coefficient, F_a, and velocity-based site coefficient, F_v, are therefore equal to 1.0. The design spectral acceleration is calculated as $S(T) = S_a(T_a)$.

5.4. Analysis Procedures

5.4.1. Nonlinear Static Procedures (NSP)

In the NSP, the global response of the building is evaluated by subjecting the structures to a monotonically increasing lateral load pattern (Pushover). These loads represent inertial forces; however, the loading is applied in a static manner

(ASCE, 2006). The structure is laterally pushed until it exceeds the target displacement. The target displacement of the control node at the roof is determined from the design response spectrum.

The target displacement could be interpreted as the maximum displacement which is likely to be experienced during the design earthquake, and the internal forces are reasonable approximations of those expected during the design earthquake.

In ASCE/SEI 41 (2006) as well as the FEMA 356 (2000), the target displacement of the structure is determined using the Displacement Coefficient Method:

$$\delta_t = C_0 C_1 C_2 S_a \frac{T_e^2}{4\pi^2} g \qquad \text{Eq. 5-2}$$

C_0 is a factor which relates spectral displacement of an equivalent single degree of freedom system to the roof displacement of the building obtained from a multi-degree of freedom (MDOF) analysis and can be determined as the 1st mode mass participation factor multiplied by the ordinate of the 1st mode shape at the control node:

$$C_0 = \phi_{1,r} \Gamma_1 = \phi_{1,r} \frac{\{\varphi_1\}^T [M] \{1\}}{\{\varphi_1\}^T [M] \{\phi_1\}} \qquad \text{Eq. 5-3}$$

$\phi_{1,r}$ is the ordinate of the mode shape corresponding to the 1st mode at the control node, $[M]$ is the diagonal mass matrix, and Γ_1 is the 1st mode mass participation factor.

C_1 is the modification factor which relates the expected maximum inelastic displacement to displacements calculated for linear elastic response:

$$C_1 = 1 + \frac{R - 1}{\alpha T_e^2} \qquad \text{Eq. 5-4}$$

Where α is the site Class factor, taken as 90 for site Class C, T_e is the effective fundamental period of the structure ($T_e = T_i\sqrt{k_i/k_e}$), and R should be calculated using Eq. 5-5:

$$R = \frac{S_a}{(V_y/W)}.C_m \qquad \text{Eq. 5-5}$$

S_a is the response spectrum acceleration at the effective fundamental period and damping ratio of the building, V_y is the yield strength corresponding to the idealized nonlinear force-displacement response, W is the effective seismic weight, and C_m is the effective mass factor.

The fundamental period of the building is modified using the idealization of the force-displacement (pushover) curve. k_i is the stiffness derived from components using modified stiffnesses, and k_e is the effective stiffness illustrated in Fig. 5-10.

C_2 is the modification factor to represent the effect of pinching, as well as cyclic stiffness and strength degradation:

$$C_2 = 1 + \frac{1}{800}\left(\frac{R-1}{T_e}\right)^2 \qquad \text{Eq. 5-6}$$

It should be noted that for fundamental periods greater than 0.7 sec, the value of C_1 should be taken as 1.0. For periods greater than 1.0 sec, the value of C_2 is taken as 1.0.

5.4.2. Nonlinear Dynamic Procedures (NDP)

The nonlinear dynamic procedure consists of performing time history analyses using multiple ground motion records. It should be noted that the responses calculated by NDP is sensitive to the characteristics of each ground motion record.

5.4.2.1. Simulated Ground Motions

Atkinson (2009) proposed a directory of simulated response histories, for sites in the eastern and western parts of Canada that could be used to match the NBCC

2005 Uniform Hazard Spectrum (Seismotoolbox, as of Feb 2013). This directory contains accelerograms and response spectra for eastern and western Canada.

The simulated records are categorized based on their intensities, site Class, and the closest epicentral distance to the fault. Each file contains 45 records, which can be used as 15 three component data sets, or 45 random components. The corresponding 5% damped response spectra for each data set is provided in the directory.

Simulated records for Eastern Canada were used in the analysis of the building in Montreal. For Vancouver, Western Canadian records were selected and scaled.

The simulated response histories were selected to match the 2% in 50 years Uniform Hazard Spectrum as proposed by Atkinson (2009). In order to identify the best records to match the UHS, the ratio of the simulated response spectra over the period range of interest is compared to the target UHS for the same site conditions by examining the ratio, $r_{match} = S_a(TargetUHS)/S_a(simulated)$. Over the selected period range, the mean and standard deviation (SD) are calculated for each set of simulated data.

For each site location (Montreal, and Vancouver), twelve data sets with the lowest standard deviation and having mean values of r_{match} between 0.5 and 2.0 were selected. The 0.5-2.0 range for the mean values was chosen to provide variations in the records. Each selected time history was then scaled by multiplying the record by the corresponding mean value of r_{match}.

The proposed CSRN guidelines (2013) indicate that the period range for matching should have an upper bound greater than or equal to twice the first-mode period, but not less than 1.5 s. The period range chosen must include the periods necessary to achieve 90% mass participation in each orthogonal horizontal direction, but not less than 0.2 times the first-mode period.

Figs. 5-11(a) and (b) show the results of spectrum matching for the selected twelve records for Montreal and Vancouver for 2% chances of exceedance in 50 years. The acceleration time history records of the selected ground motions to be

used for the time history analyses for Montreal and Vancouver are given in Fig. 5-12 and Fig. 5-13, respectively.

5.4.2.2. Damping

Rayleigh damping is assumed for modeling. The fundamental periods, T_1, and the second mode period, T_2 (which was generally lower than $0.2T_1$ for all models) were used to determine damping coefficients.

A damping ratio of 2.5% was used for all models. The value is lower than 5% damping ratio which is generally used in nonlinear modelling of short to mid-rise reinforced concrete structures. The use of these lower values was also studied in NIST GCR 10-917-8 and 9 (2010) reports. The damping matrix is formulated as a linear combination of the mass matrix and initial stiffness matrix ($C = a_0 M + a_1 K_i$, where a_0 is the mass proportional damping coefficient and a_1 is the stiffness proportional damping coefficient).

The stiffness proportional damping was not applied to the rigid truss elements connecting the frames to properly model the damping. The mass proportional damping was separately assigned to the nodes with mass. In order to avoid spurious damping, no stiffness proportional damping was assigned for the zero-length rotational springs that were used to model the plastic hinges. Therefore, the stiffness properties assigned to the elastic beam-column elements were adjusted (multiplied by 1.1, assuming $n = 10$) to account for the total damping of the component.

5.5. Analyses

The wall frame structure was analyzed using pushover analysis (nonlinear static procedure (NSP)) and time history analyses (nonlinear dynamic procedure (NDP)) according to ASCE 41.

Eigen-value analysis was carried out to determine the principal mode shapes of the structural model. The mass source was chosen the same as the seismic weight of the model (1.1D + 0.275L load combination).

The mathematical model (see Fig. 5-6) was developed. The beams and columns were modeled as elastic beam-column element, with concentrated hinges at each end.

5.5.1. Original Frame-Wall Structure

For the walls in their original condition, the effects of the lap splices in the potential plastic hinging location were considered. The maximum stress that can be developed in the #7 bars can be predicted using the model proposed in Chapter 4 (section 4-4-1-c). The development length for straight bars in tension can be calculated in accordance with the 2011 ACI Code, using expected material properties as:

$$l_d = \frac{3}{40}\frac{f_{y,e}}{\lambda\sqrt{f'_c}}\frac{\psi_t\psi_e\psi_s}{(c_b + k_{tr})/d_b}d_b = \frac{3}{40}\ \frac{(1.15 * 50{,}000)}{1\times\sqrt{4500}}\frac{1\times1\times1}{1.5/0.875}\times(0.875) \approx 32.8\ in.$$

In order to calculate the minimum lap splice length, the development length should be multiplied by 1.3 to account for the lap splice Classification.

$$l_d = 1.3\times l_b = 42.6\ in.$$

Hence, the maximum stress that can be developed in the bars at the base of the walls can be determined as:

$$f_s = \frac{l_b}{l_d}f_{y,e} = \frac{26}{42.6}\times(1.15\times50) = 35.1\ ksi$$

The structure was subjected to the first mode lateral displacement pattern, until the failure of the lap splices in the wall.

Fig. 5-14 shows the predicted response of the wall-frame structure for the original building. The initial loading response represents the wall-frame interaction. A brittle failure occurs at a predicted base shear of 399 kips, corresponding to a roof displacement of 1.34 in. (0.19% drift) due to brittle failure of the tension lap splices in the walls. Due to this brittle failure, there is a sudden drop in capacity of the wall-frame structure with only the frames resisting load. The storey drift distribution shown in Fig. 5-17(b) indicates that the inter-storey drifts are less than

0.25%. The predicted performance indicates that the structure is inadequate for both Montreal and Vancouver.

5.5.2. CFRP Retrofit

5.5.2.1. Nonlinear Static Pushover Analysis

Elastic dynamic properties of the retrofitted wall-frame structure were determined by performing an Eigen value analysis of the structure. The periods, and the modal properties of the building are given in *Appendix D*.

The pushover analysis was carried out on the structure with the CFRP retrofitted walls. Fig. 5-15(a) shows the predicted pushover response. The building is capable of reaching a maximum base shear of 816 kips, corresponding to a roof displacement of 8.38 in. (1.16% roof drift). The drop in the load carrying capacity is associated with hinging of the beams framing into the wall. Fig. 5-16(a) also shows the ability of the structure to reach a maximum shear of 837 kips, and a corresponding displacement of 10.8 in. (1.4% roof drift) if the ends of the beams framing into the walls are locally retrofitted with CFRP wrap. It was concluded that it is not necessary to retrofit the beams with CFRP wrap at their ends framing into the wall.

The P-Δ effects were included in predicting the response of the frame-wall structure. The pushover curve was idealized using the recommendations of ASCE-41. The idealized responses are shown by the dashed lines in Figs. 5-15(a) and 5.16(a). Using these idealized responses, the target displacements were determined as shown in Table 5-14 for different return period earthquakes in Montreal and Vancouver. The target displacements are identical for both CFRP retrofit on the walls only and for the CFRP retrofit on the walls and beams framing into the walls. The details for the determination of the target displacements are given in Appendix D.

Table 5-12- Target roof displacements for CFRP retrofitted walls

	δ_t *(in.)*	*Roof drift (%)*
Montreal: 2%/50years	1.85	0.3
Montreal: 10%/50years	0.67	0.1
Vancouver: 2%/50years	4.82	0.7
Vancouver: 2%/50years	2.52	0.4

Figs 5-15(b and c) and 5-16(b and c) show the storey drifts corresponding to the target displacements. It is clear from Fig. 5-15(a) that the retrofitted structure is adequate for the target displacements for 2% in 50 years for both Montreal and Vancouver. It is noted that even if the target displacements are increased by 50% (ASCE-41, 2006) the structures remain in the pre-capping region.

Figs 5-15(d and e) and 5-16(d and e) show the variation of storey shears at the target displacements and for the maximum predicted base shear. It is noted that there is considerable margin for the case of Montreal; however, there is only a small margin for the case of Vancouver.

5.5.2.2. Nonlinear Dynamic Analysis

Figs. 5-17(a) and (b) show the predicted peak storey drifts from the nonlinear dynamic analyses for the 12 selected records for Montreal and Vancouver, respectively. These records were determined for 2475-year return period (2% in 50 years). For Montreal (Fig. 5-20(a)), the median of the peak drifts determined from the 12 nonlinear analyses are slightly less than the drifts predicted using the ASCE-41 nonlinear static procedure (pushover analysis) except at the roof level. It is interesting to note that for Vancouver, the median of the peak drifts is considerably greater than the pushover predictions, contrary to the results for Montreal. This difference is larger in the top two storeys probably because of the higher mode effects. It is believed that the increased accelerations associated with Vancouver led to more significant nonlinear response than that for the structure in Montreal. Dynamic amplification is responsible for greater storey shears in dynamic analysis compared to static pushover analysis.

Figs. 5-17(c) and (d) give the predicted storey shears for Montreal and Vancouver, respectively. For both Montreal and Vancouver, the median values of the predicted peak storey shears are above the storey shears corresponding to the target displacements obtained from the pushover analyses. The median base shears from dynamic analyses are 849 kips (708 kips in walls) and 1258 kips (1014 kips in walls) for Montreal and Vancouver, respectively.

Degradation in the shear strengths of the walls was not modeled. For one 14 ft long wall, retrofitted with CFRP wrap, the nominal shear resistance of the concrete can be determined as:

$$V_c = A_{cv}(\alpha_c \sqrt{f_c'}) = (0.8 \times 168 \times 8) \times \left(2.0\sqrt{4500}\right) = 144 \text{ kips}$$

The nominal shear resistance of the 1 mm (1/25 in.) thick CFRP wrap, having an effective tensile strength ($0.3F_{t,u} = 36.3 \text{ ksi}$) is:

$$V_{CFRP} = (2\, t_f l_w) \times F_{t,eff} = (2 \times 1/25 \times 168) \times 36.3 = 488 \text{kips}$$

The total shear capacity of one shear wall is $144 + 488 = 632$ kips, hence, the capacity of two walls is 1264 kips, which exceeds the median base shear of the wall of 1014 kips, predicted for Vancouver. It is concluded that the shear capacities are adequate. In the nonlinear modeling, the resistance of the shear springs in the walls were capped to a shear of 632 kips per wall.

It is also necessary to check whether or not the beams and the columns are capable of undergoing the predicted rotations. Table 5-13 compares the maximum predicted plastic rotations in the beams with the ASCE-41 (2006) acceptance criteria (see Tables 5-6). It is noted that the average rotations of the beams in the interior (gravity) frames satisfy the Immediate Occupancy (IO) criteria for both Montreal and Vancouver. However, the beams framing into wall in the exterior frame experience higher rotation demands. These mean values of rotation in the hinges satisfy IO limits for Montreal, but for the case of Vancouver, they are closer to the Collapse Prevention (CP) margin. It is noted that the maximum predicted rotations (i.e., records Van-4, Van-5) reach 0.014 radians that is close to the

collapse prevention margin. Therefore, a higher hazard level would likely cause failure in these hinges.

It is noted that the columns are considerably stronger than the beams and have predicted maximum plastic rotations that are an order of magnitude less than the immediate occupancy (IO) limit (see Table 5-8). This is consistent with the extremely low storey drifts predicted for both Montreal and Vancouver.

Table 5-13- Average beam rotations versus ASCE/SEI 41 acceptance criteria

	Average rotation		IO	LS	CP
	Exterior Frame Beams	Interior Frame Beams	0.005	0.01	0.017
Montreal (2%/50 years)	0.003	< 0.001	Ok	Ok	Ok
Vancouver (2%/50 years)	0.011	0.004	Not OK	Not OK	Ok

It is concluded that the CFRP retrofit is suitable for both Montreal and Vancouver for the 2475-year return period hazard. However, there is chance of collapse for the building in Vancouver in case of a greater hazard.

Fig. 5-18 shows the predicted moment-rotation response at the end of the beam framing into the wall at the third floor level (beam responses were critical at 3rd ,4th and the 5th floor) for the Van-5 record. It is evident that yielding occurred in the beams at this location in both positive and negative bending. Using ATC 72-1 (2010) modeling option 3 (modified backbone shown in green) results in rotations that are close to the collapse prevention limit.

Fig. 5-19 shows the predicted moment curvature response of the wall near its base when subjected to records: Van-5, Van 10, Mtl-1 and Mtl-2 records. Van-5 and Mtl-1 records are the records resulting in maximum storey drifts for CFRP retrofitted structure. Van-10 and Mtl-2 are the records resulting in maximum base shear. These responses indicate that the reinforcing bars experienced yielding and strain hardening, but did not reach the post capping stage. Also shown in Fig. 5-19 is the moment-curvature response prediction for the walls from program Response-2000. The monotonic prediction from Response-2000 provides a reasonable backbone curve to the hysteretic response. The stress-strain relations for the

extreme concrete fibres and concentrated reinforcement are shown for these records in Fig. 5-20. The results indicate that the concrete is predicted to reach the maximum compressive strength. The strain in the reinforcement (see Fig. 5-21) shows that extensive yielding of the concentrated reinforcing bars is predicted. It should be noted that the distributed vertical reinforcement was also experiencing yielding. A limit of 0.05 on the steel strains was set to account for possible bar buckling or bar rupture. The maximum strain in the uniformly distributed vertical bars indicate that the steel strains never reached the bar buckling limiting strain.

5.5.3. FRSCC Retrofitted Walls

5.5.3.1. Nonlinear Static Pushover Analysis

Fig. 5-22(a) shows the predicted pushover analysis for the wall-frame structure with FRSCC retrofitting on the bottom two storeys and CFRP wrap above the second storey. The retrofitted structure is capable of reaching a maximum base shear of 972 kips, with a corresponding roof displacement of 8.2 in. (1.14% roof drift). The drop in the load carrying capacity after the peak load is due to the hinging of the beams framing into the wall.

Figs 5-212(b) and 5-22(c) show the storey drifts corresponding to the target displacements. The target displacements were determined in accordance with ASCE-41. Table 5-15 gives the target displacements for Montreal and Vancouver for different return periods. Due to the higher initial stiffness of the FRSCC retrofitted wall, the target displacements are smaller than those for the CFRP retrofitted case.

Although the target displacement is well below the drift at maximum shear, even if increased by 50% (ASCE-41, 2006), it is noted that there are considerable rotations in the beams that have limited ductility.

Table 5-14- Target roof displacements for FRSCC retrofitted walls

	δ_t *(in.)*	*Roof drift (%)*
Montreal: 2%/50years	1.32	0.18
Montreal: 10%/50years	0.48	0.7
Vancouver: 2%/50years	3.14	0.43
Vancouver: 2%/50years	1.65	0.23

Figs 5-22(e) and 5-22(f) show the storey shears corresponding to the target displacements for Montreal and Vancouver as well as the predicted shears corresponding to the maximum predicted base shear from the pushover analysis.

5.5.3.2. Nonlinear Dynamic Analysis

The results of the nonlinear dynamic analyses for the 12 selected records for Montreal and Vancouver are shown in Figs. 5-23(a) and 5-23(b), respectively. These records were determined for the probability of exceedance of 2% in 50 years. The median values of the peak drifts for Montreal determined from the 12 nonlinear analyses are about the same as the drifts predicted from the pushover analysis. For Vancouver, once again, the median values of the peak storey drifts are considerably greater than the pushover predictions corresponding to the target displacement.

Figs. 5-23(c) and (d) give the predicted storey shears for Montreal and Vancouver, respectively. The median values of the predicted peak storey shears are above the storey shears corresponding to the target displacements from the pushover analyses. The median values of the peak base shears from dynamic analyses are 984 kips (730 kips in walls) and 1437 kips (1214 kips in walls) for Montreal and Vancouver, respectively.

For the bottom two storeys, the nominal shear capacity of the retrofitted section (see Fig. 5-5(c)) can be determined as:

$$V_n = V_c + V_s$$

where V_c is the shear resistance provided by the fibre reinforced self-consolidating concrete jacket and the shear resistance of original web, V_s is the

shear resistance provided by both the original and the additional transverse reinforcement in the jacket. It is assumed that the presence of the reinforced concrete jacket that was pinned to the original concrete using headed bars through the wall thickness in the boundary regions provide suitable confinement for the lap spliced bars, and for the existing transverse reinforcement. Therefore, the contribution to the shear resistance of the original transverse reinforcement is taken into account.

The concrete shear resistance can be determined as:

$$V_c = 2.0\sqrt{4500} \times 8 \times (0.8 \times 168) + 2.0\sqrt{5800} \times 6 \times (0.8 \times 168) = 267\ kips$$

The nominal shear resistance of the original and the additional transverse reinforcement in the FRSCC jacket can be determined as:

$$V_s = \left(\frac{A_{v,1}}{s_1} + \frac{A_{v,2}}{s_2} \right) f_y d$$

Where $A_{v,1}$ and $A_{v,2}$ is the area of existing and additional transverse reinforcement, respectively. These bars having a spacing of $S_1 = 16\,\text{in.}$ and $s_2 = 3\ in.$. Therefore, the shear resistance can be determined as:

$$V_s = \left(\frac{0.2}{16} + \frac{0.4}{3} \right) \times 58 \times (0.8 \times 168) = 1137 kips$$

For the third storey, the shear resistance is the same as the CFRP retrofitted section determined in previous section (632 kips).

The nominal shear resistance of one of the FRSCC retrofitted walls is therefore 1404 kips which provides a total shear capacity from both walls of 2808 kips, that is considerably above the median value of the peak base shear of 1437 kips in the walls, predicted for Vancouver.

Table 5-15 compares the maximum predicted plastic rotations in the beams with the ASCE-41 (2006) acceptance criteria. Similar to the CFRP retrofitted case, the beams in the interior frames remain in the IO performance range, while the introduction of the stiffer wall at the base, has somewhat lowered the demands in

the beams in the exterior frames. The rotation demand on the columns remains small and therefore, no damage is expected in the columns.

Table 5-15- Average beam rotations versus ASCE/SEI 41 acceptance criteria for FRSCC retrofitted building

	Average rotation		IO	LS	CP
	Exterior Frame Beams	Interior Frame Beams	0.005	0.01	0.017
Montreal (2%/50 years)	0.003	< 0.001	Ok	Ok	Ok
Vancouver (2%/50 years)	0.010	0.003	Not OK	OK	Ok

Fig. 5-24 (a) and (b) show the moment-curvature response of the FRSCC retrofitted jacket when subjected to records Mtl-1 and Van-10. These two records resulted in the maximum base shear. Also shown in these figures, is the monotonic moment curvature from sectional analysis. The monotonic response provides an envelope for the hysteretic response of the wall. The moment values that are slightly greater than the monotonic envelope are a result of the limited number of displacement-based beam-column elements used to model each storey. The variation of axial stress on the fibre elements results in variation of moment capacity of the section. General flexural yielding is predicted for the Van-10 records but only slight yielding is predicted for the case of Montreal. It is noted that no significant yielding was observed in third storey where the retrofit changed from the FRSCC retrofit to the CFRP retrofit.

Fig. 5-24 (c), (d), (e), and (f) show the stress strain relationships for the concrete and the reinforcing steel. The predicted concrete stresses are below the peak concrete strength and the reinforcing bars experience some strain hardening. It is noted that the stress values in concrete and steel material for both Mtl-1 and Van-10 fell within the acceptable pre-capping range.

It is concluded that the use of a reinforced concrete jacket using fibre reinforced self-consolidating concrete (FRSCC) provides a suitable retrofit for Vancouver. For

Montreal, the CFRP retrofit is sufficient and more economical than the FRSCC retrofit.

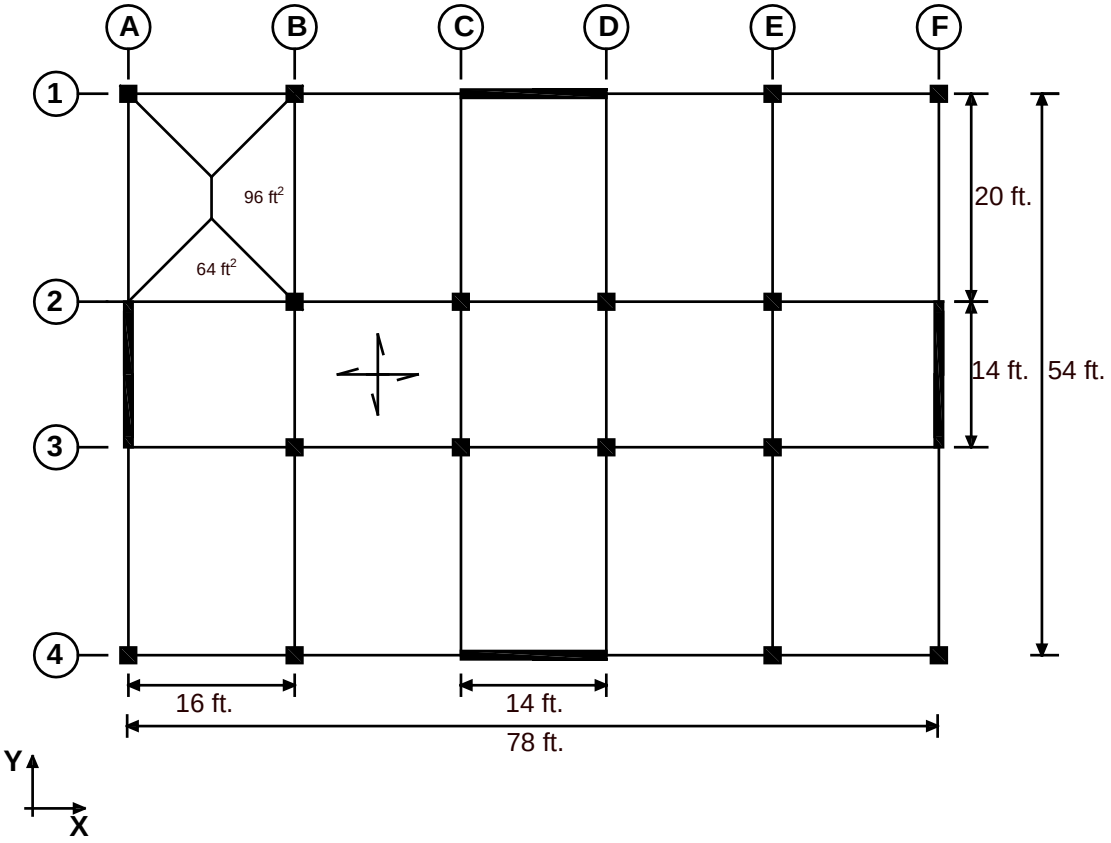

Fig. 5-1- Plan view of the prototype structure

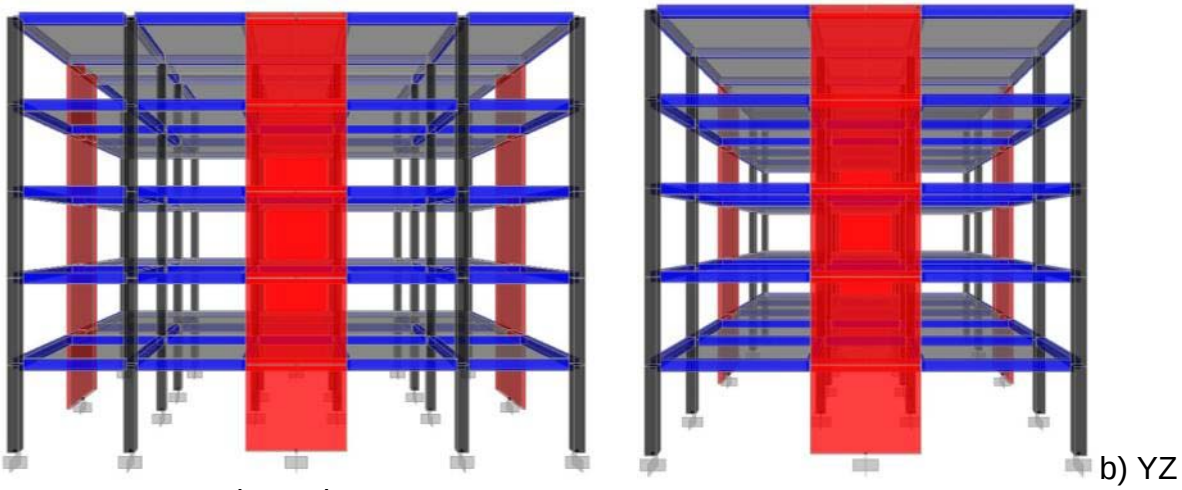

a) XZ view b) YZ view

Fig. 5-2- Perspective views of the structural system

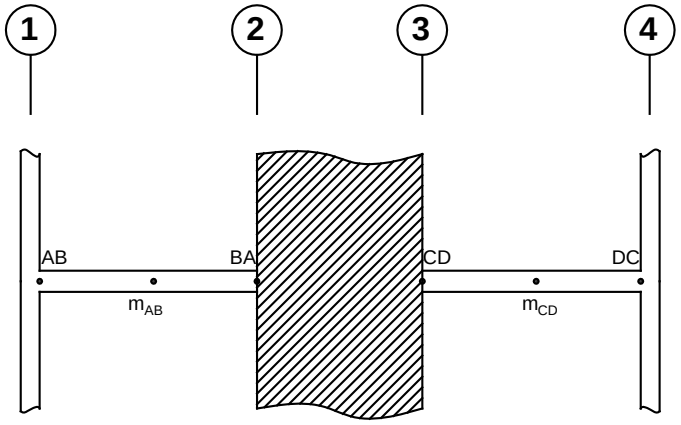

(a) Exterior Frame: Y direction

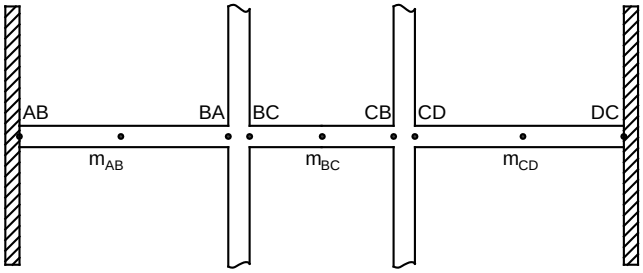

(b) Interior Frame: Y direction

Fig. 5-3- Critical moment locations in Interior and Exterior frames

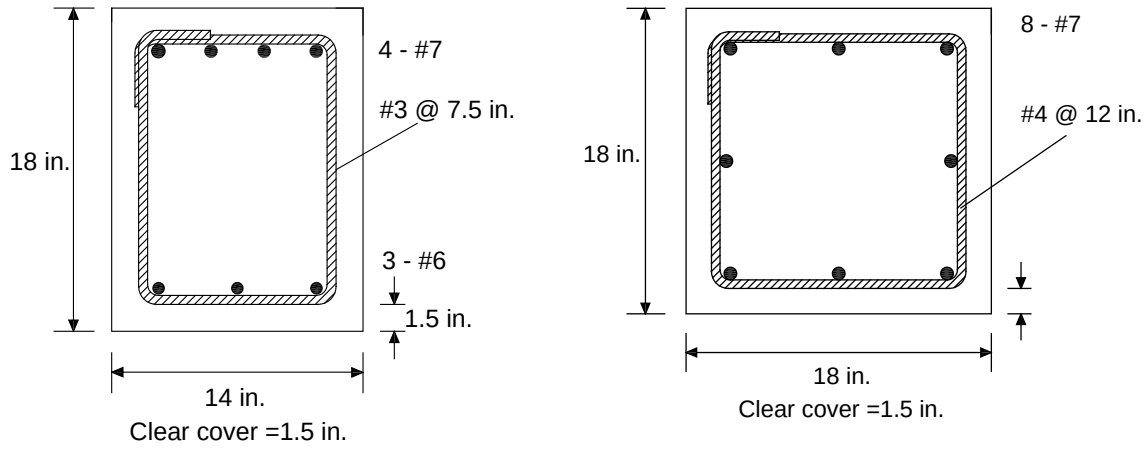

(a) Beams (b) Columns

Fig. 5-4- Cross section and reinforcing details for beams and columns

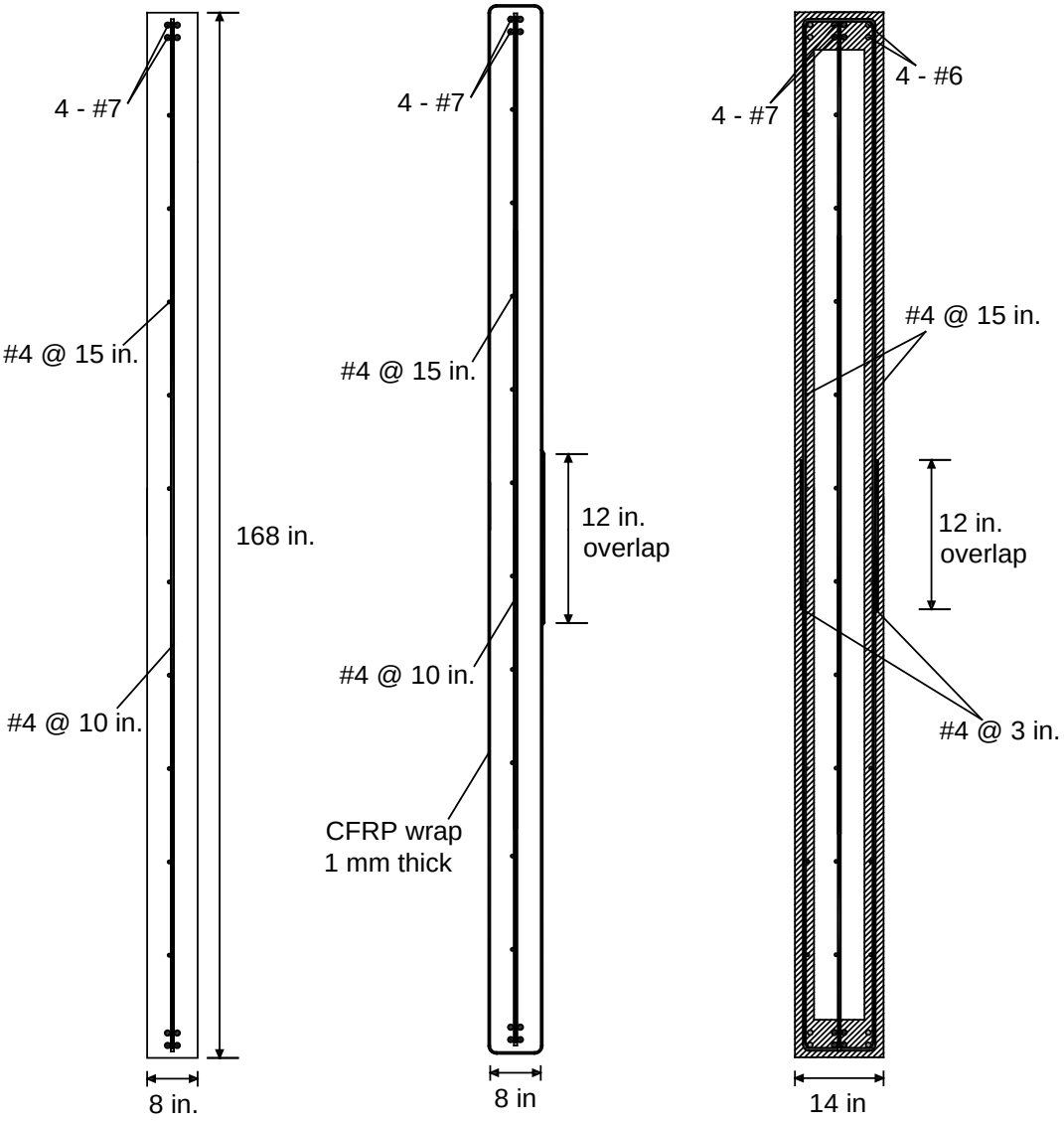

(a) As-built (b) CFRP (c) FRSCC

Fig. 5-5- Cross section and reinforcing details for walls

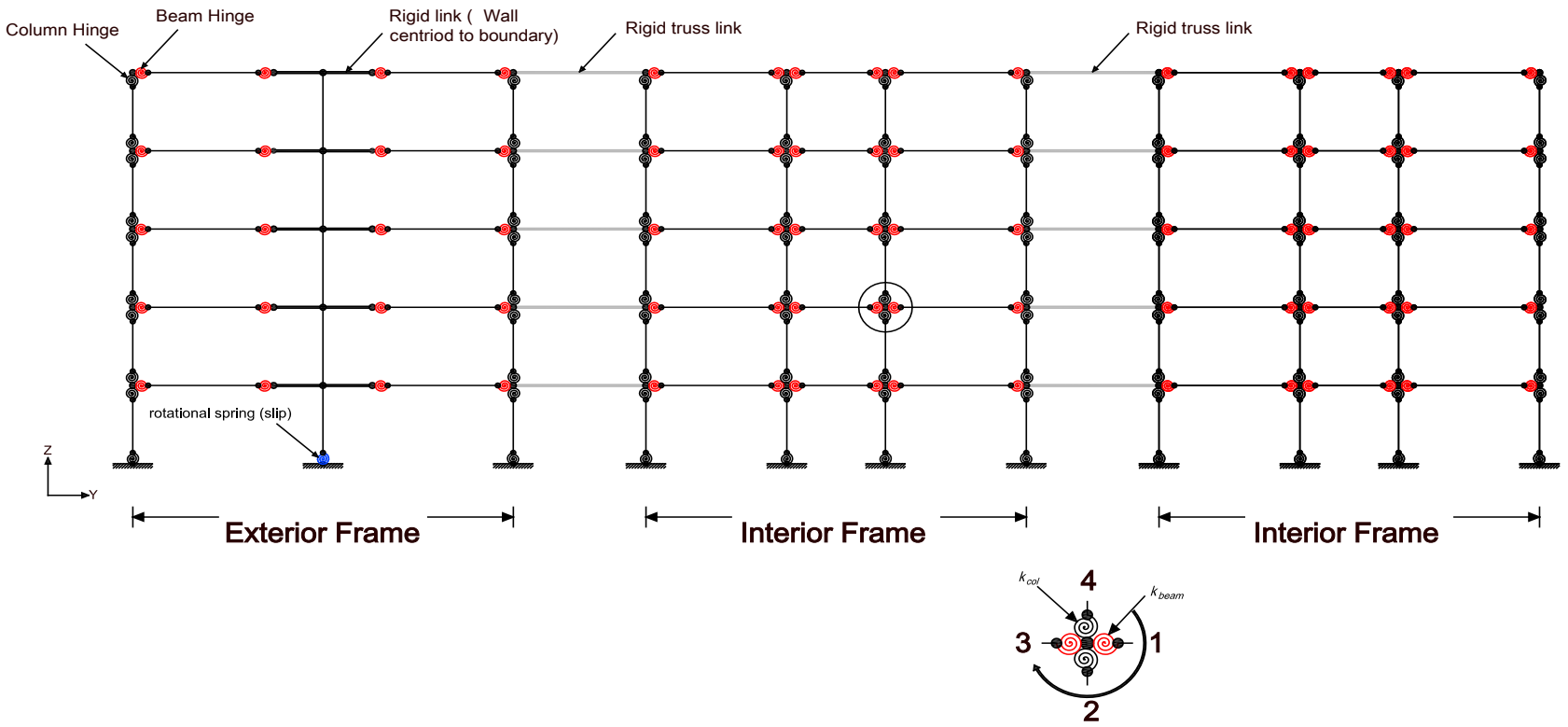

Fig. 5-6- 2D mathematical model of the building (half)

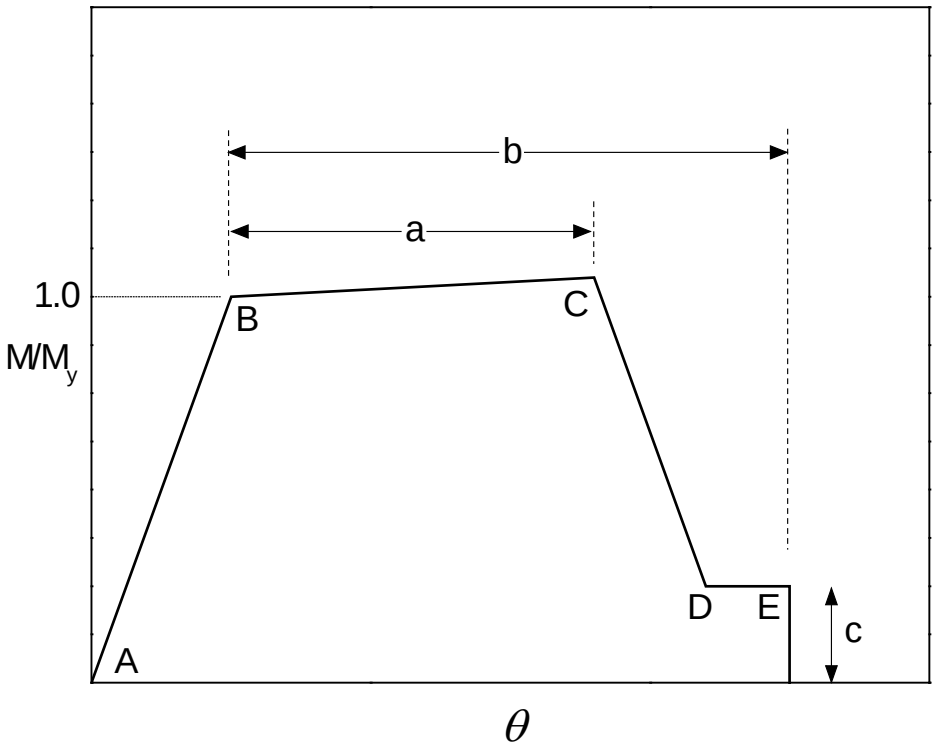

Fig. 5-7- Modeling parameters (Adapted from ASCE/SEI 2006)

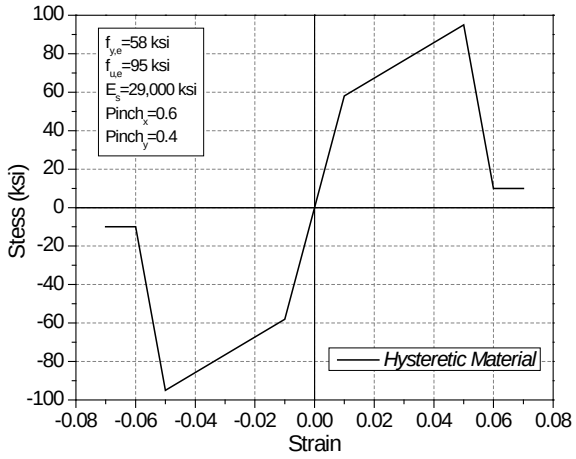

(a)

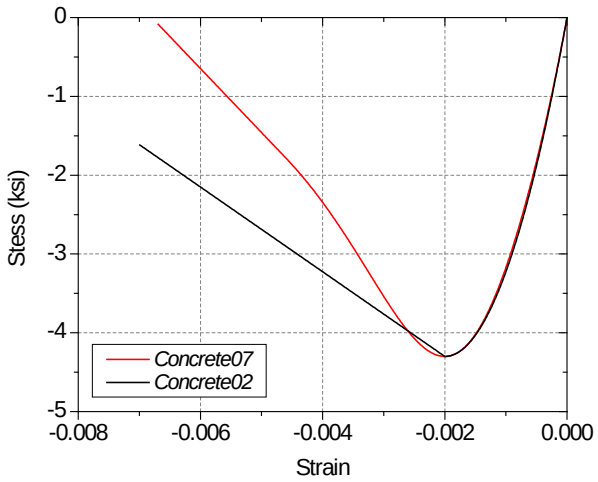

b) Compression

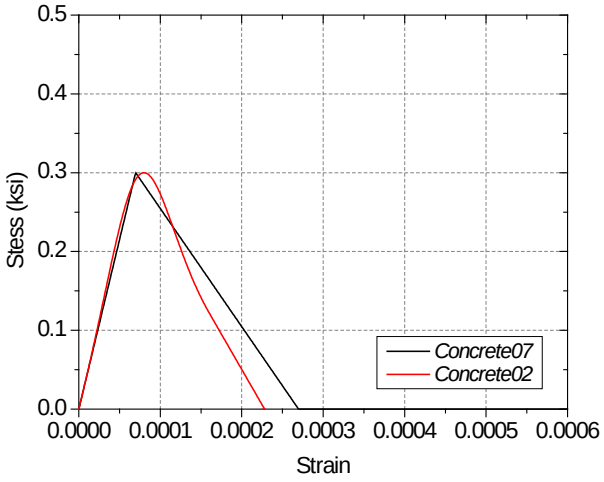

b) Tension

Fig. 5-8- Monotonic envelopes for steel and concrete

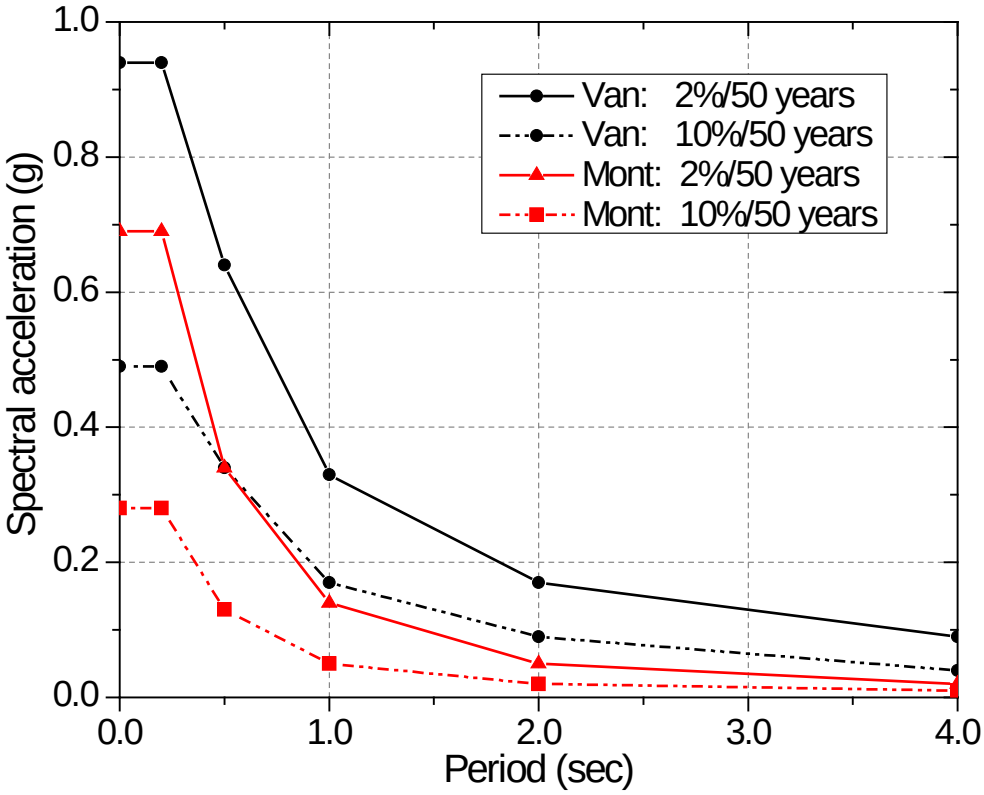

Fig. 5-9- Spectral acceleration for Montreal and Vancouver

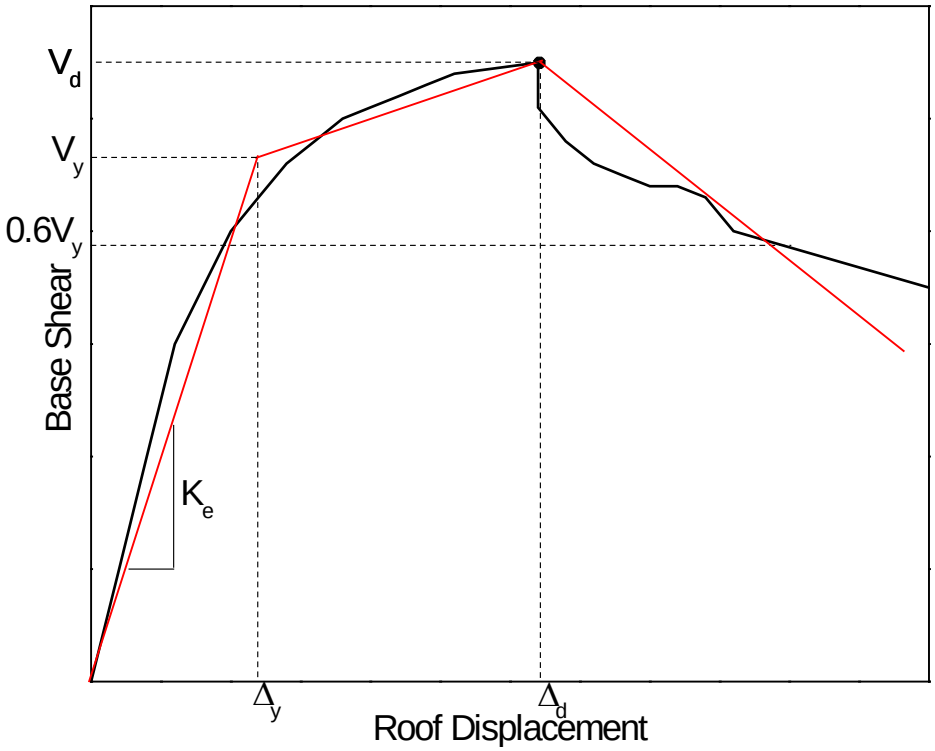

Fig. 5-10- Idealized Force-Displacement Curves (Adapted from ASCE-41, 2006)

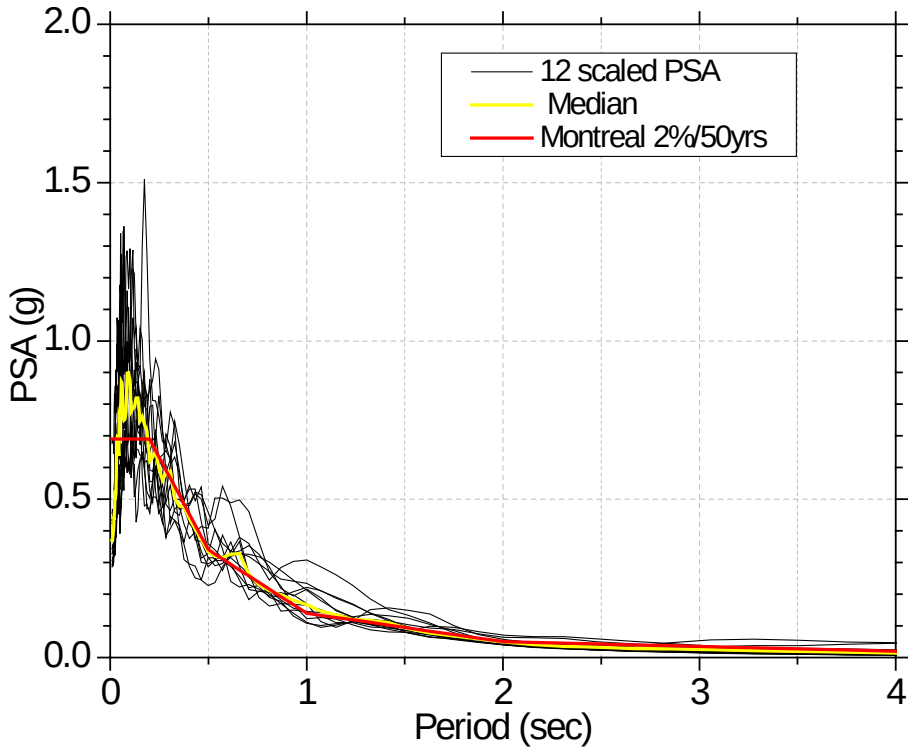

a) Montreal

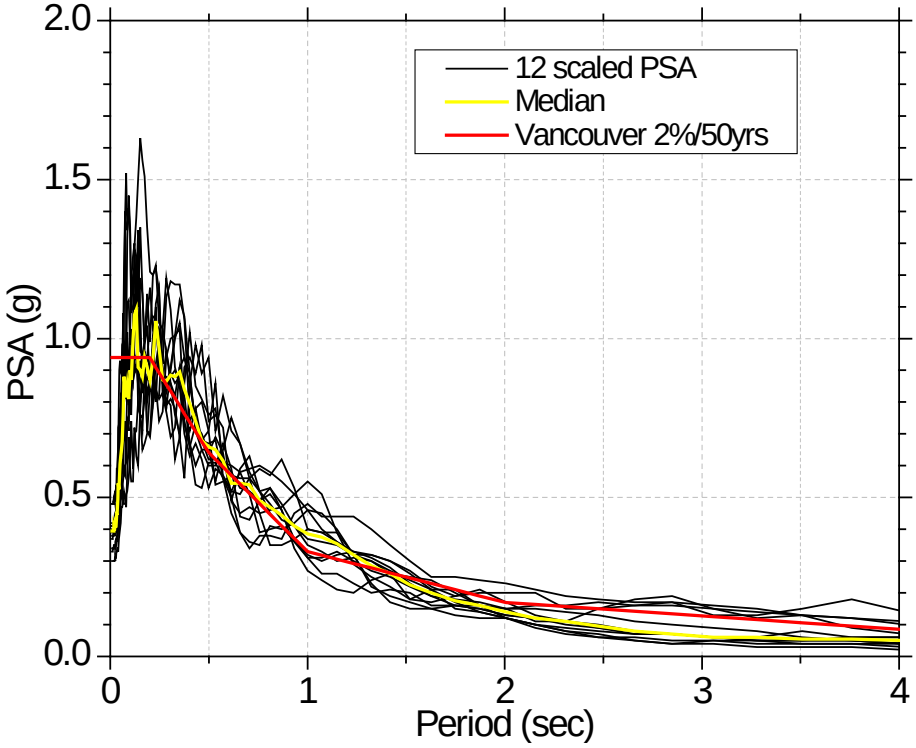

a) Vancouver

Fig. 5-11- Scaled Pseudo Spectral Acceleration (2% chance of exceedance in 50 years)

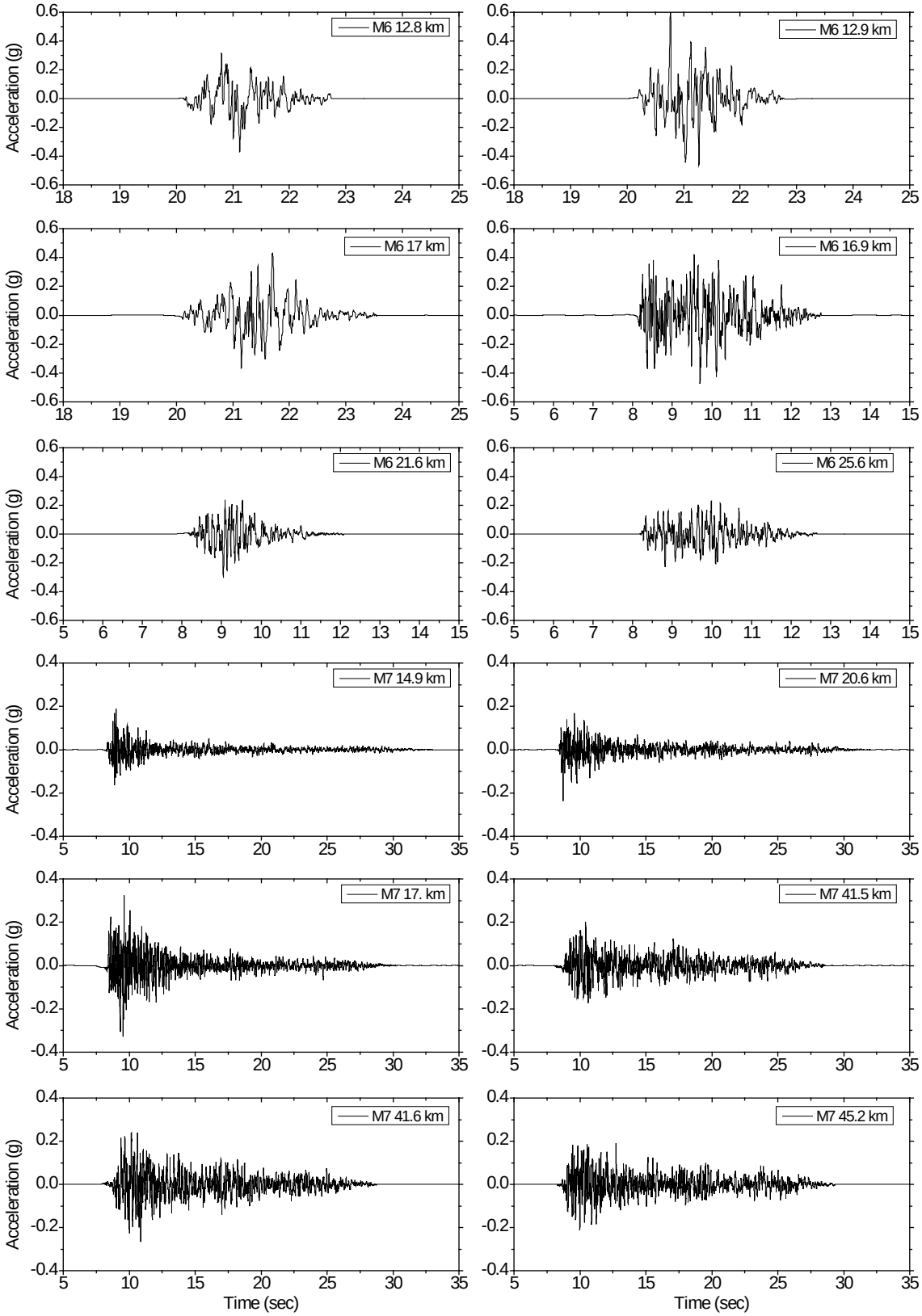

Fig. 5-12- Scaled ground motions (2%/50years) - Montreal

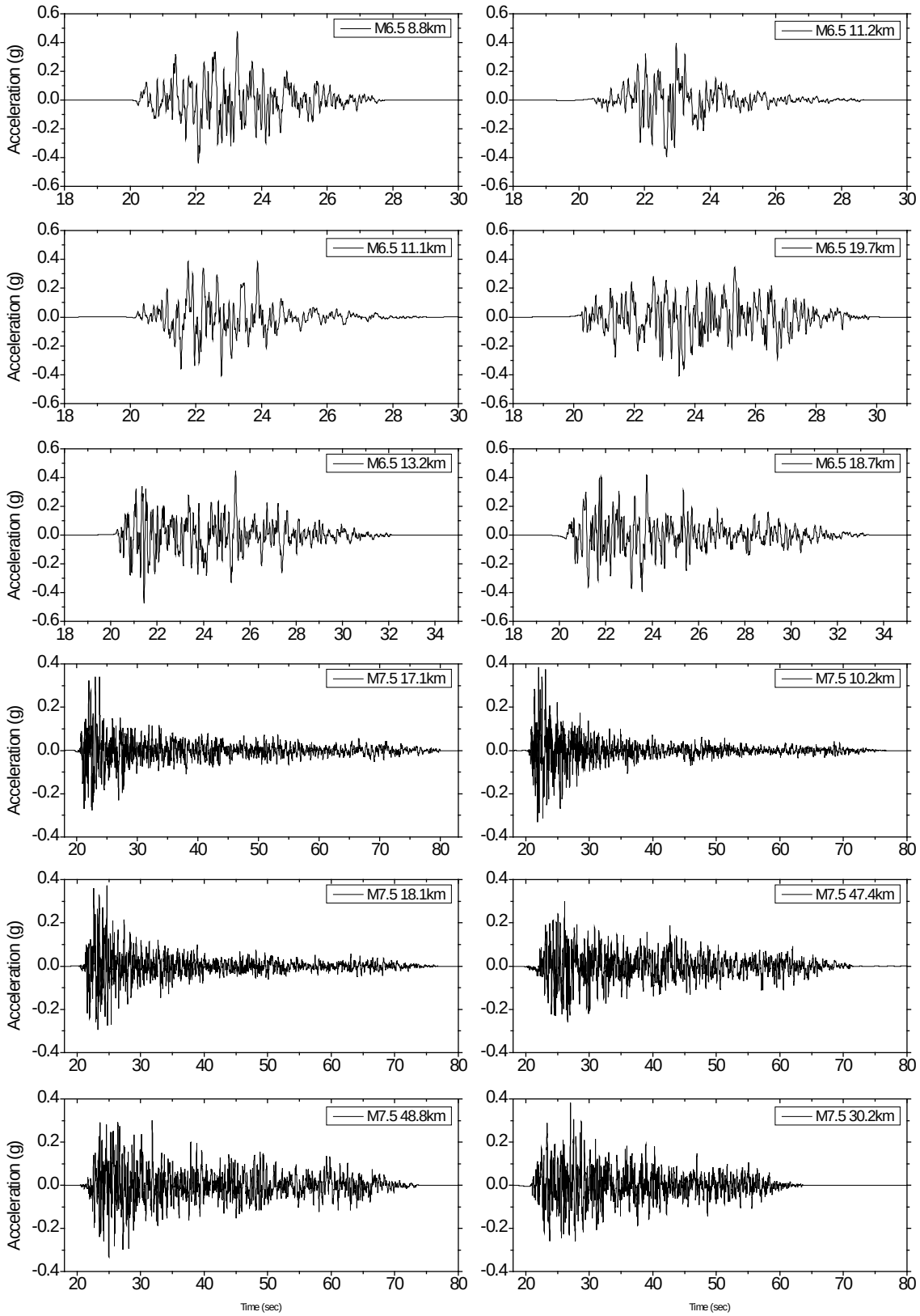

Fig. 5-13- Scaled ground motions (2%/50years) - Vancouver

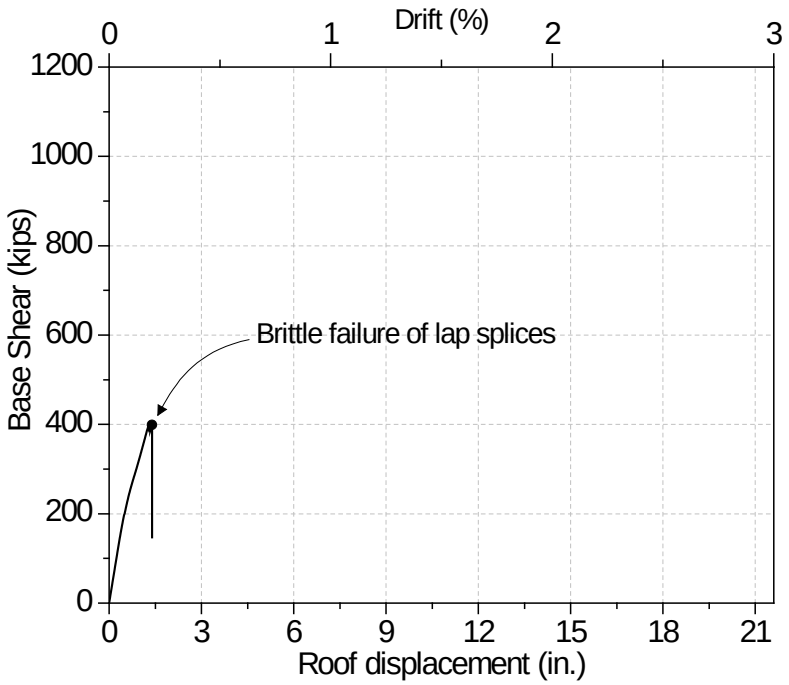

a) Pushover

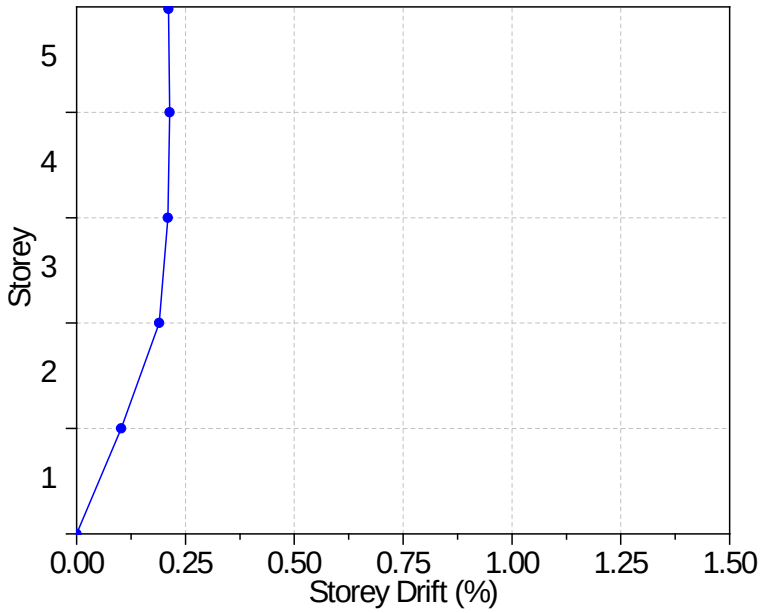

b) Variation of storey drifts

Fig. 5-14- Predicted response of original wall-frame structure at peak load

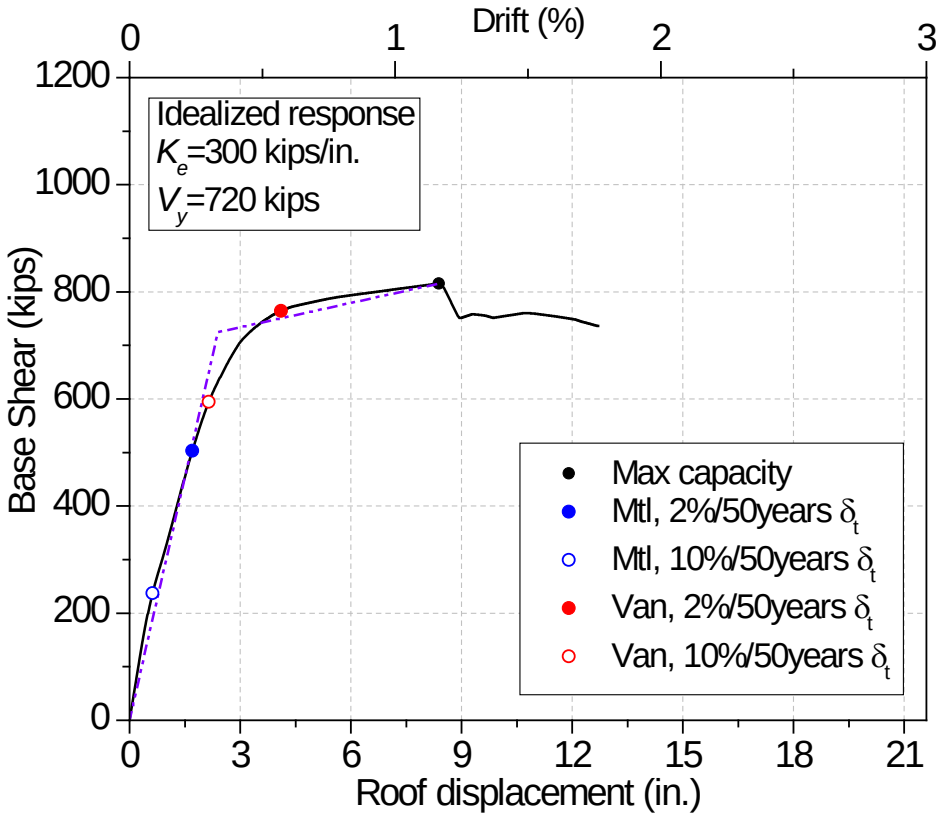

a) Pushover

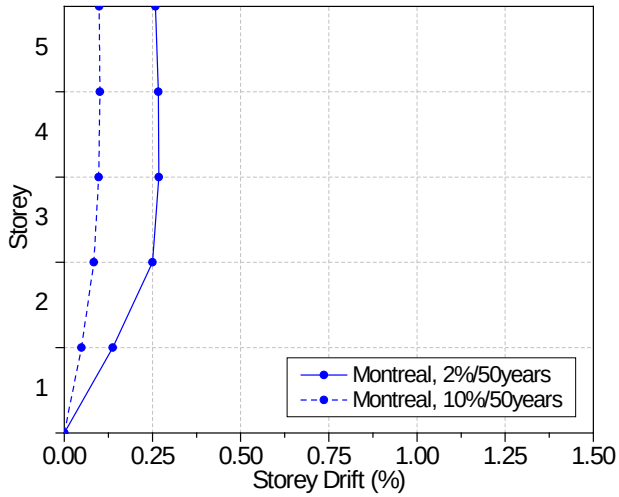

b) Variation of storey drifts - Montreal

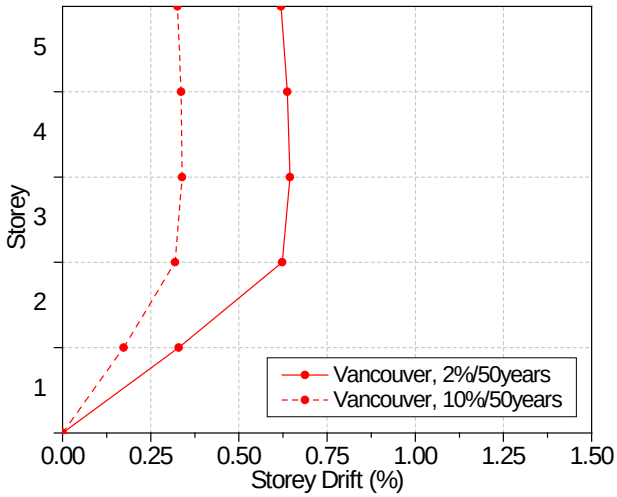

c) Variation of storey drifts - Vancouver

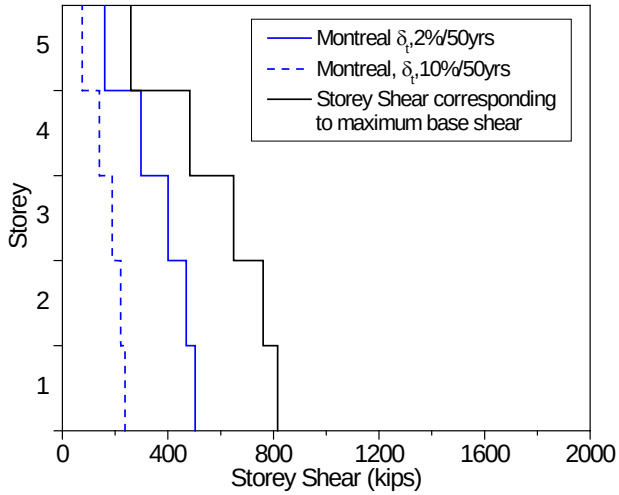

d) Storey shear - Montreal

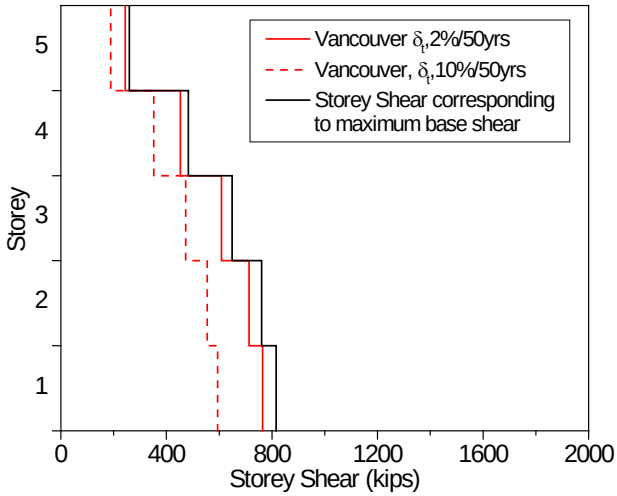

e) Storey Shear - Vancouver

Fig. 5-15- Pushover response of wall-frame structure with CFRP retrofitted walls

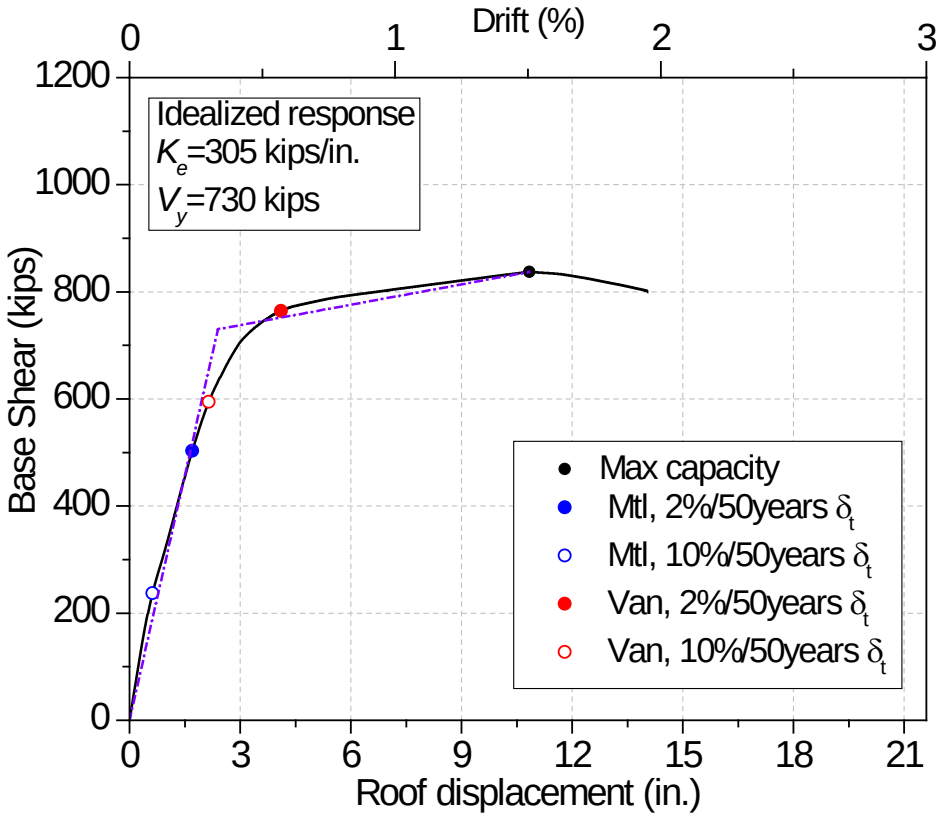

a) Pushover

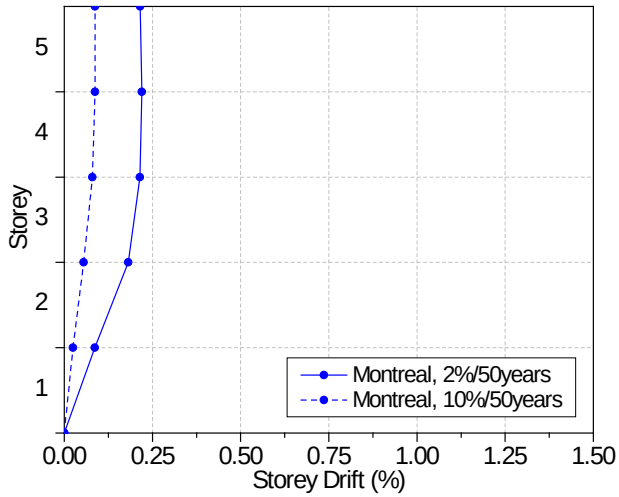

b) Variation of storey drifts - Montreal

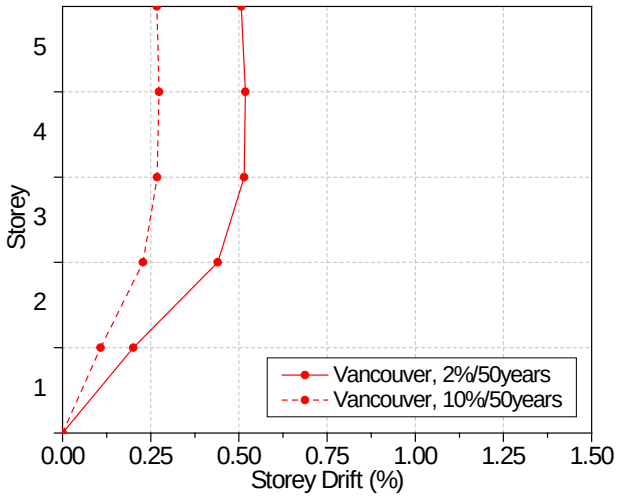

c) Variation of storey drifts - Vancouver

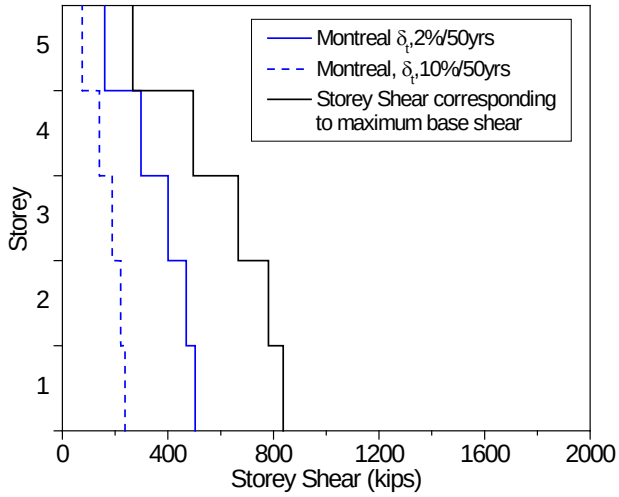

d) Storey shear - Montreal

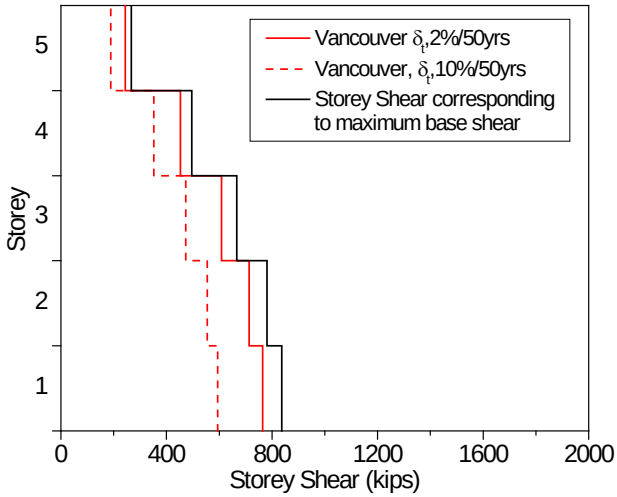

e) Storey Shear - Vancouver

Fig. 5-16- Pushover response of wall-frame structure with CFRP retrofitted walls and beams framing into walls

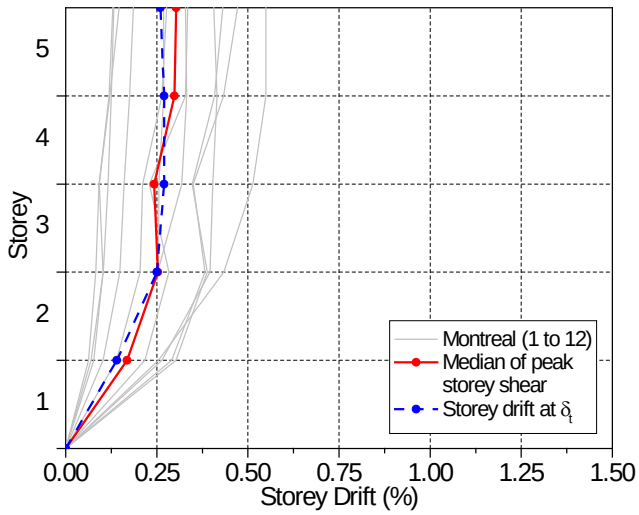

a) Montreal, peak storey drifts

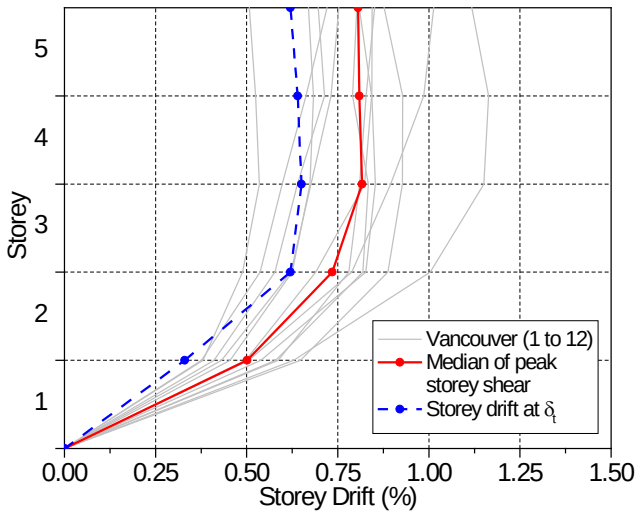

b) Vancouver, peak storey drifts

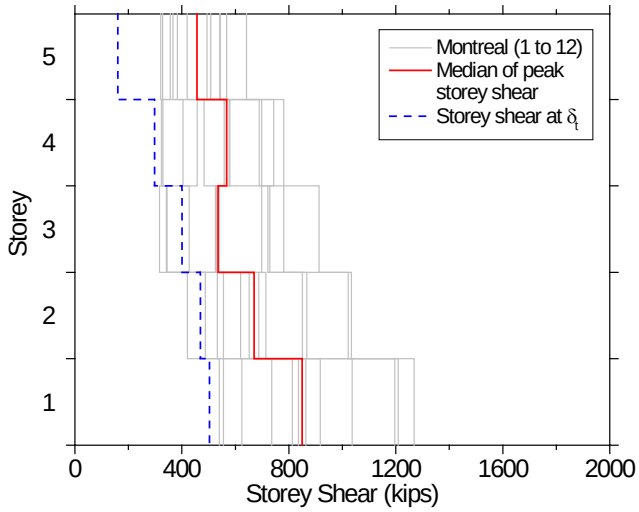

c) Montreal, peak storey shears

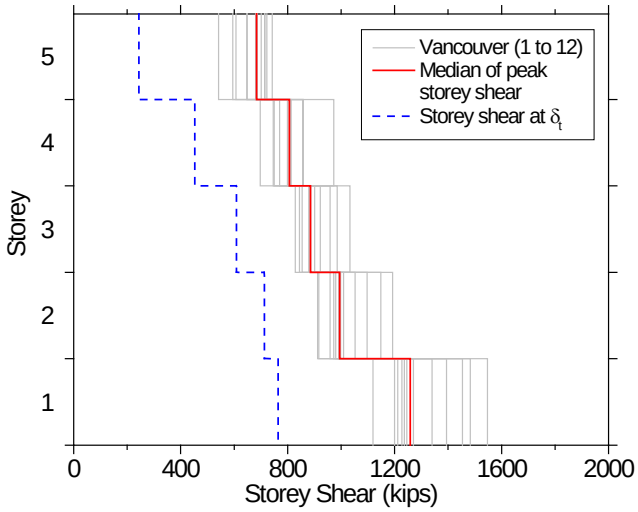

d) Vancouver, peak storey shears

Fig. 5-17- Predictions from nonlinear dynamic analyses for CFRP retrofitted structures in Montreal and Vancouver for 2% / 50 years

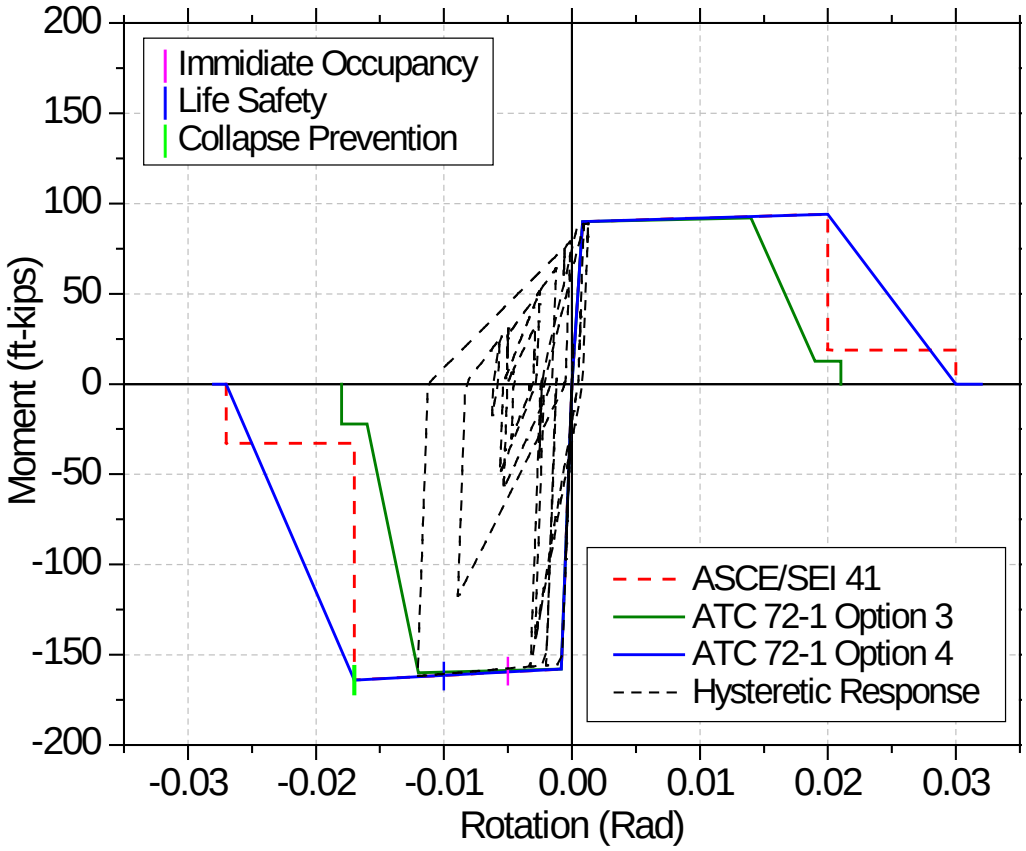

Fig. 5-18- Hysteretic response of Beams

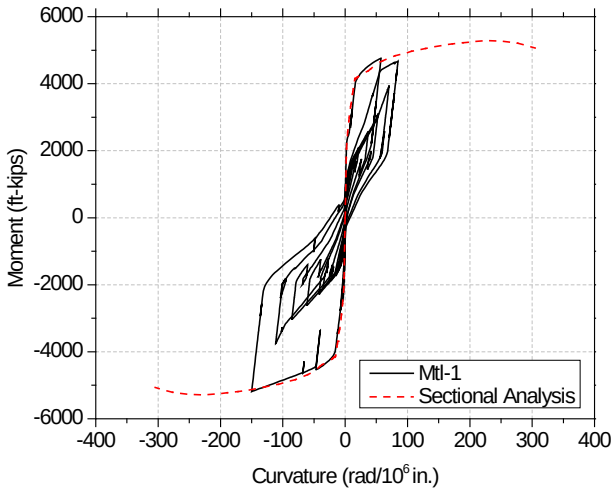

(a) Mtl-1
(record with maximum predicted drifts)

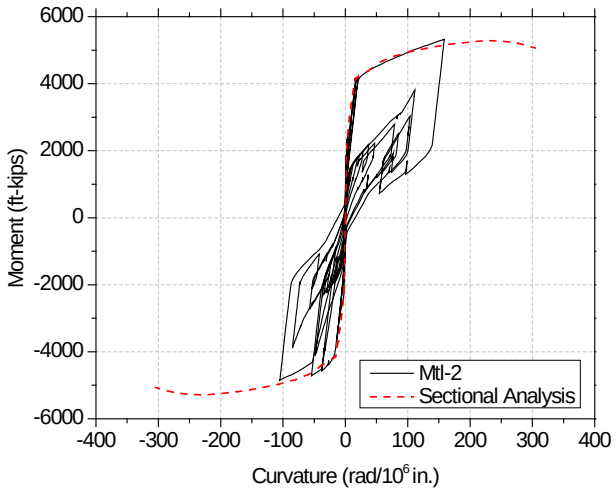

(b) Mtl-2
(record with maximum predicted base shear)

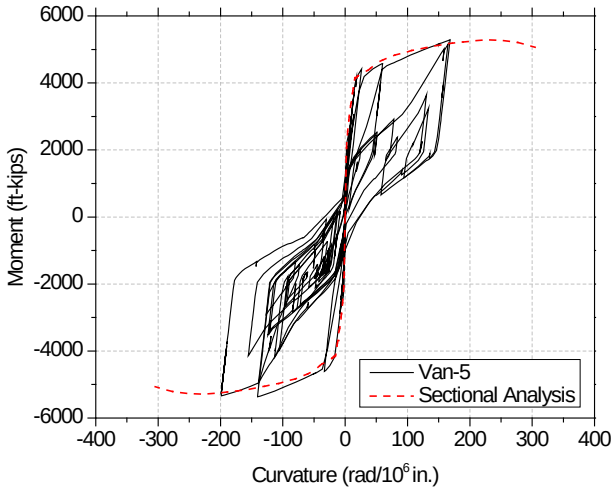

(c) Van-5
(record with maximum predicted drifts)

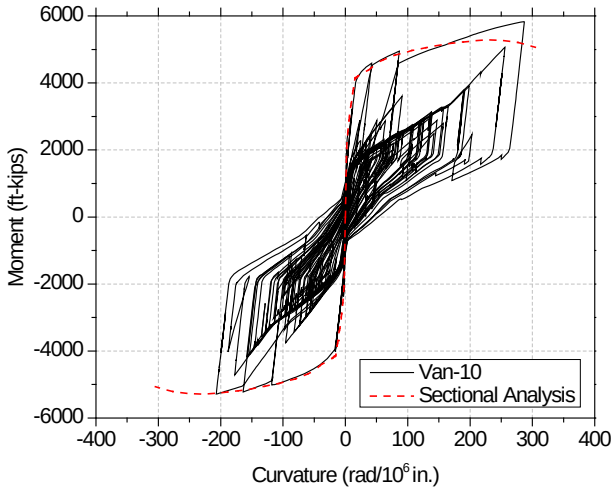

(d) Van-10
(record with maximum predicted base shear)

Fig. 5-19- Moment-curvature response of walls subjected to selected records

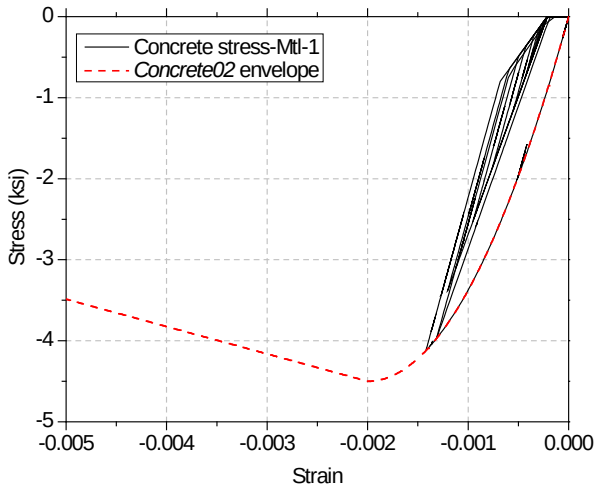

(a) Mtl-1

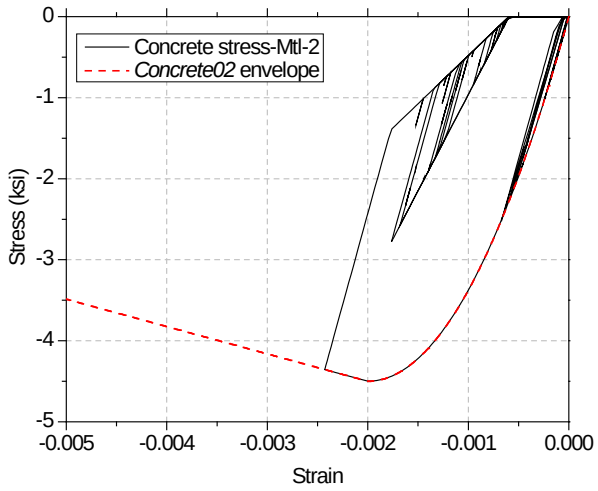

(b) Mtl-2

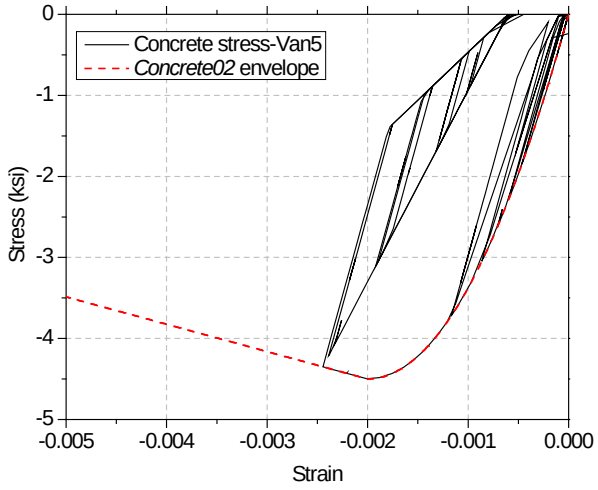

(c) Van-5

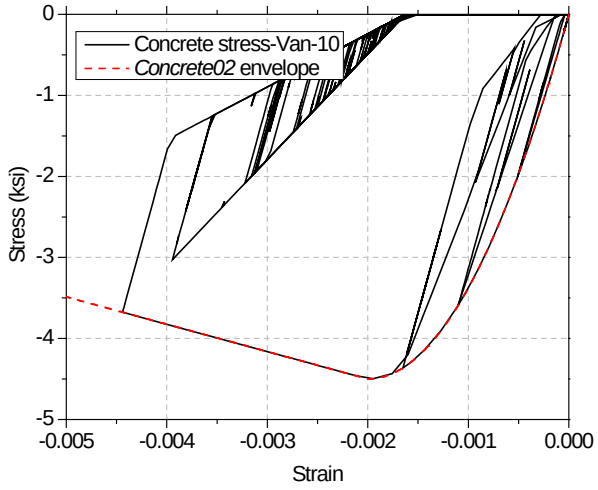

(d) Van-10

Fig. 5-20- Concrete stress (ksi) at extreme fibre

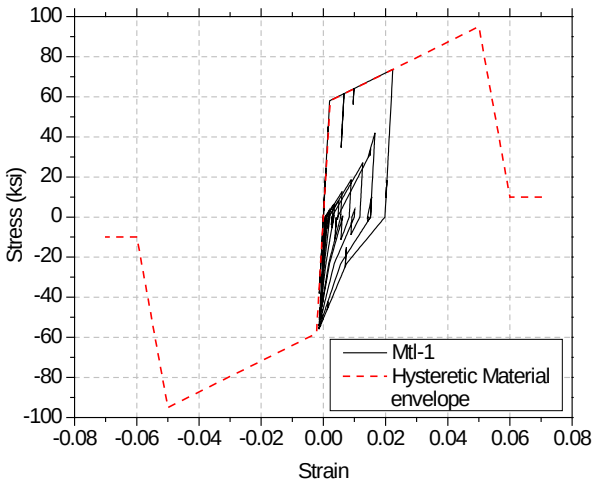

(a) Mtl-1

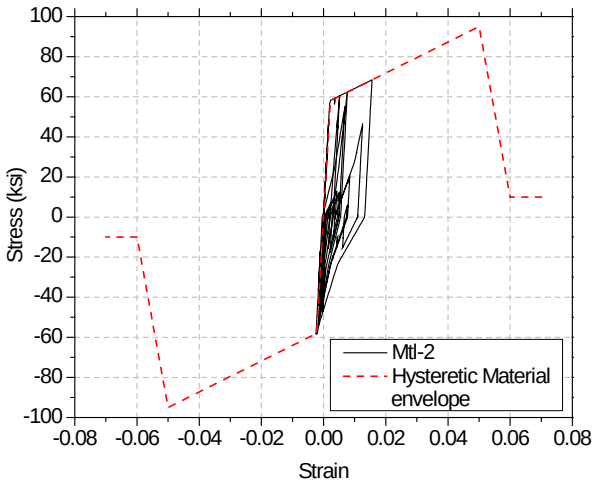

(b) Mtl-2

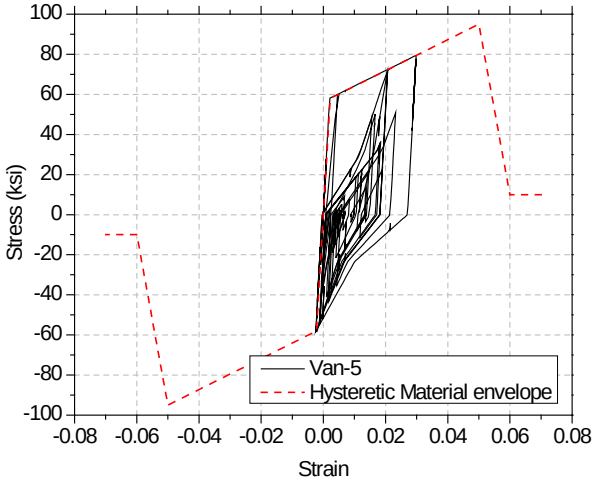

(c) Van-5

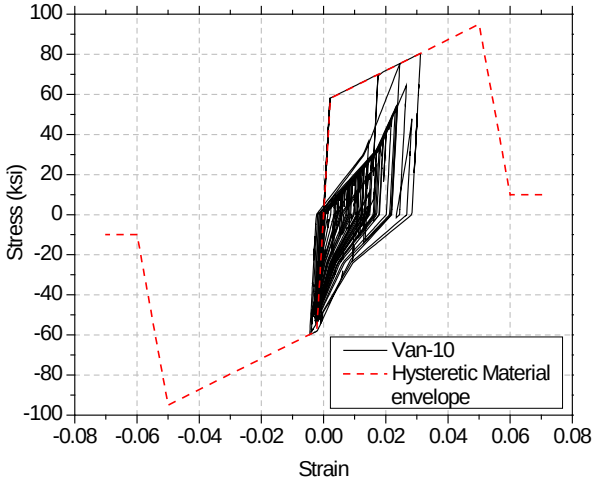

(d) Van-10

Fig. 5-21- Stress in concentrated steel reinforcement

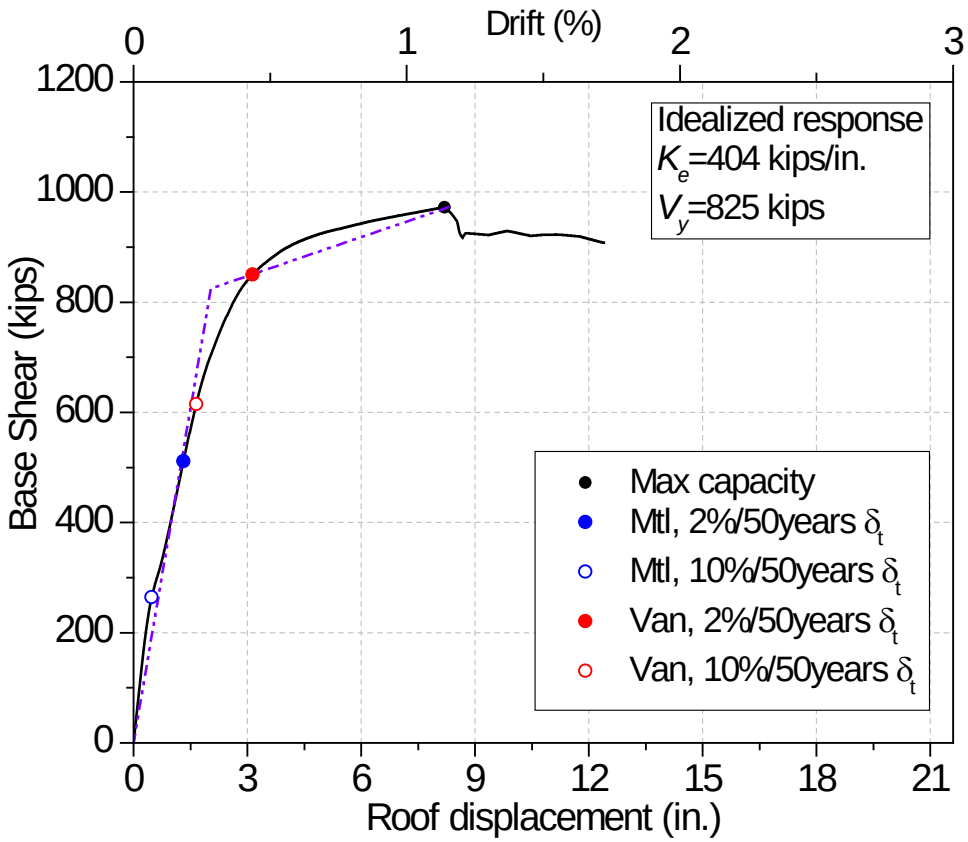

a) Pushover

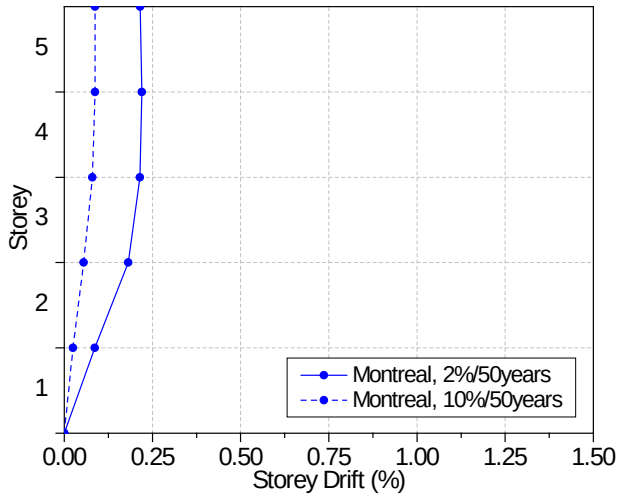

b) Variation of storey drifts - Montreal

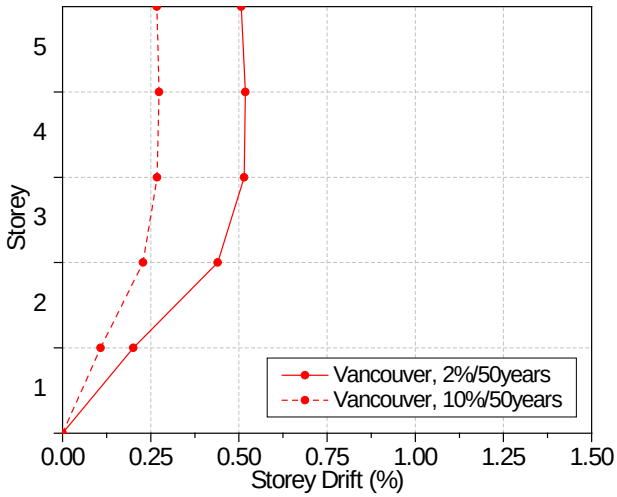

c) Variation of storey drifts - Vancouver

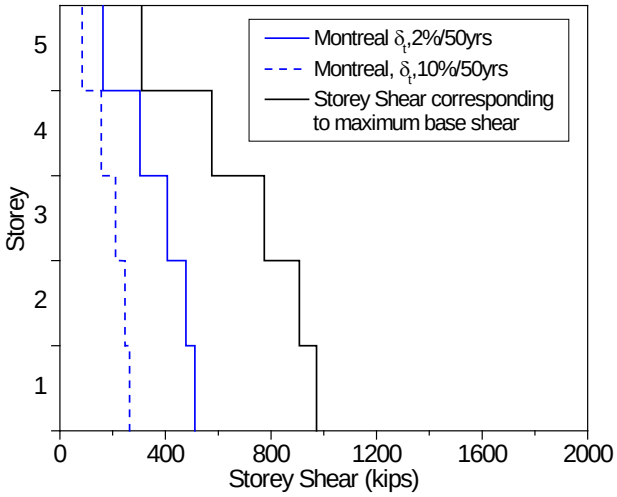

d) Storey shear - Montreal

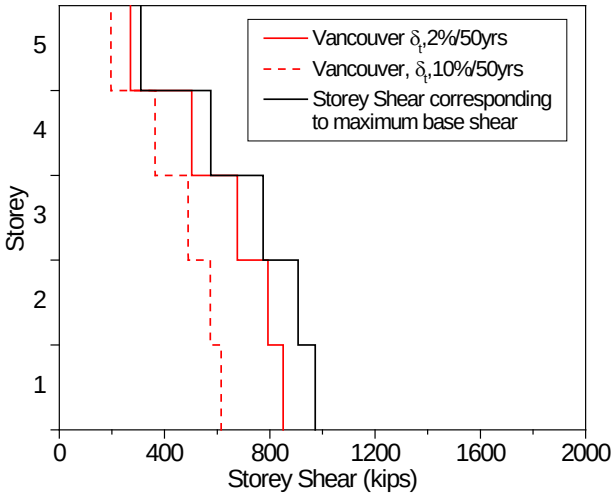

e) Storey Shear - Vancouver

Fig. 5-22- Pushover response of wall-frame structure with FRSCC retrofitted walls (1st and 2nd storeys) and CFRP retrofitted walls (above 2nd storey)

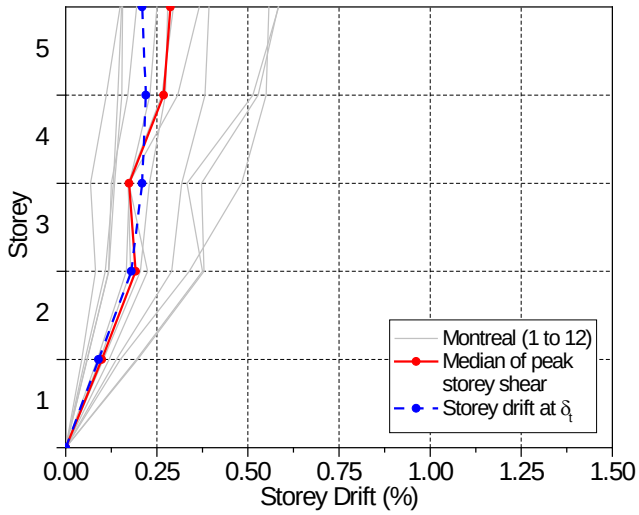

a) Montreal, peak storey drifts

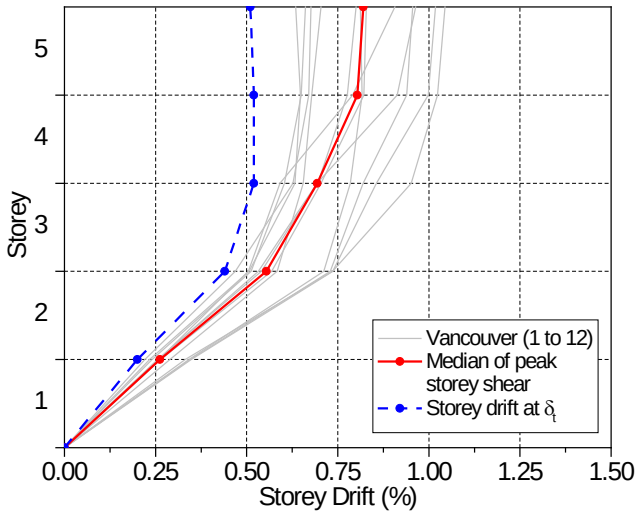

b) Vancouver, peak storey drifts

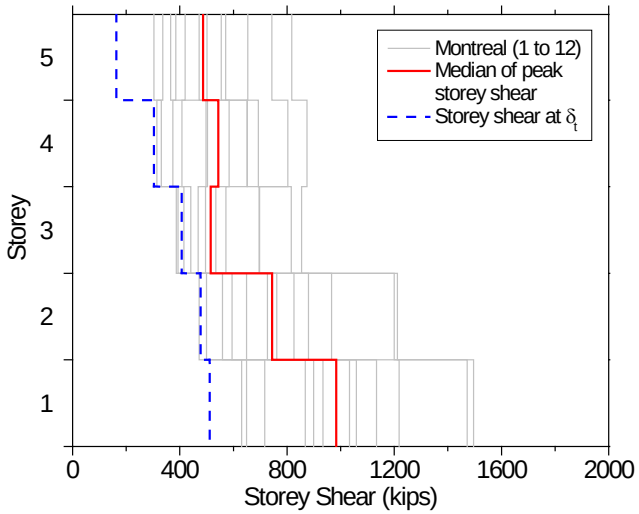

c) Montreal, peak storey shears

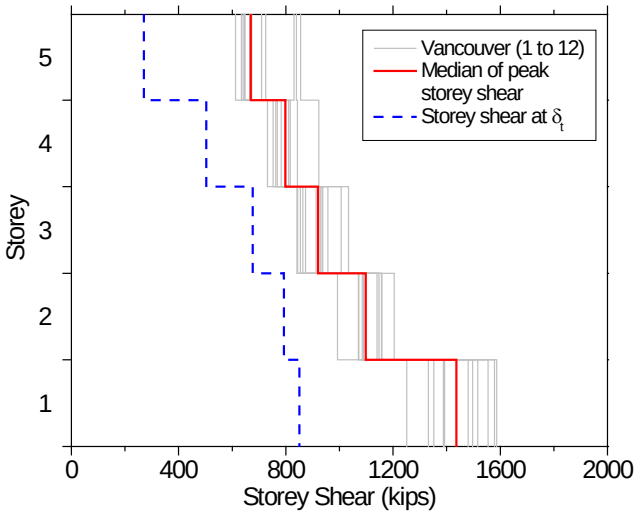

d) Vancouver, peak storey shears

Fig. 5-23- Predictions from nonlinear dynamic analyses for FRSCC retrofitted structures in Montreal and Vancouver for 2% / 50 years

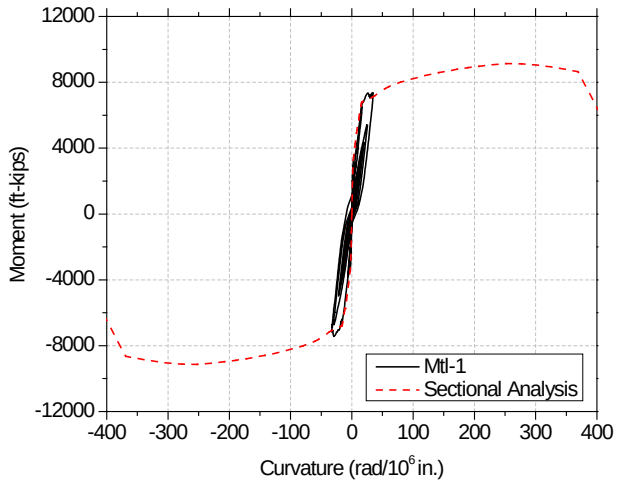

(a) Mtl-1, Moment curvature at base

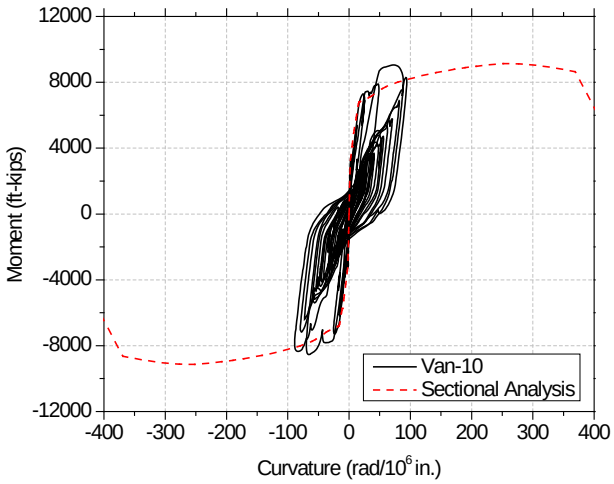

(b) Van-10, Moment-curvature at base

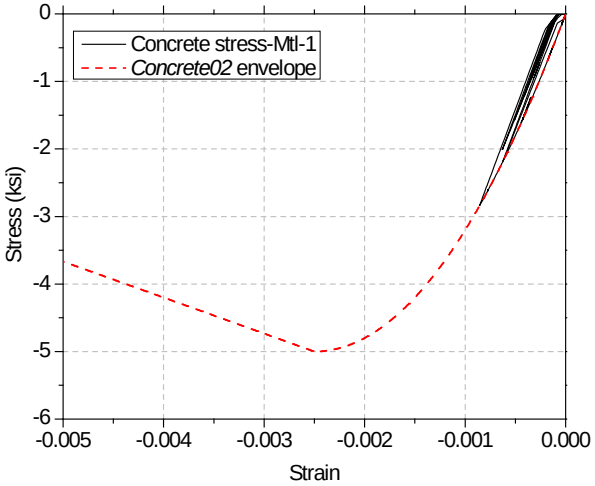

(c) Mtl-1, concrete stress at extreme fibre

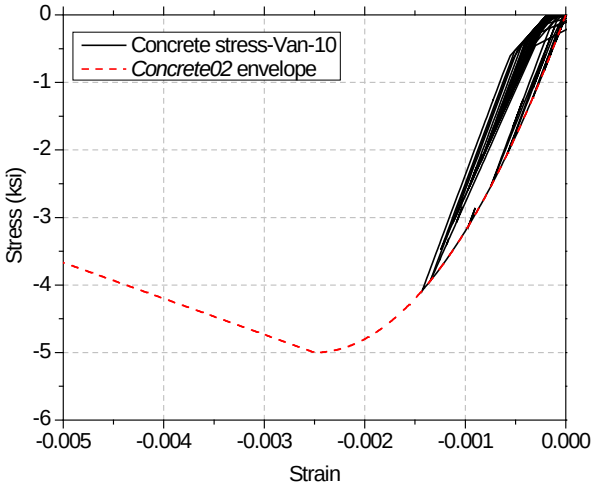

(d) Van-10, concrete stress at extreme fibre

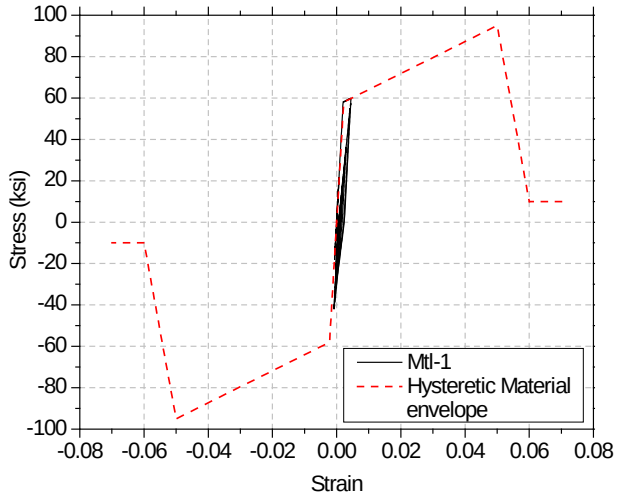

(e) Mtl-1, steel stress

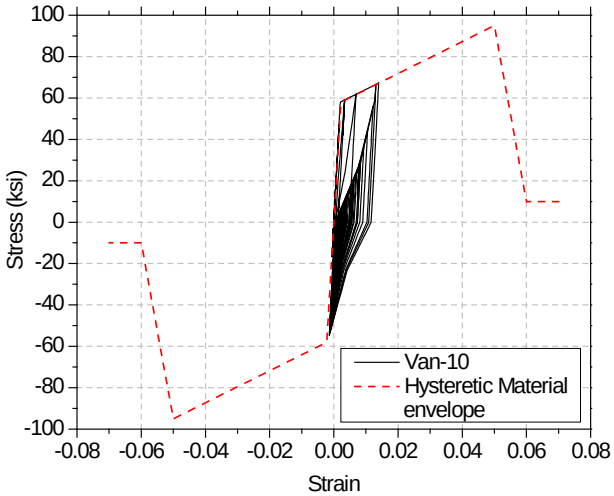

(f) Van-10, steel stress

Fig. 5-24- Response of FRSCC retrofitted walls subjected to selected records

Chapter 6
Summary and Conclusions

The following conclusions can be made from this experimental and analytical research program:

1) Thin, poorly detailed flexural walls containing inadequate lap splices in regions of potential plastic hinging fail in a brittle manner without yielding of the reinforcement when subjected to reversed cyclic loading. Thin walls having a thickness of 6 or 8 in. (150 mm to 200 mm) are common in low-rise buildings designed and built in the 1960's and early 1970's.
2) Existing methods for the evaluation of the performance of lap splices are based on research conducted on columns, and do not reflect the more brittle behaviour of lap splices in thin walls.
3) Carbon Fibre Reinforced Polymer (CFRP) wrap can be used to improve the confinement of inadequate lap splices, such that a limited displacement ductility of about 2.0 can be achieved in the wall.
4) The use of a reinforced concrete jacket using fibre reinforced self-consolidating concrete (FRSCC) can be used to repair walls damaged in an earthquake to provide increased strength, stiffness, and considerably improved ductility to about a level of 3.0. A method for designing this repair technique was developed and this technique can also be used to retrofit existing walls.
5) Adjustments to the ASCE-41 (2006) generalized force-displacement models taking into account the reduced stiffness, strength, and ductility of poorly detailed thin walls have been proposed based on the experimental research. Guidance was also developed for generalized force displacement models for the two different types of retrofit studied.

6) The retrofitted shear walls of a prototype structure were modeled using fibre displacement-based beam-column elements. These models were developed based on experimental results from this research program and the results from the literature. The beams and columns were modeled with concentrated hinge models. Hysteretic parameters suitable for predicting the complete reversed cyclic loading responses of the retrofitted walls were developed.
7) The nonlinear static procedure (pushover analyses) based on ASCE-41 (2006) was used to predict the responses of the frame-wall structure. The target displacements determined using the ASCE-41 procedure were used to judge the nonlinear responses of the walls before and after retrofit.
8) Acceleration-time histories, using a spectral matching procedure, suitable for Montreal and Vancouver were developed for a probability of exceedance of 2% in 50 years.
9) Nonlinear dynamic analyses (time history) using the OpenSees platform were carried out to study the expected performance of frame-wall structure, before and after retrofit. These analyses were carried out for both Montreal and Vancouver and for two different retrofit techniques (CFRP and FRSCC).
10) The nonlinear static procedure and the nonlinear dynamic analyses enabled an assessment of the effectiveness of the retrofit techniques.

Statement of Originality

The original aspects of this research program are described below:

1) This research provides important behavioural data on the seismic behaviour of poorly detailed thin flexural walls consistent with details used in the 1960's and 1970's. The very thin walls contained short lap splices at the base of the wall and had a single layer of inadequately anchored shear reinforcement having no confinement effects at the ends of the walls. No previous research was found in the literature for slender walls with these poor details.
2) Only a few experimental studies have been carried out using Carbon Fibre Reinforced Polymers (CFRP) to retrofit poorly detailed walls. The minimum intervention technique, using a single layer of CFRP wrap, was studied to determine the improved reversed cyclic loading response of these thin, flexural walls with inadequate reinforcement details. A method for assessing the influence of deficient lap splices on the response of the walls before and after retrofit was developed.
3) The repair of thin, poorly detailed walls that were damaged from reversed cyclic loading was studied using steel fibre reinforced concrete and added reinforcement over the critical lap splice region together with CFRP shear strips above this region. The design and detailing method chosen for the repair was successful in improving the ductility and energy absorption. This part of the research program provides a design philosophy and details for the repair of previously damaged walls. This part of the study also provides guidance on the retrofit of existing walls.
4) Behavioural models, capable of predicting the reversed cyclic loading responses of the walls before and after retrofit, were developed.
5) The responses of a deficient wall-frame prototype structure before and after retrofit were predicted using the OpenSees software. Pushover analyses

were carried out to determine the overall response of the structure. Non-linear time history analyses of the prototype structures located in Montreal and in Vancouver were carried out to assess the dynamic response of the structures before and after retrofit. These analyses enabled a comparison of the assessment of the structures using pushover and non-linear dynamic analyses.

6) This research program provides guidance to engineers faced with the difficult task of assessing the performance of older deficient walls and determining suitable retrofit techniques.

References

ACI (1963), Building Code Requirements for Reinforced Concrete (ACI 318-63). American Concrete Institute, Detroit., MI

ACI, (1971), Building Code Requirements for Reinforced Concrete (ACI 318-71). American Concrete Institute, Detroit, MI

ACI, (1977), Building Code Requirements for Reinforced Concrete (ACI 318-77). American Concrete Institute, Detroit, MI

ACI, (1983), Building Code Requirements for Reinforced Concrete (ACI 318-83). American Concrete Institute, Detroit, MI

ACI, (1989), Building Code Requirements for Reinforced Concrete (ACI 318-89). American Concrete Institute, Detroit, MI

ACI, (1995), Building Code Requirements for Reinforced Concrete (ACI 318-95). American Concrete Institute, Farmington Hills, MI

ACI, (2008), Building Code Requirements for Reinforced Concrete (ACI 318-08). American Concrete Institute Farmington Hills, MI

ACI, (2011), Building Code Requirements for Reinforced Concrete (ACI 318-11). American Concrete Institute, Farmington Hills, MI

Adebar, P.; Mutrie, J.; and DeVall, R. (2005). “Ductility of Concrete Walls: the Canadian Seismic Design Provisions 1984 to 2004”, Canadian Journal of Civil Engineering, V. 32, No. 6, pp. 1124-1137.

Aktan, A. E., Bertero, V. V. (1985). “RC Structural Walls: Seismic Design for Shear”, ASCE Journal of Structural Engineering, 111 (8), 1775-1791.

Antoniades, K. K., Salonikios, T. N., Kappos, A. J. (2003). ”Cyclic Tests on Seismically Damaged Reinforced Concrete Walls Strengthened Using Fiber-Reinforced Polymer Reinforcement”. ACI Structural Journal , 100 (4), 510-518.

ASCE/SEI 41 (2007). “Seismic Rehabilitation of Existing Buildings”, American Society of Civil Engineers, Reston, VA.

ATC (1978) “Tentative Provisions for the Development of Seismic Regulations for Buildings, Applied Technology Council”, Applied Technology Council, ATC-3-06, NBS Special Publication 510, NSF Publication 78-8, U.S. Government Printing Office, Washington, D.C.

ATC (1996). “Seismic Evaluation and Retrofit of Concrete Buildings”, Applied Tchnology Council, ATC-40. Redwood City, California

ATC (2010). “Modeling and Acceptance Criteria for Seismic Design and Analysis of Tall Buildings.” Jointly published by PEER adn the Applied Technology Counsil as PEER/ATC 72-1.

Balaguru, P., Nanni, A., and Giancaspro, J. (2009). “FRP composites for reinforced and prestressed concrete structures.” Taylor and Francis, NY.

Belmouden, Y. and Lestuzzi, P. (2007). Analytical model for predicting nonlinear reversed cyclic behaviour of reinforced concrete structural walls. Journal of Engineering Structures 29:7, 1263-1276.

Bentz, E. C., Collins, M. P. (2000) “Response-2000: Reinforced Concrete Sectional Analysis using the modified compression field theory”.

Cardenas, A. E., Magura, D. D. (1973). “Strength of High-Rise Shear Walls-Rectangular Cross Section”. Response of Multistory Concrete Structures to Lateral Forces, pp. 119-150, ACI Special Publication SP-36, American Concrete Institute, Detroit, Michigan

Chang, G. A., and Mander, J. B., (1994). “Seismic Energy Based Fatigue Damage Analysis of Bridge Columns: Part I—Evaluation of Seismic Capacity,” NCEER Technical Report No. NCEER-94-0006, State University of New York, Buffalo, N.Y., 222 pp.

Cho, J.-Y., Pincheira, J. A., 2006. “Inelastic analysis of reinforced concrete columns with short lap splices subject to reversed cyclic loads”, ACI Struct. J. 103, 280–290.Belmouden and Lestuzzi, 2006; Massone et al., 2009

CSA. (1973), Code for the Design of Concrete Structures for Buildings (CAN3- A 23.3-M73), Canadian Standards Association, Rexdale, ON.

CSA. (1977), Code for the Design of Concrete Structures for Buildings (CAN3- A 23.3-M77), Canadian Standards Association, Rexdale, ON.

CSA. (1984), Code for the Design of Concrete Structures for Buildings (CAN3-A 23.3-M84), Canadian Standards Association, Rexdale, ON.

CSA. (2004), Design of Concrete Structures, Standard CSA-A23.3–04. Canadian Standard Association, Mississauga, ON.

CSRN, (2013). “Canadian Guidelines for Seismic Evaluation and Retrofit”, Canadian Seismic Research Network, under preparation.

Clough, R. W.; Benuska, K. L; and Wilson, E. L. (1965). “Inelastic Earthquake Response of Tall Buildings” Proc. 3rd World Conference on Earthquake Engineering, New Zealand.

Elnashai, A.S. and Izzuddin, B.A. (1993). “Modelling of material non-linearities in steel structures subjected to transient dynamic loading” Earthquake Engineering and Structural Dynamics, Vol. 22, pp. 509-532

Elwood, K. J., Matamoros, A. B., Wallace, J. W., Lehman, D. E., Heintz, J. A., Mitchell, A. D., Moore, M. A., Valley, M. T., Lowes, L. N., Comartin, C. D., and Moehle, J. P., 2007. “Update to ASCE/SEI 41 concrete provisions”. Earthquake Spectra, 23, 493–523.

Fardis, M. N. (2009). “Seismic design, assessment and retrofitting of concrete buildings”, Springer, New York, e-ISBN: 978-1-4020-9842-0

FEMA. (1997). "NEHRP guidelines for the seismic rehabilitation of buildings.", FEMA 273, prepared by the Building Seismic Safety Council for the Federal Emergency Management Agency, Washington, D.C .

Federal Emergency Management Agency (FEMA). (2000). "Prestandard and commentary for the seismic rehabilitation of buildings" FEMA 356, prepared by the American Society of Civil Engineers for the Federal Emergency Management Agency, Washington, D.C.

Federal Emergency Management Agency (FEMA). (2009). "Quantification of Building Seismic Performance Factors" FEMA 695, prepared by Applied Technology Council for the Federal Emergency Management Agency, Washington, D.C.

Fiorato, A. E., Oestrele, R. G., Corley, W. G. (1983). “Behavior of Earthquake Resistant Strutural Walls Before and After Repair”, ACI Structural Journal, 80 (5), 403-413.

Filippou, F. C.; Popov, E. G., and Bertero; V. V. (1983). “Effects of Bond Deterioration on Hysteretic Behavior of Reinforced Concrete Joints”; EERC Report No. UCB/EERC-83/19; Earthquake Engineering Research Center; University of California, Berkeley

Fyfe, 2012, “Tyfo® SCH-41 Composite using Tyfo® S Epoxy”, Description of the product, verified on April 2013.”http://www.fyfeco.com/products/pdf/tyfo%20sch-41%20comp.pdf”

Giberson, M. (1967). The response of nonlinear multi-story structures subjected to earthquake excitation. Tech. report, Earthquake Engineering Research Laboratory, California Institute of Technology, Pasadena, California.

Hamad, B. S. , Rteil, A. A. , and Soudki, K. A. (2004b). “Bond strength of tension lap splices in high-strength concrete beams strengthened with glass fiber reinforced polymer wraps.” J. Compos. Constr., 8 (1), 14–21.

Harajli, M. H. (2008). “Seismic Behavior of RC Columns with Bond-Critical Regions: Criteria for Bond Strengthening Using External FRP Jackets” Asce Journal Of Composites For Construction, 69-79.

Harajli, M. H. and Khalil, Z. (2008). “Seismic FRP Retrofit of Bond-Critical Regions in Circular RC Columns: Validation of Proposed Design Methods”. ACI structural Journal, 105(6). 760-769.

Harries, K. A.; Ricles, J. R.; Pessiki, S; and Sause, R. (2006). “Seismic Retrofit of Lap Splices in Nonductile Square Columns Using Carbon Fiber-Reinforced Jackets”. ACI structural Journal, 103(6). 874-884.

Ibarra, L. F., and Krawinkler, H. (2005). "Global collapse of frame structures under seismic excitations," Technical Report 152, The John A. Blume Earthquake Engineering Research Center, Department of Civil Engineering, Stanford University, Stanford, CA.

Ibarra L.F., Medina R. A., and Krawinkler H. (2005). “Hysteretic models that incorporate strength and stiffness deterioration”, Earthquake Engineering and Structural Dynamics, 34(12), 1489-1511.

International Conference of Building Officials (1982), “Uniform Building Code”, 1982 Edition, Whittier, California.

Júlio, E. S., Branco, F., and Silva, V. D., (2003). “Structural Rehabilitation of Columns with Reinforced Concrete Jacketing”, Prog. Struct. Engng Mater. John Wiley and Sons, Ltd., 29-37.

Kabayesawa, T. H., Shiohara, S., Otani, S. and Aoyama, H. (1982). Analysis of the Full-Scale 7-Story R.C. Test Structure. Proceedings, 3rd Joint Technical Coordinating Committee, U.S. Japan Cooperative Earthquake Research Program, Building Research Institute, Tsukuba.

Kent, D. C.; Park, R. (1971). “Flexural Members with Confined Concrete”, Journal of the Structural Divison, Proceeding of the American Society of Civil Engineers (ASCE), 97 (7), 1969- 1990.

Kuang, J. S., Ho, Y. B. (2008). “Seismic Behavior and Ductility of Squat Reinforced Concrete Shear Walls with Nonseismic Detailing”. ACI Structural Journal , 105 (2), 225-231.

Kunnath, S. K., Hoffmann, G., Reinhorn, A. M., and Mander, J. B. (1995). “Gravity load-designed reinforced concrete buildings. Part I: Seismic evaluation of existing construction.” ACI Struct. J., 92(3), 343–354.

Lignos, D.G. and Krawinkler, H. (2012). “Sidesway collapse of deteriorating structural systems under seismic excitations,” Rep.No.TB 177, The John A. Blume Earthquake Engineering Research Center, Stanford University, Stanford, CA

Lynn, A. C. (2001). "Seismic evaluation of existing reinforced concrete building columns." PhD dissertation, Dept. of Civil and Environmental Engineering, University of California, Berkeley.

Menegotto, M., and Pinto; E. (1973). “Method of Analysis for Cyclically Loaded Reinforced Concrete Plane Frames Including Changes in Geometry and Non-Elastic Behavior of Elements Under Combined Normal Force and Bending”. Proc. Of IABSE Symposium on Resistance and Ultimate Deformability of Structures Acted on by Well-Defined Repeated Loads; Lisbon, Portugal.

Mar, D., Panian, L., Dameron, R. A., Hansen, B. E., Vahdani, S., Mitchell, D., and Paterson, J. (2000). “Performance-based seismic upgrade of a 14-story suspended slab building using state-of-the-art analysis and construction techniques.” Proc., 69th Annual Struct. Engrs. Assoc. of Cal. Conv. (SEAOC), Calif., 1–12.

Massone, L.; Orakcal, K. and M., Wallace, J. W. (2009). “Modeling of Squat Structural Walls Controlled by Shear”. ACI Structural Journal, 106 (5), 646-655.

Melek, M. and Wallace, J. W. (2004). "Cyclic behavior of columns with short lap splices." ACI Strc. J., 101(6).

NBCC 1965, National Building Code of Canada, Institute for Research in Construction, National Research Council of Canada, Ottawa, ON.

NIST, 2010, Evaluation of the FEMA P-695 Methodology for Quantification of Building Seismic Performance Factors, GCR 10-917-8, prepared by the NEHRP Consultants Joint Venture for the National Institute of Standards and Technology, Gaithersburg, MD.

Orakcal, K., Wallace, J. W. (2006). “Flexural Modeling of Reinforced Concrete Walls-Experimental Verification”. ACI Strcutural Journal , 103 (2), 196-206.

Orakcal, K., Wallace, J. W., Conte, J. P. (2004). “Flexural Modeling of Reinforced Concrete Walls - Model Attributes”. ACI Structural Journal, 101 (5), 688-698.

Park, R., Priestley, M. J. N., and Gill, W. D. (1982). "Ductility of square confined concrete columns." J. Struct. Div., ASCE, 108(4), 929-950.

Paterson, J., Mitchell, D. (2003). “Seismic Retrofit of Shear Walls with Headed Bars and Carbon Fiber Wrap”. Journal of Structural Engineering, ASCE, 129 (5), 606-614.

Paulay, T., Preistley, M., Synge, A. (1982, Jul). “Ductility in Earthquake Resisting Squat Shearwalls”. Journal of the American Concrete Institute, V.79, No.4, pp. 257-269.

Perform 3D, (2011), Computers and Structures Inc., Berkeley, CA

Priestley, M., Seible, F. (1995). “Design of Seismic Retrofit measures for Concrete and Masonry Structures”. Journal of Construction and Building Materials, 9 (6), 365-377.

Priestley, M.J.N., Seible, F. and Calvi, G. M. (1996). “Seismic Design and Retrofit of Bridges”, John Wiley & Sons Inc., New York, NY.

Saatcioglu, M., Palermo, D., Ghobarah, A., Mitchell, D., Simpson, R., Adebar, P., Tremblay, R., Ventura, C.E., Hong, H., (2013) "Performance of reinforced concrete buildings during the February 27, 2010 Maule (Chile) Earthquake"Can. J. of Civil Eng., in press.

Saatcioglu, M., and Razvi, S. R. (1992). “Strength and ductility of confined concrete.” J. Struct. Eng.,ASCE, 118(6), 1590–1607.

SAP2000, (2011). “Structural Analysis Program”, Version 14.2, Computers and Strcutures. Inc, Berkeley, CA, Licence: McGill University

Scott, B. D; Park, R. and Priestley, M. J. N. (1982). “Stress-Strain Behavior of Concrete Confined by Overlapping Hoops at Low and High Strain Rates”, ACI Journal Proceeding, 79(1), 13-27.

Seible, F., Priestley, M. J. N., Hegemier, G.A. and Innamorato, D. (1997). “Seismic Retrofit of RC Columns with Continuous Carbon Fiber Jackets.”, J. of Comp. for Const., ASCE, 1(2), pp. 52-62.

Sozen, M. A., and Moehle, J. P., (1993). “Stiffness of reinforced concrete walls resisting in-plane shear,” Electric Power Research Institute, Research Project 3094-01, Final Report.

Taucer. F. F.; Spacone, E. and Filippou, F. C. (1991). “A Fiber Beam Column Element for Seismic Response Analysis of Reinforced Concrete Structures”, Earthquake Engineering Research Center, University of California, Berkeley

Taghdi, M., Bruneau, M., Saatcioglu, M. (2000). “Seismic Retrofitting Of Low-Rise Masonry And Concrete Walls Using Steel Strips”. ASCE Journal of Strcutural Engineering, 126 (9), 1017-1025.

Thai, D. X. and Pimanmas, A. (2011). “Response of lap splice of reinforcing bars confined by FRP wrapping: modeling approach”, Structural Engineering and Mechanics, 37(1).

Thermou, G. E., Pantazopoulou, S. J., and Elnashai, A. S. (2007). “Flexural Behavior of Brittle RC Members Rehabilitated with Concrete Jacketing”, J. Str. Eng., ASCE, 133(10), 1373-1384.

Thomsen IV, J. H., Wallace, J. W. (2004). “Displacement-Based Design of Slender Reinforced Concrete Structural Walls-Experimental Verification.”, ASCE Journal of Structural Engineering, 103 (4), 618-630.

Vecchio, F. J., (1999) “Toward Cyclic Load Modeling of Reinforced Concrete”, ACI Structural Journal, 96(2), 193-202

Vulcano, A., Bertero, V. V. and Colotti, V. (1988). Analytical Modeling of RC Structural Walls. Proceedings, 9th World Conference on Earthquake Engineering, V. 6, Tokyo-Kyoto, Japan, 41-46.

Wallace, J. W., Thomsen, J. H. (1995). “Seismic Design of RC Structural Walls. Part II: Applications”, Journal of Structural Engineering, 121 (1), 88-101.

Wallace, J. W. (2012). “Behavior, Design, and Modeling of Structural Walls and Coupling Beams - Lessons from Recent Laboratory Tests and Earthquakes”, International Journal of Concrete Structures and Materials, 6 (1), 3-18

Zhao, J., and S. Sritharan. (2007). “Modeling of strain penetration effects in fiber-based analysis of reinforced concrete structures.”, ACI Structural Journal, 104(2), pp. 133-141.

Appendix A
Unit Conversion Table

To Convert From	multiply	to get / To Convert from	multiply	to get
Length / Area				
inch, in	25.5	millimeter, mm	0.0394	in
feet, ft. (12 in.)	304.8	millimeter, mm	0.0033	ft
Force				
pound, lb	4.44822	newton, N	0.224809	lb
kilo-pound, kip = 1000 lb	4.44822	kilo-Newton, kN = 1000 N	0.224809	kip = 1000lb
Stress				
pounds per sq. ft, lb/ft^2, psf	47.8803	Pascals, Pa = N/m^2	0.020885	lb/ft^2, psf
psf	0.04788	kilopascal, kPa, kN/m^2	20.88540	psf
kilo-pounds per sq. ft, ksf	47.8803	kPa	0.020885	ksf
pounds per sq. inch, psi	6894.76	Pa	0.000145	psi
psi	6.89476	kPa	0.145038	psi
kilo-pounds per sq. in, ksi	6.89476	Megapascal, MPa	0.145038	ksi
Bending Moment				
pound-foot, lb-ft	1.35582	Newton-meter, N-m	0.737561	lb-ft
pound-inch, lb-in	0.11298	N-m	8.850732	lb-in
Distributed Load				
pounds per foot, plf	14.5939	Newton per meter, N/m	0.0685218	plf
pounds per inch, pli	175.127	N/m	0.0057102	pli

Appendix B
Gravity and wind loads

Table B-1- Self weight of the beams, columns and walls			
	Columns	Beams	Shear Walls
	18" × 18"	14" × 18"	X, Y
Height (ft)	1.5	1.5	12.0
Width (ft)	1.5	1.167	0.67
Density (pcf)	150	150	150
Weight/length (kip/ft)	0.3375	0.2625	1.4
Self Weight of Slabs			
Slab thickness (ft)	0.667		
Density (pcf: lb/ft^3)	150		
Weight/Area (psf: lb/ft^2)	100		
Additional Dead Load			
Dead Plus (psf: lb/ft^2) [2.4 kPa]	50		

Table B-2- Live load	
Live load (psf: lb/ft^2) [2.4 kPa]	50

Table B-3- Wind load		
	Dir-Y	Dir-X
5th Story Tributary Area (ft^2)	324	468
2nd to 4th Story Tributary Area (ft^2)	648	936
1st Story Tributary Area (ft^2)	972	1404
Wind Load (psf: lb/ft^2) [1.8 kPa]	38.0	38.0
Wind/length for each wall (kip/ft)	1.03	1.48

Appendix C
Mathematical Model

Table C-1- Effective Stiffness of Beam	
Flexural	$0.3E_cI_g$
Shear	$0.4E_cA_w$
Axial	E_cA_g

Table C-2- Effective strength and stiffnesses of column components

Column	Storey	$\frac{P}{A_g f'_c}$	Stiffness modification factor, α_m	M_y	$K_{mem}=\frac{6E_cI_g}{L}$	$K_s=n.\alpha_m\frac{6E_cI_g}{L}$
		-	-	*kips.in.*	*kips.in.*	*kips.in.*
Corner	1	0.07	0.30	2160	1640250	4920750
	2	0.06	0.30	2004	1640250	4920750
	3	0.04	0.30	1872	1640250	4920750
	4	0.03	0.30	1740	1640250	4920750
	5	0.01	0.30	1608	1640250	4920750
Edge	1	0.12	0.32	2472	1640250	5248800
	2	0.10	0.30	2364	1640250	4920750
	3	0.07	0.30	2160	1640250	4920750
	4	0.05	0.30	1932	1640250	4920750
	5	0.02	0.30	1656	1640250	4920750
Interior	1	0.20	0.40	3132	1640250	6561000
	2	0.16	0.36	2808	1640250	5904900
	3	0.12	0.32	2520	1640250	5248800
	4	0.08	0.30	2196	1640250	4920750
	5	0.04	0.30	1848	1640250	4920750

Appendix D
Target Displacements

Case 1 – CFRP Retrofitted Walls

Step 1- Mode shape vectors

Mode	φ_1	φ_2	φ_3	φ_4	φ_5
1	-0.06	-0.17	-0.32	-0.47	-0.63
2	0.26	0.49	0.44	0.08	-0.48
3	-0.48	-0.37	0.29	0.42	-0.33
4	-0.54	0.24	0.32	-0.48	0.20
5	0.37	-0.50	0.48	-0.30	0.09

Step 2- Periods

	Mode 1	Mode 2	Mode 3	Mode 4	Mode 5
Ti (sec)	0.99	0.18	0.06	0.03	0.02

Step 3- Modal properties

$\begin{Bmatrix}\varphi_1\\ \varphi_2\\ \varphi_3\\ \varphi_4\\ \varphi_5\end{Bmatrix}$	0.10	-0.54	1.46	-2.73	4.05
	0.28	-1.03	1.14	1.22	-5.57
	0.50	-0.94	-0.88	1.65	5.37
	0.75	-0.16	-1.27	-2.44	-3.32
	1.00	1.00	1.00	1.00	1.00
L_1	3.24	-2.19	1.74	-1.73	1.85
Γ_1	1.40	-0.54	0.20	-0.07	0.02
M_n^*	4.52	1.19	0.36	0.13	0.03
$M_n^*/\sum M$	0.73	0.19	0.06	0.02	0.00

Step 3- Target Displacement calculations according to ASCE-41, 2006

	Montreal		Vancouver	
	2%/50yrs	10%/50yrs	2%/50yrs	10%/50yrs
T_i		0.99		
$T_e = T_i\sqrt{\frac{k_i}{k_e}}$		1.13		
$C_0 = \Gamma_1$		1.39		
$C_1 = 1 + \frac{R-1}{\alpha T_e^2}$ *	1.00	1.00	1.0	1.00
$C_2 = 1 + \frac{1}{800}\left(\frac{R-1}{T_e}\right)^2$ **		1.00		
$C_m = M_n^* / \sum M$		0.73		
S_a	0.13	0.05	0.31	0.16
$R = \frac{S_a}{\left(V_y / W\right)}.C_m$	0.58	0.21	1.40	0.73
$\delta_t = C_0 C_1 C_2 S_a \frac{T_e^2}{4\pi^2} g$ (in.)	1.70	0.62	4.11	2.15

* $Class\ C \rightarrow \alpha = 90$ and $T_e > 1.0\ sec \rightarrow C_1 = 1.00$

** $T_e > 0.7\ sec \rightarrow C_2 = 1$

Case 2 – FRSCC Retrofitted Walls

Step 1- Mode shape vectors

Mode	φ_1	φ_2	φ_3	φ_4	φ_5
1	-0.03	-0.12	-0.27	-0.46	-0.67
2	-0.17	-0.48	-0.50	-0.15	0.44
3	-0.30	-0.53	0.21	0.46	-0.32
4	0.43	0.08	-0.51	0.49	-0.17
5	-0.64	0.44	-0.29	0.18	-0.05

Step 2- Periods

	Mode 1	Mode 2	Mode 3	Mode 4	Mode 5
Ti (sec)	0.85	0.15	0.06	0.03	0.02

Step 3- Modal properties

$\begin{Bmatrix}\varphi_1\\ \varphi_2\\ \varphi_3\\ \varphi_4\\ \varphi_5\end{Bmatrix}$	0.05	-0.40	0.94	-2.49	12.57
	0.18	-1.11	1.63	-0.44	-8.55
	0.41	-1.15	-0.64	2.96	5.73
	0.70	-0.35	-1.44	-2.80	-3.44
	1.00	1.00	1.00	1.00	1.00
L_1	2.86	-2.62	1.79	-2.33	9.15
Γ_1	1.40	-0.55	0.20	-0.08	0.03
M_n^*	4.00	1.45	0.37	0.18	0.24
$M_n^*/\sum M$	0.64	0.23	0.06	0.03	0.04

Step 3- Target Displacement calculations according to ASCE-41, 2006

	Montreal		Vancouver	
	2%/50yrs	10%/50yrs	2%/50yrs	10%/50yrs
T_i		0.85		
$T_e = T_i\sqrt{\frac{k_i}{k_e}}$		1.06		
$C_0 = \Gamma_1$		1.40		
$C_1 = 1 + \frac{R-1}{\alpha T_e^2}$ *	1.00	1.00	1.0	1.00
$C_2 = 1 + \frac{1}{800}\left(\frac{R-1}{T_e}\right)^2$ **		1.00		
$C_m = M_n^* / \sum M$		0.64		
S_a	0.13	0.05	0.32	0.17
$R = \frac{S_a}{\left(V_y / W\right)}.C_m$	0.57	0.21	1.36	0.71
$\delta_t = C_0 C_1 C_2 S_a \frac{T_e^2}{4\pi^2} g$ (in.)	1.32	0.48	3.14	1.65

* $Class\ C \rightarrow \alpha = 90$ and $T_e > 1.0\ sec \rightarrow C_1 = 1.00$

** $T_e > 0.7\ sec \rightarrow C_2 = 1$